IN-DEPTH INVESTIGATION OF THE EFFECTS OF POWDER PROPERTIES ON NUCLEATION AND CONTINUOUS GRANULATION

by

Albarah Al-Afandi

A thesis in fulfilment of the requirements for the degree of

Doctor of Philosophy

Strathclyde Institute of Pharmacy and Biomedical Sciences,

Glasgow, United Kingdom

2021

Declaration of authenticity and Author's rights

This thesis is the result of the author's original research. It has been composed by the author and has not been previously submitted for examination which has led to the award of a degree.

Signed:  Date: 29th March 2021

Abstract

To modernise manufacturing practices and standards, the pharmaceutical industry is undergoing an evolutionary shift from batch processes to a continuous end-to-end operation. Twin screw granulation (TSG) has gained a lot of attention as a viable continuous alternative to traditional high shear mixing for wet granulation. Additionally, regulatory guidelines have advocated the adoption of Quality by Design principles to develop a more versatile operation to consistently deliver quality products. This includes dynamically adjusting operational parameters within an established design space to accommodate variability of input materials and yield a uniform output.

The variability of raw materials poses a threat to the Quality Target Product Profile of solid dosages produced via continuous wet granulation. This work sought to assess particle size as a Critical Material Attribute and barrel fill as a Critical Process Parameter by investigating their effects on the Critical Quality Attributes of an immediate release tablet produced via continuous wet granulation using TSG. A Quality by Design approach was taken to characterise and document the progression of the variable raw materials from powders to nuclei (in vitro and in vivo), from nuclei to granules, and from granules to tablets. Each step sought to link the properties, performance and sensitivity of the material output to the initial raw materials to determine criticality.

A novel method of engineering three distinct grades of commonly used excipients was used to evaluate the effect of particle size variability. Single drop penetration tests on bimodal formulation blends were analysed to discern the effect of particle size and packing on powder wetting and granule formation. The engineered grades were then used to assess the effect of variability on granule properties and tablet performance resulting from TSG. Whilst the drastic particle size variability manifested differences between the granules formed from the

single drop tests, the tablets produced following TSG were all of acceptable quality. Therefore, for the typical blend used, twin screw granulation proved to be robust enough to mitigate input variability. However, a consistently high proportion of fines and oversized granules highlighted a substantial yield inefficiency across all conditions.

Powder material residence time distribution was also characterised to explore the channel fill within the barrel. The analysis demonstrated that by maintaining barrel conditions via the material feed rate and screw speed, granule properties can be preserved whilst increasing throughput as a method of scaling output.

This study highlighted that whilst material attributes and process parameters can be adjusted to manipulate material output, fundamental features of the TSG design, such as short residence time and liquid addition, limit production efficiency.

Acknowledgement

I can only express my deepest gratitude to my supervisor, Professor Gavin Halbert, for his continued support, guidance and patience throughout the years. I am truly indebted for the many times he helped me get back on track in the pursuit of this thesis.

I wish to thank everyone across CMAC who has enabled me to carry out my research.

I hold the greatest appreciation for my dear parents for their dependable wisdom and reassurance; for my wife and pillar, Romana, and her inexorable devotion; and for my family and friends who have made every step possible through their encouragement, companionship and empathy.

“Once you’ve been in the dark, you learn to appreciate those around you that shine evermore,” a quote with no attributable author that I found to be unequivocally true.

Table of Contents

List of figures

List of tables

List of abbreviations

API – Active pharmaceutical ingredient

CCS – Croscarmellose sodium

CDA – Constant drawing area

CE – Conveying element

CI% - Compressibility index

CMA – Critical material attribute

CPP – Critical process parameter

CQA – Critical quality attribute

DDA – decreasing drawing area

DoE -Design of experiments

DPT – Droplet penetration test

EQPC – Diameter of a circle of equivalent projection area

FDA – U.S. Food and Drug Administration

FDT – First detection time

GSD – Granule size distribution

HPMC – Hypromellose

HSM – High shear mixer

ICH - International Council for Harmonisation of Technical Requirements for Pharmaceuticals for Human

KE – Kneading element

LAC – α-Lactose monohydrate

LSR – Liquid-to-solid ratio

MCC – Microcrystalline cellulose

MFR – Material feed-rate

MgSt- Magnesium stearate

MLR – Multiple linear regression

MRT – Measured mean residence time

OOS – Out of specification

PBD – Powder bed density

PSD – Particle size distribution

QbD – Quality by design

QTPP – Quality target product profile

RSD – Relative standard deviation

RSM – Response surface methodology

RTD – Residence time distribution

sd – Standard deviation

SS – Screw speed

THP – Theophylline anhydrate

TRT – Theoretical residence time

TSG – Twin screw granulation

TVF – Total volumetric fraction

VAR – Vertical aspect ratio

WCR – Washburn capillary rise

List of symbols

$\bar{t}_t$ – Theoretical residence time

$\bar{t}_m$ – Measured mean residence time

A – Cross section area to flow

A' – Imbibition rate coefficient

B' – Viscous spread coefficient

Bo_g^* - Bond number

C(t) – Dye concentration

C' – Inertial spread coefficient

c_v – Conveying efficiency

d – Droplet diameter

$d_{3,2}$ – Sauter mean diameter

d_{50} – Median particle diameter

d_i – Initial diameter spread

d_{max} – Maximum droplet contact diameter

d_{nuclei} – Nuclei diameter

d_v –Viscous spread

E(t) - Residence time distribution function

FFc – Flow function

f_{pore} – Surface pore fraction

f_s – Surface solid fraction

g – Acceleration due to gravity

h – Droplet height

h_{nuclei} – Nuclei height

^{k} – Imbibition rate exponent

k – Permeability

l – Length

L – Screw conveying length

m – Mass

$\dot{m}$ - Mass flow rate

^{m} – Viscous spread exponent

^{n} – Inertial spread exponent

p_c – Capillary pressure

Pe – Peclet number

Q – Volume flowrate

Q^2 – Predictive cross-validation coefficient

R – Surface roughness

r_0 – Droplet radius prior to impact

R^2 – Coefficient of determination

R_{eff} – Effective pore radius

r_{pore} – Average pore radius

S – Spreading coefficient

S_0 – Specific surface area

S_L – Screw lead

S_p – Pore surface area

t – Time

t_{fd} – First detection time

u – Velocity

u_i – Impact velocity

V – Volume

V_0 – Droplet volume prior to imbibition

V_f – Free conveyor volume

V_{imb}(adim) – Darcy's adimensional imbibition rate

V_{imb}(darcy) – Darcy flow rate

α – Tortuosity

γ – Surface tension

γ_{LV} – Surface tension at liquid-vapour interface

γ_{SL} – Surface tension at solid-liquid interface

ΔP – Pressure drop

ε – Porosity

ε_{bulk} – Porosity of bulk powder bed

ε_{eff} – Effective porosity

$\varepsilon_{macrovoid}$ – Porosity fraction of macrovoids

ε_{tapped} – Porosity of tapped powder bed

η_v – Volumetric efficiency

ϑ_{act} – Actual contact angle

ϑ_{app} – Apparent contact angle

ϑ_{eq} – Equilibrium contact angle

ρ_{bulk} – Bulk powder density

ρ_{liq} – Liquid density

ρ_{tapped} – Tapped powder density

ρ_{true} – True particle density

σ – Tensile strength

σ^2 – Residence time variance

τ – Inertial regime duration

τ_i – Calculated inertial regime time scale

l_c – Capillary length

η – Liquid viscosity

1. Introduction

1.1. Twin Screw Granulation

Granulation is ubiquitous in any industry processing fine powders and is the process of agglomerating small particles into large ones. The purpose for this process of particle enlargement is that granules possess more favourable properties than raw powders with respect to homogeneity, flowability, compaction, dust emission and segregation. In the pharmaceutical industry, wet granulation is the most common method of particle enlargement and involves agitating the powder in the presence of a liquid binder. Cohesive liquid bridges form between adjacent primary particles resulting in a larger particle known as a granule. Several methods of wet granulation exist and are utilised by drug manufacturers including high shear mixers, fluidised bed granulators and drum granulators. Each of these are batch processes. More recently, twin screw granulators have gained interest and coincide with industry ambitions of adopting continuous manufacturing. A basic depiction of a twin screw granulator is shown in Figure 1.1 and consists of a dry powder blend and liquid binder being continually introduced into a barrel housing two co-rotating screws. The screws can be configured to include various elements to modulate compression and shear forces. The material traverses the barrel within seconds and is discharged at the opposite end in the form of wet granular material. Twin screw granulation not only offers an opportunity for reduced processing time and easier scale-up, but also, greater operational control (Dhenge et al., 2012a; Tu et al., 2013; V. Lute et al., 2016) to better meet the requirements of quality risk management (ICH, 2005). However, the effects of variable raw materials on granule quality has not been fully established in the literature.

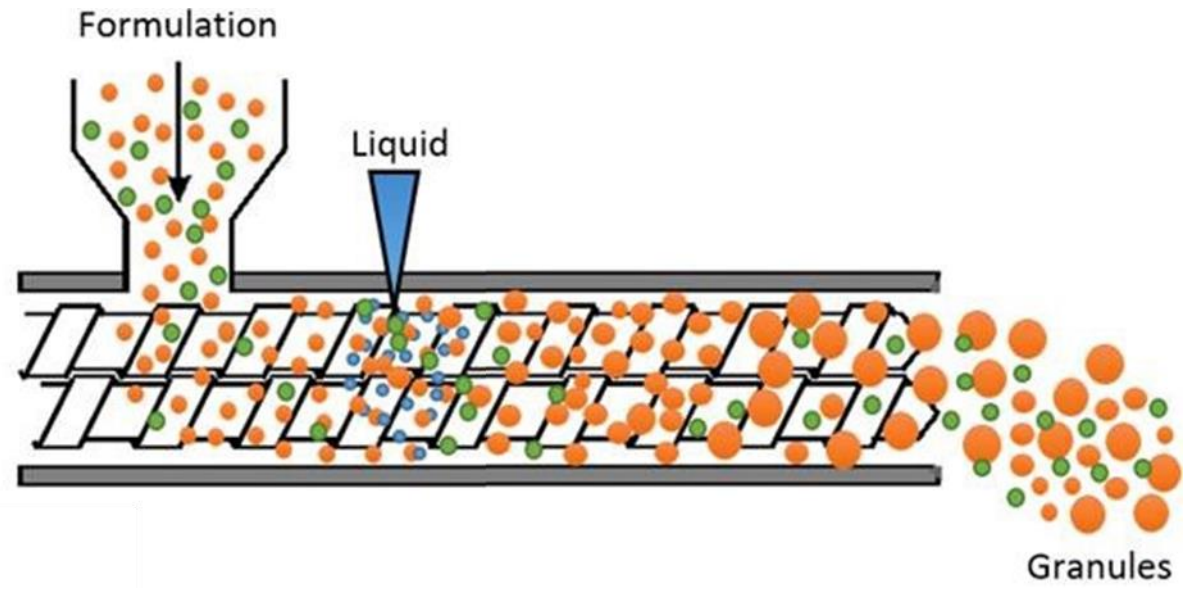

Figure 1.1 Basic diagram of a twin screw granulator in operation.

1.2. Research aims and objectives

The aim of the proposed research project is to investigate twin screw granulation's ability to accommodate variability of the raw material. Namely, to evaluate the effect of particle size distribution of commonly used excipient powders on the properties of the resulting granules. The criticality of particle size will be assessed at each stage of manufacture including powder blend, nucleation, granulation and tableting.

It is hypothesised that varying the primary particle size will result in significant changes to the granule properties because the short residence time places greater emphasis on particle wetting during nucleation than conventional wet granulation via a high shear mixer, as there is less time for mechanical dispersion of the liquid binder. It is believed that this will in turn, have an impact on the performance of the final dosage form.

A secondary aim is to assess twin screw granulation's ability to scale-up output by increasing the material throughput whilst maintaining granule quality. It is hypothesised that granule

quality can be preserved whilst increasing material throughput by adjusting process parameters to maintain the barrel fill level.

To achieve these aims the following objectives will be performed:

1) Evaluate the current state of continuous twin screw granulation, as well as the Quality by Design framework through which its application must be developed.

2) Use a novel method to engineer distinct grades of commonly used excipients, followed by characterising their particle and powder properties and behaviours.

3) Study powder wetting in vitro by measuring the effects of formulation parameters on droplet penetration and nuclei formation in a static powder bed and determine if in vitro observations are informative to in vivo production.

4) Assess particle size distribution of commonly used excipients as Critical Material Attributes by investigating the effect of variability on the properties of granules produced via twin screw granulation, and performance of the subsequent tablets.

5) Develop a means of controlling barrel fill during twin screw granulation, and subsequently assess barrel fill as a Critical Process Parameter by investigating the effect of various fill levels on the properties of the resulting granules and the ensuing tablets.

6) Assess controlling barrel fill level as a means of increasing material throughput and scaling up twin screw granulation production, whilst preserving granule quality.

1.3. Novelty of research

The novel aspects of this research include:

1) Generating distinct and normally distributed engineered grades of commonly used excipients to investigate the influence of particle size distribution on powder wetting, nuclei formation and twin screw granulation.

2) Developing understanding of powder wetting in a static powder bed by characterising and linking droplet oscillation post-impact, energy dissipation, droplet spreading, droplet imbibition, late-diffusive intra-spreading, and nuclei formation.

3) Assessing particle size distribution as a Critical Material Attribute and barrel fill level as a Critical Process Parameter determining relationship between these variables and the Critical Quality Attributes of the final tablet product.

3) Developing determination of total volumetric fraction by characterising residence time distribution during twin screw granulation to incorporate conveying efficiency to better control barrel fill level.

4) Evaluate the developed total volumetric fraction as a means of maintaining granule quality whilst increasing material throughput.

2. Literature Review

2.1. Pharma background – a changing environment

The pharmaceutical industry is one of the most regulated and research-intensive industries worldwide (McLaughlin et al., 2017; efpia, 2018). For their troubles, successful pharmaceutical companies have become top staples of their respective securities exchanges. With that said, revenue from prescription medicines has experienced modest growth in recent years – 4 % from USD 558 billion in 2010 to USD 583 billion in 2017 – and yet, internal and external pressures have seen the cost of innovation increase 28% over that same period (EvaluatePharma, 2018).

Due to comprehensive clinical trials and high candidate attrition, estimates of the average spending on research and development per successful new molecular entity (NME) have risen from USD 1.7 billion to USD 3.9 billion and the total R&D costs amount to 20% of prescription sales (Gilbert et al., 2003; Scannell et al., 2012; EvaluatePharma, 2018). Additionally, the first decade of this millennium saw the number of NME approvals stagnate at approximately 30 per annum despite an increase in the number of new drug applications (EvaluatePharma, 2018; Scannell et al., 2012). Moreover, the industry faces value-based pricing pressures from healthcare payers due to the rising incidence of costly chronic diseases such as diabetes and Alzheimer's, compounded by an aging population in most developed countries (Mathers and Loncar, 2006; United Nations et al., 2015).

Demands for more targeted treatments with improved and verifiable outcomes continues to stratify the market and has curtailed the product pipeline for blockbuster drugs (Gibson et al., 2015). Further pressure is created by the lengthy clinical trials and approval process that limit the length of patent protection for successful NMEs. It is during this protected period that the majority of expenditure can be recouped before generic manufacturers file

abbreviated new drug applications and offer more competitively priced bioequivalent alternatives.

Therefore, as one of the last stages in the R&D process, the manufacturing operation is often developed in haste to maximise sales during patent protection, as each day post-approval is potentially worth millions of dollars in revenue (Suresh and Basu, 2008). As a result, a batch failure rate of circa 16% (2.5 sigma) is considered acceptable within pharma and is comparatively much higher than other manufacturing industries where operating above 5 sigma – 3.4 defects per million – is the standard (Bruttin and Dean, 2005; Blackburn et al., 2011). This failure rate elicits extensive testing to identify defective batches, which are reworked or disposed of in order to ensure a product output above 5 sigma, and hence, the pejorative phrase "*quality by testing*" is commonly associated with the pharmaceutical industry. Some researchers have even estimated that the cumulated manufacturing inefficiencies across the industry amount to USD 50 billion each year (Macher and Nickerson, 2006).

In the past, relatively high incidence rates of out-of-specification (OOS) batches have been tolerated as high sales revenue has offset the cost of inefficiencies. Additionally, stringent regulations - in the form of a *Scale-up and Postapproval Changes* application - provided little incentive for pharma to innovate practices once a manufacturing processes had been established. However, via quality guidelines published by the International Council for Harmonisation of Technical Requirements for Pharmaceuticals for Human Use (ICH), global regulators have collectively sought to discourage the traditional quality-by-testing approach and instead promote and facilitate the adoption of *quality-by-design* (QbD) principles and the incorporation of process-analytical-tools for real time release (International Conference on Harmonisation, 2009).

Additionally, in 2017, in an effort to support modernisation of the pharmaceutical industry, the U.S. Food and Drug Administration (FDA) issued guidance on advancing the application of emerging technologies in the manufacture of quality pharmaceutical products (Center for Drug Evaluation and Research and US Food & Drug Administration, 2017). This was in response to an ever-increasing number of drug shortages resulting from disruptions in manufacture, which in turn jeopardise patient care. Hence, the FDA seeks to encourage and facilitate "a more robust drug product design and improved manufacturing with better process control, thereby leading to improved product quality and availability throughout a product's lifecycle." (Center for Drug Evaluation and Research and US Food & Drug Administration, 2017).

Subject to this internal and external scrutiny, the case is being made for moving away from the conventional batch manufacture of drugs and towards a continuous operation. This is spurred by an industry initiative to implement emerging technologies to build an agile, efficient supply chain which brings pharma closer to the patient (Arlington, 2011). It is evident that this paradigm shift is reliant on the process intensification capabilities of continuous manufacturing, such as possessing a smaller plant footprint, reduced wastage, greater equipment utilisation, reduced handling, improved safety, less idle inventory, more flexible scalability, and a narrower scope for in-process variation. The subsequent supply chain benefits include greater market dispersion, increased end-to-end responsiveness, less capital frozen in large inventory, reduced transportation, lower capital requirements, and greater supply chain control.

The sum of these efficiencies is expected to manifest as substantial financial gain and greater quality control. However, the aforementioned industry pressures, amongst many others

that have not been discussed here, have collectively contributed to the cultivation of a risk averse climate that has stifled innovation that might unnerve shareholders and buttressed adherence to conventional practices (Kaplan, 2004). Therefore, in pursuit of the rewards of continuous manufacture and to alleviate anxieties, companies have sought to disperse the risk by engaging in precompetitive collaborations that draw on the skills and expertise of manufacturers, supply vendors, academia, regulators and governmental bodies (Florence, 2017). Not only do these collaborations seek to develop the understanding and technology to make continuous manufacturing viable, but also to develop the skills and mind-set necessary to champion the continual development of manufacturing in the future.

Examples of these strategic collaborations include the Center for Structured Organic Particulate Systems (C-SOPs) which is headquartered at Rutgers University and involves three other U.S. academic institutions and over 40 industrial consortium member companies (C-SOPS, 2017); Research Centre Pharmaceutical Engineering GmbH (RCPE) located in Graz, Austria (RCPE, 2018); the Novartis-MIT Center for Continuous Manufacturing based at Massachusetts Institute of Technology (Novartis-MIT Center for Continuous Manufacturing, 2017); and the EPSRC Centre for Innovative Manufacturing for Continuous Manufacturing and Crystallisation (CMAC) which comprises a hub at the University of Strathclyde, Glasgow, six other UK universities and over 20 industry partners (CMAC, 2018). Additionally, between 2009 and 2013 Bayer Technology Services GmbH coordinated a project funded by the European Commission to research and assess the viability of Flexible, Fast and Future Production Processes (F^3 Factory) as a mode of manufacturing process intensification for chemical industries (European Commission and Bayer Tehnology Services GmBH, 2013). Further, a 2016 symposium co-hosted by CMAC and MIT resulted in a regulatory white paper (Nasr et al., 2017). The funding and attention these groups have received is a testament to

the importance of advancing manufacturing practices and its impact on the future of healthcare.

2.1.1. Continuous manufacture

Due to little innovation to its batch operations in prior decades, the manufacture of pharmaceuticals has long been surpassed by contemporary industries, such as those involved in the manufacture of bulk chemicals and household commodities. Director of the US-based Centre for Drug Evaluation and Research, Janet Woodcock, stated that "…manufacturing experts from the 1950s would easily recognise the pharmaceutical manufacturing processes of today," (FDA, 2012). Yet, she continued to state that "…manufacturing will change in the next 25 years as current manufacturing practices are abandoned in favour of cleaner, flexible, (and) more efficient continuous manufacturing."

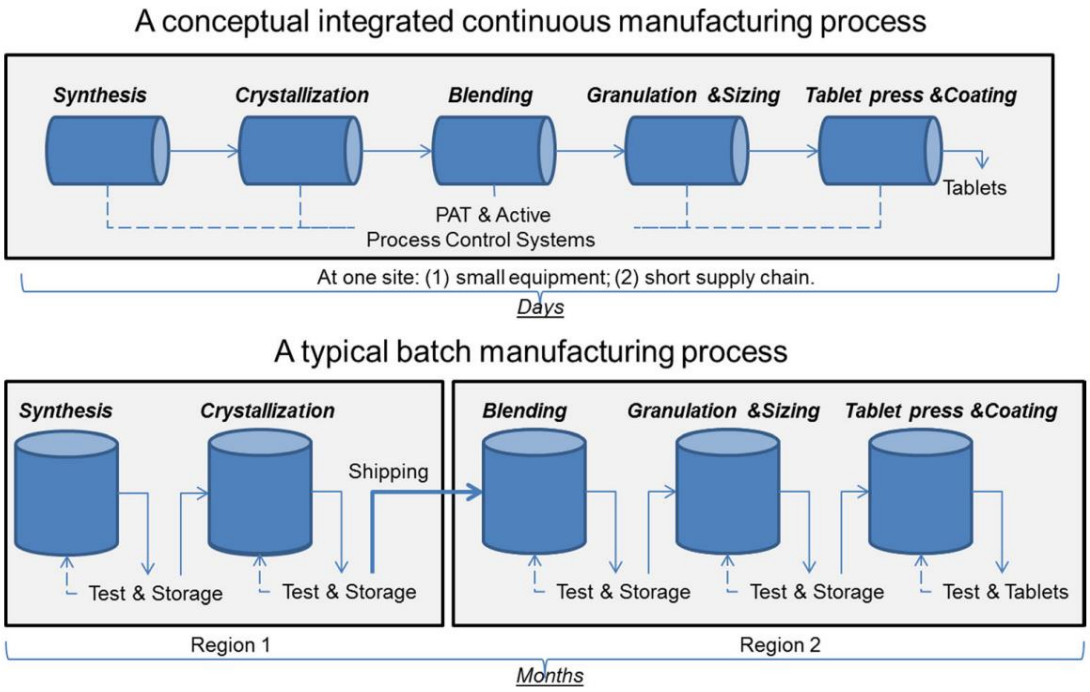

Figure 2.1 A conceptual fully integrated continuous manufacturing process (top). A typical batch manufacturing process for tablets is also presented for comparison (bottom) (Lee et al., 2015).

In recent guidance issued by the FDA, continuous manufacture was defined as "a process in which the input material(s) are continuously fed into and transformed within the process, and the processed output materials are continuously removed from…an integrated process that consists of a series of two or more unit operations" (CDER, 2019).

As contrasted in Figure 2.1, batch manufacturing involves discrete unit operations punctuated by significant periods of idle inventory whilst subjected to extensive off-line quality testing (CDER, 2004; Lee et al., 2015), and laborious material transfer (Kim and Lee, 1993; Gorsek and Glavic, 1997; Mascia et al., 2013). Other features characteristic of batch manufacture includes a large equipment foot print (Lee et al., 2015), low equipment utilisation (Tyson, 2019), significant operational start up and shut down, long production schedules (Calabrese and Pissavini, 2011), labour intensive tasks (Gorsek and Glavic, 1997), and arduous and inflexible scale-up capabilities (Faure et al., 2001; Leuenberger, 2001).

By moving away from processing large volumes of materials in segregated stages (e.g. large vessel reactors and mixers), and instead, leaning towards perpetual material flow (e.g. oscillatory flow reactors, twin-screw extruders and spray dryers), continuous manufacturing represents a form of process intensification (Gutmann et al., 2015). The lower in-process volume and greater process surface area involved allows for fewer dead spots and reduced thermal lag, resulting in greater heat transfer uniformity (Gutmann et al., 2015). Additionally, these features permit increased accessibility and closer monitoring, in addition to greater opportunities for intervention and more precise control of key process parameters such as temperature and moisture levels (Gutmann et al., 2015; Kockmann et al., 2008; LaPorte and Wang, 2007; Van Arnum, 2013). This enhanced control can manifest as a reduction in impurities and increase in product quality (Kockmann and Roberge, 2009; Roberge et al., 2008).

A further benefit of supplanting large volume processors that are disconnected with small volume alternatives that are integrated, is that energetic chemistries and toxic compounds can be handled on a smaller scale with less risk (LaPorte and Wang, 2007; Mascia et al., 2013). Furthermore, end-to-end process integration diminishes the need for material transfer and buffer inventory (Lee et al., 2015), and hence, can decrease the risk of contamination, operator exposure and degradation of sensitive in-process material (Mascia et al., 2013).

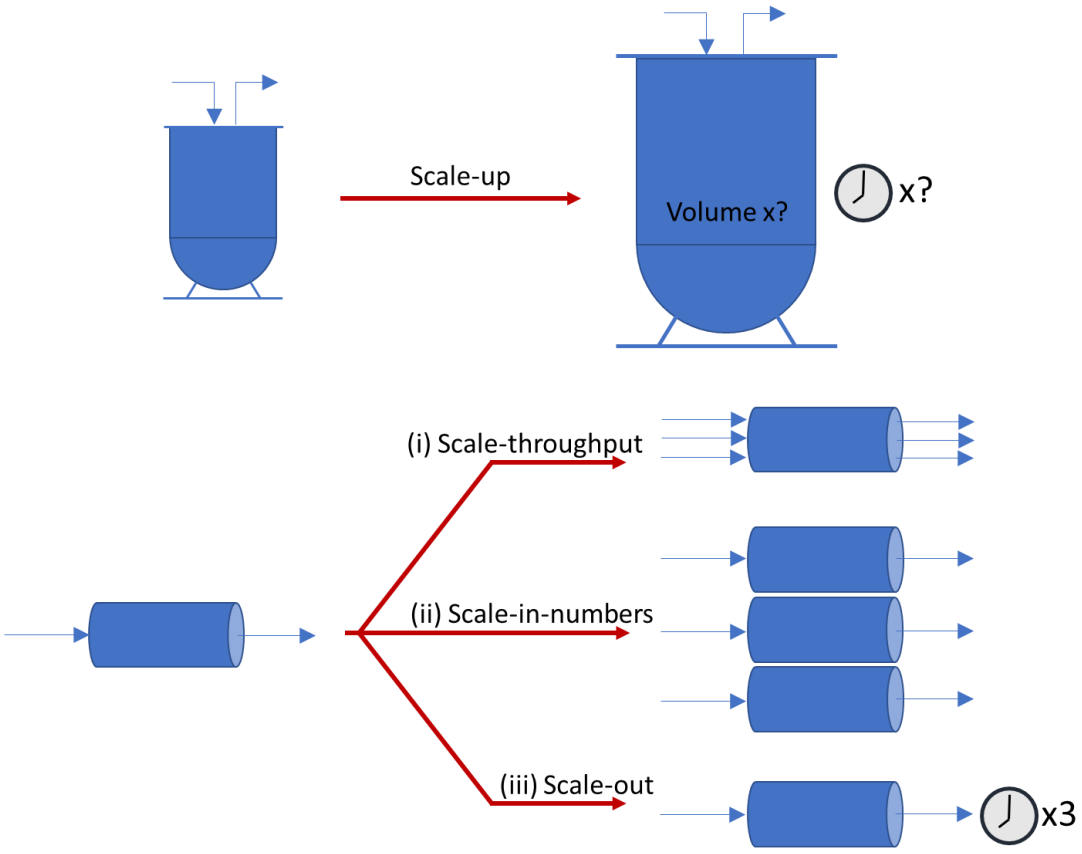

Figure 2.2 An illustrative comparison of scale-up strategies to triple output. Batch manufacture (top) involves capricious increases in equipment dimensions and operating time. Continuous manufacture (bottom) can be achieved by (i) increasing flow-rate, (ii) operating more lines in parallel, and/or (iii) extending operating time.

Another advantage of continuous processing pertains to scalability. In the past manufacturers have struggled to predict a drug's market size (Porath, 2018), which in turn has limited their ability to forecast manufacturing requirements (Bauer and Fischer, 2000).

With that said, it has been recognised that, in the post-blockbuster era, newer drugs targeting increasingly stratified populations are more likely to be produced in smaller quantities (Debnath et al., 2010). However, as often is the case, drugs can be repurposed and licenced for new indications, subsequently increasing dramatically in demand (Nguyen et al., 2018; Oprea et al., 2011). Alternatively, competitor "me-too" drugs can significantly reduce market share (Lichtenberg and Philipson, 2002), as can greater-than-anticipated reporting of adverse reactions during phase IV post-marketing surveillance (Siramshetty et al., 2016). Conversely, a competitor may experience manufacturing issues and shortages, resulting in a dramatic increase in demand for alternatives. Hence, production must possess the ability to adapt to fluctuations in demand, without jeopardising significant capital investment and product quality.

Scaling a batch process generally involves larger equipment, significant investment, and complex geometric, dynamic and kinematic considerations (Agrawal and Pandey, 2015), and is rarely a matter of proportionality (Levin, 2001; Muller and Latimer, 2009; Pandey and Badawy, 2016). Contrastingly, continuous processes offer the flexibility of scaling-out i.e. extending the duration of operation (Lee et al., 2015), scaling-throughput i.e. increasing the processing flowrate i.e. (Mascia et al., 2013), or scaling-in-numbers i.e. multiplying the number of lines operating in parallel (Allison et al., 2015; Gutmann et al., 2015), as illustrated in Figure 2.2.

Coupled with greater scalability, production agility is further enhanced by shortened production schedules. The FDA estimates that some drugs which normally take months to produce using conventional batch processing, may only take one day to make using continuous manufacturing (Lee, 2017). This enables a pharmaceutical product to be produced *just-in-time* and in response to market demand rather than having to maintain

large inventories internationally in case of regional surges in demand (National Academies of Sciences, Engineering and Medicine et al., 2019). Equally, manufacturers are better positioned to respond rapidly to drug shortages with minimal latency in the lead time (National Academies of Sciences, Engineering and Medicine et al., 2019).

Furthermore, continuous manufacturing's intensification promises manufacturing sites that occupy a smaller footprint, yield less waste (Leonard, 2019), and house fewer personnel, thus, requiring less capital (Dream, 2017; Srai et al., 2015). This incentivises manufacturers to build more production sites that are closer to their final markets, rather than current practices that involve globally centralised manufacturing sites and extensive logistics (Harrison et al., 2018). This not only results in a more environmentally friendly supply chain, but by operating closer to the end-user, the bullwhip effect resulting from fluctuations in demand is reduced, further realising *lean manufacturing* (Harrison et al., 2018; National Academies of Sciences, Engineering and Medicine et al., 2019; Srai et al., 2015). Hence, continuous manufacturing does not only add value during production, but has the potential to benefit and revolutionise the entire supply network (Harrington et al., 2017; Srai et al., 2016).

2.1.2. Technical challenges

Whilst extensive end-product testing is synonymous with batch manufacturing and pharma (Uddin et al., 2015), continued reliance on this method of quality assurance will nullify many of the efficiencies gained from continuous process (CDER, 2019). To realise real-time release, data pertaining to the input material, process conditions, in-process material and product properties must be attainable live and at-line (Colón et al., 2017; ICH, 2009; Potter, 2009; Vargas et al., 2018). Therefore, utilising process analytical technology (PAT) is a fundamental component to supporting active process control and real time parameter

adjustment to respond to material variability and process disturbances (CDER, 2004; Lee et al., 2015; Potter, 2009).

An adequate feedback control strategy during continuous manufacture warrants additional characterisation and control of input material attributes beyond compendial standards (Lee et al., 2015; Yu, 2008). To achieve continuous production during lengthy production campaigns, different batches of raw feedstock must be continuously added to the feeder system. As material attributes can vary between batches and even shift throughout a product's lifecycle, the effects of variability on process control, residence time distribution and product functionality must be well characterised and incorporated into process design (International Conference on Harmonisation, 2009; Narang, 2015; Su et al., 2019). In doing so, input variability can be proactively identified and the impact on manufacture mitigated (Yu, 2008).

Furthermore, due to the absence of discrete batches, continuous operations must possess the capability of detecting and diverting materials that are OOS or materials that are processed when out-of-range conditions occur, such as during start-up, shut-down and temporary process disturbances (CDER, 2019). In order to adequately segregate the non-conforming material downstream, PAT must be able to measure the duration and severity of the disturbance and a comprehensive characterisation of the process residence time and axial mixing is required to establish safety margins for diversion (CDER, 2019). Process designers must seek to adequately segregate OOS material without affecting the rest of the process and material flow (CDER, 2019).

2.1.3. Regulatory challenges

In addition to technical challenges to implementing continuous manufacture, manufacturers must also address regulatory considerations (CDER, 2019). Foremost, the ability to establish a continuous analogue to the lot number used in batch manufacture. A lot number is unique to a single batch and enables it to be identified with respect to its constituents, production and supply. This is important for quality and safety purposes, for example in the event of a product recall, of which 1,225 occurred in 2013 alone (Gaffney, 2014).

In batch manufacture a specific quantity of product, that is intended to have uniform quality within specified limits, is produced according to a single manufacturing order during the same cycle of manufacture. In continuous manufacture, this is not possible as there is no definitive beginning or end once steady state is achieved. Hence, a lot number would relate to an arbitrary unit of time or quantity and would not be dependent on equipment capacity (Lee et al., 2015). An additional consideration pertaining to lot identification is that during continuous operations, a single lot may include different batches of feed stock as a result of axial back mixing, and thus, obscure the ability to identify the origins of each lot. As a result, manufacturers must demonstrate a keen understanding of material mixing and propagation throughout the manufacturing process (Kumar et al., 2015). These considerations, amongst other regulatory concerns are likely to be addressed in an upcoming ICH guideline (Q13) that will promote, facilitate and clarify regulatory involvement in the development of continuous manufacturing (ICH, 2018).

The above discussion highlights some of the merits and challenges of continuous manufacturing that are at the forefront of pharmaceutical innovation and are summarised in Figure 2.3. Some cases of continuous manufacturing being actualised do exist; July 2015

marked the first continuously manufactured drug to gain FDA approval, Vertex's Orkambi (Pollack, 2015), followed by Symdeko in February 2018 (Davio, 2018) – both of which are combination drugs for the treatment of cystic fibrosis. Additionally, in April 2016 Janssen successfully transitioned the manufacture of its retroviral, Prezista, from batch to continuous production (Marriott, 2017). Likewise, industry leaders are investing significant resources into continuous manufacture R&D (Khinast, 2016) and an ever-increasing number of companies "have engaged the FDA in their efforts to develop and implement CM processes" (Gottlieb and Woodcock, 2019). This interest has drawn in equipment vendors, most notably a GEA-Siemens collaboration resulting in the ConsiGma™ Continuous Tableting Line - a plug-and-play modular platform capable of creating coated tablets from raw materials in a single continuous production line (GEA-Siemens, 2020).

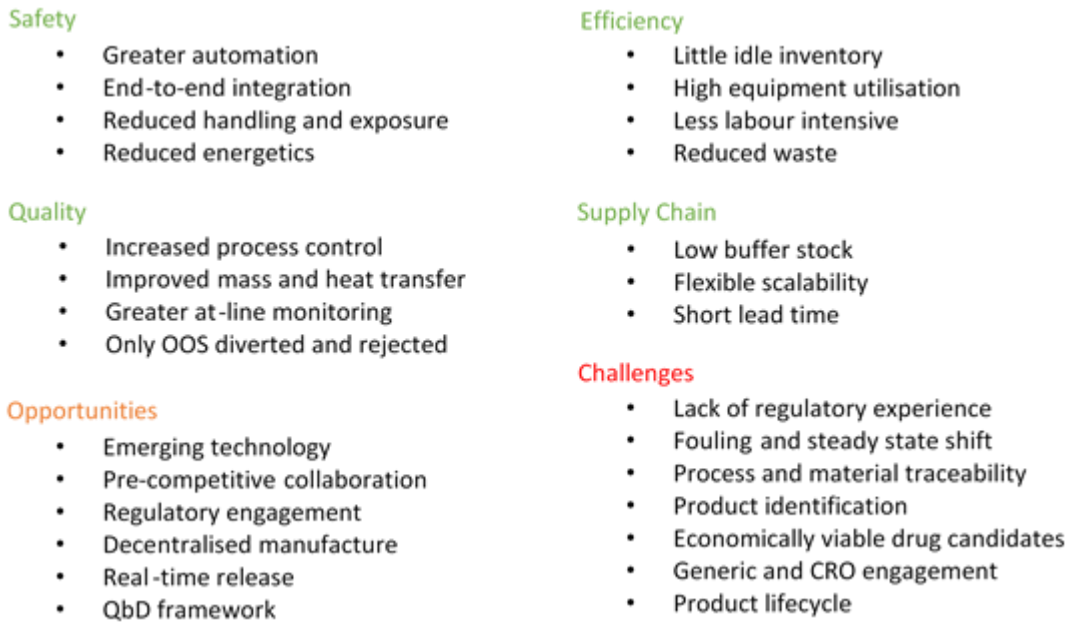

Figure 2.3 Advantages, opportunities and challenges associated with continuous drug manufacture. This list is not exhaustive.

2.1.4. Quality by Design

To gain regulatory approval, drug manufacturers must comply with Current Good Manufacturing Practice (cGMP) (EudraLex, 2011). These regulations stipulate that pharmaceutical products are subject to stringent specifications. In the third module of the Common Technical Document (CTD), section 3.2.P.3.3. titled "Description of the Manufacturing Process and Process Controls" manufacturers must detail information pertaining to all aspects of drug production (ICH, 2003):

- Manufacturing site locations
- API characterisation
- Dosage form composition
- Raw materials
- Product characterisation
- Process development
- Manufacturing process
- Analytical methods
- Specification testing of raw materials
- In-process materials and product
- Container and closure systems
- Stability testing data
- Release testing data

Traditionally, once licensing is granted, the manufacturing process becomes fixed, whereby any changes must first gain approval from a Scale-up and Post Approval Changes expert working group following submission of supplemental documentation (CDER, 1995). Hence, in the absence of regulatory permission, any deviation from the approved method is invalid.

One such problem arising from this rigid approach, is that lot-to-lot variability is inherent to many of the raw materials used in drug formulation due to their agricultural and natural origins (Dave et al., 2015; IPEC, 2008). Additionally, in the absence of an excipient industry solely serving pharma, the specification of bulk raw materials is broad and beyond the control of drug manufacturers (Dave et al., 2015; Schoneker, 2008). Therefore, a variable output is often the consequence of feeding a variable input into a fixed and unforgiving process.

A more versatile and flexible response to variability is offered by the implementation of Quality by Design (QbD) principles. A shift towards this paradigm is being advocated by regulatory bodies, most notably in a series of quality guidelines issued by the International Council for Harmonisation (ICH, 2012, 2009, 2008, 2005). In ICH Q8(R2) regulators affirmed that "the aim of pharmaceutical development is to design a quality product and its manufacturing process to consistently deliver the intended performance of the product" (ICH, 2009). Q10 posits a shift towards a QbD paradigm would allow for predetermined process adjustments to accommodate variability with the objective of producing a uniform product (ICH, 2008).

QbD is a systematic approach to process development, and it incorporates a fundamental and scientific understanding of material and process variables into quality risk management (ICH, 2009). By identifying the greatest sources of risk to the desired product properties,

then steps can be taken to mitigate those risks (ICH, 2005). Hence, quality is built into the product rather than resorting to testing the defects out.

By beginning with the patient in mind, the QbD approach first seeks to establish a quality target product profile (QTPP). QTPP is defined as "a prospective summary of the quality characteristics of a drug product that ideally will be achieved to ensure the desired quality, taking into account safety and efficacy" (ICH, 2009). Example profile targets include the route of administration, dosage strength and release profile of the drug as they pertain to clinical performance.

From the QTPP, attributes that are critical to the quality (CQA) of processed material can be identified. CQAs are characteristics of the final product or in-process material that must be within an appropriate limit, range or distribution to ensure the desired quality and performance of the product (ICH, 2009). This includes physical and chemical properties such as purity, tensile strength, content uniformity, and disintegration time.

Any material attributes or process parameter that can potentially influence the identified CQA, and are likely to exist as a range, must be studied to determine the effects of their variation (Kushner et al., 2011, 2014; Kushner, 2013; Narang, 2015; Dave et al., 2015; Maguire and Peng, 2015). Design of experiments (DoE) and multivariate data analysis methodology have been advocated to elucidate the functional relationship between material attributes and process parameters, and the CQAs (ICH, 2009). Where possible, variables should be evaluated simultaneously so that interactions can be quantified and assessed for criticality (ICH, 2009). Properties that are found to have a significant influence on CQAs, and in turn jeopardise the QTPP, are considered to be *critical material attributes* (CMA) and *critical process parameters* (CPP), and must be incorporated into a robust control strategy,

as outlined in Figure 2.4 (ICH, 2009, 2005). Conversely, attributes that have no detrimental influence on processing or product quality are tolerable, necessitating fewer monitoring and control requirements (ICH, 2009). Collectively, the multidimensional combination of material and process limits within which successful manufacturing and product quality is assured is known as a design space (ICH, 2009). These demonstrate the effect of material attributes and process parameters on CQAs.

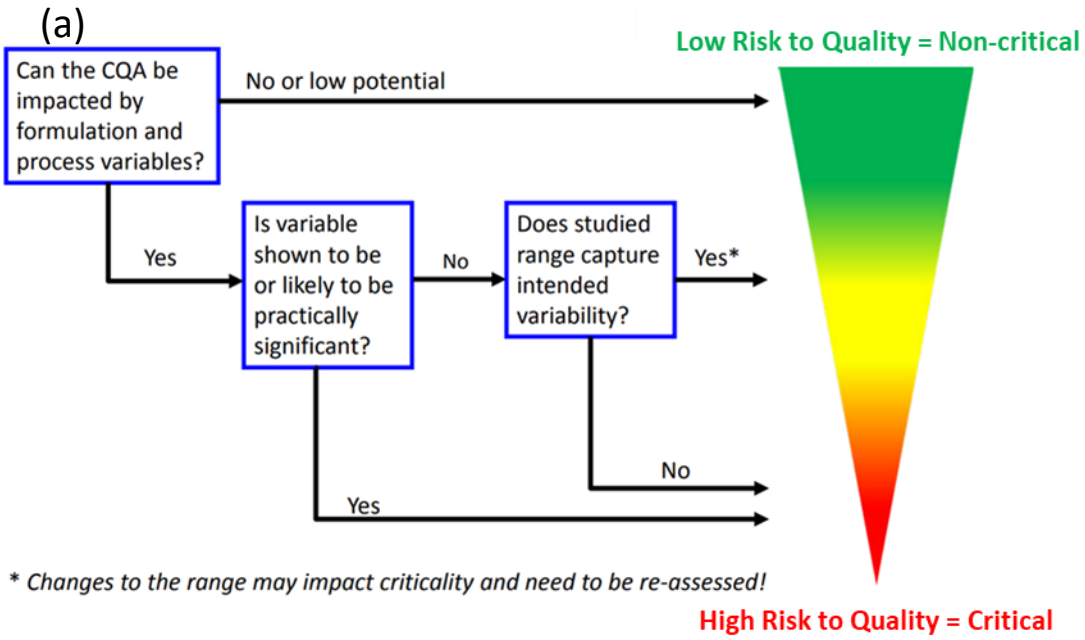

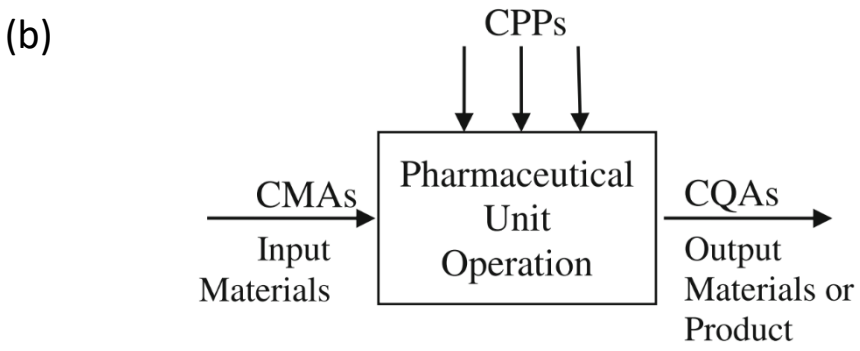

$$CQAs = f\,(CPP_1, CPP_2, CPP_3 \ldots CMA_1, CMA_2, CMA_3 \ldots)$$

Figure 2.4 (a) Schematic flow diagram for identification of CMAs & CPPs (Maguire and Peng, 2015). (b) Link between input critical material attributes (CMAs) and critical process parameters (CPPs) to output critical quality attributes (CQAs) for a unit operation (Yu et al., 2014).

Real-time monitoring capabilities and scientific understanding of CMAs and CPPs allows downstream parameters to be adjusted within a pre-approved design space, so that the process can adapt to the incoming variability (ICH, 2009). Alternatively, upstream process parameters can be adjusted based on data resulting from PAT located at the sites of output material (ICH, 2009). These feedback and feed forward loops do not represent a departure from a *state of control*, and enable the manufacturing process to be dynamic and flexible without the need for regulatory notification (ICH, 2009). The design of such a quantitative and predictive control system, based within a QbD framework, minimises the risk of producing OOS product and enables real-time release, and forms the foundation of a *Quality by Control* strategy, outlined in Figure 2.5 (ICH, 2009; Su et al., 2019).

With that said, the scientific knowledge space surrounding the product quality, material attributes and process parameters should continue to expand and be used to improve the process design throughout the lifecycle of the product with reduced post-approval submissions (ICH, 2008). In the event of any failings, a root-cause analysis should be conducted, so that the findings can inform future design and development (ICH, 2005). Hence, as part of Quality Risk Management and lifecycle management, the inclusion of an up-to-date design space pertaining to excipient specification and manufacturing controls in the Common Technical Document is recommended (ICH, 2009, 2008).

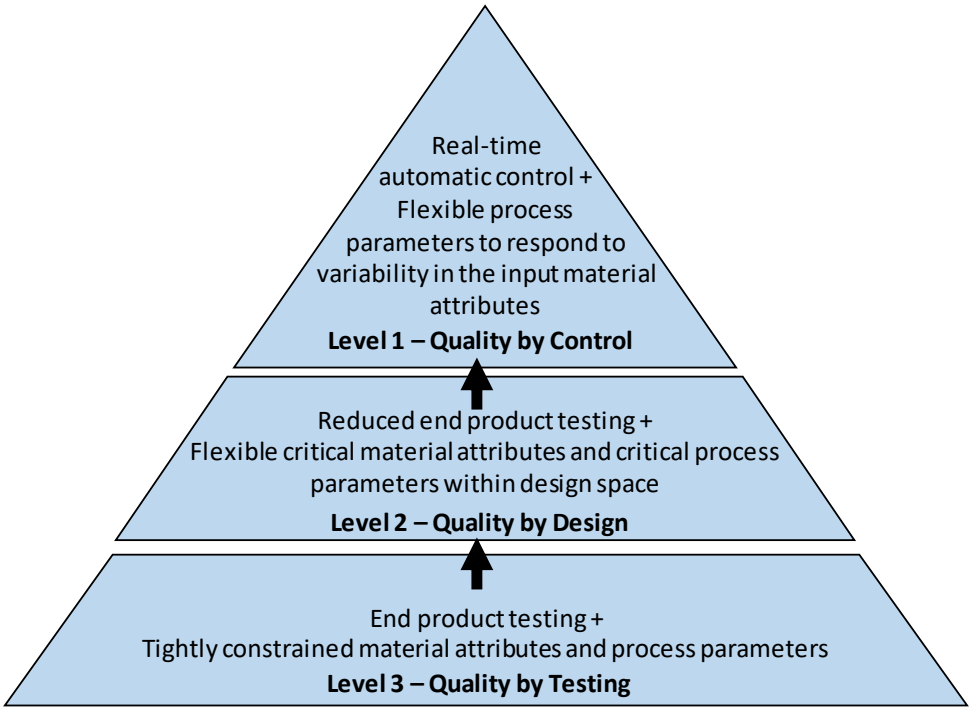

Figure 2.5 Control strategy implementation options (adapted from Yu et al., 2014)

To summarise, process development within a QbD framework is advantageous to regulators and manufacturers alike. Opportunities for "more flexible regulatory approaches" stipulate that manufacturers "demonstrate an enhanced knowledge of the product performance over a range of material attributes, manufacturing process options and process parameters" (ICH, 2009). Quality should primarily relate to product performance and product design, and development should be approached systematically to improve process capability with reduced product variability that often leads to defects, rejections and recalls. A robust quality control strategy can be considered as a process whereby (1) all critical sources of variability are identified and explained, (2) variability is managed, (3) product quality attributes can be accurately predicted, and (4) product quality can be reliably produced.

2.1.5. Conclusion

The pharmaceutical industry is under growing financial and regulatory pressure to abandon conventional manufacturing practices for the design and development of more efficient and contemporary approaches. Process intensification in the form of continuous manufacture offers numerous benefits and the potential to revolutionise the entire pharmaceutical supply chain. Evidence of this shift is currently present in the form of substantial investment, significant regulatory engagement and unprecedented cross-sector collaboration.

Technical and regulatory challenges exist as established discrete processes are replaced with the complexity of operating multiple processes simultaneously and in series. Additionally, the industry's current quality management strategy is to be reformed as the cost of quality by testing is no longer tolerable. To address both of these concurrently, it is necessary to develop a robust control strategy comprising the integration of emerging continuous technologies that offer greater control, in combination with PATs that offer increased monitoring capabilities, outlined in Figure 2.6.

To successfully incorporate real time adjustments to process conditions in accordance with live data, then quality by design principles must form the basis of the process development. Process designers must develop an in-depth understanding of material and process variability and how they pertain to product quality. From this, manufacturers can better predict the parameters for acceptable product quality and in doing so, inspire greater regulatory confidence.

Automated quality control involves the management of variability and process disturbances by way of feedback and feed forward loops, as well as the diversion of OOS materials. To achieve this, manufacturers must possess an in-depth knowledge of material progression and

mixing, and thereby demonstrating the ability to identify the origins of each product at each step of manufacture and distribution. It is therefore evident, that in order to achieve the aforementioned goals of continuous manufacture then variability of material attributes, process parameters and residence time distributions must all be investigated and characterised in tandem.

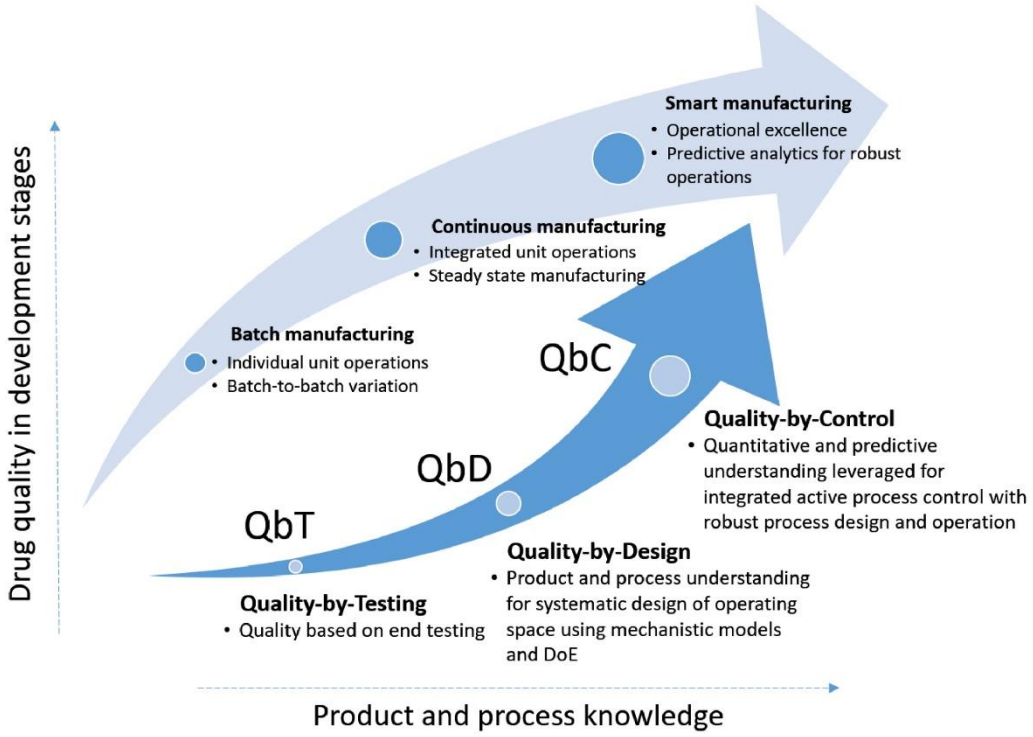

Figure 2.6 The systematic progression in quality assurance via QbT, QbD, and QbC (Su et al., 2019)

2.2. Solid dosage forms, excipients and manufacture

Oral administration is the most common route of drug delivery and often first choice for patients and prescribers. Compared to alternative drug delivery devices, solid dosage forms demonstrate greater stability, easier packaging and transport, convenient administration, improved patient adherence, and are formulated to possess different strengths, appearances, and release profiles (Conway and Gad, 2007). Solid dosage forms that are swallowed and make the active pharmaceutical ingredient (API) available for absorption during transit along the gastrointestinal tract constitute the majority of orally administered medication, of which tablets are the most frequently prescribed (Niazi, 2009).

Commercial tablets are the result of applying a compression force via a high-speed tablet press to either a powder blend of raw materials – known as direct compression - or to a collection of multi-component granules. These granules can be the result of dry granulation, whereby rollers compact a powder blend into a ribbon that is then milled into granules, or most commonly the result of wet granulation. Wet granulation involves agitating heterogeneous particles in the presence of a liquid binder. This results in cohesive forces arising from the liquid bridges between primary particles causing them to agglomerate and form granules that are subsequently compacted into tablets once dried.

Tablets, as with all pharmaceutical products, are subject to stringent regulatory scrutiny to ensure that they reliably deliver the right drug, the right dose, and with the right release profile. Hence, tablets must repeatedly demonstrate stability, integrity, content uniformity and drug release in accordance with the product specification (The British Pharmacopoeia Commission, 2017).

APIs seldom possess properties that facilitate the tablet production or performance, such as desirable flowability, wettability, solubility and compressibility. Efforts to improve API properties and developability in the areas of crystal and particle engineering are currently underway (Ahmed et al., 2019; Blagden et al., 2007; Brown et al., 2018; Datta and Grant, 2004; El-Zhry El-Yafi and El-Zein, 2015; Mirza et al., 2009; Turner et al., 2019; York, 1992), but until these endeavours come to fruition the conventional approach involves combining the API with other inactive ingredients that carry out a function to aid production and/or tablet performance (Vemavarapu et al., 2009). These functional ingredients are known as excipients and, despite being considered inert, are crucial to drug efficacy.

An example of an excipient is a disintegrant that swells upon contact with gastrointestinal fluid to subsequently rupture the dosage form and increase the liquid-solid contact area for the API to dissolve and become available for absorption through the gastro-intestinal tract. By neglecting disintegrant considerations, it is possible that the tablet would insufficiently disintegrate within the transit time of the gut, resulting in minimal API dissolution and an ineffective treatment dose. Other commonly used excipients include diluents that improve the handling and administration of the dosage form, as well as facilitate content uniformity; glidants that improve powder flow during processing; lubricants that mitigate surface friction during compression and ejection; binders that enhance tablet integrity and tensile strength; preservatives to prolong the potency and purity of the API; colours to enhance identification and appearance; sorbents to minimise API exposure to moisture; surfactants to facilitate wetting; sweeteners and flavouring to mask the taste of chewable tablets; and coating agents to aid palatability and provide protection (Gamble et al., 2010).

Excipient properties have been the subject of a plethora of studies in the literature; investigations seeking to better understand the role and properties that enable an excipient's functionality. As highlighted in Table 1, many excipients are by-products of other industries and are not exclusively used in the pharmaceutical industry (Carlin, 2009; IPEC, 2008). In fact, in comparison to the chemicals, cosmetic and food industry, drug manufacture forms only a small fraction of the recipient market (Sturtevant, 2013). Therefore, excipient specifications are driven by the needs of the larger markets and few purveyors specifically cater to the pharmaceutical industry, in that the excipients are not tailored to drug manufacturing (Carlin, 2009).

The consequence of the food and cosmetic manufacture being less regulated than pharmaceuticals manifests as broad product specifications that tolerate significant variability in terms of particle size, moisture content, crystallinity etc (Ticehurst et al., 1996; Chamarthy et al., 2009; Dave et al., 2015). A significant source of this variability is the natural origin from which many excipients are derived (Landín et al., 1993), including animal by-products (such as lactose and gelatin), vegetation (such as cellulose, stearic acid and carrageenan derivatives), and minerals (dicalcium phosphate derivatives). As a result, excipient properties are susceptible to changes in climate, location, processing and other agricultural considerations (IPEC, 2008).

Several investigations have highlighted the consequences of batch-to-batch variability on manufacturing (Gamble et al., 2010; Kushner et al., 2011; Zarmpi et al., 2017). As eliminating variability at the source is near impossible, then a management approach is required. Therefore, extensive understanding of the effects of variability are necessary for the implementation of a robust control strategy (Ruban et al., 2018).

Table 1 Details of commonly used excipients featured in this study.

Excipients	Examples	Chemical composition	Function	Mechanism of action	Source	Production	Alternative excipient	Alternate applications	Pharma market share
α-Lactose monohydrate	Pharmatose (DFE Pharma) GranuLac (Meggle)	Disaccharide simple sugar	Diluent Mild dry binder Stabiliser	Inexpensive and inert Brittle fracture Non-hygroscopic[1]	Whey of cows' milk	Crystallisation Spray-dried Grades: Milled and sieved	Mannitol Calcium carbonate Sorbitol Calcium phosphate dibasic	Cosmetics Food additive Infant formula Animal feed	~20%[1] 100,000 tonnes per annum[1]
Microcrystalline cellulose	Avicel PH (FMC Biopolymer) Vivapur (JRS Pharma) Pharmacel (DFE Pharma)	Partially depolymerised cellulose	Dry binder Mild disintegrant Diluent Texturising agent Anti-caking agent E460(i)[3]	Plastic deformation Extensive wicking action Moderate swelling capacity	Fibrous plant and wood pulp	Partial depolymerisation of cellulose via hydrolysis and then spray-dried	-	Paper Low-calorie food additive Cosmetics[2]	<2% of cellulose market[2] 35% of MCC market[4]
Hypromellose	Methocel (Dupont Pharma) Pharmacoat (Shin-Etsu)	Partly O-methylated cellulose	Wet binder Coating Emulsifier Thickening and suspending agent E464	Hygroscopic with thermal gelation property when dissolved in water	Fibrous plant and wood pulp	Alkali cellulose treated with chloromethane and propylene oxide	Hydroxypropyl cellulose	Construction Food additive Cosmetics	5-6%[5]
Croscarmellose sodium	Ac-Di-Sol (FMC Biopolymer) Vivasol (JRS Pharma) Primellose (DFE Pharma)	Crosslinked polymer of carboxymethyl-cellulose sodium	Super disintegrant Emulsifier E468	Extensive wicking action Extensive swelling capacity	Fibrous plant and wood pulp	Substitution and hydrolysis of alkali cellulose	Crospovidone Sodium starch glycolate	Food additive	-
Magnesium stearate	Parteck LUB MST (Merck)	Ester of magnesium salt and stearic fatty acid	Lubricant Flow agent Emulsifier Binder Thickening agent Anti-caking agent[6]	Adsorbent releasing agent of extremely fine particle size with low coefficient of friction	Magnesium: mineral deposits in Earth's crust Sodium stearate: Vegetable-derived stearic acid	Interacting magnesium chloride aqueous solution with sodium stearate	Talc	Food additive[6] Cosmetics & personal care	40-45% of U.S. market size[7]

[1]Roelfsema et al. 2000; [2]Galichet et al. 2006; [3]Kuhnert 2016; [4]Tiwari & Mhaisekar 2018; [5]Ranjan 2018; [6]Hobbs et al. 2017; [7]Grand View Research 2018.

2.2.1. Wet granulation

Powders are ubiquitous in the production of pharmaceuticals and pose a multitude of complex challenges throughout. The simplicity of direct compression makes it the preferred method of tablet production, but API considerations deem it impractical for production more often than not. Wide-ranging physicochemical and mechanical properties can lead to problems such as poor flow, constituent segregation, poor compaction performance, and dust emission during downstream processing. Wet granulation is employed to mitigate these issues by modifying the powder blend to have a more workable size distribution, morphology, porosity and constituent distribution.

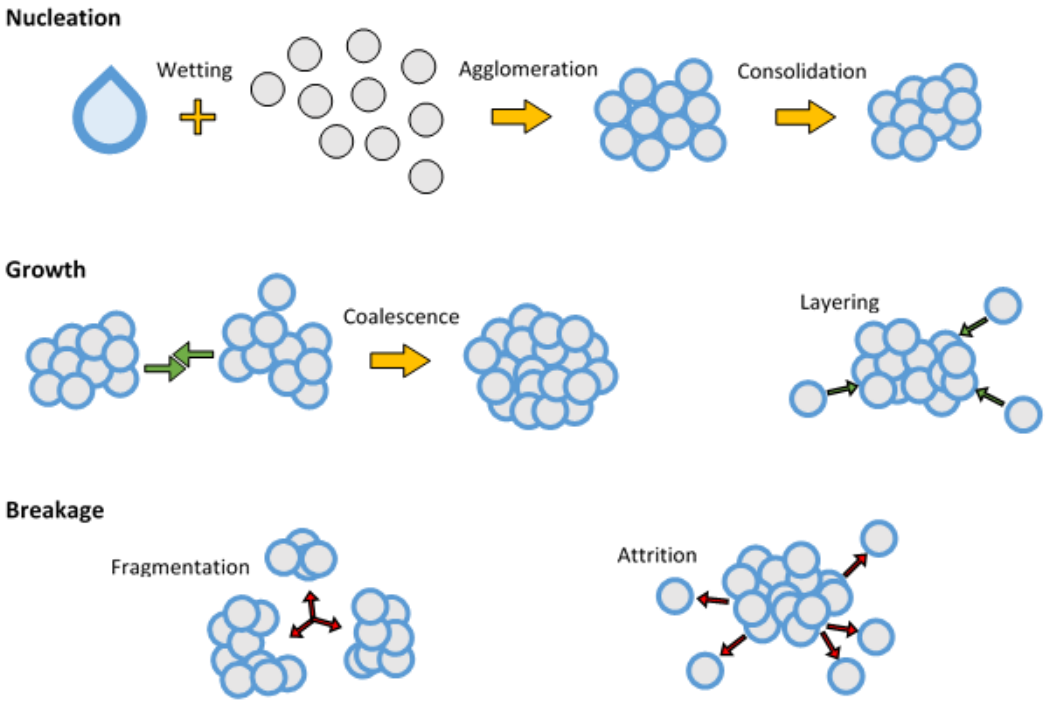

Figure 2.7 Schematic of the three rate processes of the modern approach to wet granulation, adapted from Perry and Green (1997).

Particle enlargement is achieved by agitating the dry powder blend in the presence of a liquid binder, causing the primary particles to agglomerate into granules. The mechanisms through which granules form have been the focus of countless studies (Kristensen and Schaefer, 1987;

Iveson et al., 2001; Hapgood et al., 2003; Kayrak-Talay and Litster, 2011; Pohlman and Litster, 2015; J. B. Wade et al., 2015). It is widely accepted that the initial wetting of the powder bed results in primary particles agglomerating into nuclei. These nuclei then undergo three concurrent mechanisms: (i) growth via layering and coalescence, (ii) consolidation and deformation, and (iii) breakage by fragmentation and attrition (Iveson et al., 2001). These mechanisms are illustrated in Figure 2.7. The relative magnitude of each mechanism determines the development, and subsequent properties, of the granular material (Hapgood et al., 2003). Regime maps have been proposed that outline these relationships as a function of the deformability and pore saturation (Figure 2.8), which are in turn a product of shear and impact forces, as well as liquid viscosity and concentration (Iveson and Litster, 1998a).

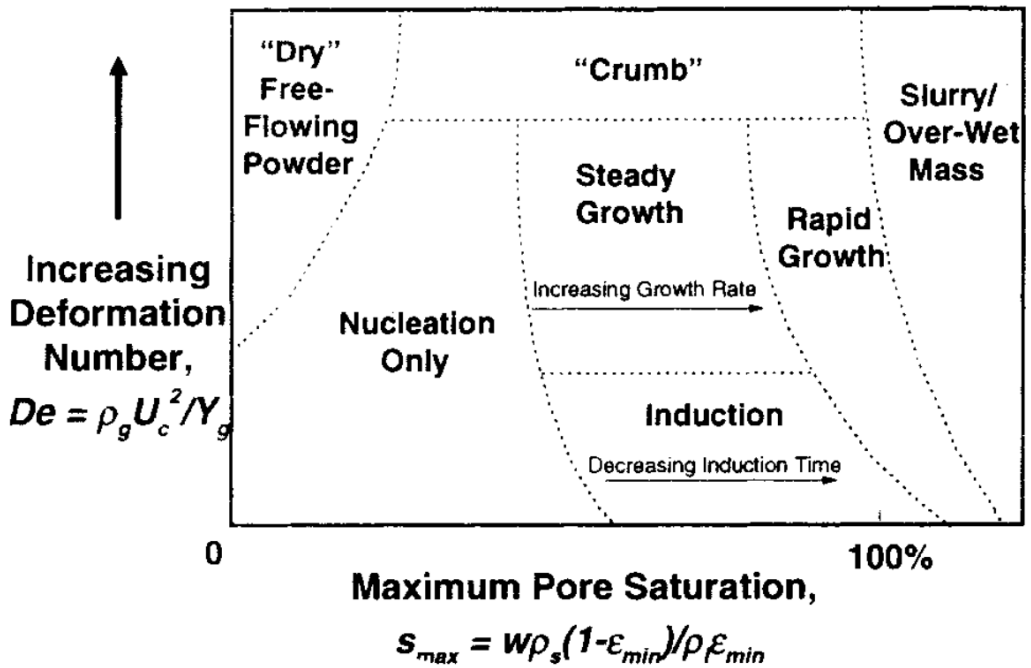

Figure 2.8 Growth regime map proposed by Iveson and Litster (1998) shows the effect on granule consolidation rate and liquid content on granulation behaviour.

Particles are primarily bound together by the attractive force of capillary bridges (Figure 2.9). To obtain viable granules post drying, a soluble component of the powder bulk must dissolve into the capillary bridge and re-crystallise upon evaporation to form a solid bridge. This can

be facilitated by including a highly-soluble binder excipient in the powder formulation or expedite the dissolution process by adding the binder directly to the granulation liquid prior to powder bed wetting. Ideal granulation conditions involve steady growth that produces a narrow granule size distribution. For this to occur the granulation liquid must be evenly distributed throughout the powder bed (Hapgood et al., 2010). It is, therefore, imperative to understand how the granulation liquid interacts with and infiltrates the powder bed, and what role each variable parameter might have on liquid dispersion.

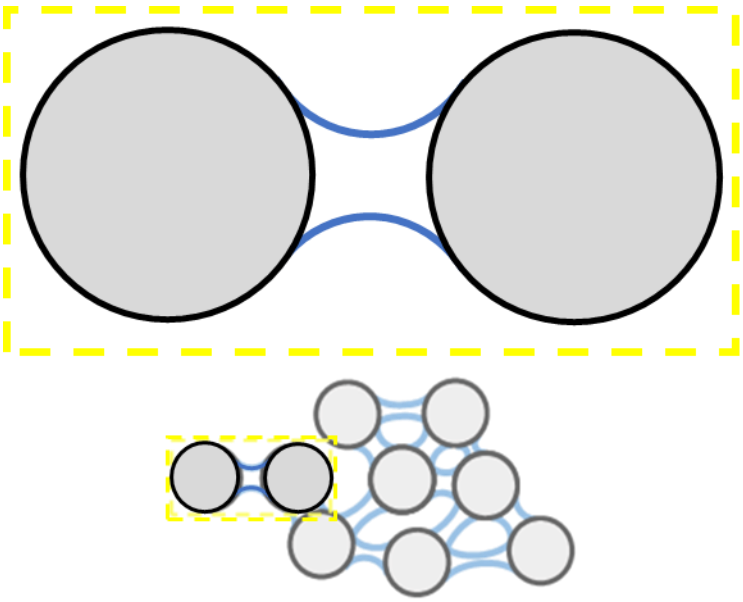

Figure 2.9 Schematic representation of a capillary bridge between two similar sized particles and its role in agglomeration at the pendular stage of wet granulation.

In the manufacture of pharmaceuticals, wet granulation has traditionally involved a large stainless-steel vessel, known as a high shear mixer (HSM) (Figure 2.10), within which a powder bed is agitated via a horizontally rotating impeller. During operation, a predetermined volume of binding liquid is sprayed onto the powder blend at a controlled rate. The liquid binder causes the powder particles to agglomerate whilst the rotating impeller promotes coalescence and densification. In addition to granule growth, breakage and attrition occur simultaneously, resulting in particle size reduction. An additional wall

mounted vertical impeller, known as a chopper, is often employed to reduce the size of oversized agglomerates.

Total operational time is in the magnitude of minutes, after which the granulated material is discharged from the batch vessel and dried. It is very important to determine the granulation endpoint as granules can become over-granulated resulting in them becoming overly dense, or oversized, or even a wet mass if over wetted - all of which can compromise tablet manufacture and performance. Several methods have been employed to determine the granulation end-point, including acoustic emissions (Whitaker et al., 2000; Rudd, 2004; Gamble et al., 2009; Watson et al., 2014), power consumption and torque rheometry (Holm et al., 2001; Chitu et al., 2011; Dave et al., 2012), near-infrared spectroscopy (Miwa et al., 2000; Otsuka et al., 2003), and even a hand squeeze test (Pandey and Badawy, 2016; Sakr et al., 2012).

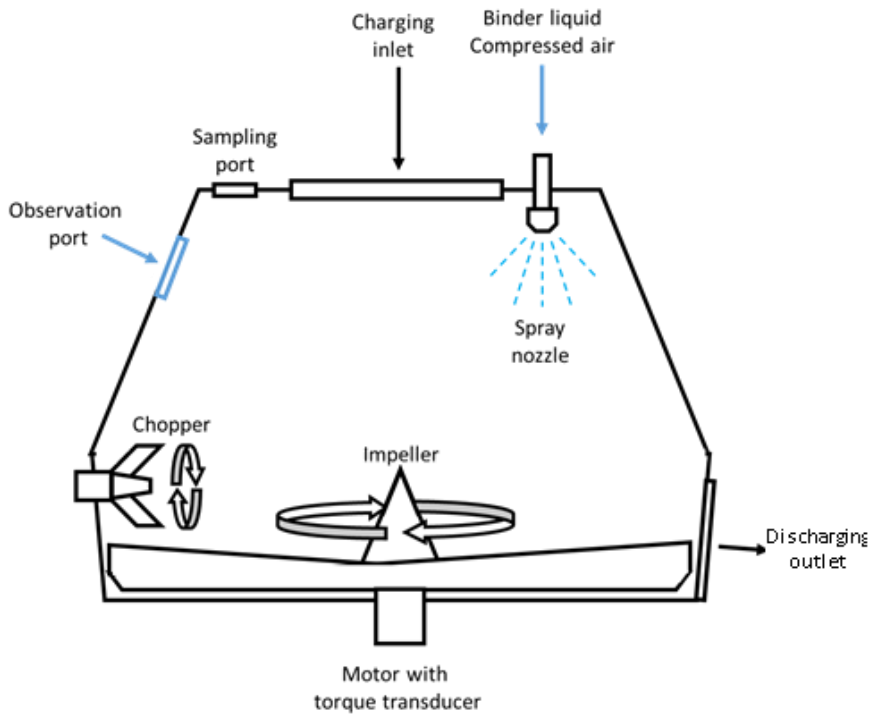

Figure 2.10 Schematic of high shear planetary mixer used for batch wet granulation. Industrial operating capacity can range from 60 to 1400L with approximate bowl dimensions (LxWxH) up to 1600x1600x900mm (GEA, 2015).

Due to the dimensions of the batch vessel and the concentric agitating method, heterogeneous regions of mass transfer and kinetic forces exist. This results in a heterogeneous output. Additionally, the dependence on distance from the impeller tip, where rotational velocity is greatest, further complicates considerations during operational scale up (Oldshue, 1985; Horsthuis et al., 1993; Rekhi et al., 1996).

A further limitation is that HSM involves a relatively long down-time when compared to operational time. This is because charging the vessel before and after operation, and thoroughly cleaning between operations are labour intensive procedures and occupy a significant proportion of a production campaign. These limitations, in addition to those discussed in section 2.1.2, have stimulated interest in alternative wet granulation techniques.

2.2.2. Twin screw granulation

Twin screw granulation (TSG) has gained much attention as a potential continuous substitute to the conventional means of particle enlargement, namely high shear mixer granulation (HSM) and fluidised bed granulation (FBG). TSG was first reported for the production of paracetamol extrudates (Gamlen and Eardley, 1986), and developed from the modification of a twin-screw hot melt extruder, namely, by removing the extrusion die at the barrel outlet (Keleb et al., 2002; E. I. Keleb et al., 2004; Lindberg et al., 1987, 1988a, 1988b; Shah, 2005).

A schematic of a typical TSG setup is shown in Figure 2.11 and features an elongated barrel with a motor at one end and the discharge outlet at the other; multiple inlets for powder and liquid feed along the upper barrel; two identical highly modifiable intermeshed co-rotating screws providing material transport and shear forces; and a short residence time in the range of seconds. When correctly characterised, the unidirectional trajectory of the in-process material presents a system whereby the material can be identified and manipulated as a

function of location and time (Tu et al., 2013; V. Lute et al., 2016), offering insights into granule formation (Dhenge et al., 2012a). Predicated on Archimedes' screw, the rotating helical surface propels the material along the horizontal barrel with limited back mixing. Hence, TSG's predominant first-in-first-out continuous flow permits it to be integrated into a continuous production line, as is the case with the ConsiGma™ Continuous Tableting Line.

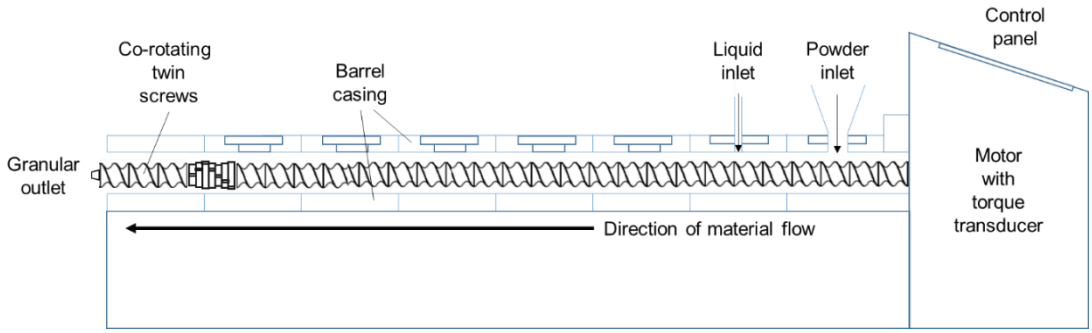

Figure 2.11 A schematic of a hot melt extruder modified for twin screw granulation (TSG). Production scale TSGs have screw diameters ranging between 16 to 25mm and extruder dimensions (LxWxH) up to 2000x320x550mm. Throughput can reach up to 70 kg/hr, formulation dependent (Thermo Fisher Scientific, 2018).

Since the early studies, TSG has been the subject of numerous published works investigating several operational aspects, including process parameters such as the influence of screw elements and screw configuration (Djuric and Kleinebudde, 2010; Pradhan et al., 2017; Sayin et al., 2015; Thompson and Sun, 2009; Van Melkebeke et al., 2008; Vercruysse et al., 2015), screw speed (Djuric et al., 2009; Lee et al., 2013), and material feed rate (Dhenge et al., 2011; Djuric et al., 2009; Djuric and Kleinebudde, 2010). Input parameters examined include the concentration and properties of the liquid binder (Dhenge et al., 2010; El Hagrasy et al., 2013a), binder addition methods (Thompson et al., 2012; Van Melkebeke et al., 2008; Vercruysse et al., 2014; Weatherley et al., 2013) binder viscosity (Dhenge et al., 2012a, 2012b, 2013; Mu and Thompson, 2012), and formulation composition (El Hagrasy et al., 2013b; Fonteyne et al., 2014b; Meier et al., 2015; Vanhoorne et al., 2016; S. Yu et al., 2014).

Additionally, studies have sought to correlate process parameters and granule properties to process conditions such as residence time distribution (Dhenge et al., 2010; A. El Hagrasy and Litster, 2013; Kumar et al., 2014a, 2015, 2016b; Mu and Thompson, 2012; T Lee et al., 2012; Vercruysse et al., 2014) and barrel occupancy fill level (Chan Seem et al., 2016; Gorringe et al., 2017; Lute et al., 2018a; Meier et al., 2017a; T Lee et al., 2012; Vercruysse et al., 2014).

Other studies have been conducted to assess TSG applicability by comparing it with HSM (Beer et al., 2014; Keleb et al., 2002; Lee et al., 2013; Tu et al., 2013), evaluating stability and viability (Vercruysse et al., 2013), appraising process analytical techniques (El Hagrasy et al., 2013a; Fonteyne et al., 2013, 2012; Kumar et al., 2015; Sayin et al., 2015; Vercruysse et al., 2014), and determining scale up considerations (Djuric and Kleinebudde, 2010; H. Liu et al., 2017a; Lute et al., 2018a; J. E. G. Osorio et al., 2017).

Previous reports have highlighted the significance of raw material attributes on HSM (S. Badawy et al., 2000; Badawy and Hussain, 2004; Kato et al., 2006; Mackaplow et al., 1997) and other wet massing operations (Alvarez et al., 2002; Soh et al., 2008), and hence, some studies have sought to understand the influence of extrinsic material attributes on the TSG process, granule properties and tablet performance, and ultimately evaluate criticality. Fonteyne et al. (2014a) examined the influence of material properties and lot-to-lot variability of six samples taken from different batches of Avicel PH101 (30% w/w) on TSG. Small differences in extrinsic particle properties (PSD) and bulk properties (densities and flowability) were found between samples but were believed to be insubstantial on TSG. Differences observed in granule size distribution, resulting from the six samples, were attributed to intrinsic differences i.e. water binding capacity as a function of the degree of crystallinity. Hence, this study warrants further investigation of the resulting tablet performance (QTPP) to determine if granule size distribution is a critical quality attribute

(CQA) and if MCC crystallinity within the typical range of variability is a critical material attribute (CMA).

El Hagrasy et al. (2013b) investigated the influence of three commercially available stock grades of α-lactose monohydrate (73.5% w/w) within a multicomponent formulation at variable liquid-to-solid ratios (LSR). Granule porosity was found to be dependent on lactose grade, however, overall the authors concluded that TSG was a robust process in response to changes in formulation properties as no significant variation in other granule properties could be ascertained as a result of different grades. To eliminate lactose particle size distribution, within the studied range, as a CMA, then the resulting granule porosity range must be shown to have no detrimental effect on the QTPP, and hence not a CQA.

In another study, Fonteyne et al. (2014b) utilised multivariate analysis techniques to compare the influence of seven different commercially available stock grades of theophylline anhydrous (30% w/w) on granule properties, tablet properties, and process behaviour. It was concluded that the particle size distribution of theophylline was a CMA as it had a significant influence on the density, porosity, and size distribution of the granules produced, as well as, tablet strength and process behaviour.

In all of the TSG studies in which the granule size distribution (GSD) was analysed, a broad and often multimodal size distribution was reported, particularly at low-to-moderate values of LSR (Dhenge et al., 2010; El Hagrasy et al., 2013a; Kumar et al., 2015; Vercruysse et al., 2014). This was attributed to heterogenous liquid distribution resulting in larger granules with a high liquid concentration, and fines that had little-to-no contact with the liquid binder (El Hagrasy et al., 2013a; Kumar et al., 2015; Sayin et al., 2015). Other studies have detailed the effects of granule size distribution on tablet production and quality (Johansson et al.,

1998; Riepma et al., 1993; Wikberg and Alderborn, 1990a; Zuurman et al., 1994), in turn, this highlights the criticality of any material attribute or process parameter that influences liquid distribution during granulation, and subsequently granule size.

Material attributes can influence the properties of granules and tablets resulting from TSG, and may arise from material-specific attributes. Many of the aforementioned studies each investigated the influence of only a single formulation component at a time. Further studies are required to investigate the effect of material attribute variation of multiple components simultaneously, in the presence of variable manufacturing parameters, to discern the presence and magnitude of interactions and to contribute to insightful formulation development (Moreton, 2009). With its short residence time, TSG lends itself to QbD as material and process variables can be assessed more efficiently than HSM with respect to time and material. This is particularly true at production scale, whereby an excess of 1000 kg of formulation mixture may be required to test one experimental condition in a batch HSM, thus limiting the resulting knowledge space. In contrast, TSG may only require 15 kg, permitting for more sophisticated and greater utilisation of DoEs.

2.2.3. Conclusion

Excipients are often the most common ingredients in the formulation of solid dosage forms, and thus, their properties can greatly influence the manufacture and performance of the final product. Excipient functionality has been shown to vary between batches due to the natural sources from which they originate, as well as variation in subsequent preparation methods. Relating excipient variability to QTPP is a vital component of developing a robust quality control strategy.

Twin screw granulation has emerged as a viable continuous alternative to traditional high shear batch granulation. As a result of the brief time the material spends within a TSG then the opportunity for liquid distribution is limited. This manifests as a broad GSD composed of large granules and small primary particles. This can prove problematic, as a bimodal granule output can lead to a non-homogenous API distribution, non-uniform drying and granule segregation during downstream operations. Although milling or sieving can narrow the GSD, these corrective operations introduce additional processing considerations and inefficiencies, thus avoiding them is desirable.

Liquid distribution has been investigated in relation to shear forces and liquid addition methods, however, an in-depth analysis of the wetting mechanics within the barrel as it pertains to powder properties and consolidation is required. From this, it can be determined if excipient variability has a significant influence on liquid distribution and what extent of variability is tolerable.

2.3. Powder wetting and nucleation

2.3.1. Wetting phenomenon

Characterising droplet behaviour and wetting phenomena has been the focus of immense scientific attention for over two centuries (Laplace, 1805; Young, 1805). This has only intensified in recent decades with the advent of high-speed cameras opening new avenues to empirically investigate a droplet's spatio-temporal development. Droplet behaviour is of significant practical application in a wide range of industries, such as administering insecticides in agriculture, developing water repellent fabrics in textiles, ink-jet printing, and wet granulation in pharmaceutical manufacture. Despite its common occurrence, droplet dynamics are complex and multiscale with many aspects yet to be fully understood.

When it comes to droplet behaviour, wettability is the most determinant physicochemical property and is often associated with, albeit separate to, solubility. It pertains to the balance of surface tensions, γ, between the liquid, solid and vapour phases and relates to a droplet's contact area via the spreading coefficient, S. Equation 2.1 presents spreading to be thermodynamically favourable ($S>0$) when the solid-vapour interface, γ_{SV}, can be replaced by the solid-liquid, γ_{SL}, and liquid-vapour, γ_{LV}, interfaces. If it is, then the cohesive forces within the liquid droplet are overcome by the adhesive forces at the solid-liquid interface and the droplet contact area increases. Most often, wettability and the balance of interfacial tensions is measured and represented as the contact angle at equilibrium, θ_{eq}. That is the angle formed by the apparent macroscopic triple-phase contact line when an equilibrated liquid is in contact with a substrate, as per the Young equation (Equation 2.2). A low contact angle ($\theta_{eq}<90^{o}$) forms when wetting is favourable, whereas a high contact angle ($\theta_{eq}>90^{o}$)

indicates a low degree of wetting (Figure 2.12). A droplet placed on a completely wetting substrate (θ_{eq}=0°) will spread to a layer of molecular thickness.

$$S = \gamma_{sv} - (\gamma_{sl} + \gamma_{lv}) \qquad \text{Equation 2.1}$$

$$\gamma_{sv} = \gamma_{sl} + \gamma_{lv} \cdot \cos\theta_{eq} \qquad \text{Equation 2.2}$$

Equation 2.1 and Equation 2.2 can be rewritten to relate the equilibrium contact angle to *S*

$$\cos\theta_{eq} = 1 + \frac{S}{\gamma_{lv}} \qquad \text{Equation 2.3}$$

Optically measuring the contact angle of a static sessile drop is relatively straightforward when the substrate of interest can be studied as an impermeable smooth surface. From Equation 2.3 it is evident from the relationship between $\cos\theta_{eq}$ and *S*, and by extension that of the contact angle and contact diameter, is inversely related; a droplet possessing a low contact angle will have a larger contact diameter than a comparable droplet with a high contact angle. However, many other factors other than wettability influence the manner in which droplet spreading occurs, some of which will be discussed here.

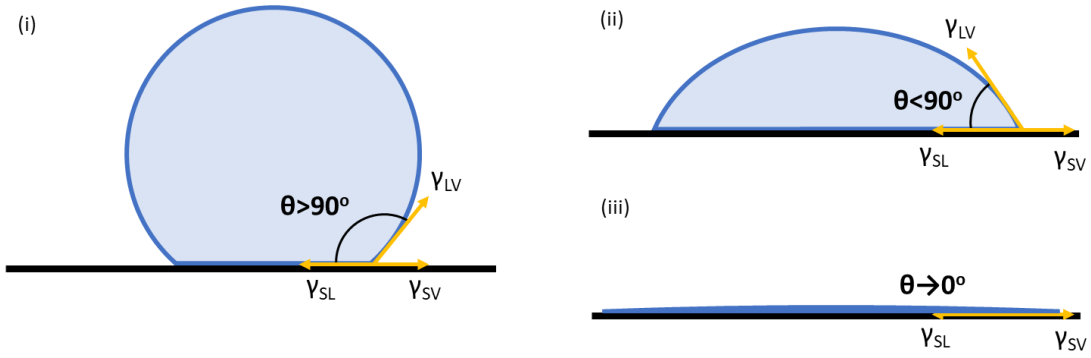

Figure 2.12 Schematics of a droplet system that is (i) non-wetting, (ii) partially wetting and (iii) completely wetting. The contact angle of the three-phase point is dictated by the balance of surface tensions (orange arrows).

2.3.2. Droplet spreading

When a droplet impacts upon a dry and partially wettable surface ($0^o<\theta_{eq}<90^o$), and considering kinetic energy from impact to be unsubstantial (Antonini et al., 2012), the droplet will undergo two consecutive regimes of radial spreading. Initially the contact area spreads quickly resulting in the droplet taking the shape of a spherical cap within a relatively short time frame (<20 ms). This is known as the inertial spreading regime and is capillary-driven, whereby the small meniscus connecting the droplet to the substrate is extremely small and induces a large gradient of Laplace pressure inside the droplet on account of the strong curvature. Therefore, liquid flows from the bulk of the droplet to the surface, resulting in a rapidly expanding contact area, manifesting as a capillary wave (Biance et al., 2004; Bird et al., 2008; Chen and Bonaccurso, 2014a). An example of this is depicted Figure 2.13b-g.

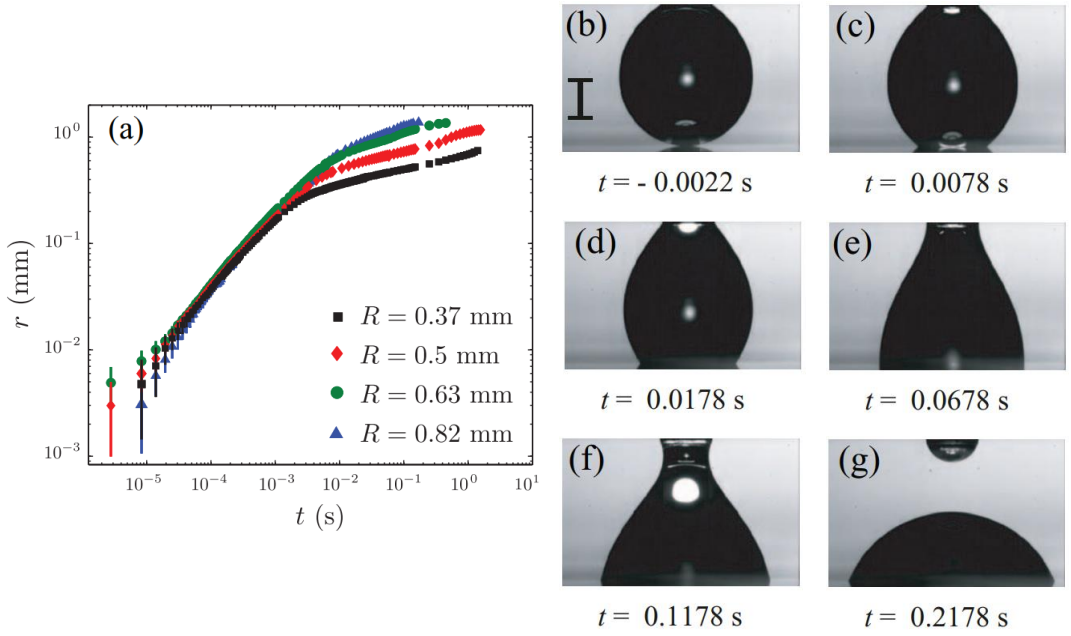

Figure 2.13 (a) Example measurements of the contact radius during early spreading of droplets of varying size. (b-g) An example of a water-glycerin droplet (η=220±5 mPa·s) undergoing inertial spreading following impact (Eddi et al., 2013).

Throughout spreading, the edge of the macroscopic portion of the droplet, visible as a spherical cap, is preceded by a microscopic precursor film at the triple-phase contact line (de Gennes, 1985), and in essence, the bulk of the droplet is spreading over an extremely thin layer of itself. This is represented in Figure 2.14. The precursor film is present throughout spreading but gradually slows until it is eventually overtaken by the spherical cap as the droplet approaches its maximum diameter spread (Wang et al., 2009a). The presence of a precursor film indicates that the θ_{eq} is not in fact the true angle of the triple-phase contact line but representative of the apparent contact angle θ_{app} measured from the angle formed by the macroscopic droplet with the surface.

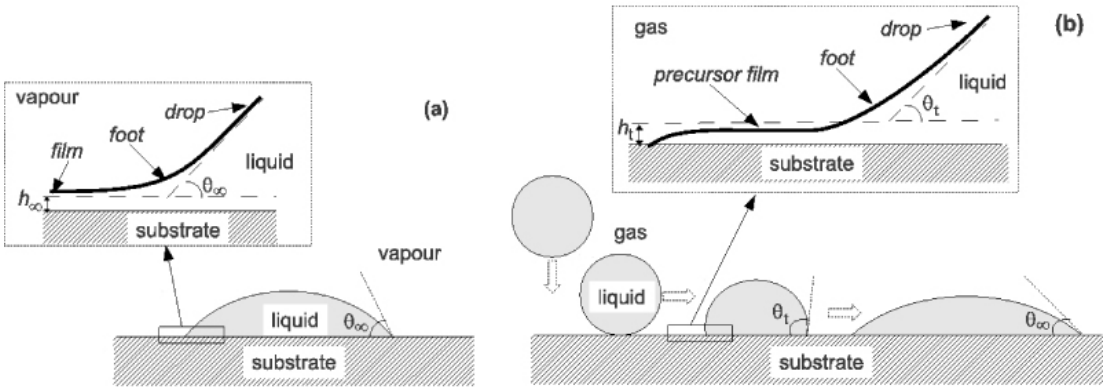

Figure 2.14 (a) Schematic drawing of a liquid droplet at equilibrium resting on an inert, flat substrate. The inset magnifies the three-phase contact line and emphasises the mesoscopic 'foot' region connecting the macroscopic spherical cap to the surface. (b) Schematic of a droplet impinging and spreading on an inert, flat and impermeable surface. The inset shows the precursor film emerging during spreading (Popescu, 2012).

The rate of inertial spreading is determined by balancing the capillary pressure, p_c – given by ~$\gamma_{lv}r_0/r_t^2$, where r_0 is droplet radius before impact and r_t is droplet spreading contact radius at time t – with the liquid inertia resisting drop deformation, ~$\rho_{liq}(\Delta r/\Delta t)^2$ – where ρ_{liq} denotes liquid density (Winkels et al., 2012). The spreading radius, r_t, of a completely wetting system can be scaled as the square root of time, t, with Equation 2.4.

$$r_t \approx \left(\frac{r_0 \cdot \gamma_{lv}}{\rho_{liq}}\right)^{1/4} \cdot t^{1/2} \qquad \text{Equation 2.4}$$

There is consensus on the scaling of the spreading radius on a completely wetting surface ($\theta_{eq}\approx0^o$) being equal to $r_t \sim t^n$ where $n\approx0.5$ (Biance et al., 2004; Mitra and Mitra, 2016; Stapelbroek et al., 2014). With that said, it has been reported that in the very early finite moments after droplet contact (t<10 ms) then the n-exponent is higher $0.5<n<1.0$ (Mitra and Mitra, 2016). However, some conflicting conclusions exist in the literature with regards to the universality of the exponent of $n\approx0.5$ for partially wetting systems. Some researchers have found the inertial power law $n\approx0.5$ to be independent of wettability (Carlson et al., 2012; Eddi et al., 2013; Grewal et al., 2015; Rioboo et al., 2002; Sikalo et al., 2002b; Tang et al., 2017). However, others have reported a decreasing value of n with increasing θ_{eq} (Bird et al., 2008; Chen et al., 2011; Chen and Bonaccurso, 2014a). Winkels et al. (2012) explained that even with decreased wettability, the $n\approx0.5$ power law of inertial spreading is initially obeyed but transitions to a viscous regime (discussed below) earlier and more gradually than perfectly wetting surfaces.

This highlights another limiting factor other than exponent n in inertial spreading; that is, the duration of the inertial regime, τ. The characteristic inertial time scale τ_i, given by $(\rho r_0^3/\gamma)^{1/2}$, can approximate the inertial time scale as $\tau\approx U\cdot\tau_i$, where U is an experimentally determined coefficient (Chen et al., 2011; Chen and Bonaccurso, 2014a). Bird et al. (2008) proposed that τ was equal to the propagation time of the capillary wave across the drop. Hence, τ_i scales the inertial time scale as the periodic motion of mass $\sim\rho r_0$ on a spring of stiffness γ (Lamb, 1945), and U accounts for the effect of viscous damping of the capillary wave (Chen et al., 2011). The duration of inertial spreading has been shown to be dependent on droplet size (Biance et al., 2004; Bird et al., 2008; Eddi et al., 2013), viscosity (Biance et al., 2004; Carlson et al., 2012; Chen and Bonaccurso, 2014a; Eddi et al., 2013), substrate surface softness (Chen et al., 2011), substrate surface microstructure (Grewal et al., 2015; Yang and Xu, 2017), liquid

surface tension (Chen et al., 2011), and impact velocity (Sikalo et al., 2002a; Tang et al., 2017; Wang et al., 2009a), but independent of wettability (Bird et al., 2008; Chen and Bonaccurso, 2014a).

Work by Chen and Bonaccurso (2014a) highlighted that droplet spreading may cease with the inertial regime for systems with a θ_{eq} above a critical angle, particularly for droplets of low viscosity. For wetting systems below this critical angle, the droplet continues to spread beyond the inertial regime, albeit at a considerably lower spreading velocity i.e. n<0.5. As the inertial forces decrease, viscous dissipation at the contact line becomes the dominant force to resist droplet spreading. Concurrently, the driving force is no longer the result of the Laplace pressure differential inside the drop, but instead the second regime is driven by either gravitational forces or available surface energy acting upon the droplet.

If the characteristic droplet length, in this case d_0, is greater than the capillary length, l_c, as determined by Equation 2.5, then surface tension and contact line dynamics have little influence on spreading (Bonn et al., 2009). Instead, spreading is gravity driven, whereby $r_t \sim t^{1/8}$ as a consequence of the balance of gravity dissipation in the bulk and viscosity dissipation at the contact line (Cazabat and Cohen-Stuart, 1986; Lopez et al., 1976).

$$l_c = \sqrt{\gamma_{lv}/(\rho \cdot g)} \qquad \text{Equation 2.5}$$

where g is acceleration due to gravity (9.81 m/s^2).

If the droplet is small ($d_0 < l_c$), then the effect of gravity is negligible and the viscous regime is dominant whereby only capillary forces arising from the available surface energy at the contact line continues to propagate the precursor film ahead of the spherical drop (Cazabat and Cohen-Stuart, 1986; Lopez et al., 1976). Assuming a conservation of volume, the viscous regime is known to obey Tanner's law presented in Equation 2.6 (Tanner, 1979).

$$r_t \approx \left[\frac{10 \cdot \gamma_{lv}}{9 \cdot q \cdot \mu} \cdot \left(\frac{4 \cdot V_0}{\pi}\right)^3 \cdot t\right]^{1/10}$$ Equation 2.6

where *q* is a non-dimensional constant set by microscopic effects like slip, long ranged forces, or a diffuse interface, and is given by $q=\ln(r/2e^2L)$ where *e* is base of the natural logarithm and *L* is a characteristic length. To highlight the relationship between the liquid properties this can be simplified to Equation 2.7.

$$\frac{r_t}{r_0} \sim \left(\frac{\gamma_{lv} \cdot t}{\mu \cdot r_0}\right)^{1/10}$$ Equation 2.7

where r_t/r_0 represents non-dimensional droplet spreading.

The power law $r_t \sim t^m$ where $m=0.1$ of the viscous regime has been well corroborated (Cazabat and Cohen-Stuart, 1986; Mitra and Mitra, 2016; Singh et al., 2013; Starov et al., 2002), as the droplet radius scales with time as a balance of the available capillary forces and resistive viscous dissipation at the contact line. As the *m* exponent suggests, droplet spreading is finite and stops once the droplet reaches an equilibrium with the opposing viscous force, to form a static contact angle with the surface.

2.3.3. Surface roughness

Considering the aforementioned principles pertaining to ideal surfaces, it is necessary to consider that most surfaces typically are non-ideal, possessing a myriad of defects, asperities and pores. The effects of surface roughness on wettability and droplet spreading have been subject to much investigation (Quéré, 2005), with a focus on two widely accepted droplet states, represented in Figure 2.15. The first of these is the Wenzel state (Wenzel, 1936), whereby the drop penetrates and wets the grooves in the surface and the net energy decrease upon wetting is related to the total area under the sessile drop (Li et al., 2013). The Wenzel equation gives:

$$cos\theta_{app} = R \cdot cos\,\theta_{act}$$ Equation 2.8

where θ_{app} in this case is the Wenzel-derived apparent contact angle and θ_{act} is the actual contact angle. The roughness factor, *R*, is the ratio between the true surface area and the projected surface area and thus, is always ≥1.

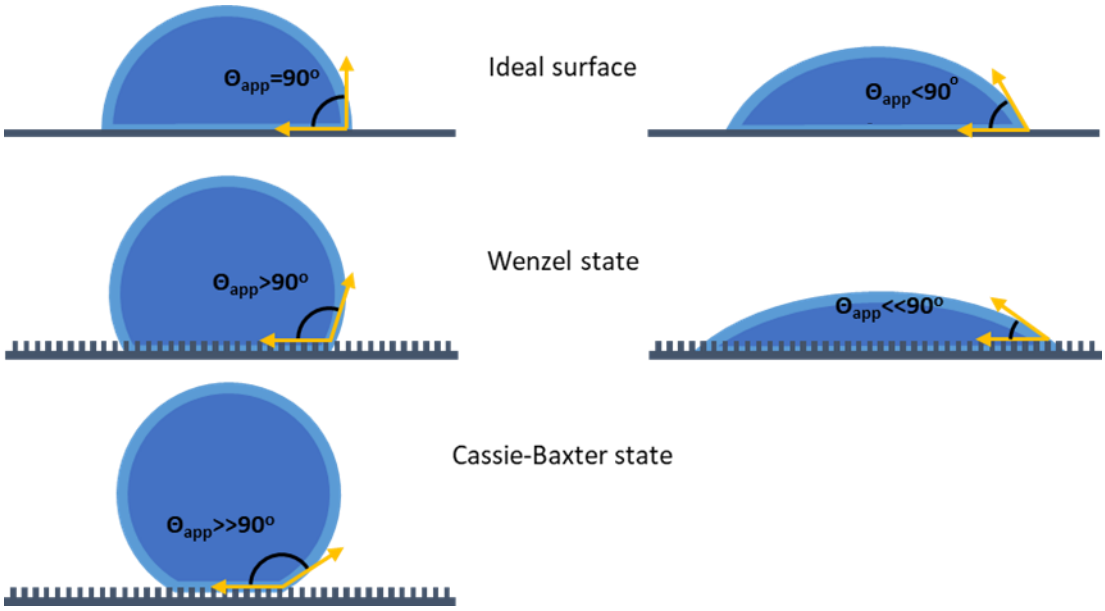

Figure 2.15 Illustrations of the various states a non-wetting droplet (left) and a partial wetting droplet (right) may assume on non-ideal surfaces and the effect of the wetting.

Consequently, a roughened surface emphasises the intrinsic wetting properties of the solid; increasing surface roughness for a wettable system enhances wetting and the θ_{eq}<90° is further reduced. Conversely, the θ_{eq}>90° of a non-wetting system is further increased with increased surface roughness (Li et al., 2013). This principle is the basis of fractal structural modification utilised to produce super-hydrophobic materials (Onda et al., 1996; Shibuichi et al., 1998).

The second state a droplet can assume was outlined by Cassie and Baxter (1944) and considers the rough surface to be chemically heterogeneous. The droplet spreads and rests upon the peaks of the asperities along with the trapped pockets of air occupying the troughs

i.e. the droplet does not penetrate and wet the grooves. Hence, the contact angle of the composite consists of the solid fraction, f_s, with contact angle θ_s and a second fraction of air f_{pore}=1-f_s with contact angle θ_{air}:

$$\cos\theta_{app} = f_s \cdot \cos\theta_s + (1 - f_s) \cdot \cos\theta_{air} \quad \text{Equation 2.9}$$

Considering the contact angle of air to be 180° to give *cos*θ=-1 then this can be rewritten as

$$cos\theta_{app} = f_s \cdot (\cos\theta_s) - (1 - f_s) \quad \text{Equation 2.10}$$

whereby, a greater air fraction reduces wettability and results in a larger contact angle, regardless of wettability upon an ideal surface of the same material. This was demonstrated by Kashaninejad et al. (2012) as shown in Figure 2.16.

Wenzel's *R*-ratio may be used in conjunction with Cassie's *f*-fractions to give a modified Wenzel-Cassie equation (Järnström et al., 2010):

$$cos\theta_{app} = f_s \cdot \left(\frac{\cos\theta_s}{R}\right) - (1 + f_s) \quad \text{Equation 2.11}$$

In addition to affecting the droplet state at equilibrium, surface topography has been found to influence droplet spreading. Spreading during the inertial regime is unencumbered by surface topography as the initial motion of r_t is not governed by the contact line but rather by the transport of liquid from the centre of the drop to the wetted region in the form of a capillary wave (Sikalo et al., 2002a; Stapelbroek et al., 2014; Tang et al., 2017). The induced Laplace pressure is easily able to drive the liquid over the topographical variations. However, observations by Wang et al. (2015) dispute this; by increasing the roughness *R*-ratio of the surface, the exponent *n* of the inertial regime decreased. Contact line friction was credited to be the determining factor, as the inherent roughness of the surface on which the drop

spreads slows down the drop compared to one spreading on a smooth substrate (Marston et al., 2013).

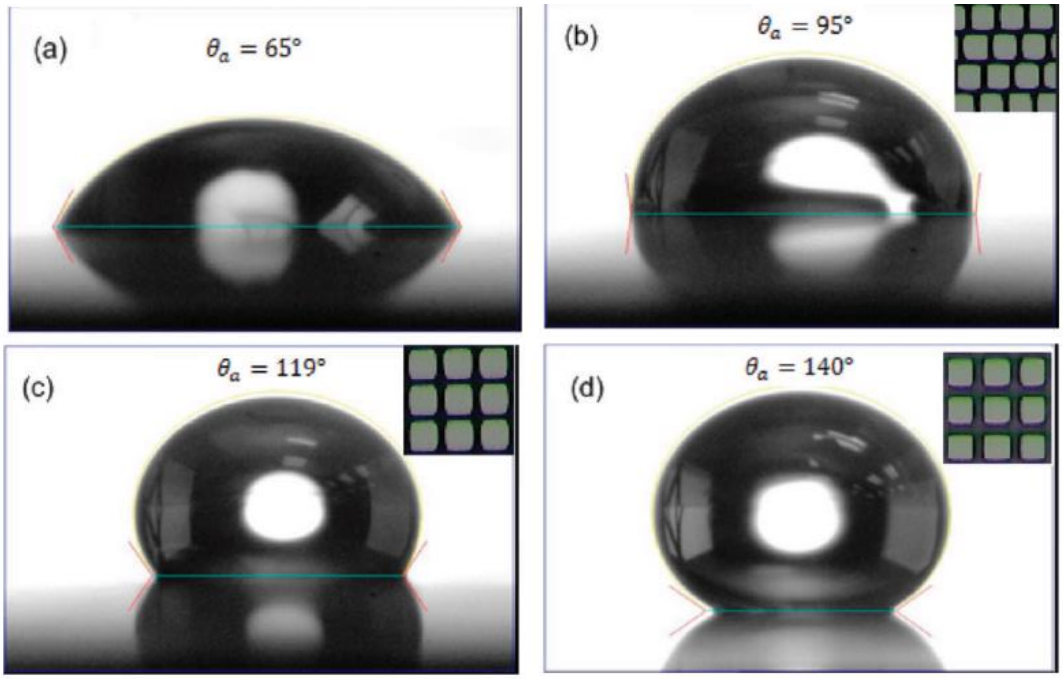

Figure 2.16 Example of the equilibrium contact angle of a static water droplet varying with the increased spatial heterogeneity. As the surface fraction of grooves increased from a smooth surface (a) to a micropatterned silicon surface (b-d) the droplet spread decreased and the contact angle increased (Kashaninejad et al., 2012).

The subsequent gravity or viscous spreading regime has also been found to deviate from the established power laws as a result of topographical variation. Cazabat and Cohen-Stuart (1986) concluded that droplet spreading on a rough surface is not governed by the advancing contact angle and internal capillary force, as is the case for smooth surfaces. Instead, it was observed that whilst the bulk of the droplet was spreading at the rate of the gravity driven regime ($r_t \sim t^{1/8}$), a transition period was observed whereby the rate of spreading significantly increased. After several seconds a liquid film emerged and preceded the spherical cap as it advanced through the "canals" in depolished glass as a result of capillary action where exponent n of $r_t \sim t^n$ ranged between ~1/2 and ~1/4. The central droplet behaved as a reservoir feeding the advancing liquid front whilst simultaneously spreading, until the rate of

spreading slowed down and eventually stopped as the totality of the droplet's volume was consumed by the topographical defects. This capillary flow was further corroborated by Apel-Paz and Marmur (1999) at low viscosity, and similarly, droplet diameter and exponent *n* were found to decrease with reduced glass roughness from n~1/2 to n~1/4. Other researchers have also made similar observations, albeit using etched silicon surfaces (Bico et al., 2001; Ishino et al., 2007; McHale et al., 2004; Yuan and Zhao, 2013). In those studies, the advancing contact line was propagated ahead of the bulk by the excess surface energy provided by the array of etched pillars. Bico et al. (2001) reported that a critical θ_{eq} existed below which the contact line propagated between the microtexture of a silicon surface at a rate of $\sim t^{1/2}$. For surfaces with a θ_{eq} above the critical value, the contact line became pinned and the droplet adopted a Wenzel state, with no infiltration of the microtexture. The critical θ_{eq} was determined by the surface roughness and the surface solid fraction. Ishino et al. (2007) too found droplet spreading on etched silicon to scale with the Washburn equation (discussed below) at $r \sim t^{1/2}$. The spreading coefficient was found to increase with pillar height until flow was balanced by friction arising from liquid viscosity and the increased contact area. Topography-driven spreading has also been demonstrated using woven fabric, whereby flow is parallel to the direction of the fibres (Arora et al., 2006).

For surface roughness to facilitate spreading then the droplet must wet the grooves, and hence, assume a Wenzel state. Some researchers found that greater roughness of wettable surfaces led to slower spreading and a smaller d_{max} (Kashaninejad et al., 2012; Sikalo et al., 2002a; Tang et al., 2017). A visual example of this is shown in Figure 2.16. Tang et al. (2017) attributed this to the droplet adopting a Cassie regime at a low Weber number resulting from a low impact velocity, causing the droplet to spread across the peaks of the substrate.

This is in agreement with work by Vaikuntanathan and Sivakumar (2014, 2016) involving a droplet impacting on a groove-textured surface; at a low Weber number the depth of the grooves did not influence droplet spreading (Vaikuntanathan and Sivakumar, 2016) but the spacing of the grooves did (Vaikuntanathan and Sivakumar, 2014). This was not the case at higher Weber numbers as increased velocity caused the droplet to penetrate and wet the grooves, and so the Wenzel state was the dominant form of spreading (Tang et al., 2017; Vaikuntanathan and Sivakumar, 2016). However, the droplet diameter during impact deformation decreased with the decreased wettability resulting from increased roughness (Li et al., 2013). It is therefore apparent, that at higher Weber numbers or following external stimuli the droplet can transition from a Cassie regime to a Wenzel regime (Li et al., 2013; Tang et al., 2017; Vaikuntanathan and Sivakumar, 2016). A temporal image sequence of this is depicted in Figure 2.17. It was also observed that spreading was dependent on the direction of the grooves, as spreading was restricted in the direction perpendicular to the grooves resulting in anisotropic coverage (Vaikuntanathan and Sivakumar, 2016).

Therefore, it is apparent that a surface's physical and chemical composition are important to wetting. The discussion until now has outlined droplet spreading on ideal and non-ideal impermeable surfaces. However, droplet behaviour and wettability measurements are further complicated by porous substrates whereby the droplet never equilibrates to form a static contact diameter or angle due to the concomitant commencement of imbibition into the substrate.

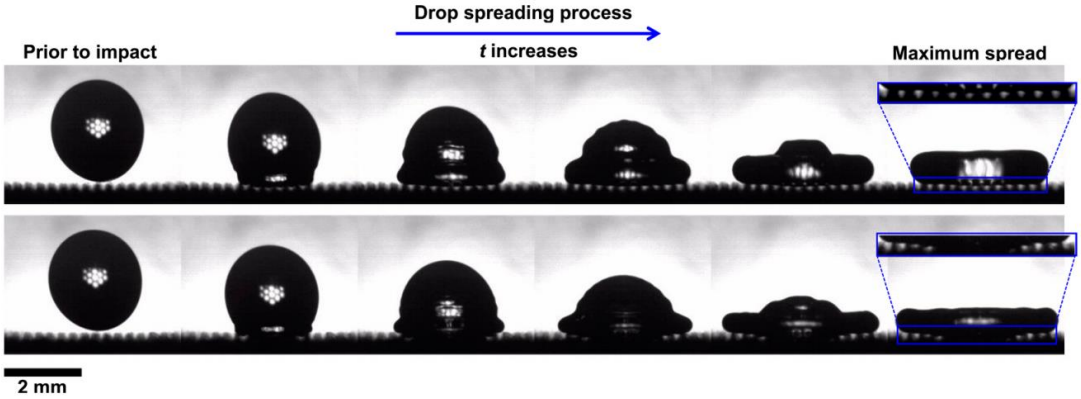

Figure 2.17 Image sequence depicting droplet impact and the subsequent spreading states. Cassie-Baxter spreading (top) is characterised by no groove penetration, whereas Wenzel spreading (bottom) involves groove penetration and results in a greater spreading diameter (Vaikuntanathan and Sivakumar, 2016).

2.3.4. Droplet imbibition and the Washburn Capillary Rise Method

A porous material such as a powder bed introduces additional complexity to the wetting phenomenon, particularly when attempting to directly measure the Young's contact angle. The contact angle of a partially wetting system ($\theta_{eq}<90^{o}$) never completely equilibrates on a powder bed. Instead, the droplet is in a constant state of flux as the triple-line contact angle advances during spreading until droplet imbibition nears completion and causes the contact line to rapidly recede (Prestidge and Tsatouhas, 2000). In addition to this, the surface is spatially heterogeneous (rough) and so gives rise to an angle at the three-phase contact line that varies locally depending on the orientation of the particles and pores (Muster and Prestidge, 2002).

All powders are inherently porous as air permeates the bulk to form a matrix of particles and voids. Pores can be characterised in terms of size (e.g. micro-, meso- and macro-pores), formation (intra- or inter-particle), and configuration (open and interconnected or closed and secluded). The cumulative volume of these pores constitutes a powder's porosity, ε, which

is expressed as a percentage and is derived from the disparity between the density of the powder bed, ρ_{bulk}, and the intrinsic density of the material, ρ_{true} (Equation 2.12).

$$\varepsilon = \left(1 - \frac{\rho_{bulk}}{\rho_{true}}\right) \cdot 100 \qquad \text{Equation 2.12}$$

The powder bed of fine and elongated particles is more likely to possess a higher porosity than a coarse powder (Lowell and Shields, 1991; Yu et al., 1997, 1996). This is because the smaller and irregular particles possess a greater surface area-to-mass ratio, and therefore, are more susceptible to a greater number of frictional and cohesive forces - namely van der Waals - arising at the particle-particle interfaces (Hamaker, 1937; Israelachvili, 1989). The effect of these forces diminishes with increasing particle size because the influence of gravitational forces acting on the individual particles is substantially greater, on account of their larger mass. Moreover, there is lower potential for particle-particle interactions due to possessing a smaller surface area (Israelachvili, 1989). Hence, coarse particles pack into a more efficient arrangement, resulting in greater air displacement and a lower porosity. With that said, a coarse powder with a narrow size distribution will always maintain a network of voids; the interstitial volume between particles will remain present, increasing proportionally with particle size, even when densely packed (Gauss, 1831). Mechanical interlocking of elongated particles can also impede efficient particle packing and is relatively independent of gravity (Wouters and Geldart, 1996).

The prevalence and size distribution of pores is not only dependent on particle properties, but also on externally applied forces during handling history that influence consolidation (Davis et al., 2017). The application of a normal stress in the form of a compression force will initially overcome cohesive and frictional forces to break agglomerates resulting in particle reorientation and a more efficient particle arrangement. However, if further

compression is not reciprocated with improved packing efficiency, then the powder may experience particle deformation (if the material has plastic properties) and/or fragmentation (if the material's ultimate tensile strength is exceeded), as is the case during tablet compaction. Applying limited shear stress between particles in confined conditions – during tapping for example - can also promote consolidation of the powder bed by overcoming intermolecular forces. However, in unconfined conditions, extensive shear can dilate the powder bed to incorporate a greater volume of air into the bulk and increase porosity – for example, during low shear mixing (Faqih et al., 2006; Reynolds, 1885).

To overcome the complications that porosity introduces to the sessile drop method, attempts have been made to minimise its influence. An approach has been taken to make contact angle measurements of powders more feasible by compressing a sample to form a compact or disc of diminished surface roughness and powder porosity, thereby impeding droplet absorption (Buckton and Newton, 1986; Holm et al., 2016). However, the results are often inaccurate and difficult to replicate (Lazghab et al., 2005; Muster and Prestidge, 2005). Additionally, it is tricky to correlate the test to granulation conditions, as particle fragmentation, deformation and bonding fundamentally transform the material's microstructure and bulk properties (Alghunaim et al., 2016; Buckton, 1990; Mangwandi et al., 2015; Muster and Prestidge, 2005). Further, several authors have reported efforts to prevent droplet penetration to be futile, as absolute droplet equilibrium proved unattainable (Karde and Ghoroi, 2014; Prestidge and Tsatouhas, 2000). In addition, powder hygroscopicity causes the droplet to eventually be absorbed regardless, albeit, at a slower rate than pore penetration.

For these reasons it is not possible to directly measure the actual contact angle formed between a liquid and pharmaceutical powder. Consequently, alternative methods of

inferring the apparent contact angle of porous material are the subject of many studies (Alghunaim et al., 2016; Depalo and Santomaso, 2013; Galet et al., 2010; Kiesvaara and Yliruusi, 1993; Link and Schlünder, 1996; Z. Liu et al., 2017; Popovich et al., 1999; Susana et al., 2012; Wang et al., 2018; Yuan and Lee, 2013). One such method known as the Washburn capillary rise method (WCR) is extensively used in the pharmaceutical industry for wettability studies (Buckton and Newton, 1986, 1985). WCR involves measuring the rate at which the liquid front of the test liquid rises through a powder-packed column (Figure 2.18) and comparing it to a reference liquid that completely wets the powder, $\theta_{eq} \approx 0^o$ (Bruil and van Aartsen, 1974). This permits wettability to be uncoupled from the pore structure of the powder bed, so that the contact angle of the test liquid can be estimated using Washburn's equation (Washburn, 1921):

$$l_{wcr}^2 = \frac{r_{pore} \cdot t_p \cdot \gamma_{lv} \cdot cos\theta}{2 \cdot \eta} \qquad \text{Equation 2.13}$$

where l_{wcr} is the depth of intrusion, γ_{lv} is the liquid-vapour surface tension, θ is the contact angle to be derived, η is the liquid viscosity, t_p is the penetration time, and r_{pore} represents the average pore radius.

To understand the Washburn equation, it helps to see how it is derived from Poiseuille's law (Equation 2.14), which gives the pressure drop of fluids in laminar flow flowing through a long cylindrical pipe of constant cross section.

$$\Delta p_c = \frac{8 \cdot \eta \cdot l \cdot Q}{\pi \cdot r^4} \qquad \text{Equation 2.14}$$

where Q is volume flow rate given by $\Delta V/\Delta t$, and in turn $\Delta V = \pi r^2 l$. Δp_c is capillary pressure derived from the Young-Laplace equation

$$\Delta p_c = \frac{2 \cdot \gamma \cdot \cos(\theta)}{r} \qquad \text{Equation 2.15}$$

Hence, together and rearranging to make infiltration rate, $\Delta l/\Delta t$, the subject gives

$$\frac{dl}{dt} = \frac{1}{4} \cdot \frac{r \cdot \gamma \cdot \cos\theta}{\mu \cdot l} \qquad \text{Equation 2.16}$$

Therefore, by measuring the depth of infiltration as a function of time for a completely wetting reference liquid ($cos\theta \approx 1$) of known surface tension and viscosity, it is possible to determine the pore radius for a given packed-powder column. As a result, the apparent contact angle can be determined by repeating the capillary rise with the test liquid to establish $cos\theta_{app}$.

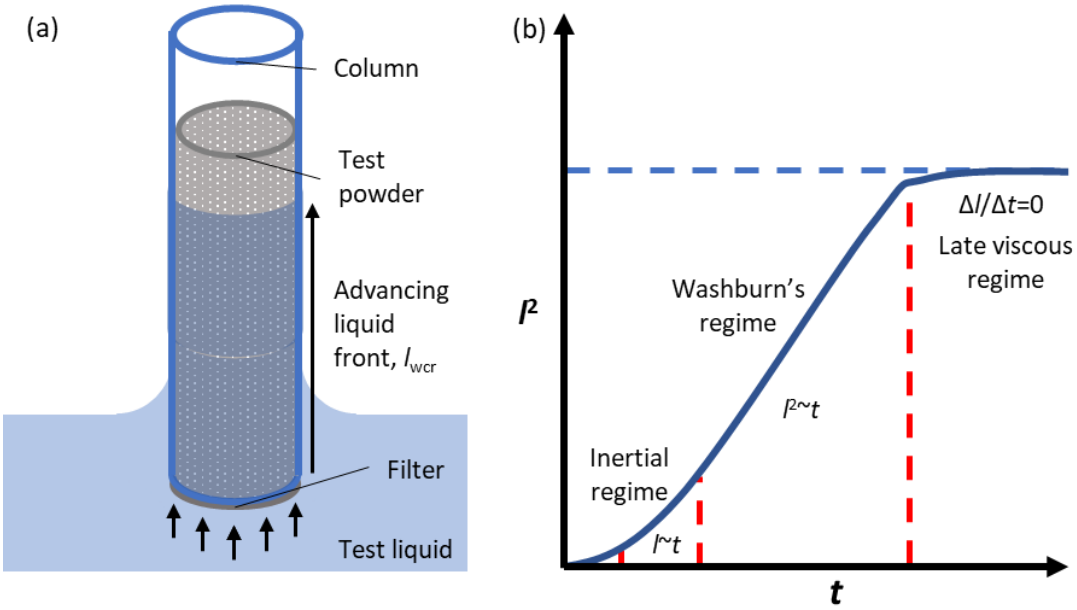

Figure 2.18 Schematic of (a) Washburn capillary rise setup and (b) plotted measurements of the advancing liquid front as a function of time to derive the contact angle from the linear Washburn portion of the curve.

In the absence of shear and compressive forces to mechanically distribute the granulation liquid, capillary action is the cardinal means by which the liquid is dispersed throughout the bulk of a static powder bed. Therefore, as the Washburn equation indicates, penetration is driven by the liquid's interfacial properties, $l_w/t \sim \gamma_{lv} cos\theta$, and flow is resisted by viscous dissipation, $l_w/t \sim 1/\eta$. The role of pore geometry, represented by r_{pore}, during imbibition is

complex but generally r_{pore} must be sufficiently narrow, typically with a Bond number below 1, for surface tension to dominate and for dynamic pressure to be maintained. With that said, the rate of infiltration is modelled with respect to a constant pore radius and therefore penetration scales with pore radius, $l_w^2/t \sim r_{pore}$. However, Schoelkopf et al. (2002) and Alava et al. (2004) highlighted that liquid imbibition was not always faster in larger pores. This was attributed to the effects of inertia at the initial moments of liquid penetration, whereby hydrostatic forces favour smaller pore geometry. In analysis of liquid flow through serial heterogenous capillary doublets, work by Chatzis and Dullien (1983) was followed up by, and in agreement with, Sorbie et al. (1995), where it was found that at high Reynold's number, indicating dominant inertial forces, the imbibing liquid favoured the smallest capillaries. This is represented by Jurin's law shown in Equation 2.17 (Jurin, 1719), whereby liquid propagation l_j resulting from hydrostatic induced capillary pressure p_c is inversely proportional to pore radius, $l_j \sim 1/r_{pore}$.

$$l_j = \frac{2 \cdot \gamma \cdot \cos\theta_{eq}}{r \cdot \rho_{liq} \cdot g} \qquad \text{Equation 2.17}$$

where l_j is the elevation of the liquid column, ρ_{liq} is the liquid density and g is acceleration due to gravity.

These contradictory relations to r_{pore} can be understood by considering that the scaling regime along a capillary tube during imbibition changes with the applicability of each model, as shown in Figure 2.18b. Initially, the *inertial* regime ($l \sim t$) resulting from the hydrostatic pressure at the opening of the entry pores is dominant and viscous resistance is negligible, and so Jurin's law is applicable. The Washburn equation better explains the subsequent *early viscous* regime ($l_{wcr} \sim t^{1/2}$), whereby the liquid propagates along the capillary and inertial

effects are negligible. During the final *late viscous* regime, resistive forces – gravitational and/or viscous - become dominant and infiltration slows to a halt ($\Delta l_{wcr}/\Delta t$=0).

Therefore, by only factoring a single value for the pore radius, the Washburn equation ignores acceleration resulting from inertia based on the assumption that it is only present during the initial stages of pore entry and is otherwise negligible for much of penetration in comparison to the velocity resulting from surface tension (Bosanquet, 1923). However, a porous medium consists of a network of interconnected voids, whereby the path of the penetrating liquid is characterised by a non-uniform radius. Therefore, the velocity of the imbibing liquid likely fluctuates as the liquid front accelerates when passing through a narrow pore radius and decelerates when navigating a large pore radius. As a result of the potential summing effect of inertia in the interconnected void network, the value of exponent *n* of $l \sim t^n$ is likely to deviate from 0.5, as originally highlighted by Bell and Cameron (1906). According to Bosanquet's modifications to the Washburn equation, which incorporates inertial flow, *l* is directly proportional to *t* i.e. *n*=1 (Ridgway et al., 2002), which is in line with Jurin's law. With that said, over the years the Washburn equation square-root time dependency has proven effective (Yang et al., 1988), but this does not nullify the role of inertial flow (Schoelkopf et al., 2002).

Furthermore, the role of pore radius is also dependent on wetting dynamics, namely viscosity, whereby imbibition of relatively inviscid liquids increases with narrower pores, whereas the flow of viscous liquids benefits from larger pore radii. In this regard, Chen et al. (2017) concluded that a substrate with a broad multiscale pore distribution observed faster wicking than a narrow uniform pore distribution, as the size distribution was able to provide a fraction of pores of an optimal size that promoted capillary pressure with minimal viscous friction.

2.3.5. Droplet penetration method

Another commonly reported technique for measuring powder wettability is the droplet penetration method (DPM). DPM involves depositing a single droplet onto the surface of a powder bed and analysing droplet absorption. Work by Denesuk et al. (1993) and Middleman (1995) produced an equation that applied Washburn principles of interfacial-driven flow resisted by viscous dissipation (Equation 2.18). It was able to estimate the contact angle (θ_{app}) from the time required for complete penetration (t_p) of a droplet of known volume $V_0^{2/3}$, viscosity η and surface tension γ_{lv}, in addition to the porosity of the powder bed, ε.

$$t_{CDA} = 1.35 \cdot \frac{V_o^{2/3}}{\varepsilon^2 \cdot R_{pore}} \cdot \frac{\eta}{\gamma_{LV} \cdot cos\theta} \qquad \text{Equation 2.18}$$

where CDA denotes a constant drawing area imbibition regime (see below), and R_{pore} is the estimated average pore radius. R_{pore} can be estimated from the surface area, porosity and density of the powder bed using the Kozeny equation (Hapgood et al., 2002; Sweeney and Mayo, 1999)

$$R_{pore} = \frac{2 \cdot \varepsilon}{(1-\varepsilon) \cdot SA_0 \cdot \rho_{bulk}} \qquad \text{Equation 2.19}$$

where SA_0 is the specific surface area and ρ_{bulk} is the powder bed density.

A limitation of the Denesuk-Middleman equation is that it models the porous substrate as a collection of vertically orientated capillary tubes of equal distance and constant radius. A powder bed consists of a collection of particles that form a network of interconnected voids of variable size, with larger voids impeding, or even preventing, liquid flow (Kaye, 1998). Bernadiner (1998) studied liquid flow in glass structures consisting of homogenous and random micro-capillaries. The homogenous model propagated the liquid uniformly and

filled evenly. For the random model, narrower capillaries filled first and filled faster while larger capillaries were by-passed and remained unfilled under conditions of limited supply volumes of fluid. That is to say, that a preferential flow pathway exists within the interconnected glass capillaries. This preferential flow was later shown to be true for interconnected pores within a powder bed (Börjesson et al., 2017, 2014; Hapgood et al., 2002; Law et al., 2013).

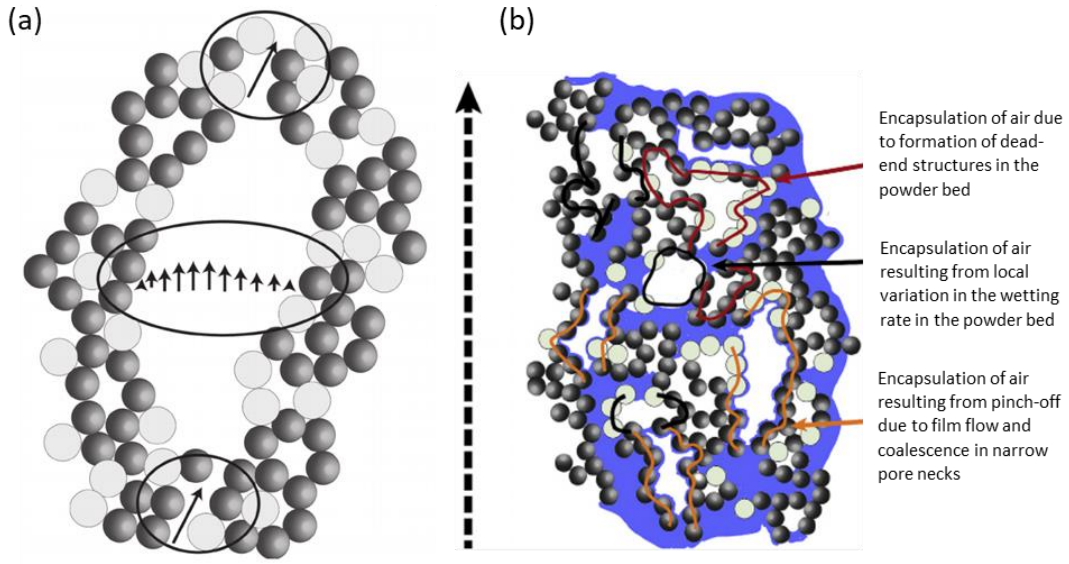

Figure 2.19 Schematic (a) illustrates the effect of pore diameter on flow velocity, whereby dark grey spheres represent particles in agglomerates and light grey spheres are single primary particles in the powder bed (Börjesson et al., 2016). Schematic (b) illustrates some of the possible phenomena causing air to become trapped during liquid imbibition of a powder bed. The dashed arrow indicates the direction of liquid flow (Börjesson et al., 2017).

Law et al. (2013) investigated the influence of non-uniform liquid penetration in a powder bed, as well as the prevalence of inaccessible voids. It was shown that aggregates resulting from cohesive fine particles were not penetrated by the imbibing liquid. Similarly, in a series of studies, Börjesson et al. (2017, 2014) distinguished between large secluded spaces within a powder bed that had a limited effect on liquid flow but a large effect on porosity, as well as narrow channels that were believed to have had a substantial effect on liquid flow but

contributed little to porosity (Figure 2.19). In one study, up to 75% of the total void space did not take part in liquid imbibition as a result of inefficient particle packing (Börjesson et al., 2017).

Hapgood et al. (2002) coined pores that did not contribute to liquid flow as *macrovoids* (Figure 2.20), and sought to eliminate their fraction of porosity, $\varepsilon_{macrovoids}$, from penetration calculations

$$\varepsilon_{macrovoids} = \varepsilon_{bulk} - \varepsilon_{tap} \quad \text{Equation 2.20}$$

$$\varepsilon_{eff} = \varepsilon_{tap}.(1 - \varepsilon_{macrovoids}) = \varepsilon_{tap}.(1 - \varepsilon_{bulk} + \varepsilon_{tap}) \quad \text{Equation 2.21}$$

where ε_{bulk} and ε_{tap} are the bulk and tapped porosity of the powder bed, respectively.

The resulting effective porosity ε_{eff} was then used, along with the Sauter mean diameter $d_{3,2}$ and particle shape factor φ, to obtain the effective pore radius R_{eff}

$$R_{eff} = \frac{\varphi \cdot d_{3,2}}{3} \cdot \frac{\varepsilon_{eff}}{(1-\varepsilon_{eff})} \quad \text{Equation 2.22}$$

Given that,

$$\varphi = \frac{4A}{\pi \cdot (d_{ML})^2} \quad \text{Equation 2.23}$$

where A is the projected surface area of a nominal particle and d_{ML} is the maximum Feret's diameter.

In an extensive study, Hapgood et al. (2002) showed that by adjusting the Denesuk-Middleman model for ε_{eff} and R_{eff}, the time for droplet absorption was better estimated

$$t_{CDA} = 1.35 \cdot \frac{V_o^{2/3}}{\varepsilon_{eff}^2 \cdot R_{eff}} \cdot \frac{\eta}{\gamma_{LV} \cdot cos\theta} \quad \text{Equation 2.24}$$

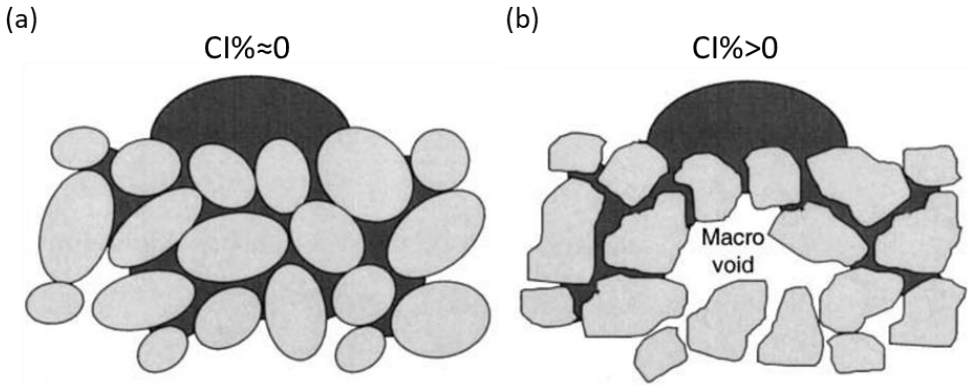

Figure 2.20 (a) Capillarity and liquid flow are relatively uninhibited through a powder bed with efficient particle packing. (b) A powder bed with inefficient particle packing and a heterogenous pore structure containing macrovoids will tend to halt liquid flow when the pore radius increases suddenly. The macrovoid does not contribute to the effective capillary volume or surface area (Hapgood et al., 2002).

As the penetration time is significantly shorter than dissolution times (Liu et al., 2017), Equation 2.24 assumes that the liquid properties and powder bed microstructure remain unchanged throughout the penetration. Additionally, Marmur (1988) detailed two penetration regimes with respect to the temporal development of the droplet contact angle and contact diameter (Figure 2.21). The constant drawing area (CDA) regime involves a droplet radius that remains relatively unchanged for much of penetration whilst the contact angle gradually approaches zero. The decreasing drawing area (DDA) regime exhibits a continually receding contact line whilst the contact angle is relatively constant.

These regimes were later modelled by Denesuk et al. (1993) from the complete penetration time, t_{CDA} or t_{DDA}, and droplet diameter, d_0

$$d(t) = d_0 \cdot \left(1 - \sqrt{\frac{t}{t_{CDA}}}\right)^{\frac{1}{3}} \qquad \text{Equation 2.25}$$

$$d(t) = d_0 \cdot \left(1 - \sqrt{\frac{t}{t_{DDA}}}\right) \qquad \text{Equation 2.26}$$

From the above power law disparity, it is evident that the CDA is the faster of the two regimes. Also, from the literature it appears that CDA is most applicable and is observed more often than DDA, and hence it is used in the Denesuk-Middleman model.

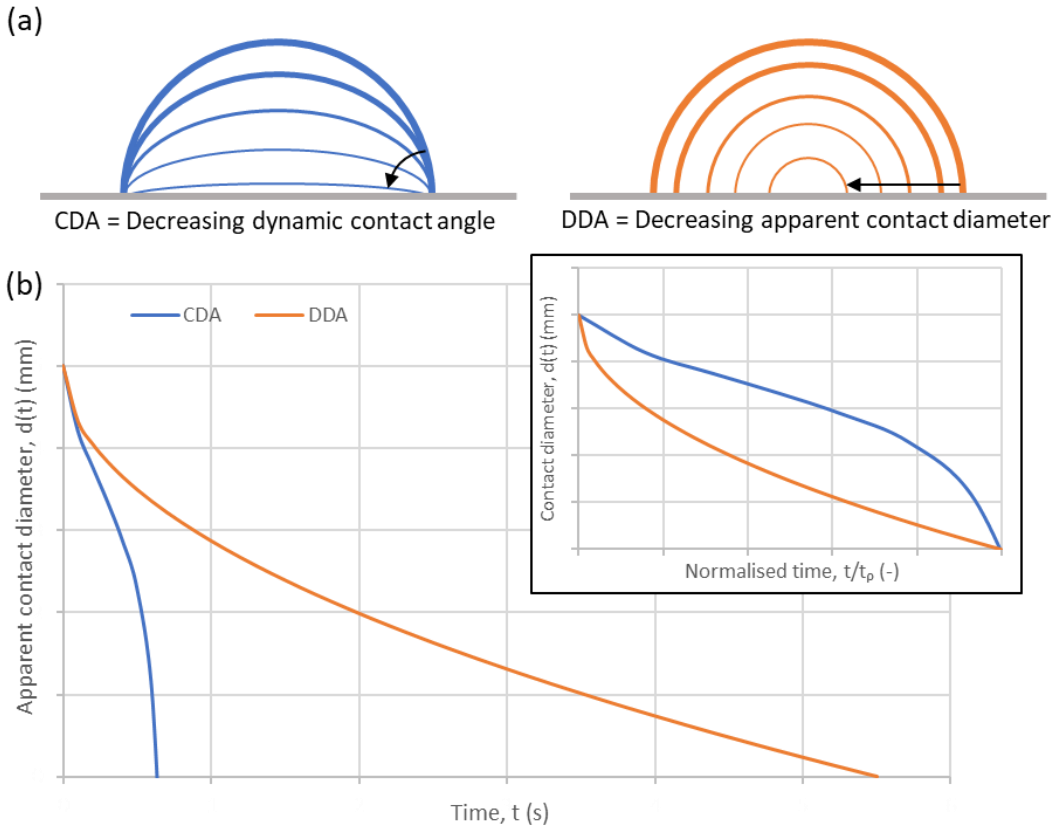

Figure 2.21 (a) Schematics of the temporal development of a droplet's contact diameter and contact angle during imbibition as proposed by Marmur (1998). (b) The contact diameter modelled as a function of time by Denesuk et al. (1993) for both regimes using Equation 2.25 & 2.26. Models are shown with normalised time inset to assist profile comparison.

Following the empirical work of Holman et al. (2002) and Clarke et al. (2002), Hilpert and Ben-David (2009) recognised that the CDA and DDA models failed to account for droplet spreading, and therefore, proposed an additional *increasing drawing area* regime (IDA). Further, it was shown that IDA, CDA and DDA are not mutually exclusive regimes, but rather, sequential regimes of the same penetration process (Hilpert and Ben-David, 2009).

By implementing temporal image analysis, Liu et al. (2017) and Wang et al. (2018) developed an alternative method to characterise powder wettability based on the penetrated volume profile and did not require complete absorption. Much like the WCR method, the contact angle measurements were decoupled from the powder bed microstructure by performing supplementary experiments with a reference liquid that completely wets the powder substrate.

However, for the purposes of this work and continuing from the above discussion, it is evident that the microstructure of the powder bed is fundamental to droplet penetration and, by extension wet granulation, where rapid imbibition is desirable (Hapgood et al., 2003; Schaafsma et al., 2000). It is therefore pertinent to relate the droplet flow rate, *Q,* through the powder bed to the microstructure via Darcy's law

$$Q = \frac{\Delta V}{\Delta t} = -\frac{k \cdot A . \Delta P}{\eta \cdot L} \qquad \text{Equation 2.27}$$

where *k* corresponds to the intrinsic permeability of the powder bed, *A* is the cross-sectional area to flow and *L* is the length over which the pressure drops Δ*P*.

Permeability represents a substrates viscous resistance to flow. Several approaches exist for estimating permeability of a porous substrate, the most notable of these being the Kozeny-Carman formula (Carman, 1937; Kozeny, 1927) which relates permeability to porosity, specific surface area and tortuosity. A representation of the formula adapted by Arns et al. (2005) is shown below

$$k = \frac{f_{pore} \cdot \left(V_{pore}/SA_{pore}\right)^2}{2 \cdot \alpha} \qquad \text{Equation 2.28}$$

where V_p and SA_{pore} represent the volume and internal surface area of the pore space, respectively, and the ratio V_p/SA_{pore} provides an estimate of the pore size comparable to r_{pore}.

f_{pore} is the surface fraction of pores and α represents pore tortuosity (Grzelakowski et al., 2009).

Tortuosity is used to describe how twisted and convoluted the path of travel is during liquid penetration. In its simplest form it is a ratio between the length of interconnected pores between two points and the absolute displacement. It can be estimated from the nominal median particle size, d_{50}, specific surface area , SA_0, and porosity, ε, with Equation 2.29 adapted from Matyka et al. (2008)

$$\alpha - 1 \propto \frac{d_{50}}{4} \cdot \frac{SA_0}{\varepsilon} \qquad \text{Equation 2.29}$$

Tortuosity is the product of the number and size of the inflections encountered by the penetrating liquid which increases with particles size and surface area, but it is inversely proportional to porosity.

As a core feature of imbibition models, particle properties have been investigated in both WCR (Galet et al., 2010; Kiesvaara and Yliruusi, 1993; Kirchberg et al., 2011) and DPM studies (Charles-Williams et al., 2011; Hapgood et al., 2009; Holman et al., 2002; Nguyen et al., 2009) with mixed results. Hapgood et al. (2009, 2002) found that droplet penetration time decreased with increased particle size for lactose monohydrate and glass ballotini. Charles-Williams et al. (2011) recorded a decrease in penetration time of liquid binders with increased lactose grade, as did Nguyen et al. (2009) for lactose and salicylic acid. Kirchberg et al. (2011) observed a linear increase in liquid penetration during WCR tests of iron silicon and magnetite powders with increased size fraction. Additionally, Yang et al. (1988) found the same trend with siliconized beads, whereby the rate of penetration increased with increased particle size.

In other studies, the trend between particle size and penetration has been less linear. Kiesvaara and Yliruusi (1992) found that a significant increase in the liquid penetration rate in lactose was observed by increasing the sieve fraction from <106 µm to 106-212 µm, whereas only a modest increase in penetration was observed with a further increase to >212 µm. These findings are similar to those by Yang et al. (2014) for molybdenite powder; decreasing the particle size below 20 µm was found to decrease penetration but particle size change above 20 µm had little influence on the rate of penetration.

Conversely, Galet et al. (2010) was not able to identify any affirmative relationship between particle size and liquid penetration in WCR experiments. However, in that study, the reason for a lack of trend is not given and may be the result of the particle shape and surface area of each grade – which were not reported - not correlating with the particle size.

Porosity is also expected to influence imbibition. Siebold et al. (1997) critically analysed WCR methodology and demonstrated the importance of controlling particle packing during liquid penetration tests, due to its impact on flow rate. Yang and Xu (2017) investigated DPM of macro-porous sintered copper substrates and found that penetration time decreased with increased porosity. Galet et al. (2010) utilised centrifugal forces as a method to ensure reproducible and controllable particle packing. In that study, it was shown that the liquid penetration of talc powder increased with decreasing porosity, however, the same was not observed for calcium carbonate powder. Hapgood et al. (2002) investigated DPM involving numerous powder-liquid combinations and found that decreased porosity increased penetration rate of inviscid liquids (water) but decreased the penetration rate of viscous liquids (PEG 600). The effect of porosity on the penetration time of droplets of moderate viscosity (PEG 200) was dependent on particle properties.

The relationship between contact area and imbibition is not fully characterised by Darcy's law as it does not account for simultaneous spreading and infiltration. As imbibition and spreading occur on a similar time frame and have competing mechanisms it is necessary to consider one in conjunction with the other (Charles-Williams et al., 2011; Grzelakowski et al., 2009; Haidara et al., 2008; Holman et al., 2002; Mundozah et al., 2018). Holman et al. (2002) recognised that rapid infiltration allowed less time for the droplet spreading to occur, limiting its maximum spread. Grzelakowski et al. (2009) identified that increased tortuosity and narrower pores impeded droplet imbibition but facilitated spreading. It has been proposed that hydrostatic forces generated within the droplet cause the droplet to depress and capillary forces from the surface pores "pin" the contact line to impede further spreading (Haidara et al., 2008). As a result, droplet spreading over a porous substrate during the viscous regime have been observed to scale well below the expected Tanner's law of n~0.1, with higher imbibition rates resulting in greater spreading suppression (Grzelakowski et al., 2009; Haidara et al., 2008). Hydrostatic depression of the contact line is a separate but compounding mechanism to that described by Vaikuntanathan and Sivakumar (2014) and Bico et al. (2001), whereby the droplet became pinned on rough surfaces in a Wenzel state due to the contact line being unable to surmount the asperities or due to a loss of surface energy at the droplet edge (Li et al., 2017) (Figure 2.22). It stands to reason that the higher capillary-induced hydrostatic pressure in the body of the remaining drop could make the contact line more sensitive to topographical variation (Charles-Williams et al., 2011).

Furthermore, according to Charles-Williams et al. (2011), droplet spreading peaked within one-tenth of the total penetration time and corresponded with a critical imbibed volume fraction of the droplet (V_f=[V_0-V(t)]/V_0). This threshold was shown to be inversely

proportional to liquid viscosity, as it was observed that high viscosity binders were able to spread further than less viscous liquids but were pinned at a lower volume fraction, V_f.

Therefore, it is important to consider the evolving droplet contact area in relation to volume depletion. Experimentally, Darcy's flow rate can be profiled throughout imbibition as V_{imb}(Darcy) (in m·s^{-1}) by measuring the temporal change in volume $[(V_0\text{-}V(t))/t]$ through the contact area ($^7/_9 \cdot d(t)^2$):

$$V_{imb}(Darcy) \sim \frac{(V_0 - V(t))}{\frac{7}{9} \cdot d(t)^2 \cdot t} \sim \frac{m^3 \cdot s^{-1}}{m^2} \qquad \text{Equation 2.30}$$

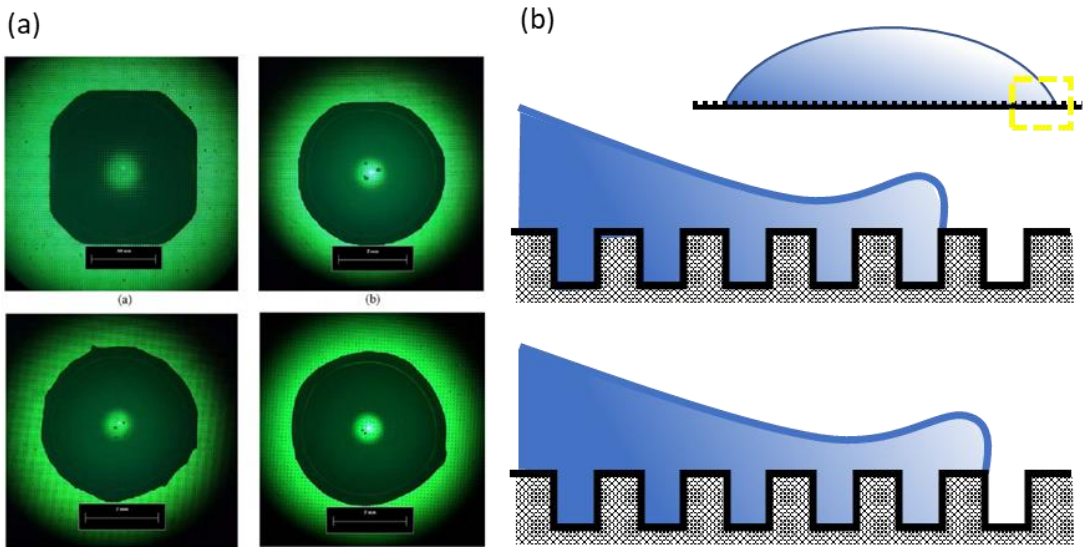

Figure 2.22 (a) Overhead images presenting examples of droplets experiencing directional pinning at the contact line due to the properties of the micro-textured silicon surface arising from the dimensions of the arrayed micro-pillars (Li et al., 2013). (b) Schematic of pinning at the contact line due to spatial heterogeneity resulting in an insurmountable asperity (top) or because of a lack of surface energy beyond the asperity (bottom) (adapted from Li et al., 2017).

Grzelakowski et al. (2009) modified Equation 2.30 to present and compare Darcy's flow rate as a dimensionless parameter by relating the imbibed volume fraction $[(V_0\text{-}V(t))/V_0]$ and the normalised spread area $(d(t)/d_0)^2$ at time t. This was termed the *Darcy adimensional imbibition rate*, V_{imb}(adim):

$$V_{imb}(adim) \sim \frac{[(V_0 - V(t))/V_0]}{(d(t)/d_0)^2 \cdot t} \sim \frac{Imbibed\ volume\ fraction\ per\ second}{Normalised\ contact\ area} \qquad \text{Equation 2.31}$$

The resulting V_{imb}(adim)-versus-time profile can then be scaled as ~Bt^m, where the coefficient B and exponent m can be related to microstructure properties. With permeability proportional to pore radius, $k \propto r_{pore}$, Darcy's law rearranges to an inverse approximation of the Washburn equation, and it is expected that droplet penetration scales as $V_{imb} \sim \sqrt{t}$ accordingly (Schoelkopf et al., 2002). However, Liu et al. (2017) obtained $V_{imb} \sim t^{0.8}$ which highlighted the limitations of traditional DPM analysis derived from the Washburn equation, in which the penetration process is approximated in one dimension. The root dependency of t for imbibition during WCR is a factor of the linear direction of liquid penetration. Although, this further conflicts with findings that droplet penetration originating from a single source point imbibes radially as $V_{imb} \sim t^{1/3}$ (Xiao et al., 2012).

2.3.6. Granule formation

Droplet penetration into a powder bed typically results in particle agglomeration and the formation of a nuclei. Following evaporation, the morphological attributes of the resulting granule further provide information pertaining to the droplet penetration process (Alkhatib, 2015; Emady et al., 2011, 2013a, 2013b; Lee and Sojka, 2012; Marston et al., 2010; Mundozah et al., 2018). Emady et al. (2011, 2013a) developed a regime map, shown in Figure 2.23a, whereby a granule's diameter-to-height aspect ratio could be related to the imbibition mechanism, which in turn, was largely governed by the particle size-derived bond number, Bo_g^* (Equation 2.32). For drop penetration tests (DPT) involving a fine powder and $Bo_g^* > 65{,}000$, a *tunnelling* process was observed, which featured limited droplet spreading and a protracted penetration. The resulting granule was spherical with an aspect ratio close to unity. Coarse powders with a $Bo_g^* < 65{,}000$ demonstrated a *spreading* mechanism,

whereby the droplet spread extensively during penetration, resulting in a shallow disk-shaped granule with a high vertical aspect ratio (VAR).

$$Bo_g^* = \frac{\gamma \cdot \cos\theta}{d_{3,2}^2 \cdot \rho_{true} \cdot g}$$ Equation 1.32

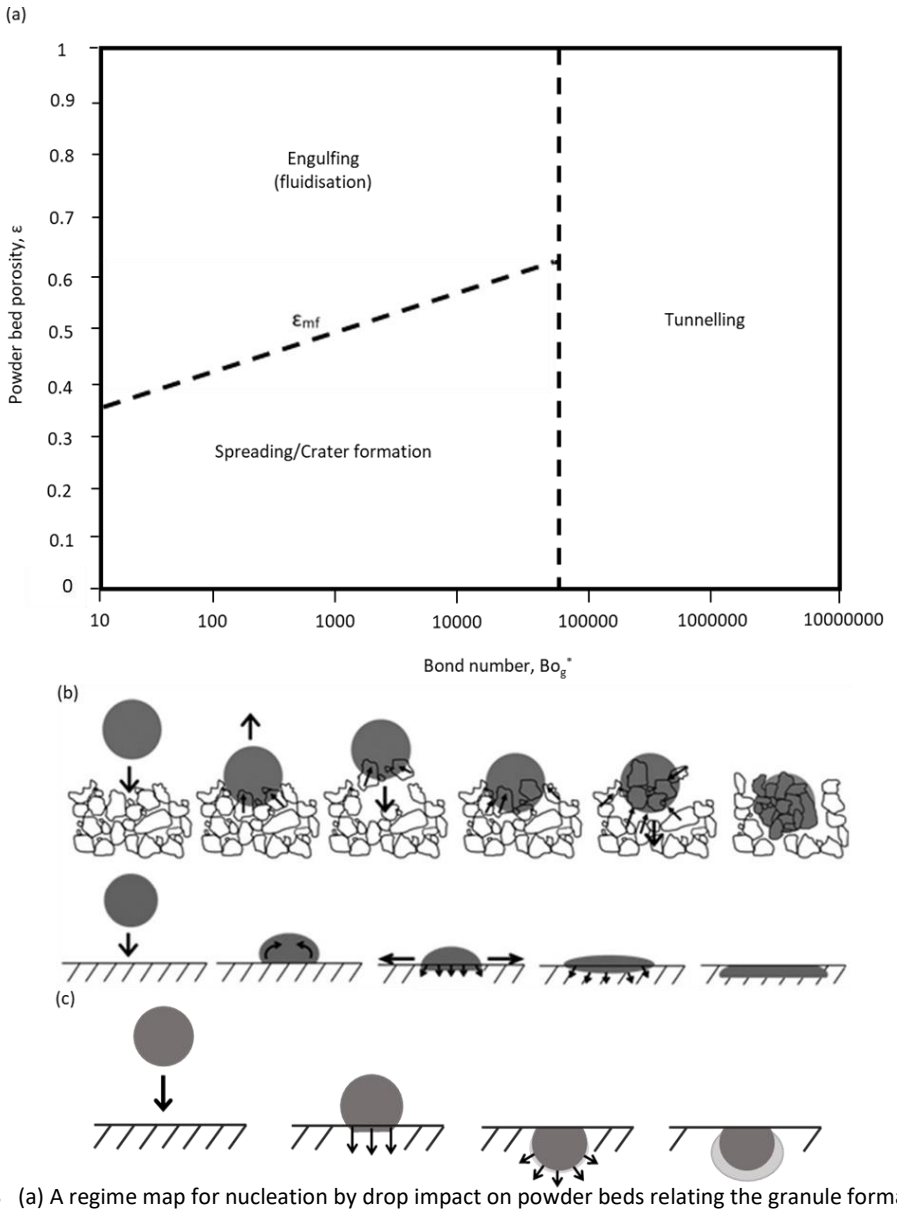

Figure 2.23 (a) A regime map for nucleation by drop impact on powder beds relating the granule formation mechanism to the powder bed properties (Emady et al., 2013). (b) Schematic of the tunnelling and spreading droplet penetration methods resulting in spherical and disk-shaped granules, respectively (Emady et al., 2011). (c) Schematic of late-diffusive intra-spreading resulting in a mushroom-shaped granule composed of a saturated core and unsaturated outer layer, adapted from Nguyen et al. (2009).

Bo_g^* represents a balance between the adhesion tension, $\gamma cos\theta$, of the capillary force acting on a particle (of order $d_{32}\gamma cos\vartheta$) and the gravitational force acting on the particle (of order $d_{32}^3\rho_{true}g$). Thus, here the Bond number is a measure of the relative magnitude of the cohesive force acting on the particle due to liquid bridges (Emady et al., 2013b).

In addition to the spherical and disk-shaped granules, mushroom-like granules with distinct "stalk" and "cap" features have also been reported (Davis et al., 2017; Emady et al., 2011, 2013b, 2013a; Hapgood, 2000; Nguyen et al., 2009). These granules result from nucleation of powders at the transitional boundary between the *tunnelling* and *spreading* mechanism and is also promoted by greater impact velocity upon coarse particles resulting in a *crater formation* mechanism (Emady et al., 2011). Nguyen et al. (2009) describes the origin of the mushroom shape from two distinct regions during penetration; the saturated core during droplet penetration forms the stalk, and the semi-saturated outer layer resulting from radial diffusion forms the cap. These penetration mechanisms are illustrated in Figure 2.23b.

Using X-ray computed tomography (XRCT), Davis et al. (2017) analysed the microstructure of granules resulting from droplet penetration on alumina powders of varying particle size distributions (Figure 2.24). Granules manifested as spherical, mushroom shaped and disk-shaped corresponding to fine (0.5 and 5 µm), medium (25 µm) and coarse (108 µm) powder grades, respectively (Figure 2.24a). XRCT revealed the frequency of macrovoids to be inversely related to particle size (Figure 2.24b). Moreover, by sieving the fine powder and breaking up cohesive aggregates, the size of the pores significantly decreased. This observation indicates that macrovoids in granules are attributed to the powder bed microstructure prior to imbibition and not due to particle migration during liquid evaporation (Davis et al., 2017), as previously reported (Pagnoux et al., 2009).

Mundozah et al. (2018) found the effects of powder hydrophobicity to be analogous to those reported by Emady et al. (2011, 2013) with respect to particle size. At elevated concentrations of magnesium stearate, droplet spreading was increasingly restricted, as was the case during the *tunnelling* mechanism. The subsequent lactose granules decreased in diameter and increased in height to exhibit a diameter-to-height ratio of approximately 1. In addition, by comparing the granule diameter with the footprint of the droplet upon complete imbibition, it was revealed that *late-diffusive intra-spreading* occurred, whereby the liquid continued to radially infiltrate the powder bed following imbibition (Figure 2.23c)

Late-diffusive intra-spreading is responsible for observations made by Nguyen et al. (2009, 2010), whereby granules formed from increasingly hydrophobic formulations could be separated according to their formation mechanism. The semi-saturated outer layer was weak due to limited liquid diffusion and hence, it detached from the stronger saturated core. Further, with increased fraction of the hydrophobic component (salicylic acid) the granule decreased in size and strength as the hydrophobic particles impeded liquid penetration and liquid bridge formation (Nguyen et al., 2009).

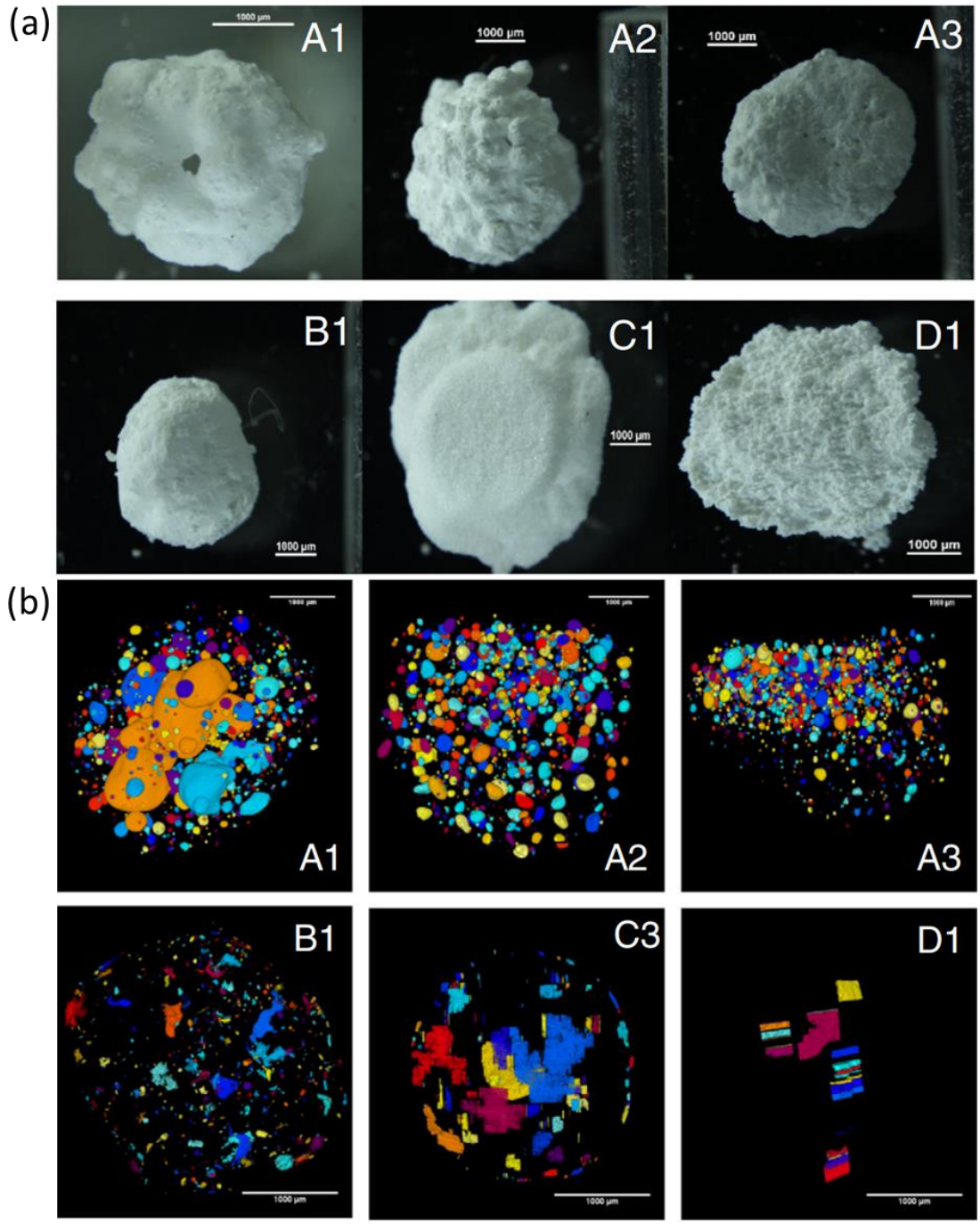

Figure 2.24 (a) Microscopic images of alumina granules whereby A, B, C and D correspond to powder grades of d50=0.5, 5, 25 and 108 µm, respectively. 1, 2 and 3 represent the mesh aperture through which the powder was first sieved; 1.4 mm, 750 and 500 µm, respectively. (b) Images depicting 3D macro-void reconstruction resulting from X-ray computed tomography (Davis et al., 2017). Pores of the same colour are connected.

2.3.7. Conclusion

Liquid distribution during wet granulation has been identified to be highly determinative on the resulting granule size distribution. A disparity in liquid concentration throughout the powder bulk results in an undesirable multimodal size distribution; oversized granules resulting from regions of high concentration, and fine granules or ungranulated powder resulting from regions of low liquid concentration. Homogenous liquid distribution results in a narrow granule size distribution (GSD) that has more favourable properties for tablet manufacture.

Liquid distribution is impeded by materials with poor wetting properties, however, powder wettability has proven a difficult quality to quantify. Droplet spreading and penetration have been shown to be useful metrics for quantifying the interaction between a liquid binder and a powder bed. However, liquid-powder interactions are further complicated by surface roughness, surface pore fraction, and capillarity, which are in turn affected by particle size distribution and particle packing. In the bulk, the powder bed microstructure also contributes to liquid propagation beneath the surface resulting in drastically different granule morphologies.

Droplet penetration tests and nuclei formation are yet to be investigated with respect to bimodal raw materials. This has the potential to manipulate the particle packing and porosity of a powder bed by supplementing the bulk constituent with another grade with a complementary PSD. Additionally, little work has been conducted using multi-component powders, as would be typical in formulations used in wet granulation. Furthermore, the literature possesses a distinct absence of hygroscopic powders.

3. The Effects of Powder Microstructure on Droplet Penetration and Static Nucleation

3.1. Research focus

From a deep body of published work, it is abundantly apparent that the microstructure of the powder bed is of great influence on the nucleation process. A powder bed's microstructure is complex to define and quantify, but manifests as the cumulative effect of surface chemistry, particle shape, size distribution and packing. Operationally, this is further complicated by particle movement during mixing and transport. As a result, well characterised powder properties are fundamental to nucleation control.

The literature features a limited number of powder materials in drop penetration studies, and there exists a noticeable absence of hygroscopic materials. Considering that cellulose-derived powders are significantly hygroscopic and some of the most used excipients in drug formulation, there exists a gap in the fundamental understanding of nucleation.

Many excipients commonly used in wet granulation are derived from animal and plant sources, such as lactose monohydrate and cellulose derivatives (IPEC, 2008). Consequently, the particle properties of these excipients are susceptible to lot-to-lot variability (Dave et al., 2015; IPEC, 2008). Additionally, the PSD specification of commercially available grades are typically broad with only two *not-more-than* or *not-less-than* size limits, and hence, are capable of accommodating a significant degree of variability (Carlson and Hancock, 2006). Moreover, treatment of bulk powders during production, storage, handling, and transport can be inconsistent, invoking further variability.

Therefore, the influence and associated risk of variance on product manufacture and product performance should be understood and managed, as per the QbD guidelines outlined in ICH

Q8(R2) and ICH Q9. It is necessary to investigate variability of all factors simultaneously within the operational space to elucidate an understanding of secondary interactions and compounded variance (L. X. Yu et al., 2014).

In this study, the influence of powder bed microstructure on drop penetration and resulting nuclei morphology will be manipulated and assessed by varying the particle size distribution and doping the main constituent with a second constituent of varying PSD. Furthermore, the porosity of the multi-component wet granulation formulation will be varied to simulate potential consolidation conditions in a continuous twin screw granulator.

3.2. Aims and objectives

The aim of this chapter is to manipulate the microstructure arising from the particle size distribution and consolidation of a multi-component powder bed in order to determine their influence on wetting phenomena and nuclei formation.

3.3. Materials

Two commonly used excipients were used in this investigation: three grades of α-lactose monohydrate (GranuLac 70, 140 and 230, Meggle, Germany) and three grades of microcrystalline cellulose (Avicel PH200, PH105 and PH101, FMCBiopolymer, USA), shown in Figure 3.1. α-Lactose monohydrate, LAC, is a soluble sugar derived from dairy and is utilised as a diluent with brittle fragmentation properties (Al-Ibraheemi et al., 2013). Microcrystalline cellulose, MCC, is an insoluble polymerised cellulose derivative commonly used in solid dosage formulation for its wicking and plastic deformation properties (Lahdenpää et al., 1997).

Each excipient was sieved and then re-constituted into three pseudo-grades termed *Lo*, *Med*

and *Hi* – as detailed in the method below. These pseudo-grades were used to prepare binary mixtures with a 70:30 composition ratio. The inclusion of diluent 70% w/w in prior wet granulation studies forms the rationale for this ratio (Chan Seem et al., 2016; Dhenge et al., 2011; El Hagrasy et al., 2013b; Gorringe et al., 2017; Lee et al., 2012; J. G. Osorio et al., 2017; Saleh et al., 2015; Sayin et al., 2015). Furthermore, as established in the literature, this ratio allows for the greatest particle packing for multi-component powder beds (Aghajan et al., 2019; Bai et al., 2017; Börjesson et al., 2014; Kouraytem et al., 2016; Lam and Nakagawa, 1994; McGeary, 1961; Nordström et al., 2018; Rassouly, 1999; Santiso and Müller, 2002; Ye et al., 2018; Yerazunis et al., 1965; Yu and Standish, 1993)., and hence, allows for the greatest manipulation and experimental range.

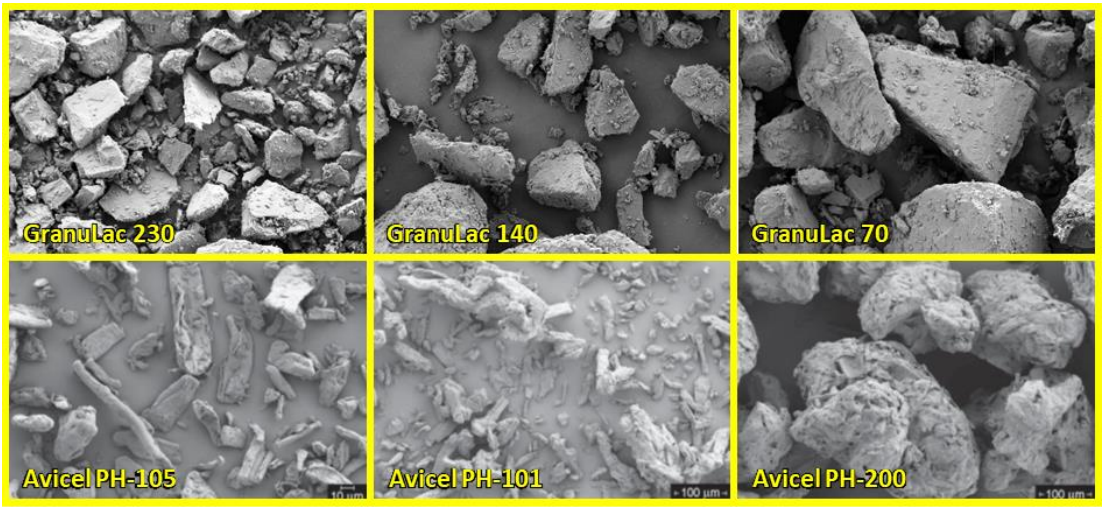

Figure 3.1 SEM images of various stock grades of LAC (top) and MCC (bottom) (Meggle Pharma, 2019, Rowe et al., 2012).

Hypromellose (Pharmacoat 603, Shit-Etsu, Japan), HPMC, solutions were prepared at concentrations of 0 (water), 2.5 and 5% w/v and were used as the penetrating liquid binder. First, a 5% w/v solution was prepared by solubilising 10 g HPMC into 200 mL purified water (Milli-Q Water Purification System, Merck Millipore, USA) using a magnetic stirrer and hotplate heated to 50°C. After 12 hours, 100 mL was removed and cooled, whilst the remaining solution was diluted to 2.5% w/v with the addition of 100 mL purified water and

further heated and stirred. The solution was covered throughout preparation and storage to prevent evaporation.

3.4. Method

3.4.1. Pseudo-grade creation and formulation

The commercial grades of LAC and MCC were sieved across a nest of ten 400 mm sieves consisting of R40/3 meshes (25, 38, 45, 53, 63, 75, 90, 106, 125 and 150 µm, FRITSCH GmbH, Germany) using an electromagnetic driven sieve shaker (Titan 450, Endecotts, UK), resulting in 11 size fractions. Each fraction was divided into eight equal parts using a rotary sample divider (LABORETTE 27, FRITSCH GmbH, Germany). The eighths were then reconstituted to create three pseudo-grades, denoted Hi, Med and Lo. This is shown in Figure 3.2 for LAC and Figure 3.3 for MCC.

Each formulation consisted of a binary *A*:*B* mixture with a 70:30 weighting. Ingredient *A* was always one of the three LAC pseudo-grades, whilst *B* was either a LAC pseudo-grade or a MCC pseudo-grade. Each mixture consisted of one pseudo-grade being "doped" with another pseudo-grade, resulting in a unimodal PSD if the two pseudo-grades matched or a bimodal PSD if the two pseudo-grades differed.

The naming convention used henceforth consists of the excipient, followed by the concentration and pseudo-grade. For example, a formulation composed of the coarse pseudo-grade, *Hi*, of LAC doped with the fine pseudo-grade, *Lo*, of MCC will be referred to as LAC_70_Hi:MCC_30_Lo. Where absolute specificity is not necessary, or no ambiguity exists, an abbreviation of this format may be used for expedience.

Batches were prepared as 300 g batches and blended for 15 minutes in a 1 L cone vessel with a tumble speed of 15 rpm and agitator speed of 200 rpm (AgiBlend AB-015, Pharmatech, UK).

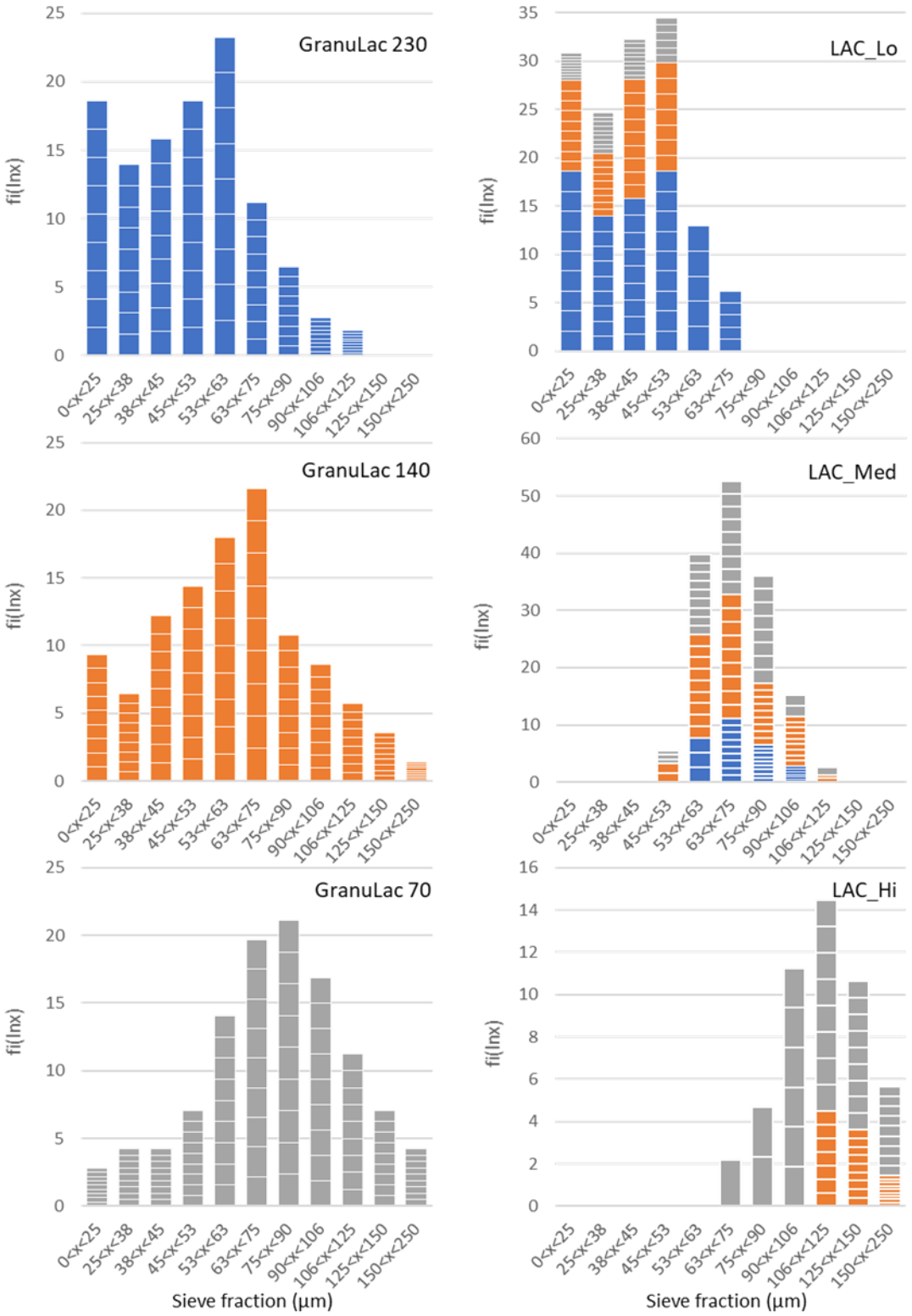

Figure 3.2 Lactose sieve fractions of commercial grades (left) and sieve fractions of reconstituted pseudo-grades (right). Each sieve fraction of the commercial grades was divided into eight equal parts - represented here by individual blocks. These were then reconstituted into the pseudo-grades, with colour representing the originating commercial grade. Where $f_i(\ln x)$ is the lognormal distribution of mass frequency (f) of particles of diameter x in sieve fraction with size interval i. Note: y-axes are not equal.

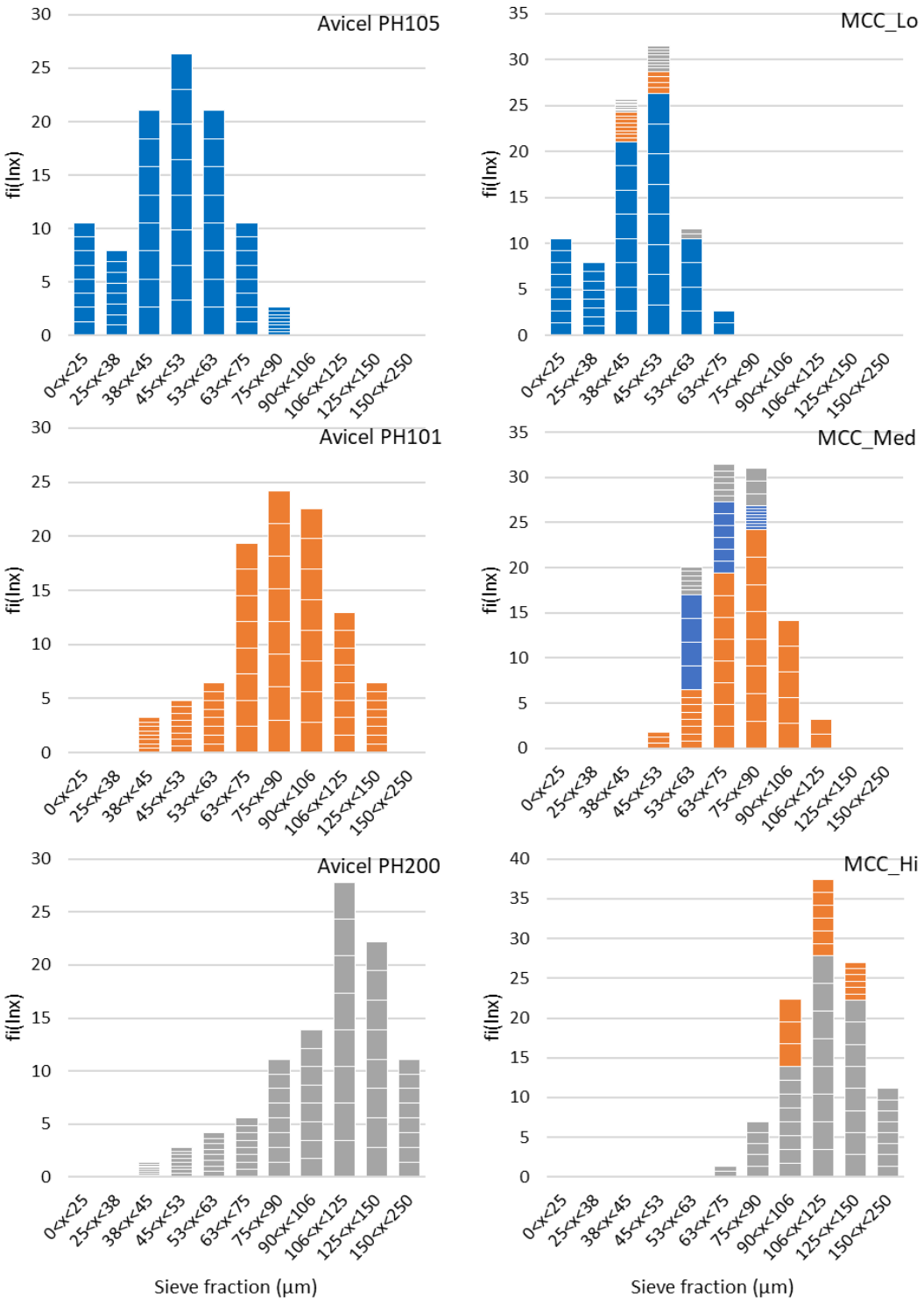

Figure 3.3 Microcrystalline cellulose sieve fractions of commercial grades (left) and sieve fractions of reconstituted pseudo-grades (right). Each sieve fraction of the commercial grades was divided into eight equal parts - represented here by individual blocks. These were then reconstituted into the pseudo-grades, with colour representing the originating commercial grade. Where $f_i(\ln x)$ is the lognormal distribution of mass frequency (f) of particles of diameter x in sieve fraction with size interval i. Note: y-axes are not equal.

3.4.2. Material characterisation

The particle and powder properties of each ingredient, grade and formulation permutation were characterised. The particle size and shape distribution were measured in triplicate using a QICPIC with the RODOS dispersing system (Sympatec GmbH, Germany). An FT4 Powder Rheometer (Freeman Technology, USA) was used to measure the flow function, FF_c, of each sample using the 25 mm setup. Additionally, the powder rheometer was used to measure the bulk density following a conditioning cycle, as described - and verified to be comparable to the USP method - elsewhere (Hughes et al., 2014). Tapped density was measured using automated tapping apparatus (Autotap, Quantachrome, UK) in accordance with USP 616 (United States Pharmacopeial Convention, 2015). The true particle density was obtained from 10 measurements using helium displacement (Accupyc II 1340 Pycnometer, Micromeritics, USA). The BET specific surface area was measured from nitrogen adsorption isotherms obtained using gas sorption analysis (Autosorb iQ, Quantachrome, UK).

After calculating the density of each test liquid ($\rho_{liq}=m/V$), the viscosity, η, was determined experimentally using the Höppler principle utilising a falling sphere setup and Equation 3.1. The time, t, for a chrome steel ball bearing (d=15 mm) to sink through a constant length of descent (l_d=400 mm) of test liquid in a measuring cylinder was recorded to determine the sphere's descent velocity ($u=l_d/t$).

$$\eta = \frac{2\cdot(\rho_{sph}-\rho_{liq})\cdot g\cdot {r_{sph}}^2}{9\cdot u} \qquad \text{Equation 3.1}$$

where ρ_{sph} and ρ_{liq} are the respective densities of the test sphere and liquid, g is acceleration due to gravity, and r_{sph} is the radius of the test sphere. Even though HPMC does possess non-Newtonian properties, the falling sphere test was chosen to determine viscosity for its

simplicity, instead of profiling viscosity as a function of temperature and shear using a rheometer. Further, HPMC demonstrates Newtonian behaviour at low concentrations (≤10%) and relatively low temperatures (≤70°C) (Silva et al., 2008), which meets the conditions of the droplet penetration test. The properties of the test liquids are listed in Table 2.

Table 2 Measurements of the physical properties of the test liquids.

HPMC conc. (%w/w)	Density, ρ_{sph} (g/ml)	Viscosity, η (mPa·s)	Surface tension, γ (mN/m)	Drop diameter, d_0 (mm)	Capillary length, l_c (mm)	Weber number, We (-)
0	0.997	1.01	72.59*	2.21	2.72	8.21
2.5	1.003	4.27	46.4*	2.03	2.17	9.13
5	1.011	14.33	46.3*	2.11	2.16	4.10

*Values taken from literature.

3.4.3. Drop penetration test

Drop penetration tests, DPT, were performed for each of the formulation permutations. This involved a single droplet being dropped from a small height onto the surface of a static powder bed whilst being recorded via high-speed image capture. This allowed the movement, dimensions, contact angle and imbibition of the droplet to be measured as a function of time.

The powder bed of each ingredient and formulation was tested at three consolidation conditions (PBD): loosely consolidated (bulk density, ρ_{bulk}), fully-consolidated (tapped density, ρ_{tap}) and semi-consolidated ($\frac{\rho_{tap}-\rho_{bulk}}{2} + \rho_{bulk}$). As in other studies (Emady et al., 2013a; Z. Liu et al., 2017), the FT4 Powder Rheometer – with the 23.5 mm blade setup – was used to ensure the powder bed densities were reproducible. To prepare the loose consolidation condition each powder bed was subjected to a conditioning cycle, whereby the rotating blade repeatedly traversed up and down the powder bed until no further changes in

rotational torque were detected. For fully-consolidated conditions the powder bed was tapped 2000 times, or until no further decrease in volume was observed. To produce the semi-consolidated condition the powder bed was first conditioned and then subjected to gradual tapping. The number of taps administered to the conditioned powder bed was incrementally increased until a density equidistant from the bulk and fully-consolidated density was achieved.

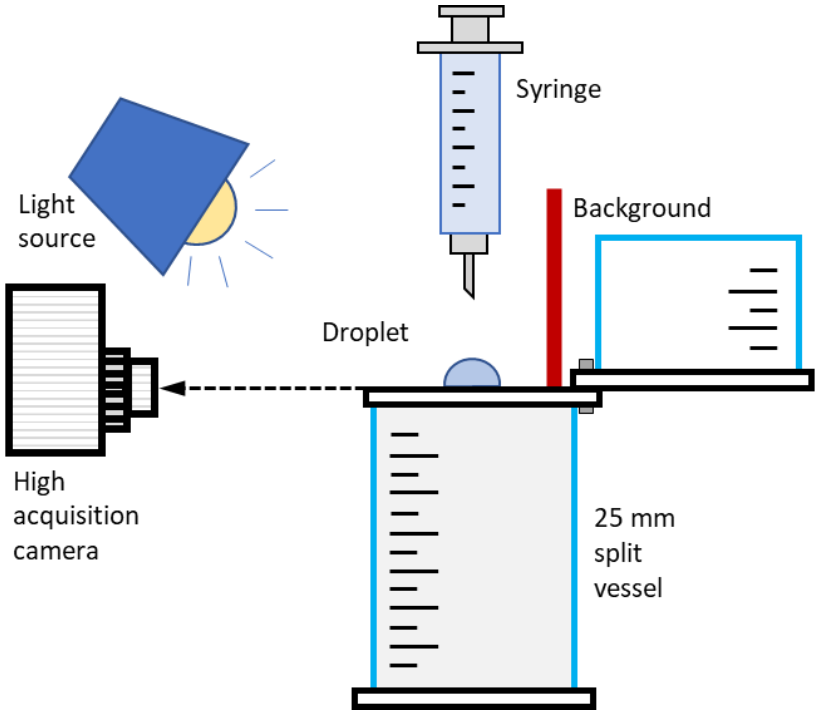

Figure 3.4 Experimental setup for the droplet penetration tests.

The FT4's split vessel (25 mm x 25 ml) was used to contain the powder bed as the splitting mechanism allowed a smooth surface to be revealed with minimal disturbance to the bulk, as previously described (Emady et al., 2013a; Wang et al., 2018). The mass of the powder bed was then measured, and the density calculated.

A vertically orientated syringe discharged a droplet of liquid binder from a height of 5±0.5 mm above the powder bed surface and off-centre. After each test the FT4 vessel was rotated approximately 70° and the test was repeated to obtain a total of five tests per prepared

powder bed (n=5, except for the centre points n=9 - see section 3.4.5 *Experimental Design* below). This was repeated three times resulting in 15 granules per experimental condition.

To obtain droplets of approximately 10 µL a 30-G needle was used for water and a 28-G needle was used for the HPMC liquids (BD Micro-Fine Plus 0.5ml, Becton Dickinson, USA). A digital camera with 40x slow motion capabilities (Sony DSC-RX100 V, Sony Corporation, Japan) was positioned level with the powder bed surface and recorded each DPT at an image acquisition rate of 960 frames per second. This allowed a temporal accuracy to ±1.04 ms. A schematic of the DPT setup is shown in Figure 3.4. Only one DPT was recorded and analysed per experiment condition.

The impact velocity, u_i, was calculated from the image sequence prior to impact and was found to be approximately 0.792±0.079 m/s, 0.712±0.073 m/s and 0.679±0.068 m/s for 0, 2.5 and 5% w/w HPMC, respectively.

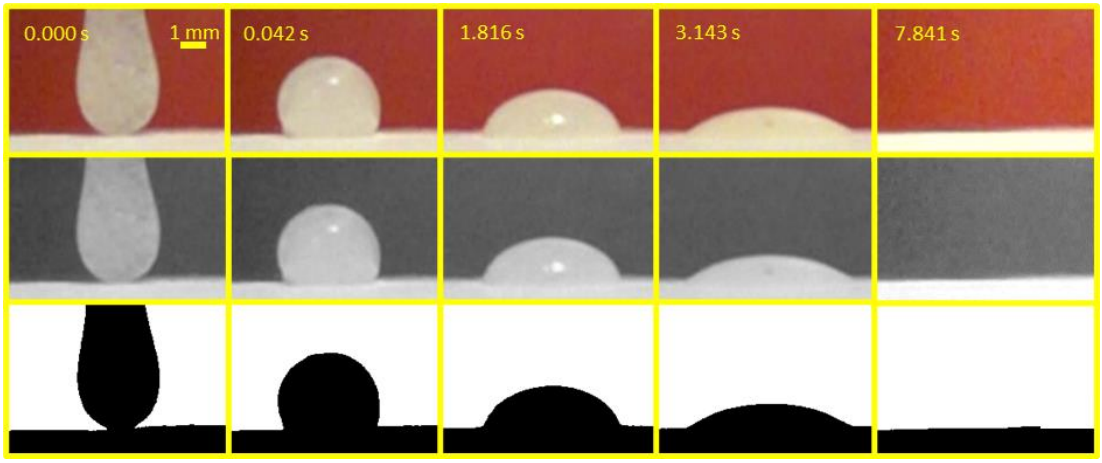

Figure 3.5 A representation of the treatment process by converting each image frame (top) to 8-bit greyscale (middle) and then to 1-bit binary (bottom) for reproducible edge detection.

Each frame from the video footage was extracted into individual images (VideoPad Video Editor v4.30, NCH Software, Australia) and analysed using image processing software (ImageJ 1.51j8, National Institute of Health, USA). By transforming each image into a binary black

and white image in accordance with a predetermined threshold value (170), it ensured that edge detection was consistent for all images and tests (Figure 3.5). A macro was created to treat and segment each frame into a series of horizontal slices, one pixel in height, and the droplet diameter (d_i) within each horizontal slice was measured (Figure 3.6). The spatial resolution was 16.2 µm per pixel.

In the literature, it is common for the volume of the droplet fraction yet to be imbibed at time *t* to be estimated from *d*(t) and *h*(t) by assuming it to be a spherical cap and using Equation 3.2 (Berthier, 2013).

$$V_t = \frac{\pi}{6} \cdot h_t \cdot (3d_t^2 + h_t^2) \qquad \text{Equation 3.2}$$

In the current study, the droplet often did not immediately assume a spherical cap shape, and Equation 2.2 was found to underestimate the volume during the early stages of imbibition, particularly for experimental conditions involving higher viscosities and fine pseudo-grades. Therefore, an alternative approach was employed in this work. Assuming the droplet was axisymmetric and circular, the droplet volume yet to be absorbed at time *t* was estimated to be the cumulative volume of a series of stacked cylinders, each one pixel in height (0.0162 mm), using Equation 3.3. The contact area of the droplet-surface interface was determined from the diameter of the bottom-most slice (Figure 3.6).

$$V_t^{2/3} = \sum_{i=1}^{n} \pi \cdot \left(\frac{d_t}{2}\right)^2 \cdot h \qquad \text{Equation 3.3}$$

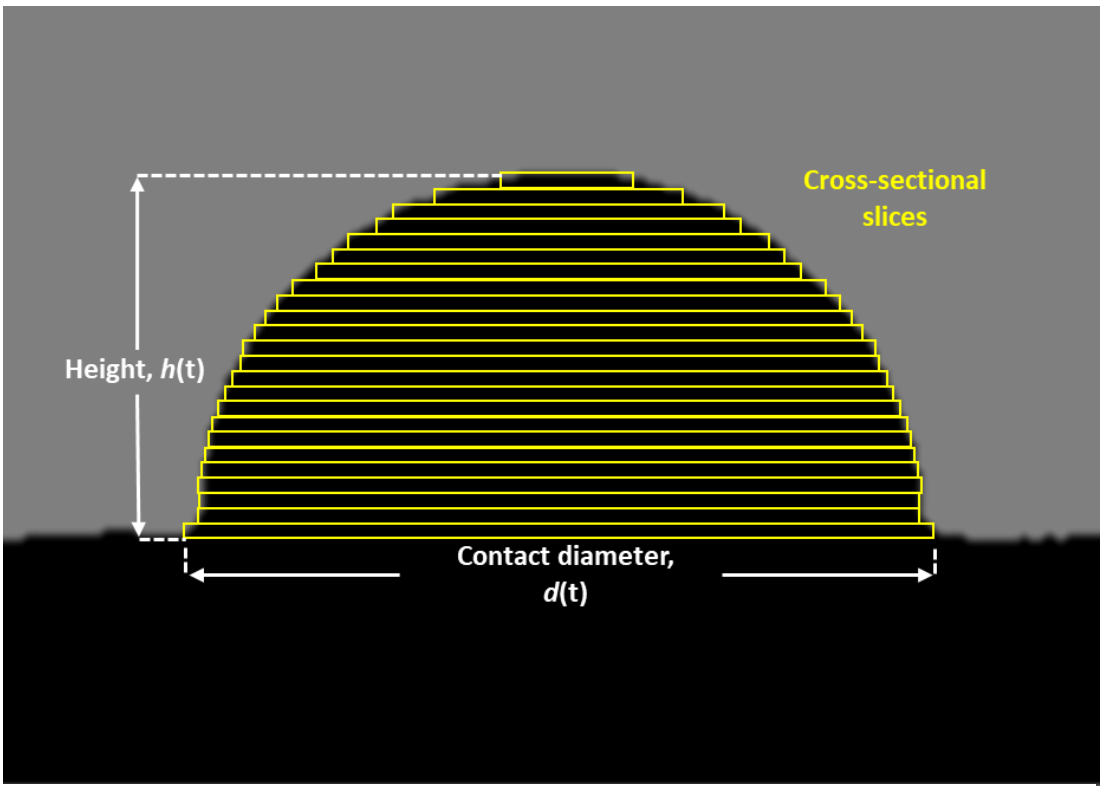

Figure 3.6 A representation of measurements obtained from image analysis (not-to-scale). In practice each cross-sectional slice had a height of 1-pixel, corresponding to 16.2 µm.

3.4.4. Granule characterisation

Following imbibition, the subsequent powder bed was left to dry at ambient conditions for 72 hours before being gently sieved using a 500 µm mesh sieve to retain the nuclei. The mass of each individual nucleus was recorded, and the overhead and side profile projection area of each nucleus was measured from digital photographs taken from a fixed distance against a contrasting surface. ImageJ software was used to isolate each nucleus and measure the corresponding area, as shown in Figure 3.7. From this, the diameter of a circle of equivalent projection area (EQPC) was calculated.

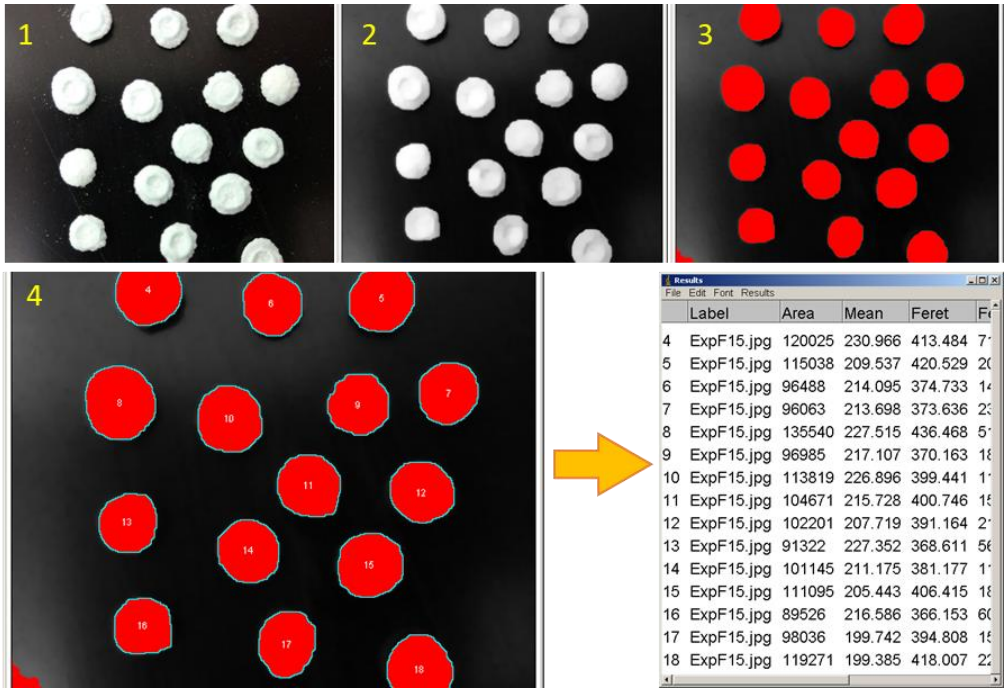

Figure 3.7 Sequential treatment process used to measure granule dimensions and area. (1) initial image, (2) conversion to 8-bit greyscale image and gaussian blur to eliminate small particles, (3) adjust threshold to mark structures, (4) label each structure to match corresponding measurements.

Archimedes' principle was used to measure the envelope volume of the nuclei. The envelope volume corresponded to the granule exterior, so that the internal pores and fractures were included. The volume of 150 g of free-flowing glass ballotini (d_{50}=27.3 µm, SiLibead, Sigmund Lindner GmbH, Germany) was measured after 100 taps in a 250 mL glass measuring cylinder.

This was then gently poured over a sample of 15 granules in a second 250 mL glass measuring cylinder. This was then tapped 100 times and the increase in volume was recorded. This was used to calculate the mean average envelope volume. The mass was then gently sieved using the 500 µm aperture mesh to retrieve the granules. The measured mass and volume were used to calculate the mean nuclei density and porosity.

3.4.5. Experimental design and analysis

Each powder consisting of a single excipient and grade was characterised. To evaluate the 70:30 binary mixtures, a full factorial design of experiments was used to evaluate the influence of PSD on the flow and packing properties of each formulation combination. This involved 9 experimental conditions for each blend of two pseudo grades as LAC:LAC or LAC:MCC, as outlined in section 2.3 and presented in Table 3. As the $d_{3,2}$ of LAC_Med and MCC_Med were not equidistant between the *Lo* and *Hi* pseudo-grades, a non-zero value was assigned as the medium level accordingly i.e. -0.16 and -0.32 for the medium grades of LAC and MCC, respectively.

Table 3 Full factorial DoE of binary mixtures consisting of two pseudo-grades to evaluate powder properties. The levels correspond to the values listed beneath.

	LAC_70	LAC_30	MCC_30
1	-1	-1	-
2	-1	-0.16	-
3	-1	+1	-
4	-0.16	-1	-
5	-0.16	-0.16	-
6	-0.16	+1	-
7	+1	-1	-
8	+1	-0.16	-
9	+1	+1	-
10	-1	-	-1
11	-1	-	-0.32
12	-1	-	+1
13	-0.16	-	-1
14	-0.16	-	-0.32
15	-0.16	-	+1
16	+1	-	-1
17	+1	-	-0.32
18	+1	-	+1

LAC, $d_{3,2}$ (µm)		MCC, $d_{3,2}$ (µm)	
+1	114.7	+1	206.8
-0.16	68.9	-0.32	93.4
-1	37.7	-1	39.3

For the drop penetration tests and nucleus formation, two sets of central composite face-centred designs, involving 27 experimental conditions each (including three repeated centre points) were performed to evaluate the main and secondary effects of each factor (LAC_70 PSD, LAC/MCC_30 PSD, HPMC and PBD). One set included LAC_30 as the secondary "doping" component and the other set included MCC_30. The design of experiments is outlined in Table 4.

Multiple linear regression (MLR) models were derived from the data set for each response and are presented as coefficient plots and response surfaces (RSM). A confidence level of 95% was applied throughout to determine statistical significance, and coefficient (Q^2).

The experimental design and analysis were performed using Modde 12.1 (Umetrics, Sartorius AG, Sweden).

Table 4 Central composite face-centred DoE including repeated centre points - experiments 25, 26 and 27. The levels for each variable correspond to the values listed beneath.

	LAC_70	LAC_30 or MCC_30		HPMC	PBD
1	-1	-1		-1	-1
2	+1	-1		-1	-1
3	-1	+1		-1	-1
4	+1	+1		-1	-1
5	-1	-1		+1	-1
6	+1	-1		+1	-1
7	-1	+1		+1	-1
8	+1	+1		+1	-1
9	-1	-1		-1	+1
10	+1	-1		-1	+1
11	-1	+1		-1	+1
12	+1	+1		-1	+1
13	-1	-1		+1	+1
14	+1	-1		+1	+1
15	-1	+1		+1	+1
16	+1	+1		+1	+1
17	-1	-0.16	-0.32	0	0
18	+1	-0.16	-0.32	0	0
19	-0.16	-1		0	0
20	-0.16	+1		0	0
21	-0.16	-0.16	-0.32	-1	0
22	-0.16	-0.16	-0.32	+1	0
23	-0.16	-0.16	-0.32	0	-1
24	-0.16	-0.16	-0.32	0	+1
25	-0.16	-0.16	-0.32	0	0
26	-0.16	-0.16	-0.32	0	0
27	-0.16	-0.16	-0.32	0	0

LAC, $d_{3,2}$ (µm)		MCC, $d_{3,2}$ (µm)		HPMC (%w/w)		PBD (packing)	
+1	114.7	+1	206.8	+1	5	+1	Full
-0.16	68.9	-0.32	93.4	0	2.5	0	Semi
-1	37.7	-1	39.3	-1	0	-1	Loose

3.5. Results

3.5.1. Excipient characterisation

The measurements obtained from dynamic particle sizing, powder rheometry, gas sorption and pycnometry are outlined in Table 5. Figure 3.8 shows that the powder properties that were most sensitive to PSD were bulk density, surface area, flow function and compressibility index, whereas aspect ratio and tapped density were less dependent. From Figure 3.9, particle size distributions of the pseudo-grades were characterised by a more normal distribution, narrower span, and reduced overlap than their stock grade counterparts.

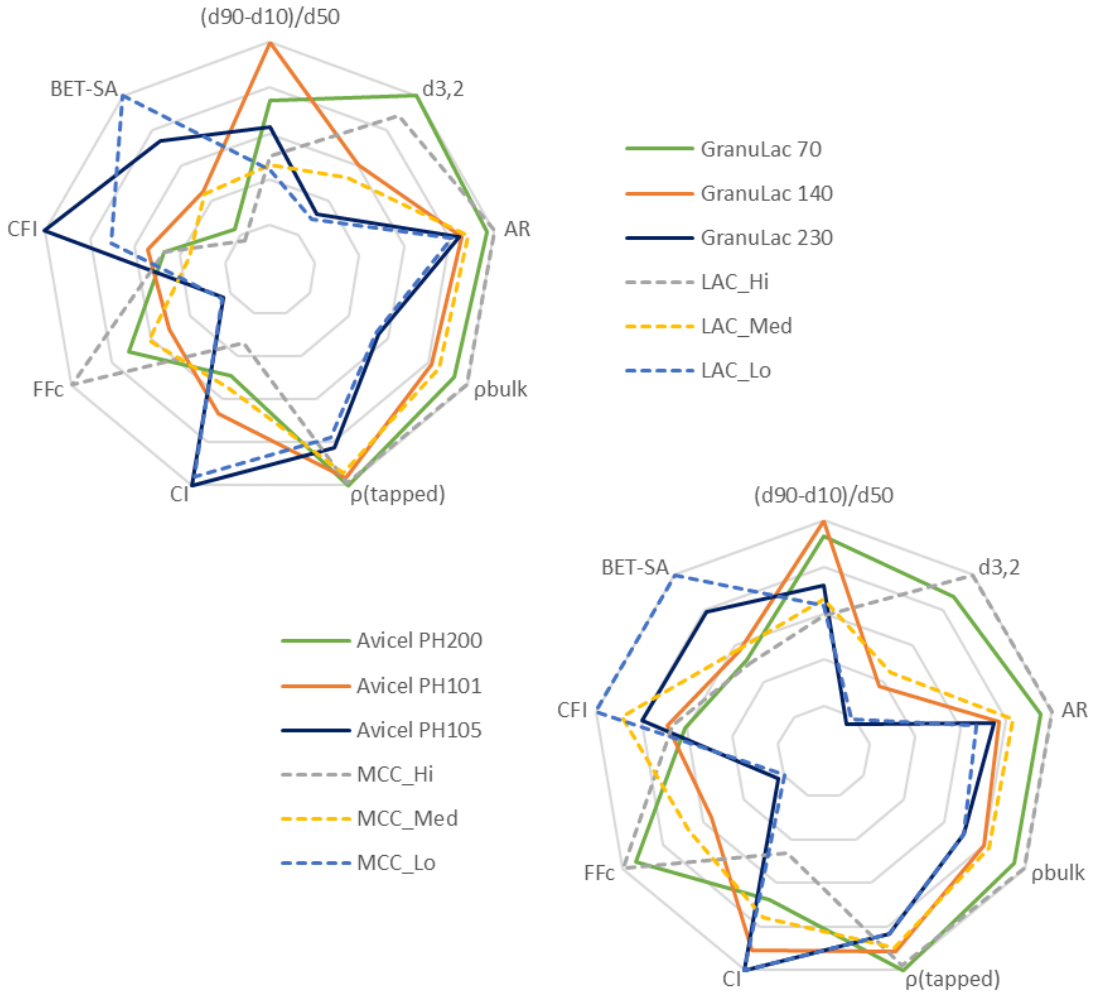

Figure 3.8 Radar chart comparing normalised powder properties for LAC (top) and MCC (bottom) commercial grades and pseudo grades. Where $(d_{90}-d_{10})/d_{50}$ is PSD span, $d_{3,2}$ is Sauter mean diameter, AR is aspect ratio, ρ_{bulk} is bulk density, ρ_{tapped} is tapped density, CI is compressibility index, FF_c is flow function, CFI is consolidation flow index, and BET-SA is specific surface area.

Table 5 Measurements of the physical properties of the stock grades, pseudo-grades and sieve fractions of LAC and MCC.

	QICPIC						Accupyc	FT4 Rheometer			Autosorb		
	d_{10} (µm)	d_{50} (µm)	d_{90} (µm)	Span $(^{d90/d10}/_{d50})$	SMD $d_{3,2}$ (µm)	Aspect ratio	True density (g/cm^3)	Bulk density (g/cm^3)	Tapped density (g/cm^3)	Compressibility index (%)	Multi-point BET surface area (m^2/g)	Total pore volume (µl/g)	Average pore radius (nm)
GranuLac 70	41.3	127.3	223.1	1.43	129.9	0.81	1.545	0.71	0.90	21.1	0.22	1.159	14.87
GranuLac 140	24.3	68.5	155.3	1.91	78.2	0.72	-	0.62	0.87	28.7	0.42	2.344	11.42
GranuLac 230	18.8	40.4	67.4	1.20	42.2	0.71	-	0.42	0.74	43.2	0.69	4.534	9.80
LAC Hi	87.4	168.2	248.7	0.96	114.7	0.84	-	0.76	0.89	14.6	0.16	1.090	14.95
LAC Med	37.2	63.2	93.2	0.89	68.9	0.74	-	0.65	0.85	23.5	0.41	2.171	10.99
LAC Lo	17.9	28.3	41.6	0.84	37.7	0.68	-	0.41	0.70	41.4	0.93	4.880	7.29
LAC 106-125 µm	117.9	142.3	226.5	0.34	151.1	0.81	-	0.78	0.87	10.3	0.15	0.988	14.58
LAC 53-63 µm	46.7	62.1	78.0	0.52	72.2	0.76	-	0.68	0.80	15.0	0.39	2.051	11.51
LAC 25-38 µm	22.6	34.2	43.8	0.62	41.7	0.77	-	0.44	0.69	36.2	0.78	4.492	7.98
Avicel PH200	87.2	204.7	366.3	1.37	180.4	0.78	1.591	0.38	0.47	19.1	1.01	5.419	9.51
Avicel PH101	34.9	70.4	137.9	1.47	76.5	0.63	-	0.32	0.43	25.5	1.16	6.012	11.52
Avicel PH105	16.6	31.1	49.5	1.06	32.1	0.61	-	0.28	0.39	28.2	1.54	13.819	13.03
MCC Hi	170.4	286.6	421.3	0.87	206.6	0.82	-	0.4	0.46	13.0	0.94	5.359	9.66
MCC Med	50.3	92.3	138.8	0.97	93.3	0.68	-	0.33	0.42	21.4	1.13	5.968	11.48
MCC Lo	14.7	27.4	39.7	0.93	39.3	0.55	-	0.28	0.39	29.7	1.62	12.720	14.83
MCC 125-150 µm	222.5	289.6	425.8	0.70	281.5	0.86	-	0.41	0.45	8.8	0.91	5.223	9.72
MCC 53-63 µm	58.5	87.1	102.1	0.51	91.2	0.64	-	0.35	0.41	14.6	1.13	5.931	11.85
MCC 25-38 µm	19.7	33.2	46.9	0.82	37.6	0.48	-	0.27	0.38	28.9	1.56	12.852	13.29

An analysis of variance (ANOVA) shows that pseudo-grade PSDs possessed lower variance values (sd^2) than the stock grades. However, only LAC_Med was significantly different statistically from GranuLac 140 (p=0.002), whereas LAC_Hi and LAC_Lo were statistically insignificant from their stock counterparts (p=0.381 and p= 0.217, respectively). With that said, the differences between LAC_Hi and LAC_Med, and LAC_Med and LAC_Lo were statistically significant ($p \leq 0.01$) whereas the difference between GranuLac 70 and GranuLac 140 was not (p=0.135).

Although pseudo-grades MCC_Hi, MCC_Med and MCC_Lo had lower variance values, they were not statistically different from Avicel PH200 (p=0.368), Avicel PH101 (p=0.368), and PH105 (p=0.258), respectively. The difference between the three pseudo-grades was significant (p<0.001).

MCC had a significantly greater surface area and porosity than LAC despite a comparable PSD. By considering the method of manufacture and the scanning electron microscope (SEM) images shown in Figure 3.1, the source of these differences becomes apparent; α-lactose monohydrate particles resulted from crystallisation and are tomahawk-shaped (Edge et al., 2006), whereas MCC was prepared via spray drying and present as elongated fibres (Galichet, 2006). Consequently, MCC had a significantly more porous structure than LAC with the vast majority of the measured surface area being internal (Doelker, 1993). Hence, the surface area of MCC was not solely dependent on the PSD as was the case for LAC (Gamble et al., 2011). This was because MCC's coarser particles were in fact, a collection of tightly aggregated smaller primary particles (Gamble et al., 2011).

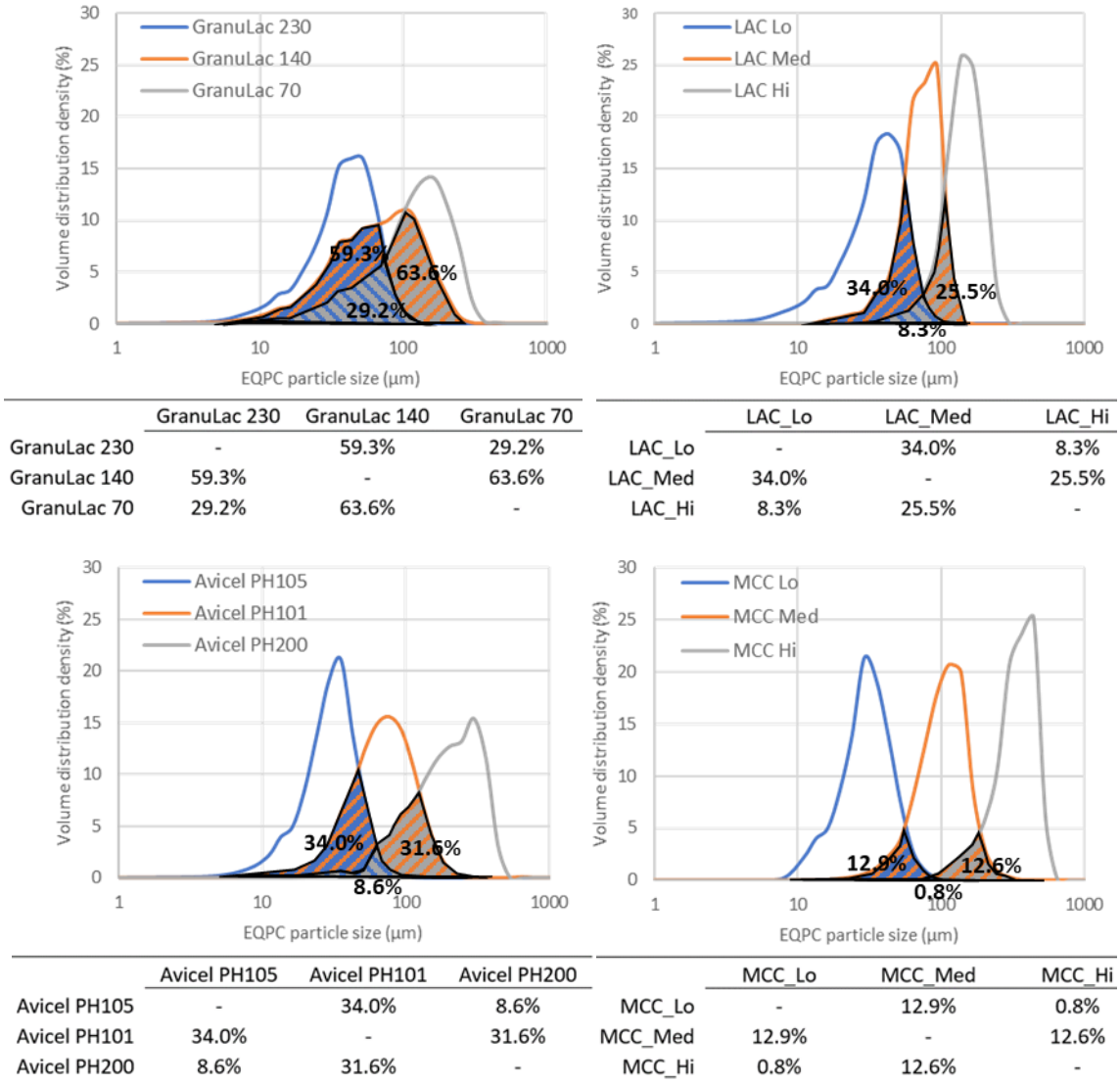

	GranuLac 230	GranuLac 140	GranuLac 70
GranuLac 230	-	59.3%	29.2%
GranuLac 140	59.3%	-	63.6%
GranuLac 70	29.2%	63.6%	-

	LAC_Lo	LAC_Med	LAC_Hi
LAC_Lo	-	34.0%	8.3%
LAC_Med	34.0%	-	25.5%
LAC_Hi	8.3%	25.5%	-

	Avicel PH105	Avicel PH101	Avicel PH200
Avicel PH105	-	34.0%	8.6%
Avicel PH101	34.0%	-	31.6%
Avicel PH200	8.6%	31.6%	-

	MCC_Lo	MCC_Med	MCC_Hi
MCC_Lo	-	12.9%	0.8%
MCC_Med	12.9%	-	12.6%
MCC_Hi	0.8%	12.6%	-

Figure 3.9 Particle size distribution of the stock grades (left) and pseudo grades (right) of α-lactose monohydrate (top) and microcrystalline cellulose (bottom) as obtained via QICPIC particle sizing (averaged from triplicate measurements). The shaded region and accompanying tables indicate the PSD overlap between the various associated grades. EQPC is the diameter of a circle with an equivalent projection area as the measured particle.

Typical particle size related behaviours were observed, such as lower flow function (FF_c) and increased compressibility index (CI%) with decreasing particle size (Figure 2.11 and Figure 2.12, respectively), indicating reduced flowability (Köhler and Schubert, 1991; Liu et al., 2008, 2015; Ouchiyama and Tanaka, 1986). The increase in shear yield strength and decrease in packing efficiency was the result of increased area-to-mass ratio with decreasing particle size,

as particles smaller than 100 µm typically have a greater potential for cohesive inter-particle interactions to arise and were less susceptible to gravitational and shear forces (Israelachvili, 1989; Visser, 1989). Hence, PSD measurements have been the basis of models used to predict flow behaviour of new powdered pharmaceutical materials (Leyva and Mullarney, 2009), along with particle shape (Yu et al., 2011), surface area and surface energy (Barjat et al., 2020).

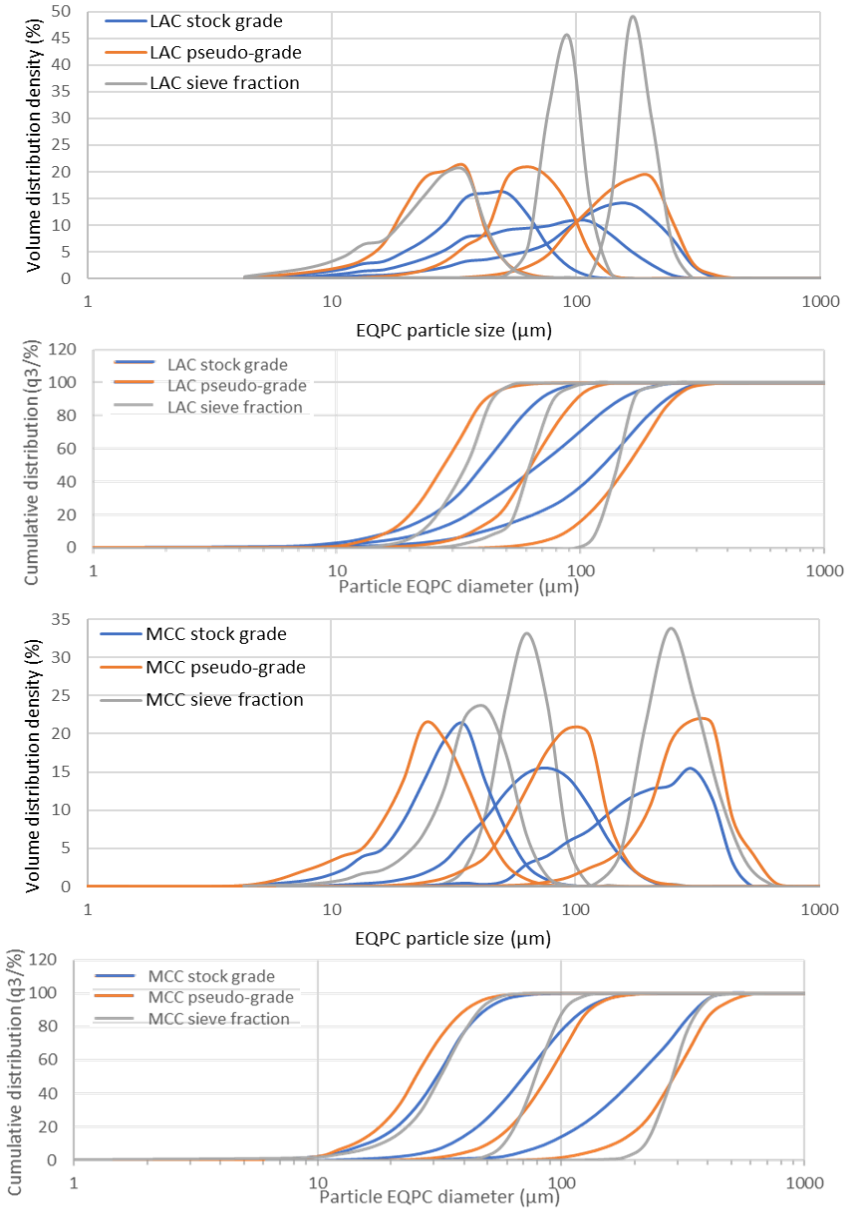

Figure 3.10 Particle size distribution and cumulative distribution of stock grades, pseudo-grades and sieve fractions of α-lactose monohydrate (top) and microcrystalline cellulose (bottom) as obtained via QICPIC particle sizing (averaged from triplicate measurements). EQPC is the diameter of a circle with an equivalent projection area as the measured particle.

2.5.2 Effect of PSD span

Figure 3.10 compares the PSD of the stock grades, pseudo-grades and sieve fractions. By comparing the porosity of the stock grades, pseudo-grades and sieve fractions with comparable d_{50}, the effect of the size distribution span [$(d_{90}$-$d_{10})/d_{50}$] on particle packing became apparent (Table 5). Generally, with decreasing span (stock grade>pseudo-grade>sieve fraction) the conditioned bulk density increased, and powder porosity decreased. This indicates that a broader size distribution promoted the presence of macro-voids within the bulk of a loose powder bed (Hapgood et al., 2002). This was likely because of the presence of finer particles within the distribution that were cohesive and agglomerated to form larger pores within the powder bed when loosely packed. However, when the powder bed was consolidated following extensive tapping, these multi-particle agglomerates were broken up and the smaller particles percolated into, and occupied, the voids created in between adjacent larger particles (Lam and Nakagawa, 1994; Zou et al., 2011). Consequently, when compared to the pseudo-grades and sieve fractions, the broader size distribution of the stock grades demonstrated a lower bulk density following the FT4 conditioning cycle and lower porosity after tapping (Figure 3.11). This was also reflected by higher compressibility indices (Figure 3.12). These findings concur with those of Kudo et al. (2019), whereby sieved samples of granulated lactose resulted in a lower angle of repose and CI% than the commercially-available original grade. Likewise, Liu et al. (2008) found that sieved ibuprofen fractions possessed lower compressibility yet a higher flower function than the original ibuprofen powder that had a much broader PSD.

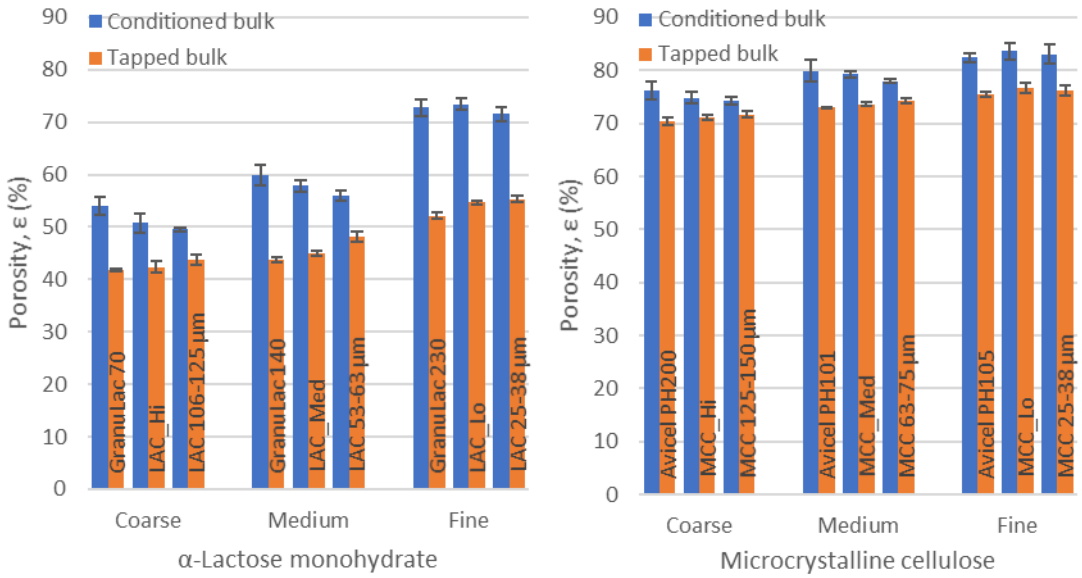

Figure 3.11 Compressibility index (mean ±sd, n=3) of the stock grades, pseudo-grades and sieve fractions of LAC (left) and MCC (right).

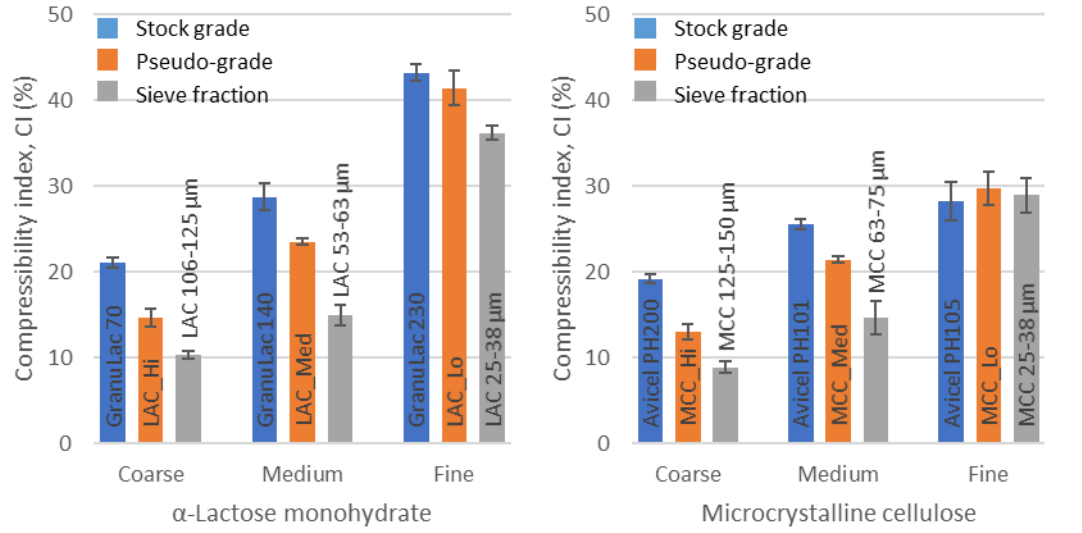

Figure 3.12 Powder bed porosity (mean ±sd, n=3) of the stock grades, pseudo-grades and sieve fractions of LAC (left) and MCC (right) when loosely consolidated following a FT4 conditioning cycle (blue) and when fully consolidated following tapping (orange).

It should be noted that the fine MCC sample grades (Avicel PH105, MCC_Lo and MCC 25-38 µm) did not follow this trend. Despite efforts to manipulate the PSD, very little reduction in PSD span was measured between the samples (p=0.354), therefore, the differences between the particle packing and compressibility observed were statistically insignificant (p=0.471).

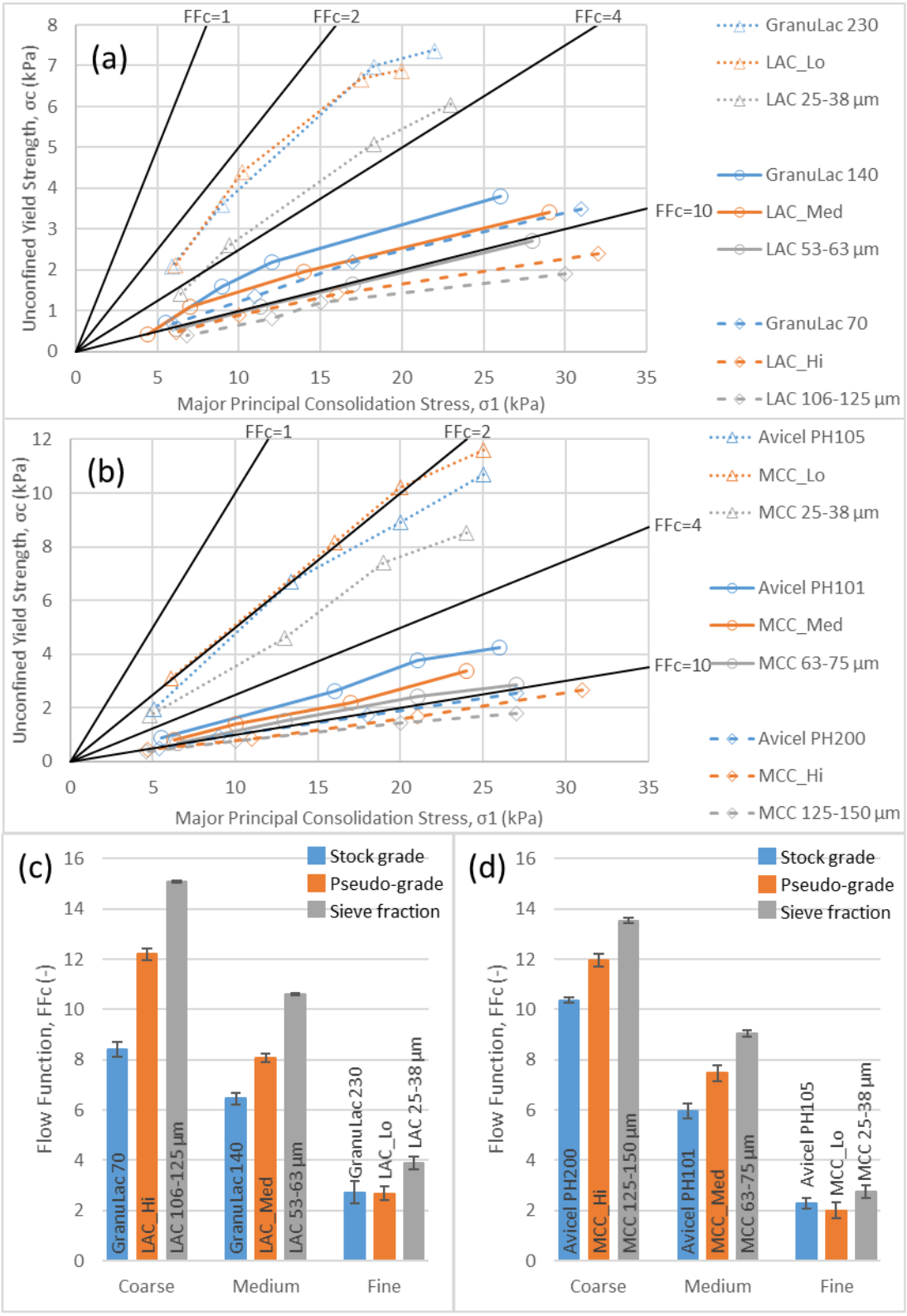

Figure 3.13 Flow function of the various grades of LAC (a & c) and MCC (b & d) resulting from FT4 shear cell test, where FFc<1 is non-flowing; 1<FFc<2 is very cohesive; 2<FFc<4 is cohesive; 4<FFc<10 is easy-flowing; and 10<FFc is free-flowing.

Narrowing the particle size span of the various LAC and MCC grades resulted in higher FF_c values, as shown in Figure 3.13. Similarly, Kurz and Münz (1975) observed the flow function of limestone samples with narrow PSDs to be greater than those with broad PSDs despite possessing comparable average particle diameters.

Figure 3.14 shows compressibility index and flow function plotted against PSD measurements d_{10}, d_{50} and d_{90}. With R-squared values of 0.872 and 0.914 for LAC and MCC, respectively, it is evident that d_{10} is a significant and strong predictor variable of CI% (p<0.01). Measurements d_{50} and d_{90} presented significant (p<0.05) but weaker correlations with CI%. Moreover, d_{10} returned even higher R-squared values for FF_c for LAC and MCC (0.961 and 0.984, respectively; p<0.01). This further supports the conclusion that the presence of fine particles is the most determinative factor on particle packing and powder flow on account of cohesive interparticle forces, namely van der Waals, being dominant over particle weight and gravitational forces (Podczeck, 1998). Goh et al. (2018) and Kudo et al. (2019) too found that the d_{10} value of granulated material was the single most important property affecting flow parameters.

Interestingly, although LAC d_{90} was statistically significant (p<0.05), it did not correlate strongly with CI% and FF_c (R^2=0.517 and 0.505, respectively). Hence, the larger particles of a distribution are a weaker predictor of the smaller particles. With that said, MCC d_{90} was found to still correlate well with CI% (R^2= 0.711; p<0.01) and FF_c (R^2= 0.903; p<0.01). However, the reason for this difference between LAC and MCC is not apparent in this investigation.

If the compressibility index were to be used as an indicator of a powder's sensitivity to handling and storage conditions, it is evident that the microstructure of the powder bulk

becomes more sensitive to handling and storage conditions as the PSD broadens and with the presence of finer particles as the compressibility index increases (Figure 3.12). Narrower size distributions are likely to pack more uniformly in the absence of consolidating forces (e.g. vibrations and movement) whereas, powders possessing a broader PSDs . Particle packing and consolidation of powders are dictated by the cohesive interactions of fine particles - typically <100 µm (Israelachvili, 1989; Visser, 1989). Hence, PSD modification methods, such as sieving and granulation, allow fine particles to be removed or minimised, offering powders with more favourable processing properties. An alternative solution is the addition of a flow aid that coats the fine particles to form a monolayer that disrupts van der Waals forces and subsequently interparticle adhesion. These additives include talc, fumed silica and magnesium stearates (Fulchini et al., 2017; Gold et al., 1966; Liu et al., 2008; Mazumder et al., 1997; Pingali et al., 2011; Podczeck, 1998; Tomas and Kleinschmidt, 2009; Yang et al., 2005).

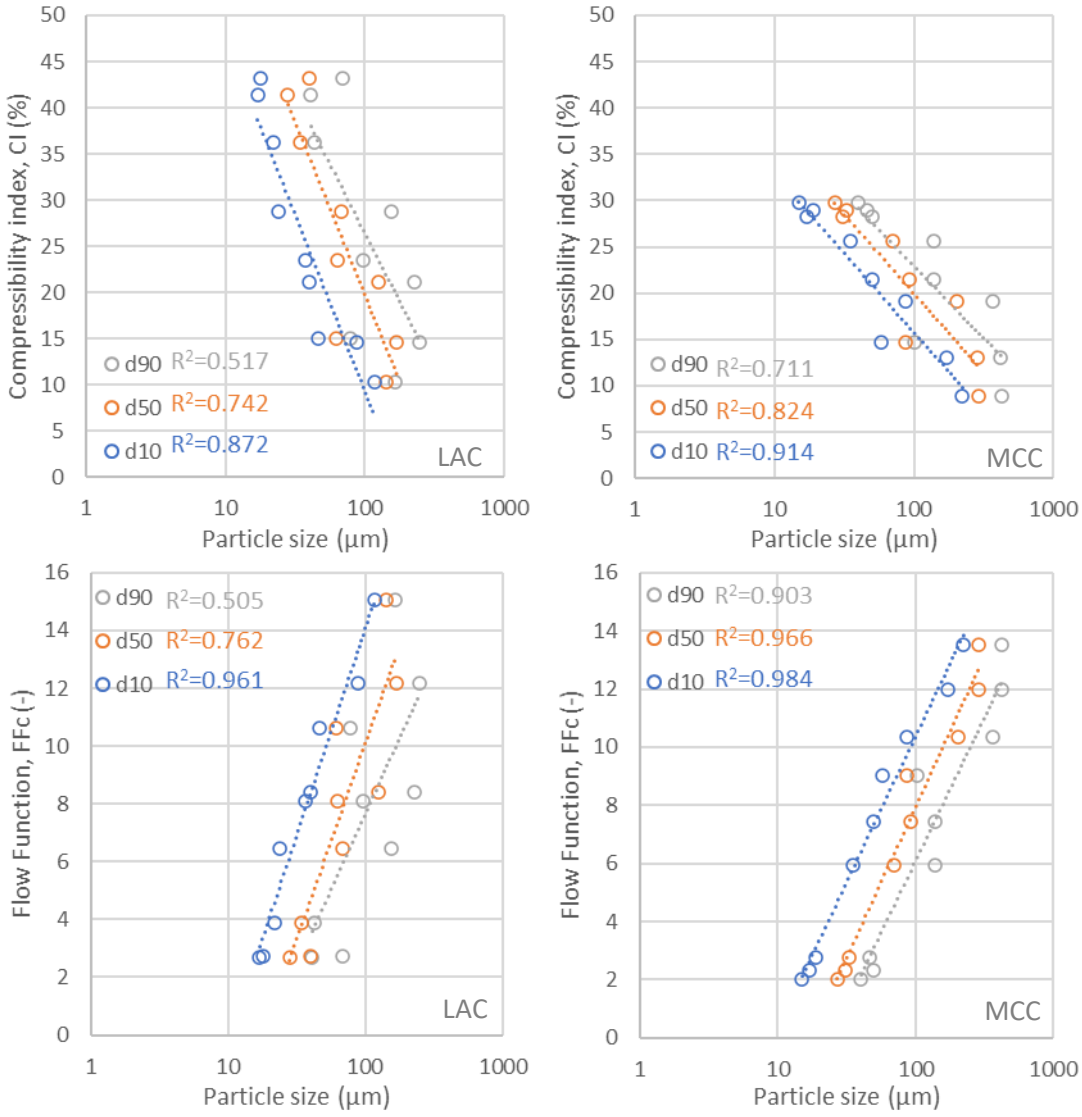

Figure 3.14 Compressibility index (top) and flow function (bottom) plotted against particle size measurements of the various grades of LAC (left) and MCC (right) with corresponding R-squared values.

2.5.3 Binary formulation mixture characterisation

The bulk properties of the binary LAC:LAC pseudo-grade permutations are represented graphically in Figure 3.15. Overall, the grade of LAC_70 - Lo, Med or Hi - had the greatest influence on the powder bed porosity but the grade of LAC_30 also had a significant, albeit smaller, effect on particle packing. Following the work of Furnas (1931, 1930) and Westman and Hugill (1930), it is widely accepted that the packing density of a bimodal mixture is greater than that of either single grade. That is evidenced here, as the tapped powder density, ρ_{tap}, increased and powder porosity decreased, ε_{tap}. Numerous studies have shown that maximum particle packing is achieved when the large particles constitute 60-80% of the mixture (Aghajan et al., 2019; Bai et al., 2017; Börjesson et al., 2014; Kouraytem et al., 2016; Lam and Nakagawa, 1994; McGeary, 1961; Nordström et al., 2018; Rassouly, 1999; Santiso and Müller, 2002; Ye et al., 2018; Yerazunis et al., 1965; Yu and Standish, 1993).

Hence, LAC_70_Hi:LAC_30_Lo (ρ_{tap}=0.93 g/cm^3) possessed a greater density than LAC_70_Lo:LAC_30_Hi (ρ_{tap}=0.74 g/cm^3). This was because the smaller particles of LAC_Lo occupied the voids in-between larger particles that would otherwise be vacant in a unitary powder bed consisting of only LAC_Hi (Westman and Hugill, 1930). Further, as the diameter ratio, *DR* - listed in Table 6, between the two grades increased so did the packing density, hence, LAC_Hi:LAC_Lo (DR=6.00) had a more dense particle packing than LAC_Hi:LAC_Med (DR=2.25) and LAC_Med:LAC_Lo (DR=2.67). This relationship has been shown to be true across a number of materials (Fedors and Landel, 1979; Kouraytem et al., 2016; McGeary, 1961; Rassouly, 1999; Westman and Hugill, 1930; Yerazunis et al., 1965; Zheng et al., 1995). Therefore, it is believed that tapped bimodal mixtures possessed a narrower and more uniform pore structure, than their tapped unimodal counterparts.

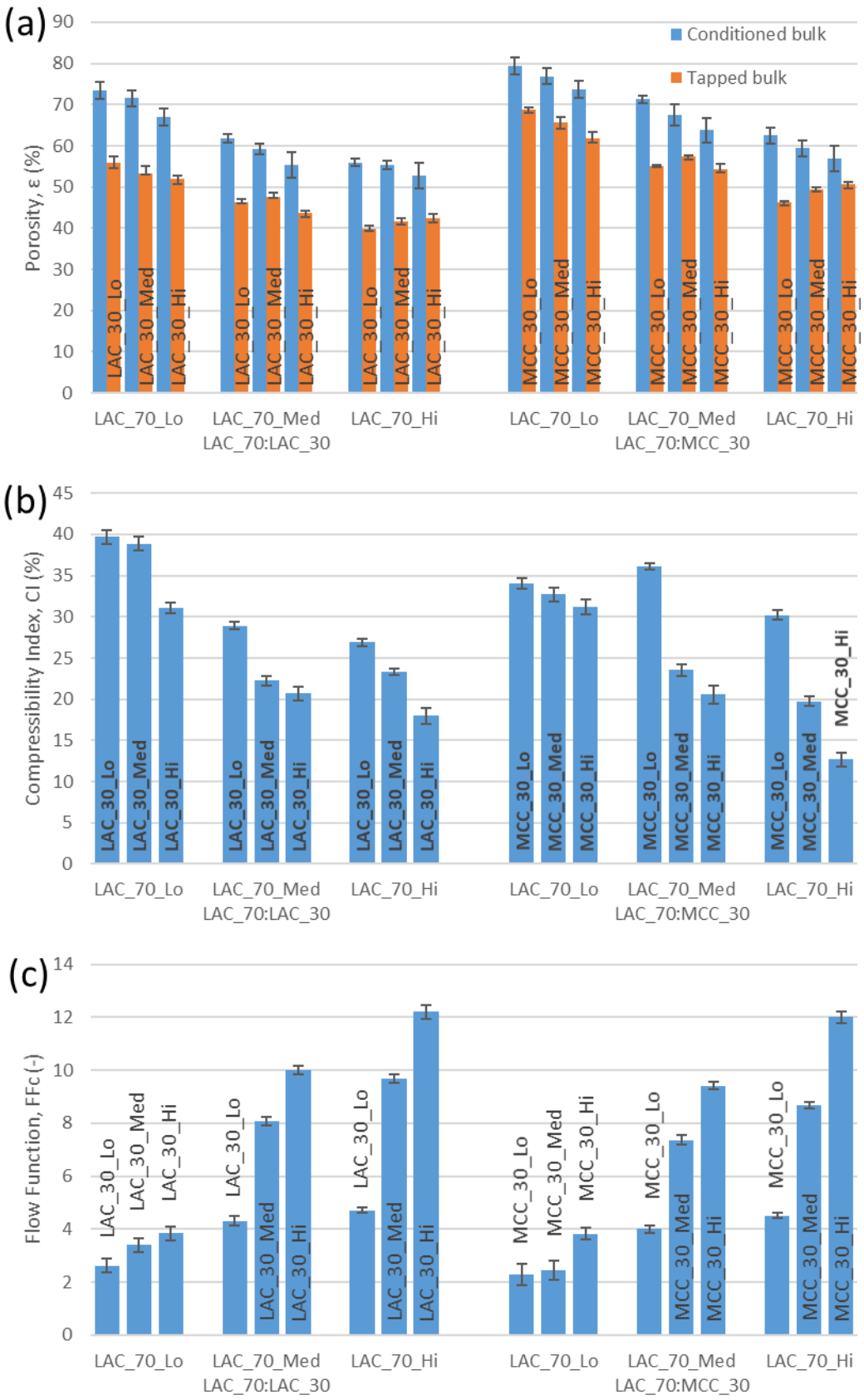

Figure 3.15 Properties of LAC:LAC (left) and LAC:MCC (right) binary mixtures; conditioned and tapped porosity (a), compressibility index (b), and flow function (c) (mean ±sd, n=3).

However, the above trends did not apply to conditioned loose mixtures; the powder bed became more porous as particle size decreased and as the proportion of smaller particles increased, irrespective of LAC_70 and diameter ratio. In the absence of shear forces induced during tapping to disrupt interparticle cohesion and promote particle rearrangement, then the fine particles of LAC_Lo exist as loose aggregates and are unable to percolate into the voids in-between the larger particles of LAC_Hi and LAC_Med, as similarly reported in the literature (Soppela et al., 2010; Thalberg et al., 2004). Therefore, the bulk porosity of LAC_70_Hi increased with the doping of LAC_30_Lo despite decreasing the tapped porosity. As previously discussed, by including the fine particles of LAC_Lo into a powder mixture then the compressibility index increased, indicating that the mixture was more sensitive to handling and storage conditions.

Table 6 Nominal diameter ratio, DR, between particles in binary mixtures.

70 %w/w		30 %w/w	Diameter Ratio, DR
LAC_Hi	:	LAC_Med	2.25
LAC_Hi	:	LAC_Lo	6.00
LAC_Med	:	LAC_Lo	2.67
LAC_Hi	:	MCC_Hi	0.59
LAC_Hi	:	MCC_Med	1.83
LAC_Hi	:	MCC_Lo	6.22
LAC_Med	:	MCC_Hi	0.22
LAC_Med	:	MCC_Med	0.68
LAC_Med	:	MCC_Lo	2.33
LAC_Lo	:	MCC_Hi	0.1
LAC_Lo	:	MCC_Med	0.3
LAC_Lo	:	MCC_Lo	1.04

Moreover, the flow function derived from the powder rheometer shear tests, indicate that the inclusion of LAC_Lo always resulted in a greater resistance to shear. This can be attributed to the greater surface area and higher potential for cohesive forces. This increased resistance to shear was indicative of the greater tendency for a heterogeneous pore structure in the absence of consolidation; particles were more likely to inefficiently adhere to adjacent particles because of van der Waals forces instead of reorienting and percolating homogenously as a consequence of gravitational forces. Thalberg et al. (2004) reported a similar impediment to flow when micronised lactose and fine lactose were added to a coarse lactose grade. Comparably, Kaerger et al. (2004) and Soppela et al. (2010) both studied the flow properties of binary mixtures of paracetamol and MCC. Despite an increase in tapped density, the authors observed a similar reduction in flow with increasing concentrations of the fine paracetamol particles. Similar to previous reports, the inclusion of a fine powder, in this case LAC_30_Lo, diminished the effect of LAC_70 and dominated the flow properties of the bulk powder even though it was the minority component (Soppela et al., 2010).

The bulk properties of the LAC:MCC mixtures demonstrated similar trends to that of LAC:LAC, however, the porosity was generally higher due to MCC particles being more porous and possessing a larger aspect ratio than LAC particles (see Table 5).

3.6. Conclusion

Commercially available stock grades of α-lactose monohydrate and microcrystalline cellulose were fractionated and reconstituted into pseudo-grades with narrower and more distinct normally distributed particle size distributions. This was intended to offer a more precise opportunity to examine the effects of PSD on powder behaviour, however, only LAC_Med

was deemed statistically significant from its GranuLac 140 counterpart (p<0.01). In addition to this, the PSD span and modality were varied by permuting a binary mixture of two pseudo-grades so that the microstructure of a powder bed could be manipulated in conjunction with the consolidation conditions.

Increasing PSD and consolidation resulted in a powder bed with a more homogeneous and smaller pore size distribution. Increasing the bimodality, and span, of the powder bed decreased the average pore size when consolidated but also increased the heterogeneity when loosely consolidated. Thus, it was evident that increased PSD span caused the powder bed to become more sensitive to handling and consolidation conditions. Conversely, a coarse PSD with a narrow span proved to be least sensitive to consolidation.

Varying the properties of the binary mixture and degree of consolidation allowed a larger range of powder properties and behaviours to be examined, offering greater insight into excipient selection and formulation.

3.7. Drop penetration method

3.7.1. Qualitative features

Images depicting the development of a typical droplet penetration test can be seen in Figure 3.16. Due to the short descent and low impact velocity, no lamella projection, splashing, bounce or satellite droplet detachment was observed. The pinch-off of a daughter droplet did manifest for some of the tests with water and 2.5% w/w HPMC. Similarly, there was no evidence of significant surface deformation or crater formation as a result of impingement. The minimal discharge height and low impact velocity did allow for some droplets to roll laterally prior to coming to rest, particularly for fine PSD formulations.

Additionally, when deposited on a fine powder bed consisting of LAC_Lo, the portion of the droplet that came into contact with the surface during impact deformation, rapidly became coated with particles (Figure 3.16). The entrained particles then went on to migrate to the top of the droplet resulting in complete coverage. This was not observed for LAC_Hi, indicating that fine particles demonstrate a similar phenomenon to that observed during the early stages of marble formation with hydrophobic powders (Eshtiaghi et al., 2009; Hapgood and Khanmohammadi, 2009; Marston et al., 2010; McEleney et al., 2009; Nguyen et al., 2009; Supakar et al., 2016). However, unlike those studies, the particles then permeated through the surface of the droplet and into the bulk. The particles were still visibly intact inside the droplet indicating that permeation was not a consequence of dissolution.

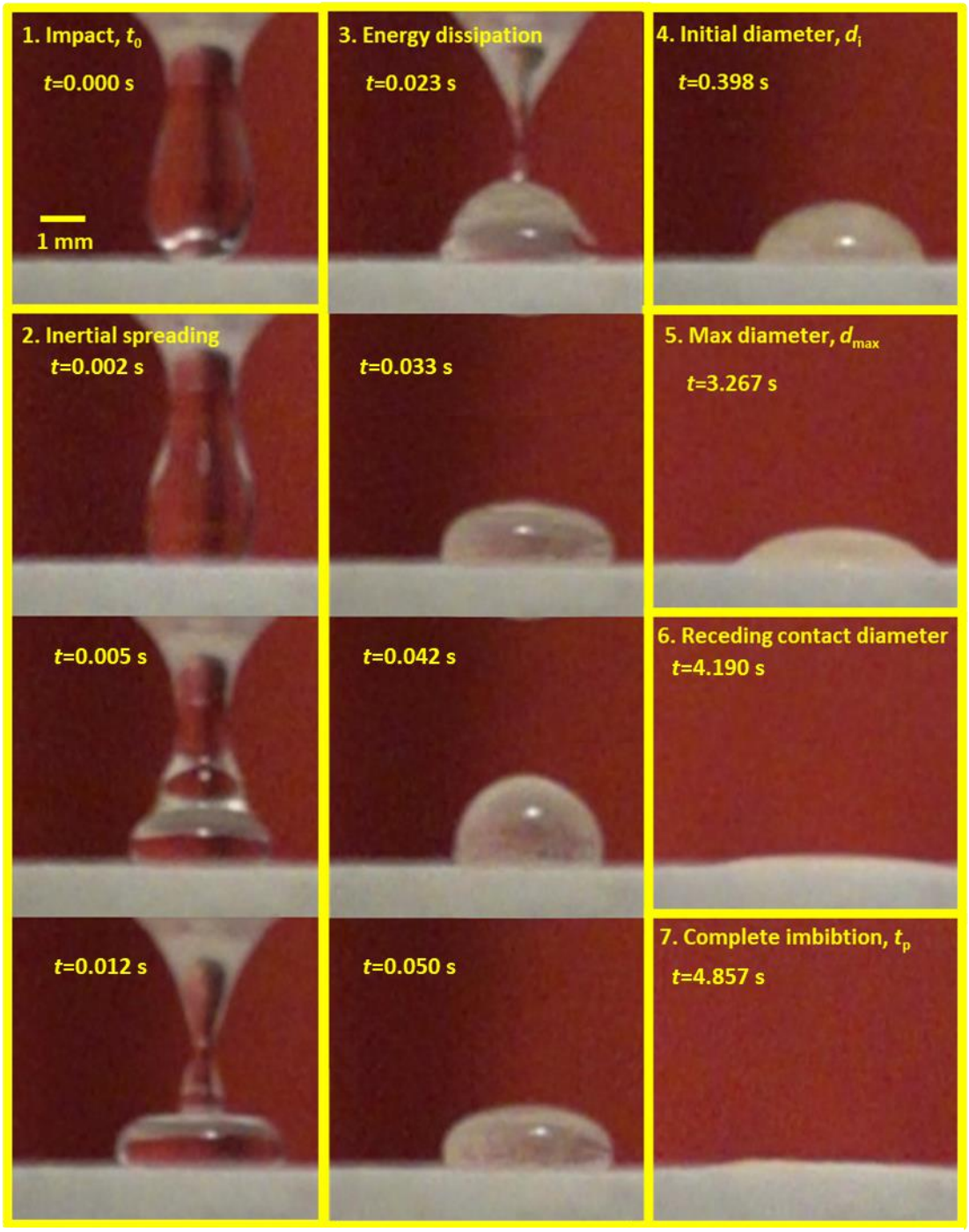

Figure 3.16 Time lapse of key moments during droplet penetration from impingement to complete imbibition.

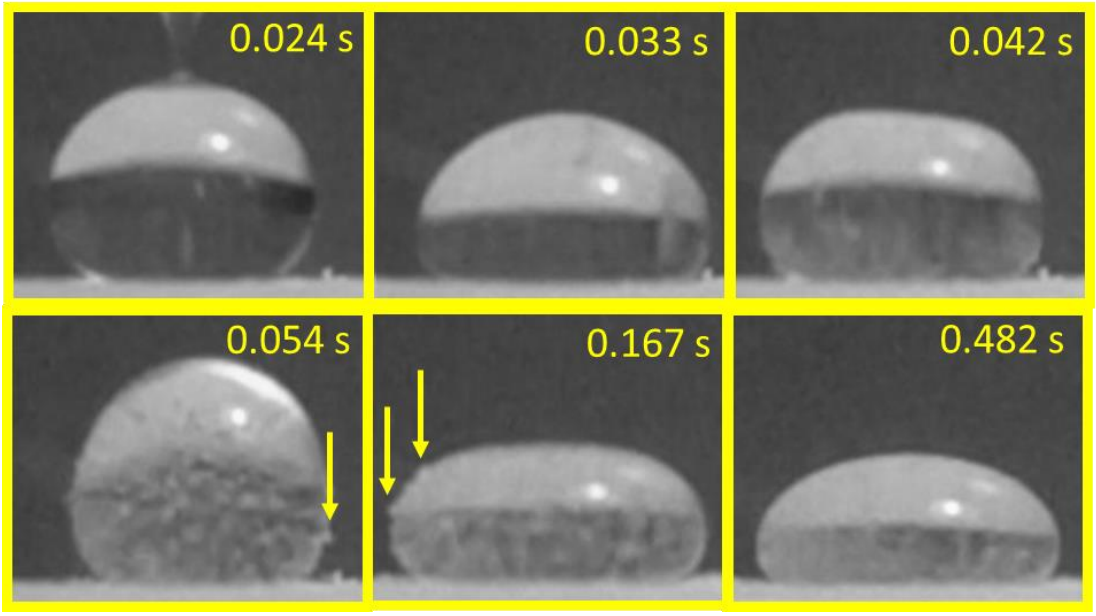

Figure 3.17 Time lapse depicts entrainment of particles to droplet surface during impact. Arrows highlight entrained particles that eventually permeate into the droplet. A 0% w/w HPMC droplet impinging on a loosely-consolidated LAC_70_Lo:LAC_30_Lo powder bed.

Throughout droplet penetration several droplet properties were measured including contact diameter, height, and apparent volume (Equation 3.2). A typical representation of these measurements is depicted concurrently in Figure 3.18 with key features highlighted in Figure 3.19. The imbibed volume was calculated by deducting the apparent volume (calculated using Equation 3.2) at time, t, from the initial droplet volume from d_0 at t_0 (Table 2). Upon impact the droplet's contact line spread rapidly, indicative of inertial spreading, and the progression of the capillary wave is visible for the least viscous test liquids. This diameter spreading is a consequence of the opposing gravitational and normal forces causing the droplet to radially deform (Yang et al., 2019). The droplet's viscoelastic properties caused it to recoil, and the diameter and height continued to oscillate between local maxima and minima with decreasing amplitude as the kinetic energy dissipated due to the dampening effect of viscous friction and surface energy conversion (Banks et al., 2014; Lin et al., 2018). This is highlighted in the inset of Figure 3.19.

As the droplet ceased to reverberate, it formed a quasi-equilibrium spherical cap, of diameter d_i, comparable to a droplet on a non-porous surface. In some cases, the apparent contact angle was visibly greater than 90^o during the early moments of penetration, as seen in Figure 3.17, indicating a hydrophobic interface despite using a formulation composed of hydrophilic excipients.

During the subsequent quiescent period the contact diameter slowly spread until reaching the maximum droplet spread, d_{max}, demonstrating an *increasing drawing area* regime, IDA. For some experimental conditions, a period of *constant drawing area*, CDA, was apparent as the contact diameter remained relatively constant. This was followed by a *decreasing drawing area*, DDA, featuring rapid droplet recession, as imbibition approached completion. The droplet height and volume exhibited a linear relationship throughout most of the imbibition, albeit the gradient decreased dramatically as imbibition approached completion. It can be seen from the inset of Figure 3.18, that the contact diameter-time curves correlate better with the CDA regime of Equation 2.25 than the DDA regime of Equation 2.26

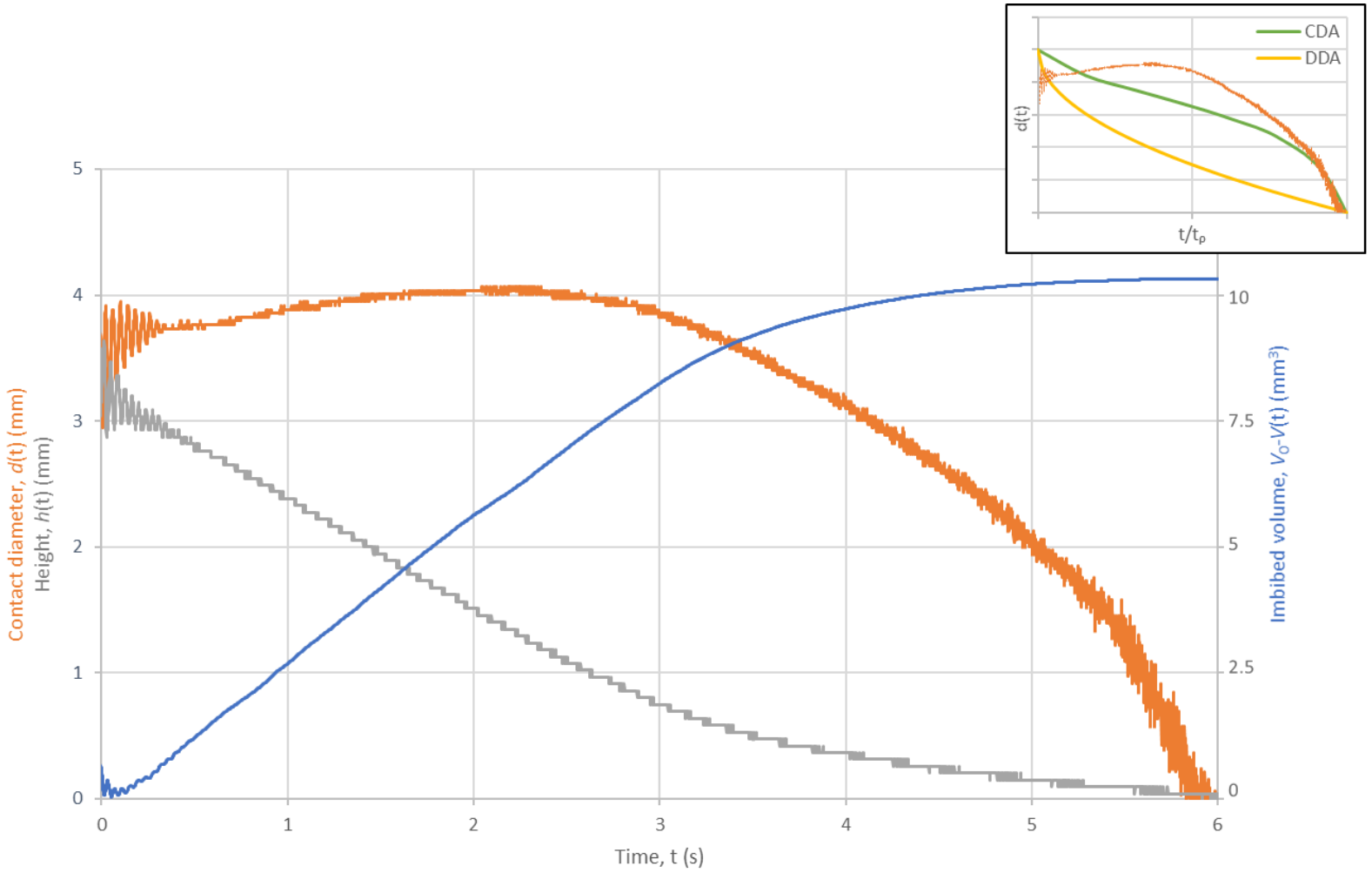

Figure 3.18 Typical representation of the measurements obtained for the droplet contact diameter (orange line), droplet height (grey line) and penetrated volume (blue line) plotted as a function of time. Figure 2.21b is shown inset comparing the constant drawing area and decreasing drawing area imbibition regimes with the experimental results superimposed.

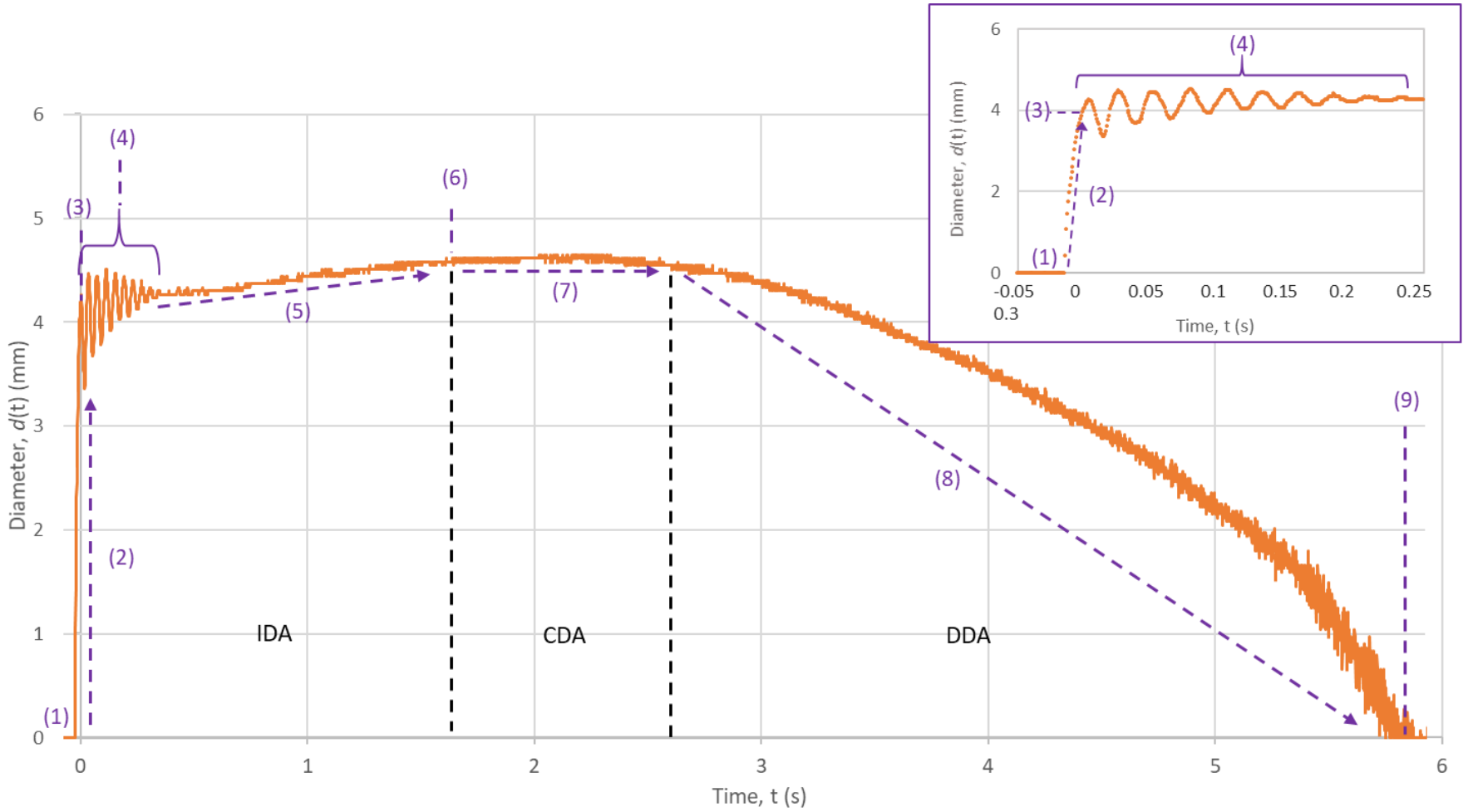

Figure 3.19 Droplet contact diameter plotted as a function of time with key moments and features highlighted: (1) Droplet contact, t0; (2) Inertial spreading; (3) Initial spread diameter, d*i*; (4) Energy dissipation; (5) Viscous spreading; (6) Maximum spread diameter, d_{max}; (7) Constant diameter; (8) Droplet receding; and (9) Complete imbibition, t_p.

3.7.2. Energy dissipation

As the height of impact was controlled the kinetic energy incurred during droplet impingement was kept reasonably consistent, and so the duration of energy dissipation and the number of oscillations were indicative of the surface wettability and liquid properties (Banks et al., 2014). Examples of energy dissipation are shown in Figure 3.20.

Some distortion during the first oscillation was the result of difficulties measuring the droplet height due to droplet deposition and pinch off. The oscillations of the height and contact diameter are of the same frequency but are opposite in phase. The amplitude of the contact diameter is smaller than that of height and dissipates earlier. This is likely due to droplet height, h(t), being measured at the vertical maxima, whereas the contact diameter, d(t), was measured at the base of the droplet and not the horizontal maxima, where displacement was greatest. Furthermore, the amplitude of the vertical oscillations generally increased with decreased contact diameter due to the inverse relationship between contact diameter and droplet height. A taller droplet had greater vertical freedom, and hence a larger range of motion and amplitude, during oscillation. Figure 3.21 compares the effect of each variable on droplet oscillation and energy dissipation. It is evident from Figure 3.21 that droplet spreading is taking place concurrently, as the contact diameter trends upwards throughout the energy dissipation period.

As can be seen the kinetic energy dissipation process varied between experimental conditions. The number of oscillations ranged from 3 to 19, and the time for the droplet to come to *"rest"* was between 0.256 and 0.681 s. The coefficients of the multiple linear regression models (MLR) and response surfaces (RSM) for energy dissipation on LAC:LAC powder beds are presented in Figure 2.22 and Figure 2.23, respectively.

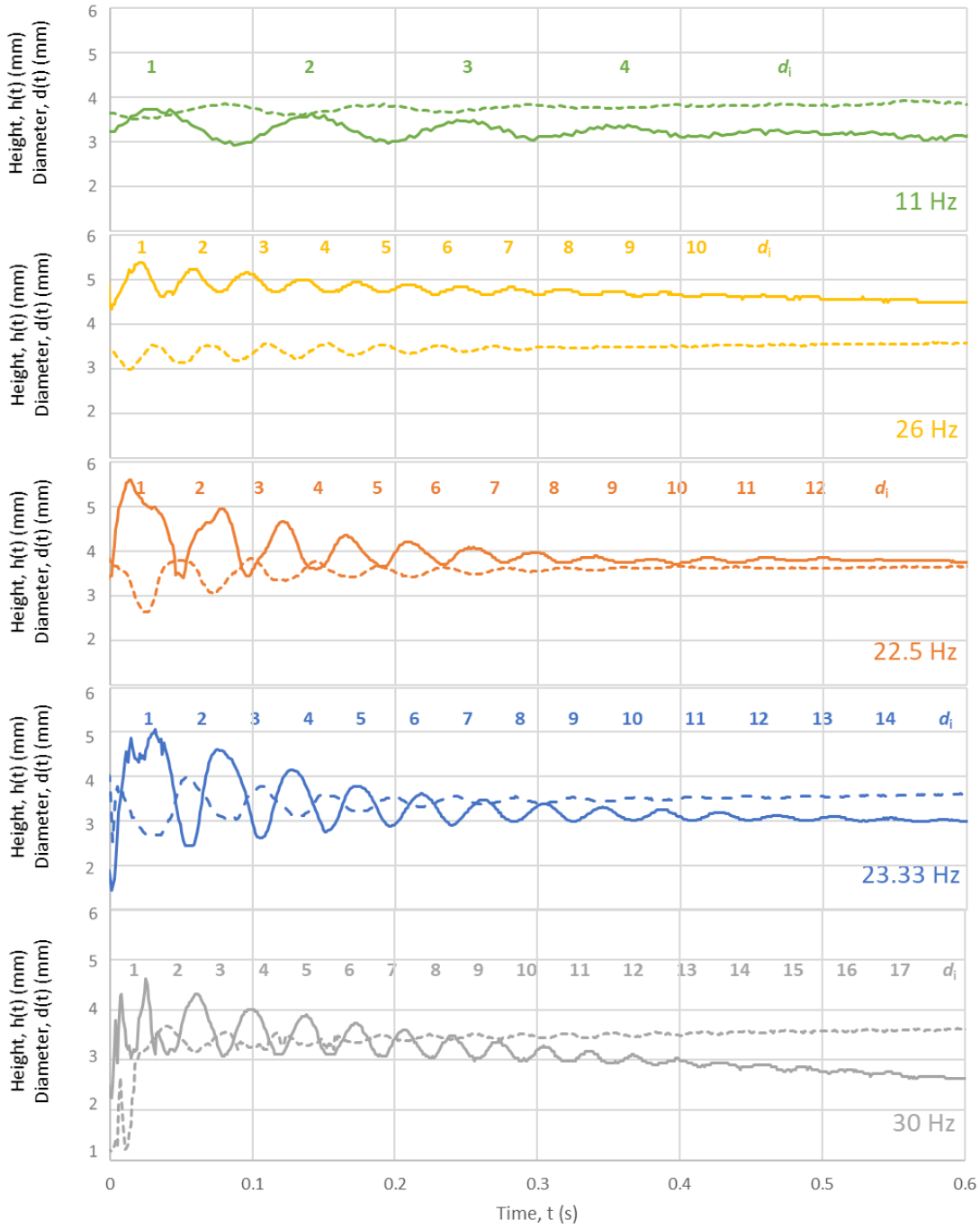

Figure 3.20 Examples of droplet height (solid line) and contact diameter (dashed line) oscillating during energy dissipation. The oscillations are numbered and the frequency is highlighted.
From top to bottom: Exp8 - LAC_Hi:LAC_Hi, 5% w/w HPMC, loose; Exp16 - LAC_Hi:LAC_Hi, 5% w/w HPMC, fully consolidated; Exp24 - LAC_Med:LAC_Med, 2.5% w/w HPMC, fully consolidated; Exp11 - LAC_Hi:LAC_Lo, 0% w/w HPMC, fully consolidated; Exp12 - LAC_Hi:LAC_Hi, 0% w/w HPMC, fully-consolidated.

Droplet viscosity had the greatest influence on the oscillation frequency and duration of oscillation for the range of conditions studied – as the viscosity increased, the kinetic energy dissipated faster with slower oscillations. This observation confirms previous studies (Banks et al., 2014; Katsuragi, 2011; Lin et al., 2018; Manglik et al., 2013), although Katsuragi (2011) found no obvious trend between viscosity and oscillation time for droplets deposited on 50 µm glass beads. Additionally, the amplitude of the oscillations decreased with increased viscosity, as the internal friction resisted droplet motion (Leblanc et al., 1999).

Increasing the particle size distribution of LAC_70 resulted in shorter oscillation durations and a higher frequency, as well as hastening energy dissipation. Katsuragi (2011) reported similar observations for droplets of low viscosity deposited on powder beds of silicon carbide and glass beads. This is likely due to a smaller surface pore fraction and decreased surface roughness resulting in higher surface energy and increasing kinetic energy conversion (Boinovich and Emelyanenko, 2008; Crick and Parkin, 2010).

The significance of LAC_70*HPMC (p<0.05) indicates an interaction, and as the response surface illustrates, the effect of LAC_70 on energy dissipation diminishes as HPMC increases. This interaction between viscosity and particle size has been reported elsewhere (Katsuragi, 2011), whereby the effect of particle size on oscillation duration diminished with increased viscosity. This suggests that the effect of powder wettability on energy dissipation has a dependence on low liquid viscosity (Banks et al., 2014; Manglik et al., 2013).

Varying the PSD of LAC_30 proved to be insignificant as a main effect with regards to droplet oscillation, as it had no discernible effect on LAC_70_Hi and LAC_70_Med. However, an interaction with LAC_70_Hi was significant (LAC_70*LAC_30 p<0.05); decreasing the PSD of LAC_30 in the presence of LAC_70_Hi resulted in a higher oscillation frequency and slightly

shorter duration of oscillation. Again, this can be attributed to a reduction in powder porosity and surface pore fraction.

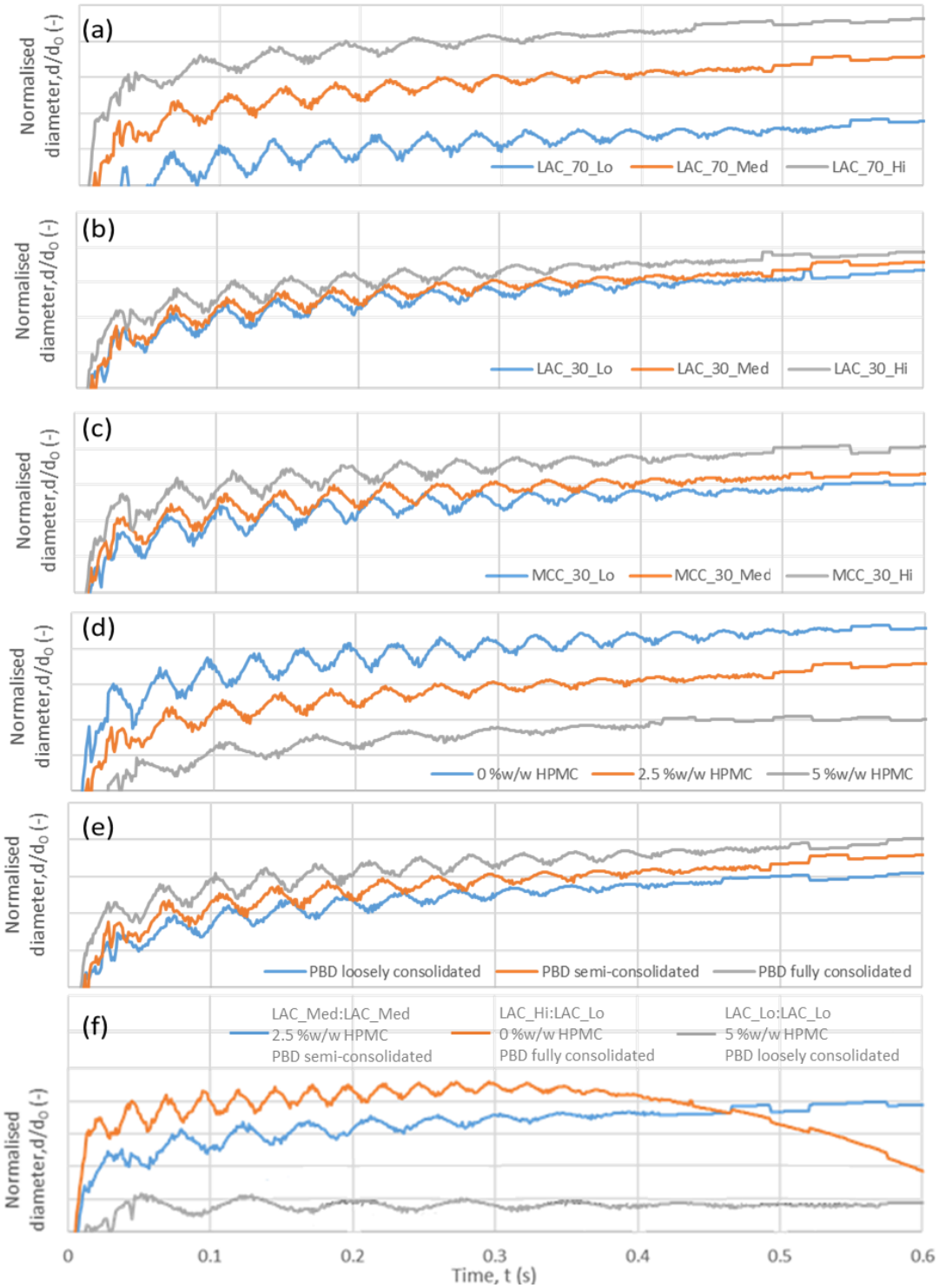

Figure 3.21 Normalised contact diameter (d/d0) with (a-e) comparing the main effects of each factor on energy dissipation and (f) comparing the shortest - Exp10 - and longest penetration tests – Exp5 – with DoE centre point – Exp 25.

The particle size distribution and inclusion of MCC_30 resulted in similar trends observed for LAC_30 (MLR coefficients and response surfaces not shown). However, a slight overall reduction in oscillations and dissipation duration was observed for coarser MCC pseudo-grades indicating greater wettability.

Increasing the extent of consolidation and powder bed density (PBD) of all powder mixtures resulted in an increase in oscillation frequency and shortened the duration of oscillation. The reduction in porosity decreased the hydrophobic pore fraction. PBD also demonstrated a significant interaction with LAC_70 (LAC_70*PBD, $p<0.05$). Interestingly, oscillation frequency was more sensitive to changes in PBD for LAC_70_Hi than for LAC_70_Lo; this is despite LAC_Hi exhibiting a smaller range of density (0.76-0.89 g/mL) than LAC_Lo (0.41-0.70 g/mL). Contrastingly, the opposite relationship was observed for oscillation duration, in that LAC_70_Lo was more sensitive to PBD than LAC_70_Hi. In this present study no reason could be identified to explain these conflicting relationships.

Based on these results, a potential hypothesis is that droplet oscillation may further be influenced by consolidation, as a loose powder bed would dampen the impact of the droplet and absorb some of the kinetic energy, resulting in a smaller amplitude and shorter oscillation duration. In contrast, a tapped powder bed would present a more rigid surface and offer less damping, resulting in a longer oscillation duration. This is hypothesised because of work by Mangili et al. (2012) and Chen et al. (2016) whereby softer surfaces resulted in a less pronounced droplet recoil following impact and a significantly shorter duration of oscillation. In the case of this study, it is difficult to differentiate the effects of surface softness and the effects of porosity, as both are a function of consolidation. However, Chen et al. (2016) reported surface softness had no significant effect on droplet

oscillation at low impact velocity (0.5 m/s), which is in the region of this study, and hence it is assumed that the effects of surface softness on droplet oscillation were negligible.

In summary, increasing particle size, bimodality and consolidation all contributed to reduced porosity, and consequently, reduced oscillation duration. Several authors have correlated shorter oscillating times to increased wettability (Banks et al., 2014; Lin et al., 2018; Wang et al., 2009b) and others have correlated wettability to porosity (Holm et al., 2016; Lee et al., 2016a; Vu et al., 2011; Yang and Xu, 2017) and surface pore fraction (Jopp et al., 2004; Murakami et al., 2014; Yang et al., 2008). In that regard, decreasing porosity increased wettability and resulted in greater surface energy conversion due to greater spreading (Ukiwe et al., 2005) as per section 3.6.4, and greater viscous energy dissipation because of longer oscillating motion (Banks et al., 2014; Lin et al., 2018). In contrast, increasing porosity reduced wettability and resulted in reduced surface energy conversion because of a smaller contact area, and less viscous dissipation from a shorter oscillating motion. It is therefore reasonable to suggest that increasing the particle size of LAC_70, increasing the bimodality via LAC_30 and increasing particle packing efficiency via PBD consolidation improved wettability by decreasing the porosity, and in turn, the fraction of hydrophobic air-filled pores in the powder bed surface.

With that said, porosity alone does not explain the variability in oscillation behaviour. The powder beds of experiment 9 (LAC_Lo:LAC_Lo fully consolidated), experiment 21 (LAC_Med:LAC_Med semi-consolidated), and experiment 4 (LAC_Hi:LAC_Hi loosely consolidated) had comparable porosities of 54.7, 51.5 and 50.8%, respectively. Despite this, the oscillation process still exhibited differences in duration and frequency. This is indicative that surface roughness, arising from surface area, contributed to droplet oscillation post-impact. Hence, assuming a Cassie spreading regime during the initial moments following

drop impact, then the area available for surface energy dissipation and spreading was greater (Murakami et al., 2014). If the droplet had assumed a Wenzel state during impact due to a higher velocity, it is likely that the larger surface area of a more porous surface would have quickened dissipation, rather than prolonging it (Vaikuntanathan and Sivakumar, 2014).

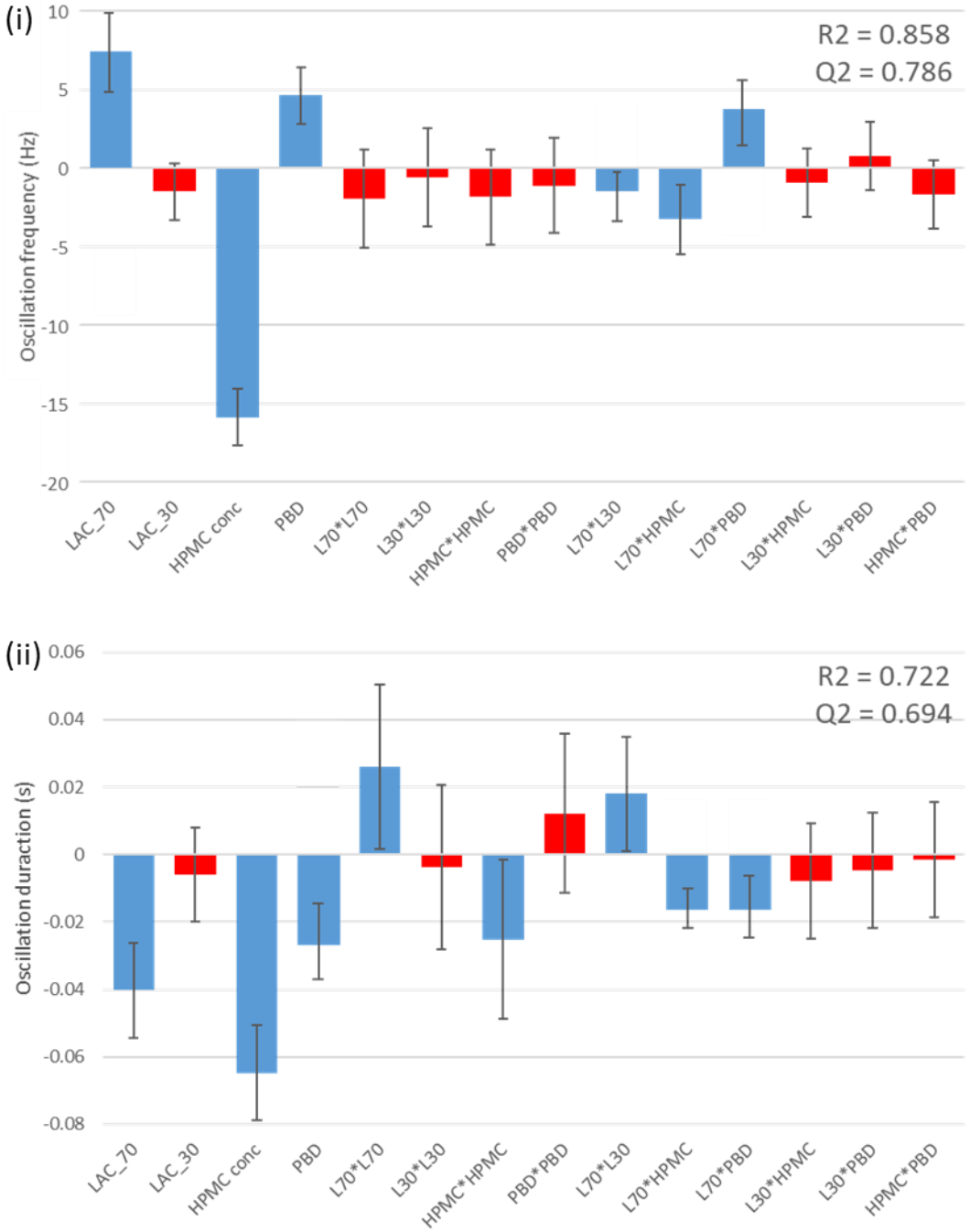

Figure 3.22 Multiple linear regression coefficients pertaining to (i) the oscillation frequency and (ii) duration required for energy dissipation for droplets deposited on LAC:LAC powder beds. Significant coefficients ($p<0.05$) are coloured blue.

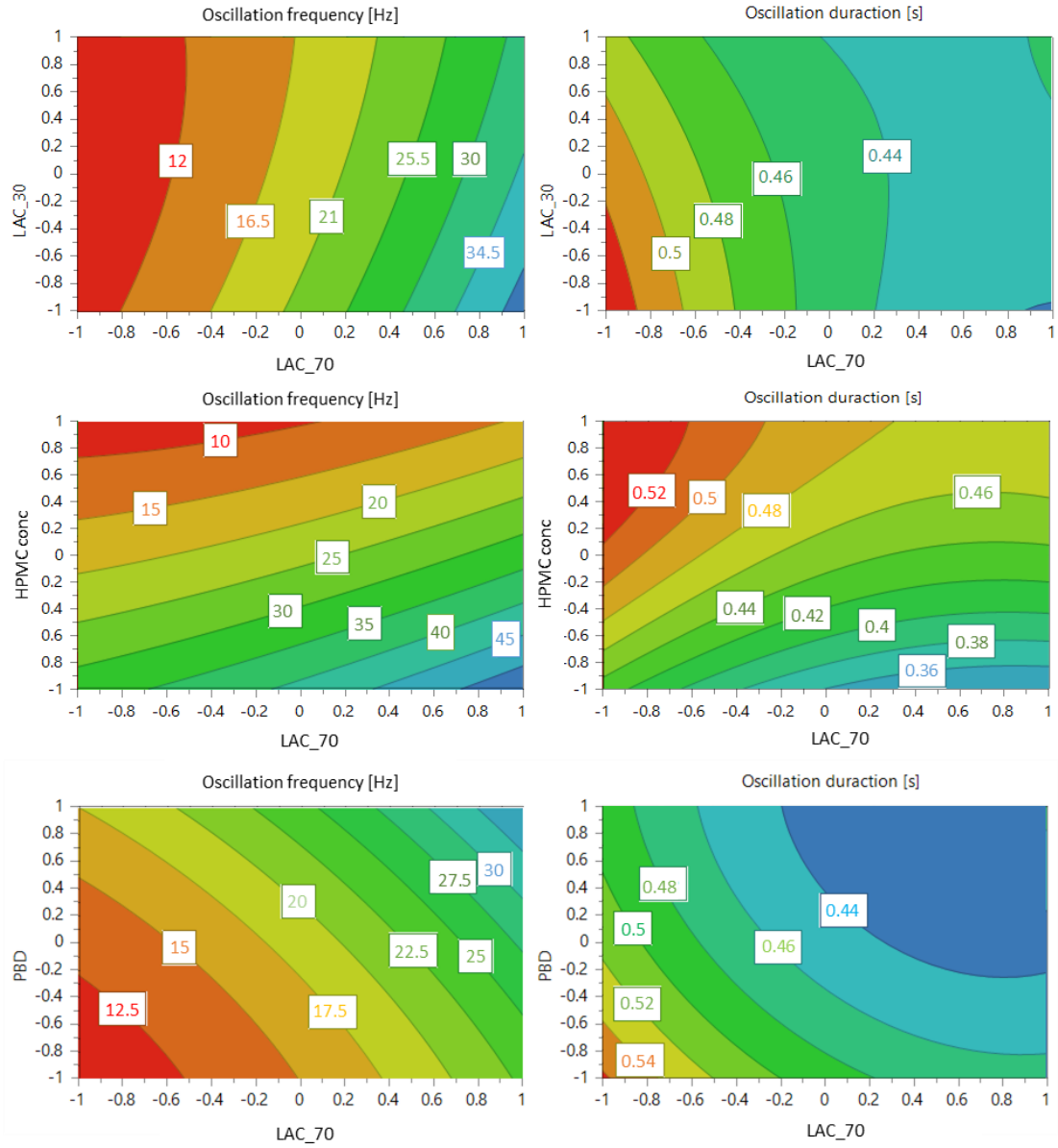

Figure 3.23 Response surfaces illustrating the MLR models pertaining to the oscillation frequency (left) and duration (right) required for energy dissipation for droplets deposited on LAC:LAC powder beds. The -1 to +1 range across the x- and y-axes corresponds to the experimental DoE levels outlined in Table 4.

As the oscillations of the droplet follow a damped harmonic motion, some authors (Manglik et al. 2013; Banks et al. 2014) have sought to model droplet oscillation as a function of the damping ratio (derived from the viscous damping coefficient) and the undamped angular frequency (derived from the characteristic mass and spring constant). These elements have

been demonstrated to scale with the droplet viscosity, surface tension and velocity (Manglik et al. 2013; Banks et al. 2014). However, to date no attempts have been made to use the damped harmonic oscillator to model droplet oscillations as a function of the surface properties. Although this is beyond the scope of this study, deriving these parameters to represent powder properties is worthy of further investigation.

3.7.3. Penetration time

The penetration time is representative of overall wettability and permeability of a powder bed (Hapgood et al., 2002). All the experimental conditions tested demonstrated complete imbibition. Figure 3.24 compares the main effects on droplet penetration. The times ranged from 0.885s indicating rapid penetration, to 7.728s for the least wetting conditions (Figure 3.24f). This illustrates an almost 9-fold difference arising from the variation in physical properties despite the materials possessing the same chemical properties.

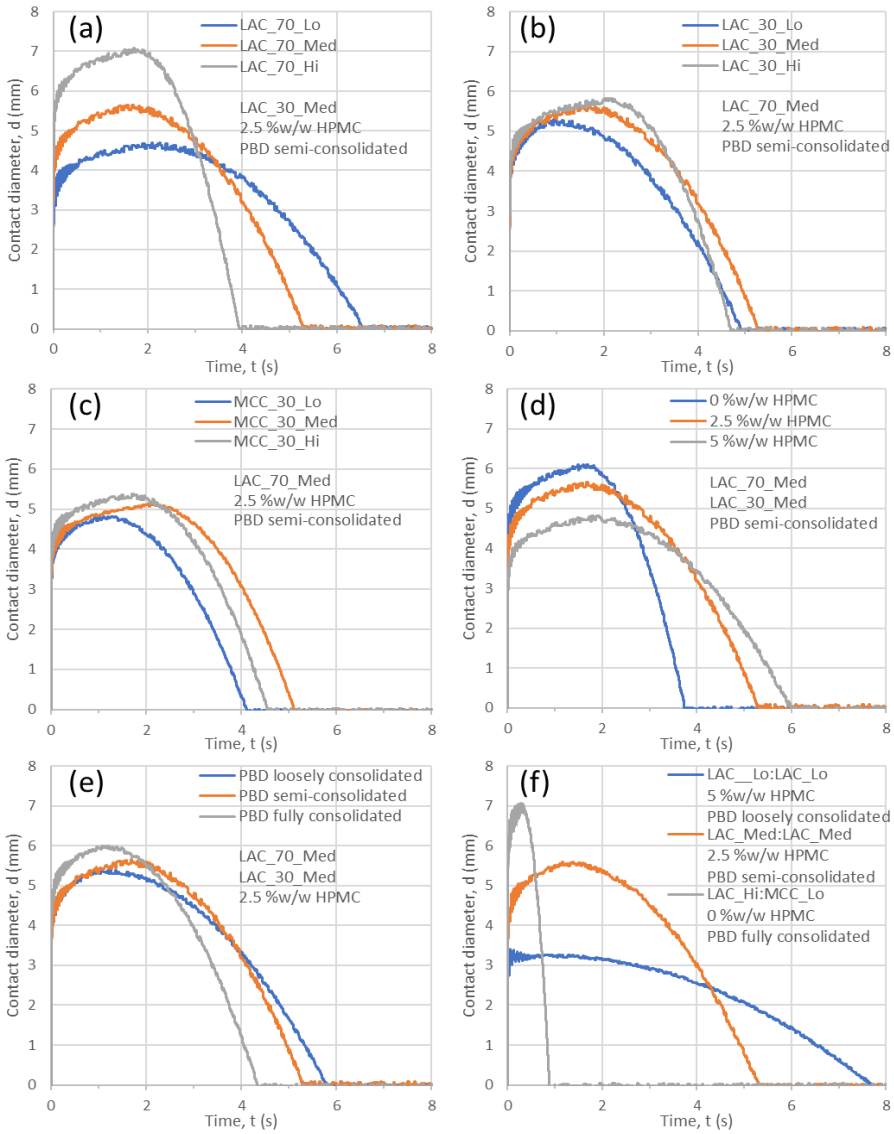

Figure 3.24 Droplet contact diameter plotted as a function of time (10-point moving average). Graphs (a-e) compare the main effects of each factor. Graph (f) displays the fastest – Exp10 - and slowest penetration tests – Exp5 - with DoE centre point – Exp 25.

For the LAC:LAC formulations, it is evident that the particle size distribution of the LAC_70 pseudo-grade, HPMC concentration and powder bed consolidation all had a significant influence on penetration time (Figure 3.25a). The effect of LAC_30 on the penetration time was dependent on LAC_70, hence the significance of the LAC_70*LAC_30 term in the MLR.

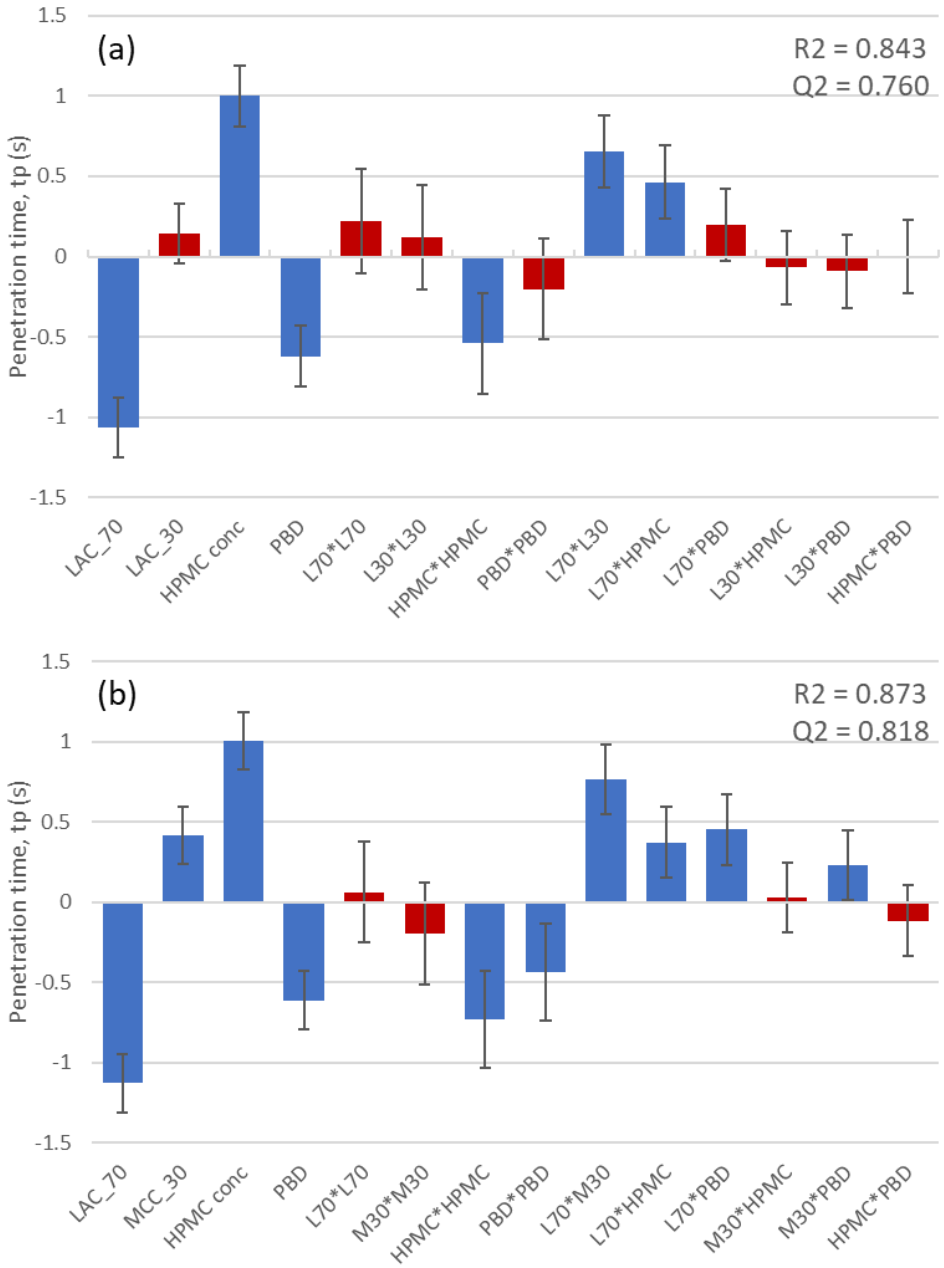

Figure 3.25 MLR coefficients pertaining to complete penetration time, t_p, for (a) LAC:LAC powder beds and (b) LAC:MCC powder beds. Significant coefficients ($p<0.05$) are coloured blue.

The effect of particle size distribution of LAC_70 on penetration time is visually presented as sequential time images in Figure 3.26. Increasing the PSD of LAC_70 decreased the penetration time. Previous studies have reported similar observations for drop penetration tests involving lactose (Charles-Williams et al., 2011; Han, 2017; Hapgood et al., 2009, 2002; Nguyen et al., 2009), glass ballotini beads (Hapgood et al., 2009), siliconised beads (Katsuragi, 2011), starch (Oostveen et al., 2015) and sintered copper (Yang and Xu, 2017). Wettability studies using Washburn capillary rise method have also demonstrated faster rates of penetration with increased particle size (Depalo and Santomaso, 2013; Kiesvaara and Yliruusi, 1993; Kirchberg et al., 2011; Yang et al., 1988). However, other wettability studies have not observed a relationship between particle size and liquid penetration (Galet et al., 2010; Schoelkopf et al., 2002; Subrahmanyam et al., 1999, 1996; Yang et al., 2014).

The cohesive quality of LAC_Lo caused it to agglomerate and create a broad pore size distribution, including prominent macrovoids, as previously described in the literature (Hapgood et al., 2002; Zou et al., 2011). It has previously been demonstrated that large pores contribute to overall porosity but do not contribute to liquid imbibition (Börjesson et al., 2017; Hapgood et al., 2002). Following sessile drop tests on porous stones, Lee et al. (2016a) explained that only narrow pores induced capillary action at the surface, whereas air became trapped in larger pores and did not contribute to penetration. These were visible as entrapped air bubbles in the base of the spherical cap (Lee et al., 2016a).

As mentioned above, experiments 4, 9, and 21 had comparable porosity (50.8-54.7%) but differed in PSD. This allowed the effect of PSD to be studied independently from other factors contributing to microstructure. The penetration time still increased with decreased PSD. Yang and Xu (2017) and Hapgood et al. (2009) reported similar observations when the porosity was controlled independently of the PSD of sintered copper and ballotini beads,

respectively. This slower imbibition was likely due to LAC_Lo possessing a more tortuous pore network and larger internal surface area (Grzelakowski et al., 2009). By considering Darcy's law in Equation 1.27 and the Kozeny-Carmen formula in Equation 2.28, it is evident that the increased specific surface area, reduced pore diameter and tortuosity arising from LAC_Lo resulted in reduced permeability (Fu et al., 2012; Le et al., 2010; Matyka et al., 2008), and in turn slower imbibition (Clarke et al., 2002).

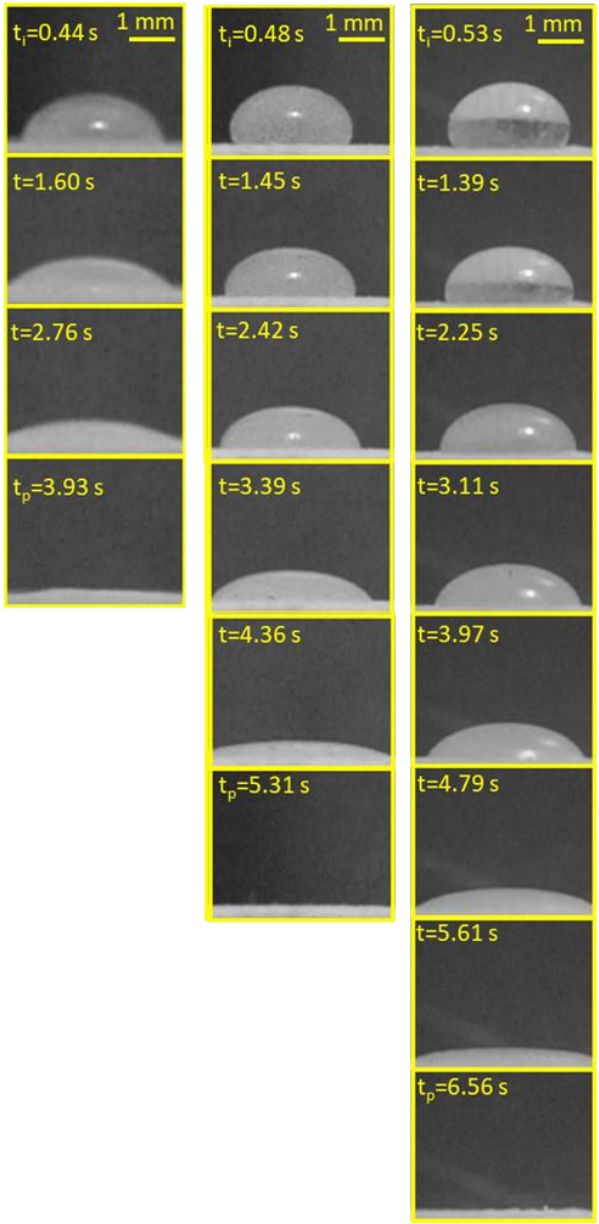

Figure 3.26 Time lapse of a 2.5% w/w HPMC droplet imbibing into a semi-consolidated powder bed consisting of LAC_Hi:LAC_Med (Left), LAC_Med:LAC_Med (centre), and LAC_Lo:LAC_Med (right) mixtures. Left-to-right: Exp 18, 25 and 17.

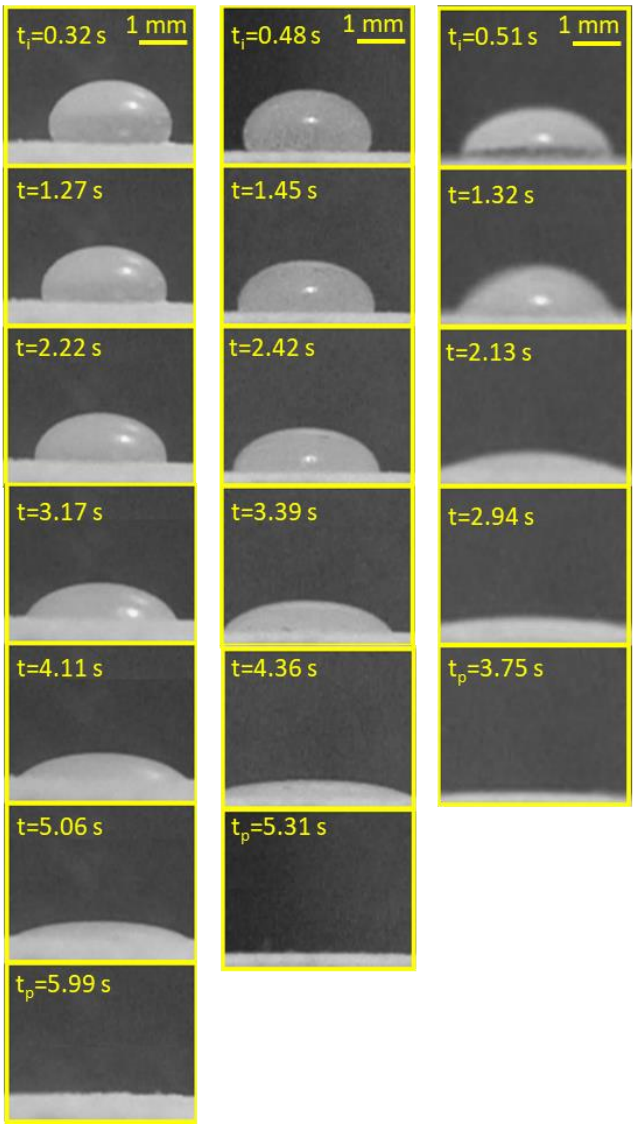

Figure 3.27 Time lapse of an aqueous droplet consisting of 5% w/w HPMC (left), 2.5% w/w HPMC (centre), and 0% w/w HPMC (right) imbibing into a semi-consolidated powder bed made up of LAC_Med:LAC_Med. Left-to-right: Exp 22, 25 and 21.

The effect of HPMC concentration on penetration time is visually presented as sequential time images in Figure 3.27. Increasing the viscosity of the liquid droplet by increasing the concentration of HPMC was found to increase the penetration time in all instances. This is in agreement with the literature examining liquid penetration of powders (Hapgood et al., 2009, 2002; Katsuragi, 2011; Mundozah et al., 2018) and nano-porous alumina membranes (Grzelakowski et al., 2009; Haidara et al., 2008). Increasing HPMC concentration increased

penetration time non-linearly (HPMC*HPMC $p<0.05$), as increasing the concentration from 0% w/w to 2.5% w/w resulted in a greater increase in penetration time than the increase from 2.5% w/w to 5% w/w. This did not correspond with the non-linear increase in viscosity (1.01, 4.27 and 14.33 mPas, respectively) or the direct proportionality reported by others (Haidara et al., 2008; Hapgood et al., 2002). An interaction between LAC_70 and HPMC was evident (LAC_70*HPMC $p<0.05$) as the use of HPMC 5% w/w diminished the influence of LAC_70 PSD, whereas, HPMC 0% w/w was highly dependent on the LAC_70 pseudo-grade (Figure 3.28).

LAC_30 pseudo-grade had a significant influence on the penetration time only when bimodality was achieved (LAC_70*LAC_30 $p<0.05$) and the powder bed was consolidated (LAC_30*PBD $p<0.05$). That is to say, changing from a unimodal powder bed (LAC_Hi:LAC_Hi or LAC_Lo:LAC_Lo) to a bimodal (LAC_Hi:LAC_Lo or LAC_Lo:LAC_Hi) consolidated powder bed resulted in a reduction in penetration time. Varying LAC_30 in the presence of LAC_70_Med had little influence on the penetration time, due to limited bimodality. As seen above, bimodality has the potential to narrow pores as smaller particles occupy voids between larger particles, and in turn induces greater capillary forces. Hapgood et al. (2002) found the droplet penetration time of unfractionated lactose to be longer than a fractionated grade of similar mean diameter. Likewise, Kirchberg et al. (2011), Kirdponpattara et al. (2013), and Dang-Vu & Hupka (2005) observed unsieved powders with a broad PSD to result in a reduced and uneven penetration rate during WCR tests. However, these studies did not study the effects of binary PSD mixtures on liquid penetration. As presented earlier (see section 3.5.3), a larger size ratio between the fine and coarse particles and an approximate 30:70 packing fraction results in greater packing density, whereas a large PSD span resulted

in less efficient packing. Therefore, the bimodal mixtures resulted in a more homogenous pore distribution which increased the rate of penetration in this current study.

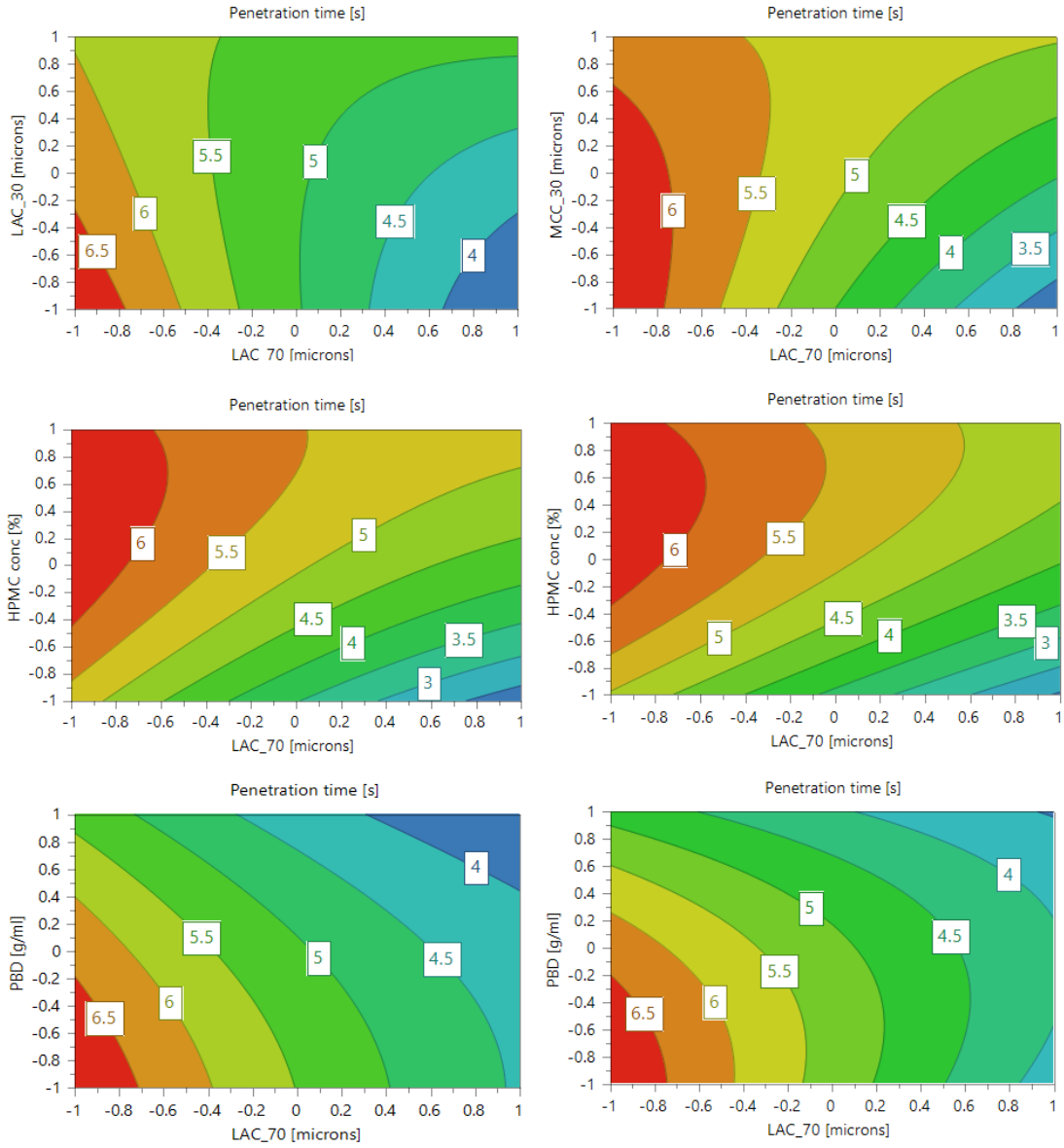

Figure 3.28 Response surfaces illustrating the MLR models (above) and pertaining to the time for complete penetration for LAC:LAC powder beds (left) and LAC:MCC powder beds (right).

Work by Oostveen et al. (2015), Galet et al. (2010) and Hapgood et al. (2002) showed that decreasing the porosity of a powder bed resulted in faster liquid penetration. Correspondingly, increasing the PBD resulted in a decrease in penetration time for all LAC_70 pseudo-grades, however, this effect was more pronounced for LAC_Lo than for LAC_Hi (LAC_70*PBD $p<0.05$), likely due to a larger CI%. This relationship was only evident at 0% w/w and 2.5% w/w HPMC, whereas increases in PBD when using 5% w/w HPMC resulted in an increased penetration time (HPMC*PBD $p<0.05$). The penetration time of water and 2.5% w/w HPMC in relation to consolidation and bimodality is indicative of increased capillarity and Poiseuille flow with decreased porosity on account of a smaller and narrower pore distribution. Whereas, the behaviour of 5% w/w HPMC is due to increased resistive viscous flow as a result of smaller pores at increased consolidation. Similarly, Hapgood et al. (2002) described penetration time of a water droplet to decrease with decreased porosity, but penetration of a viscous PEG600 droplet increased. Comparably, Galet et al. (2010) observed material dependent effects, as decreased porosity of talc resulted in faster capillary action during WCR tests. However, in that study the authors could not delineate between the capillary rise kinetics and the porosity of calcium carbonate powder.

In contrast with results above, Schoelkopf et al. (2002) reported penetration rates of calcium carbonate powder to be independent of particle size and to increase with increased porosity. However, the authors applied compressive forces to their samples to study porosity at a lower range (20-40%) than those cited above (Galet et al., 2010; Hapgood et al., 2002; Oostveen et al., 2015) and this present study (≥40%). This deviation form Poiseuille flow indicates that reduction below a porosity threshold results in a net loss of penetrability owing to insufficient viable pathways for liquid to navigate, despite increased fluid acceleration (Schoelkopf et al., 2002).

When MCC_30 was included as the second component then the penetration times were generally shorter than those obtained for the LAC:LAC mixtures under the same conditions. This is attributable to MCC's vigorous wicking action (Desai et al., 2012; Lerk et al., 1979) and was most evident for water as increasing the HPMC concentration diminished the influence of MCC_30. Further, decreasing the PSD of MCC_30 resulted in a shorter penetration time. This was likely because MCC's highly hygroscopic properties were accentuated by the significantly larger surface area offered by MCC_Lo (Desai et al., 2014, 2012; Rojas et al., 2012; Spence et al., 2005). Hence, the finer MCC_Lo particles were more widely distributed, and therefore, more accessible to the imbibing liquid (Rojas et al., 2012).

Like LAC_30, the effect of MCC_30 on the penetration time was dependent on the LAC_70 PSD but this was not due to bimodality, as was the case for LAC_30. Varying MCC PSD had a greater effect when included in a mixture with LAC_70_Hi than LAC_70_Lo. This was likely due to the stronger capillarity transport of LAC_70_Hi resulting in distributing the imbibing liquid to a greater number of MCC particles (Zhao and Augsburger, 2006), and better elucidating the difference in surface-area controlled absorption rates (Rojas et al., 2012). Similarly, increasing PBD further highlighted the effects of varying the PSD of MCC_30 on penetration time (MCC_30*PBD $p<0.05$). Under fully consolidated conditions and in the presence of HPMC 0% w/w, the effect of varying MCC_30 PSD was most evident.

3.7.4. Spreading analysis - Inertial spreading regime and initial diameter spread

Early droplet spreading was assessed and categorised into two regimes. The first regime involved inertial spreading between droplet impact, t_0, and the first recoil. As the radius of the droplets were smaller than the capillary length, l_c, the inertial spreading regime transitioned to a viscous spreading regime and the effects of gravity on the spreading process were assumed to be negligible. This transition from the inertial regime to the viscous regime was identifiable by a significant reduction in the rate of spreading. Key measurements are depicted in Figure 3.29.

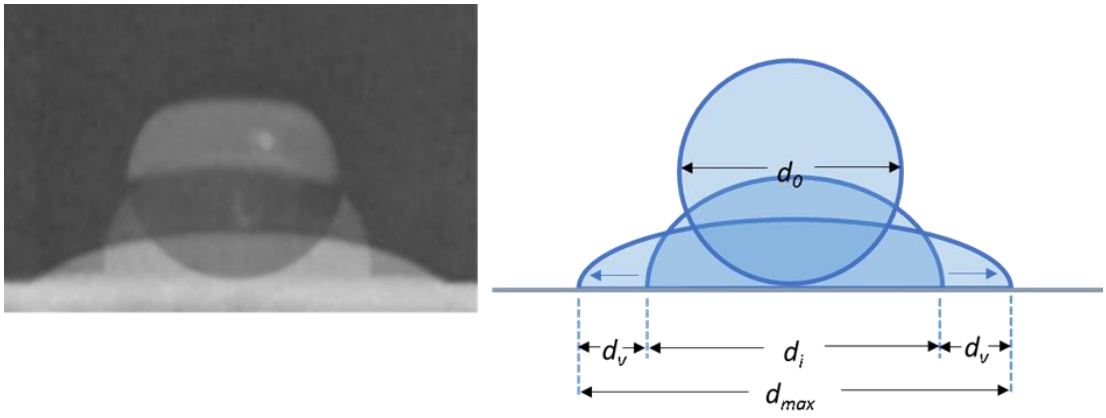

Figure 3.29 Super-imposed images (left) and schematic (right) of droplet measurements during impingement and surface spreading: droplet diameter at impact, d_0; droplet contact diameter following inertial spreading, d_i; and droplet contact diameter following viscous spreading, d_{max}. The extent of viscous spreading is represented by d_v.

A typical sequence depicting all the frames pertaining to inertial spreading and the propagation of the capillary wave is shown in Figure 3.30. As the droplet came into contact with the surface it rapidly spread radially. This is plotted graphically for all test conditions in Figure 3.31. Due to the image acquisition capabilities of the camera used in this study, only a limited number of measurements – 11 to 14 images – could be made during the inertial period allowing for a 7.1-9.0% temporal error. With that said, the measurements obtained

appear to be sufficient for the purposes of discerning the values of the *C*-coefficient and *n*-exponent of $d(t) \sim Ct^n$ from the resulting diameter-time curves.

During the initial moments of spreading (≤12 ms), the power law $d(t) \sim t^{1/2}$ held true for the majority of experimental conditions. However, deviations from $n \approx 0.5$ were evident for 5% w/w HPMC and LAC_70_Lo, as the inertial spreading was observed to transition to the viscous regime earlier and more gradually than other experimental conditions. Hence, low viscosity and large PSD resulted in values of *n* approaching 0.5, however, at high viscosity and decreased PSD *n* decreased to values as low as 0.339.

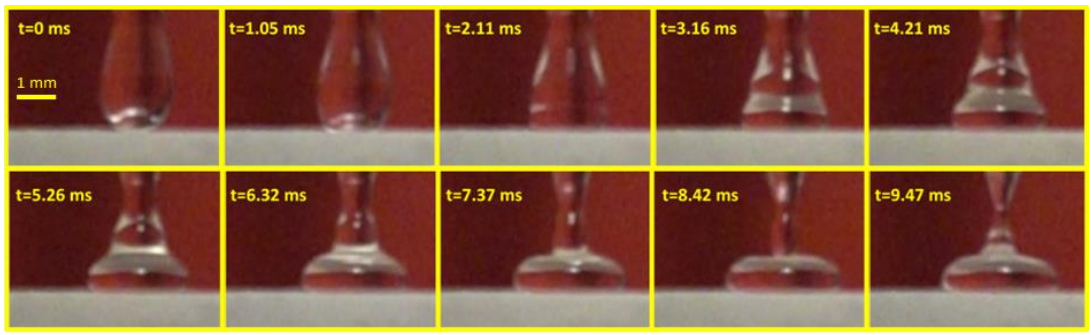

Figure 3.30 Sequential images depicting the propagation of the capillary wave and inertial spreading during droplet deposition. The time interval between two successive images is ~1.05 ms.

These observations conflict with the universality of $n \approx 0.5$ claimed by earlier studies (Biance et al., 2004; Carlson et al., 2012; Chen and Bonaccurso, 2014b; Eddi et al., 2013; Grewal et al., 2015; Rioboo et al., 2002; Sikalo et al., 2002a; Stapelbroek et al., 2014; Winkels et al., 2012; Wu et al., 2004), as well as, the proposed theory that the Laplace pressure from the capillary induced wave overcomes surface topography and heterogeneity unimpeded (Eddi et al., 2013; Stapelbroek et al., 2014). Further, others reported that the power law was insensitive to liquid properties (Chen et al., 2011; Chen and Bonaccurso, 2014b). Nevertheless, these observations are consistent with other experimental studies that have shown the n-exponent of the inertial regime to be dependent on the substrate properties

(Bird et al., 2008; Chamakos et al., 2016; Chen et al., 2011; Wang et al., 2015; Yang and Xu, 2017), as well as numerical solutions (Das et al., 2018; Frank et al., 2015; Milacic et al., 2019).

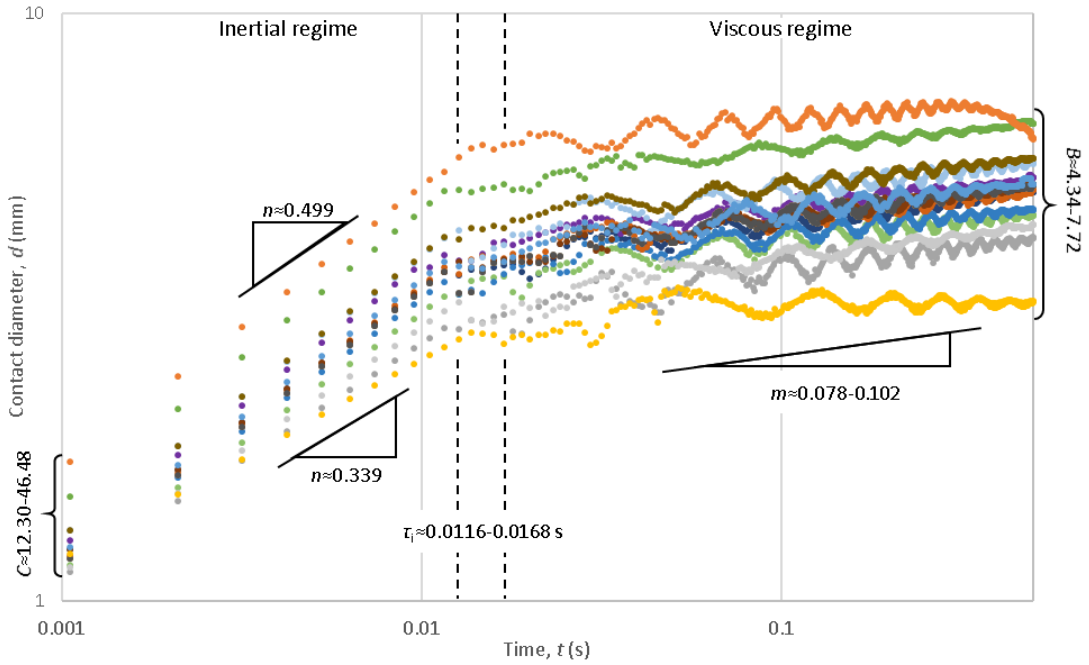

Figure 3.31 Log-log plot of the contact diameter during the first 0.5 s of droplet spreading following impact for all the experimental tests. Colouring is for purposes of distinguishing experiments from one another but not for identification purposes.
The range of C-coefficient, n-exponent and inertial time (τ) are highlighted for the inertial regime. The B-coefficient and m-exponent are highlighted for the viscous regime.

Following tests on a variety of substrates, Winkels et al. (2012) and Stapelbroek et al. (2014) noted that initially all wetting conditions exhibited $n\approx0.5$, but with decreased substrate wettability, the transition of droplet spreading to the viscous regime ($n\approx0.1$) commenced earlier. It is possible that this was the case in this study, however, the limited number of measurements during the inertial spreading phase (10-12 frames) restricted the ability to discern within the inertial time when the deviation from $n\approx0.5$ occurred. Instead the value of the *n*-exponent was calculated from the inertial spreading duration in its entirety.

Eddi et al. (2013) considered the spreading exponent to decrease throughout spreading, and an increased contact angle prompted an earlier departure from the inertial power law,

whereas increased viscosity resulted in a later and more gradual transition to the viscous regime. The powder grade was found to have no discernible effect on the inertial time τ, whereas increased viscosity did delay the onset of the viscous regime. The inertial regime lasted 11.6±1.04 ms for water (n=9) and 16.8±2.08 ms for 5% w/w HPMC (n=9), which are comparable to the estimated inertial times using $\tau_i \approx (\rho r_0^3/\gamma)^{1/2}$ (Biance et al., 2004), which are 14.2 and 17.9 ms, respectively. This is consistent with findings by Chen and Bonaccurso (2014b), whereby surface wettability had no influence on the inertial duration, but viscosity extended it substantially. Yet there is no consensus, as Biance et al. (2004) found the duration of the inertial regime decreased with increased liquid viscosity.

Frank et al. (2015) proposed that the reduced n-exponent to be a result of slowed spreading. To overcome the energy barriers in the presence of topographic or chemical patterns that lead to a spatial variation of the local surface energy, an additional source of energy is required in the vicinity of the contact line. This energy must come from the kinetic energy of the flow inside the droplet but was limited due to the low impact velocity. Similarly, Lee et al. (2016a) explained using porous stones, that air became trapped beneath the droplet during spreading causing hydrophobic non-wetting behaviour.

Figure 3.32a-e compares the main effect of all the factors on inertial spreading, as well as inertial spread during the fastest and slowest tests (Figure 2.31f). The C-coefficient ranged from 12.3 to 46.48, and was found to decrease with increased viscosity and decreasing powder grade, and is in agreement with the literature (Bird et al., 2008; Das et al., 2018; Eddi et al., 2013; Frank et al., 2015; Winkels et al., 2012; Yang and Xu, 2017). However, the effects of particle size appeared to diminish with increased viscosity, i.e. the C-coefficient resulting from 5% w/w HPMC was insensitive to particle size, as was the case in prior studies (Bird et

al., 2008; Chen and Bonaccurso, 2014b). Conversely, Wu et al. (2004) experimentally demonstrated the *C*-coefficient to be independent of liquid properties.

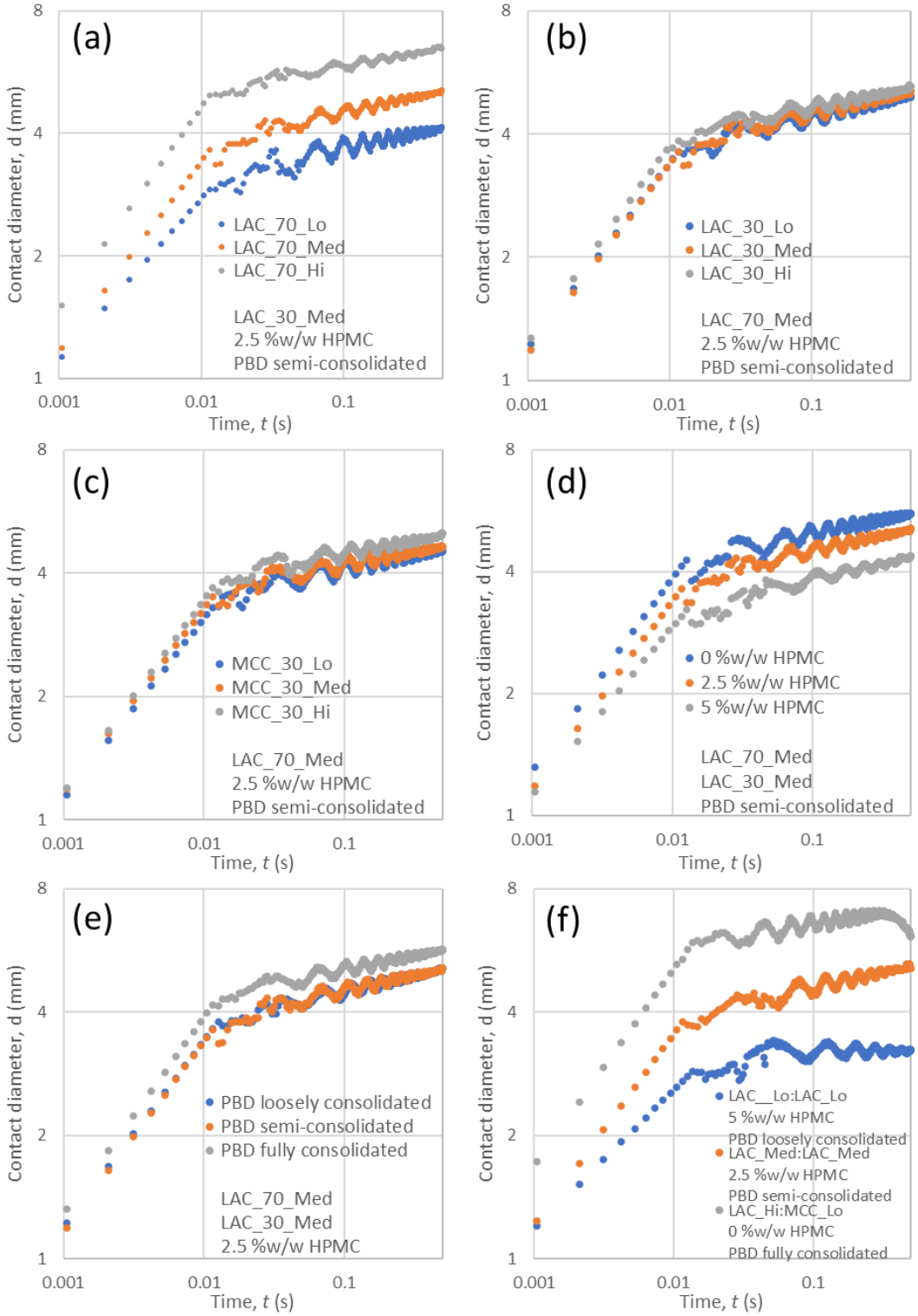

Figure 3.32 Graphs (a-e) compare the effect of varying each factor on inertial spreading. Graph (f) compares the inertial spreading of fastest -Exp10 - and slowest penetration tests – Exp5, as well as the DoE centre point- Exp26.

There was no evidence of the excipient nor the pseudo-grade of the second component, be it MCC_30 or LAC_30, having any significant influence on inertial spreading (Figure 3.33). Inertial spreading was also found to be independent of powder bed consolidation. With that said, it should be noted that due to the significant temporal error introduced by the limited frame rate, it is difficult to determine anything but the most significant and influential trends during inertial spreading from the current data.

The initial diameter spread, d_i, was the diameter of the droplet following inertial spread and ranged from 2.88 to 5.32 mm. d_i was the result of both *C*-coefficient and *n*-exponent, and therefore, only LAC_70 and HPMC were discerned to influence d_i, whereby a finer pseudo-grade and a greater viscosity resulted in a smaller footprint. Additionally, an interaction between these two factors was observed (LAC_70*HPMC $p<0.05$), as increased HPMC diminished the influence of LAC_70 PSD, as evidenced from Figure 3.34.

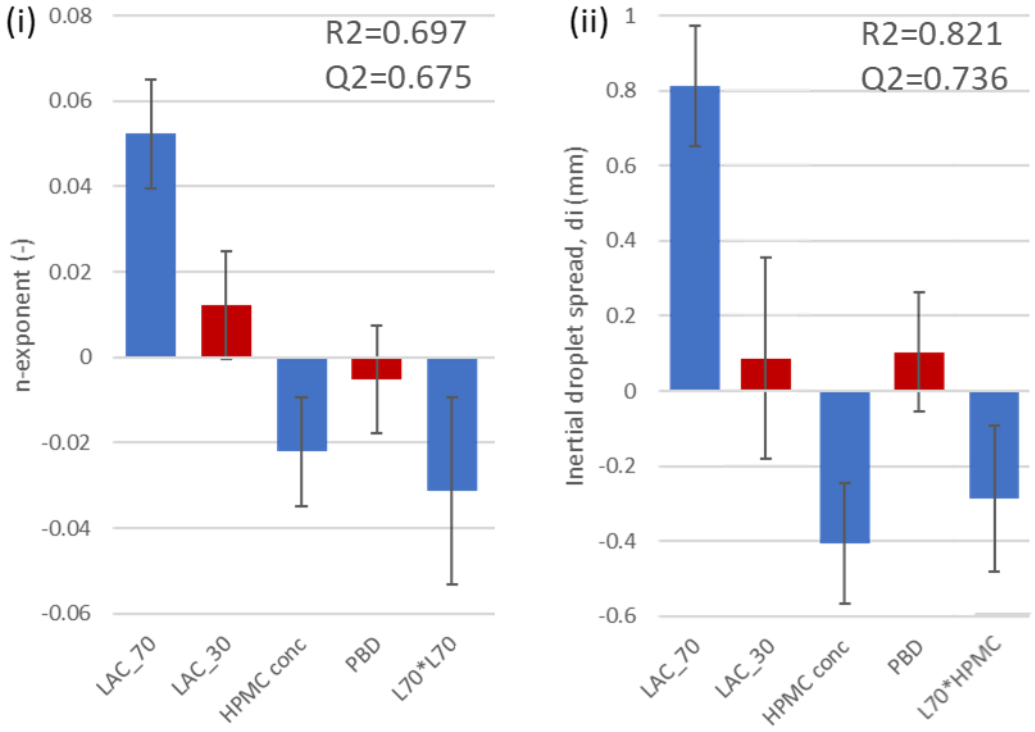

Figure 3.33 MLR coefficients pertaining to (i) the n-exponent during inertial spreading and (ii) the initial spread diameter, d_i, following inertial spread on LAC:LAC powder beds. Significant coefficients ($p<0.05$) are coloured blue.

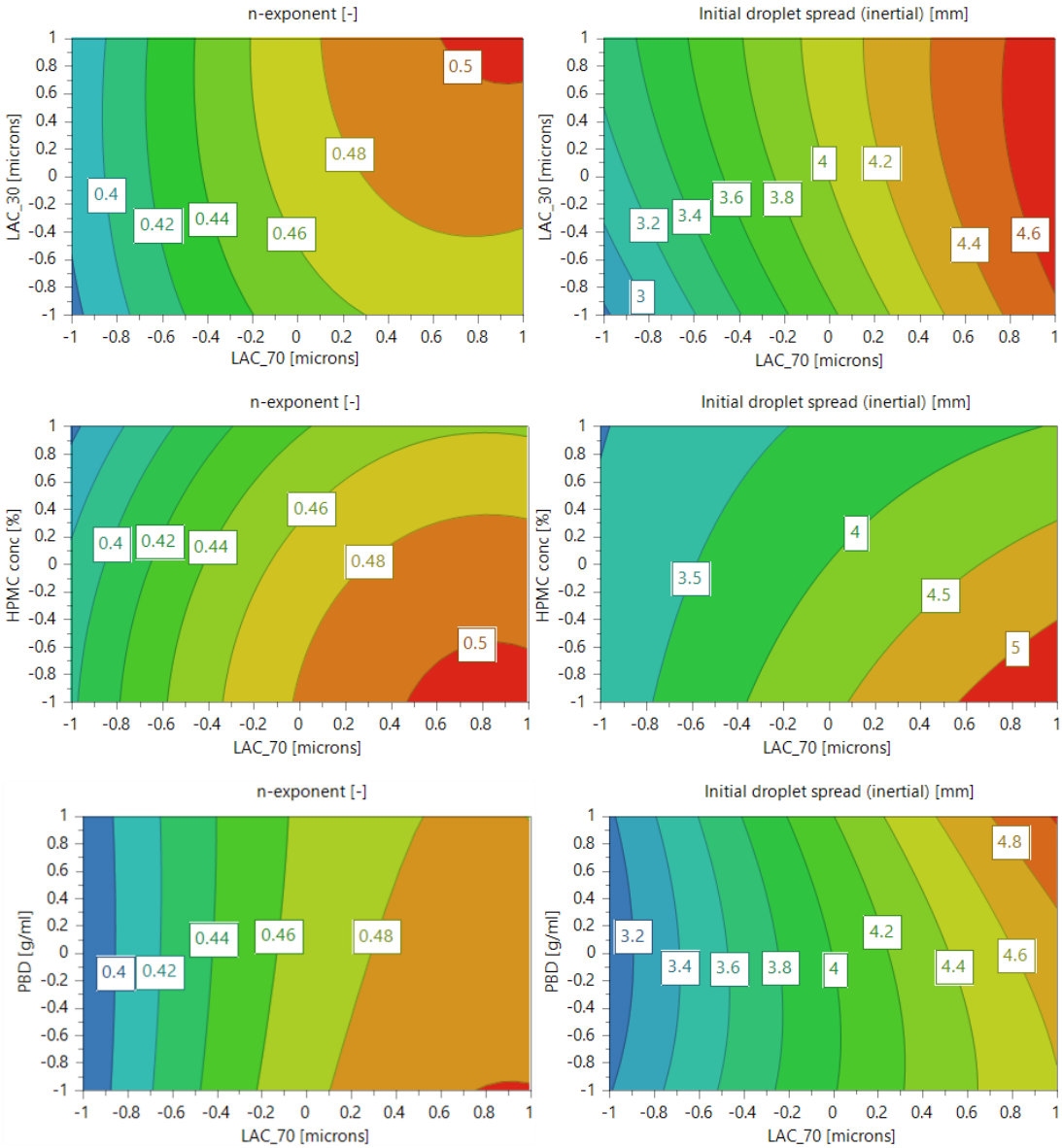

Figure 3.34 Response surfaces illustrating the MLR models pertaining to the n-exponent (left) and initial droplet spread, di (right) on LAC:LAC powder beds.

3.7.5. Spreading analysis - Viscous spreading regime and maximum diameter

Measuring the power law of the viscous regime following transition from inertial spreading was difficult, as the initial fluctuation arising from droplet impact and the corresponding deformation obscured the trend. Additionally, for some experimental conditions that resulted in rapid absorption, there is little to no distinction between the energy dissipating fluctuations and the recession of the droplet - that is to say, no linear region was visible. Therefore, when necessary a line of best fit has been inferred from the fluctuations of the contact diameter.

Figure 3.35 presents the MLR coefficients for the m-exponent and viscous spread and Figure 2.36 shows the corresponding response surfaces. For the majority of experimental conditions, the viscous regime scaled according to Tanner's law and obeyed $d(t) \sim Bt^m$, where m approximated 0.1 and B ranged between 4.34 to 7.72. As a result, droplet spreading beyond the inertial regime, $d_v = d_{max} - d_i$, was proportional to the duration of the viscous regime. However, for droplet conditions that induced rapid penetration (e.g. Exp10), the exponent m was suppressed as low as 0.078. This can be ascribed to hydrostatic pressure arising within the droplet of the imbibing liquid and causing the contact line of the droplet to be pinned to the porous surface, thereby impeding viscous spreading (Charles-Williams et al., 2011; Haidara et al., 2008). Liquid flow into the surface pores became more favourable than liquid flow at the three-phase contact line and across the heterogenous powder surface, indicating that viscous spreading and imbibition were competing droplet behaviours (Mundozah et al., 2018). Therefore, for conditions that resulted in a short penetration time, the spreading potential during the viscous regime was limited by rapid imbibition. For example, a water droplet impinging on LAC_70_Hi resulted in a short viscous regime, as the contact diameter demonstrated a quick transition to a *decreasing drawing area*. With that said, conditions

that resulted in longer penetration times did not necessarily cause viscous spreading to continue for longer. LAC_70_Lo was responsible for some of the longest penetration times, however, droplet spreading quickly transitioned from the viscous regime to a *constant drawing area,* i.e. a static footprint. This is likely due to the greater roughness and porosity at the powder surface (Marston et al., 2013), and hence, insufficient adhesive forces to overcome liquid adhesion in the bulk of the droplet to thermodynamically promote further extension at the contact line (Cazabat and Cohen-Stuart, 1986; Leese et al., 2013; Lopez et al., 1976).

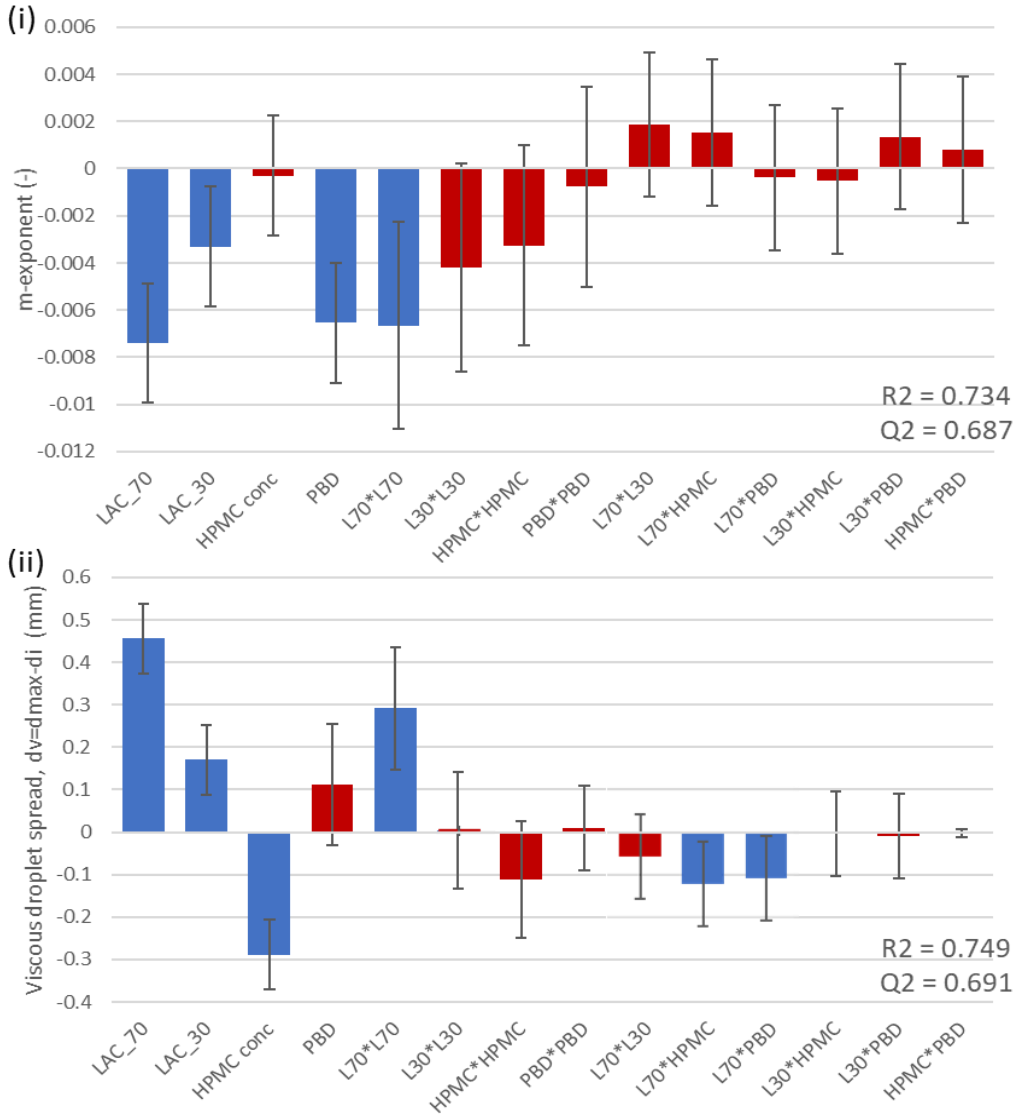

Figure 3.35 MLR coefficients pertaining to (i) the m-exponent for the viscous spreading regime and (ii) the viscous spread diameter, d_v, on LAC:LAC powder beds. Significant coefficients ($p<0.05$) are coloured blue.

The effect of PSD on spreading can be further understood by considering the capillary forces induced by the powder bed following impingement. The pore network of LAC_Hi transported the imbibing liquid radially away from the droplet-surface contact area (Börjesson et al., 2017; Lee et al., 2016b). As the surface adjacent to the contact line became wetted it facilitated spreading of the macroscopic bulk (Apel-Paz and Marmur, 1999; Cazabat and Cohen-Stuart, 1986). The lack of capillary action in the LAC_Lo resulted in the droplet being absorbed into the powder bed as a function of gravity with limited radial imbibition. This is consistent with conclusions made from examining nuclei morphology by Emady et al. (2011), even though no measurements of droplet spreading were made.

Therefore, by considering that LAC_70_Med prolonged viscous spreading when compared to LAC_70_Hi and LAC_70_Lo, it is evident that the PSD of LAC_70 had a non-linear relationship with viscous spreading (LAC*LAC $p<0.05$). This was because LAC_70_Med provided a compromise to promote viscous spreading; viscous spreading was impeded less by imbibition-induced hydrostatic forces and rapid absorption, as was the case with LAC_70_Hi; and viscous spreading was less hindered by surface non-wettability arising from a high surface pore fraction, as was the case with LAC_70_Lo.

After the pseudo-grade of LAC_70, liquid viscosity was the second most influential variable and inversely correlated on viscous spreading (Mundozah et al., 2018; Werner et al., 2007). With increased HPMC concentration the influence of the other variables diminished, as the viscous regime became less sensitive to powder bed conditions. Although increased HPMC concentration prolonged penetration time, it shortened the duration of the viscous regime, transitioning to a *constant drawing area* sooner on account of the increased viscous friction resisting spreading (Grewal et al., 2015). Further, the suppression of the *m*-exponent that was observed for water droplets was not observed for 5% w/w HPMC when penetrating into

identical powder bed conditions. This indicates that viscous spreading at the three-phase contact line was not hindered by capillarity-induced hydrostatic forces.

The influence of the LAC_30 pseudo-grade on viscous spreading was significant but small. Interestingly, the effect of PSD of LAC_30 on viscous spreading did not correspond to bimodality and instead, increasing the PSD of LAC_30 increased d_v only in the presence of LAC_70_Lo and to a lesser extent, LAC_70_Med. This further supports the conclusion that reducing the surface area, and therefore the roughness factor r, increased the extent of viscous spreading (Marston et al., 2010).

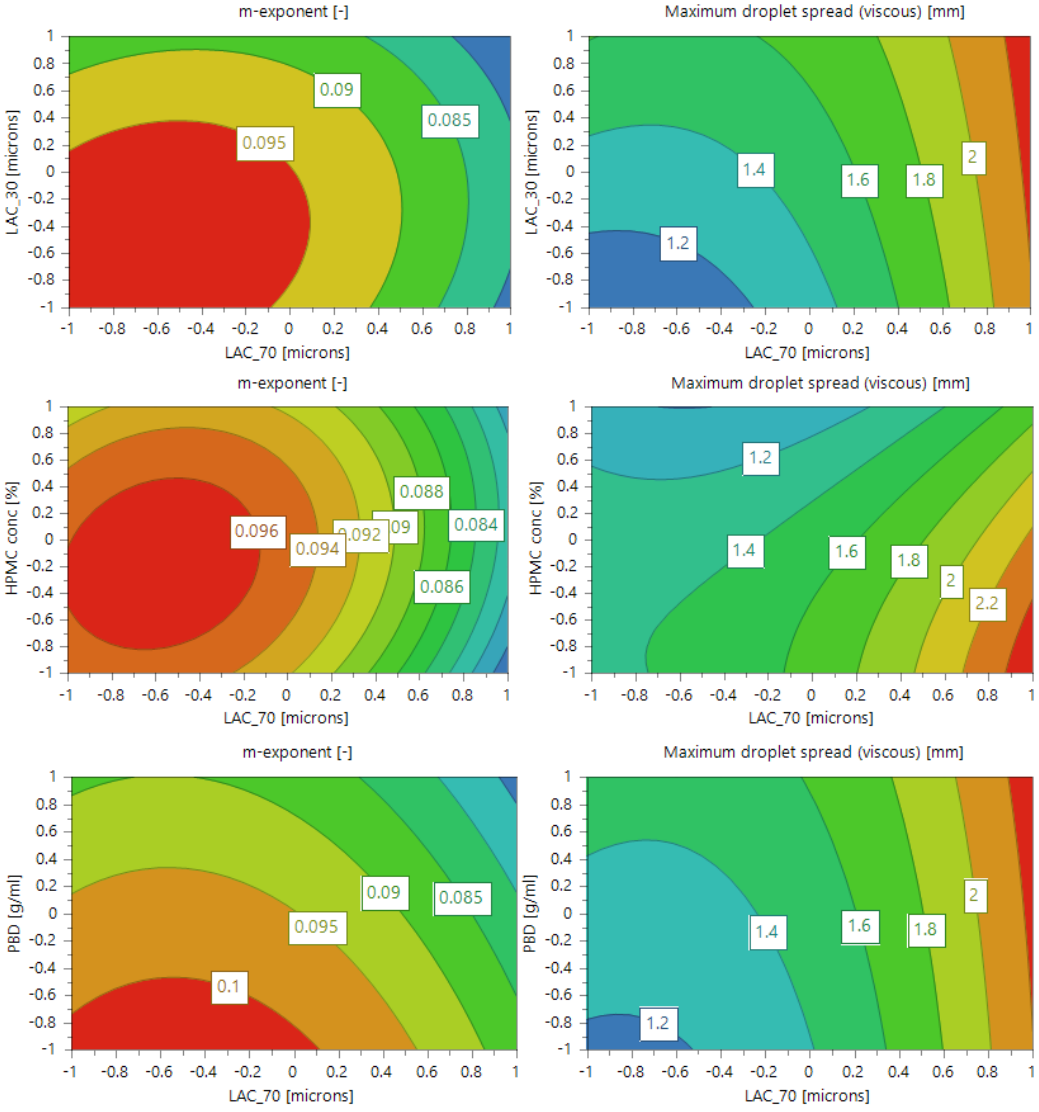

Figure 3.36 Response surfaces illustrating the MLR models pertaining to the m-exponent (left) and viscous droplet spread, dv, (right) on LAC:LAC powder beds.

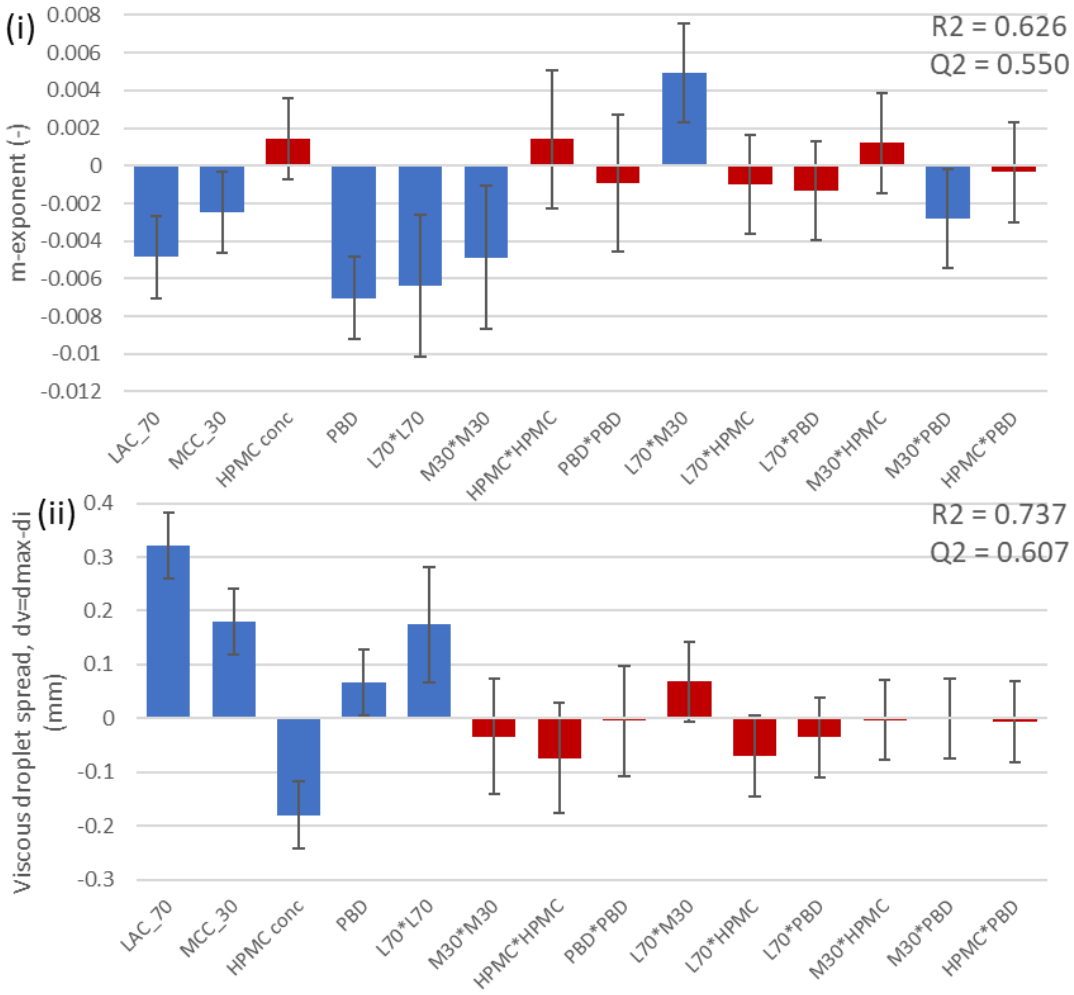

Figure 3.37 MLR coefficients pertaining to (i) the m-exponent for the viscous spreading regime and (ii) the viscous spread diameter, dv, on LAC:MCC powder beds. Significant coefficients ($p<0.05$) are coloured blue.

The effect of powder bed consolidation on d_v was also found to be significant with a dependency on LAC_70 pseudo-grade (LAC_70*PBD $p<0.05$). Despite decreasing the penetration time, increasing the state of consolidation of a LAC_70_Lo powder bed promoted viscous spreading and increased d_v. However, the decreased penetration time resulting from increased consolidation reduced the duration of viscous spreading of LAC_70_Med, as well as suppressing exponent m below 0.1. As LAC_70_Hi exhibited very little spreading after the inertial regime, the consolidation state had no discernible effect on d_v.

Figure 3.37 and Figure 3.38 respectively show the MLR coefficients and response surfaces for LAC:MCC formulations. The addition of MCC_30 decreased the duration of viscous spreading when compared to like-for-like LAC_30 conditions. This can be expected as the inclusion of MCC_30 in the binary mixture decreased the penetration time. The hygroscopic properties of MCC promoted imbibition and pinned the contact line to suppress exponent *m* below 0.1. Increasing the PSD of MCC_30 was observed to permit greater viscous spreading when compared to MCC_30_Lo, as evidenced by a larger d_v. Unlike LAC_30, this was irrespective of the LAC_70 pseudo-grade. These observations are attributable to larger MCC particles occupying a smaller surface fraction than MCC_Lo particles, and less able to suppress *m*.

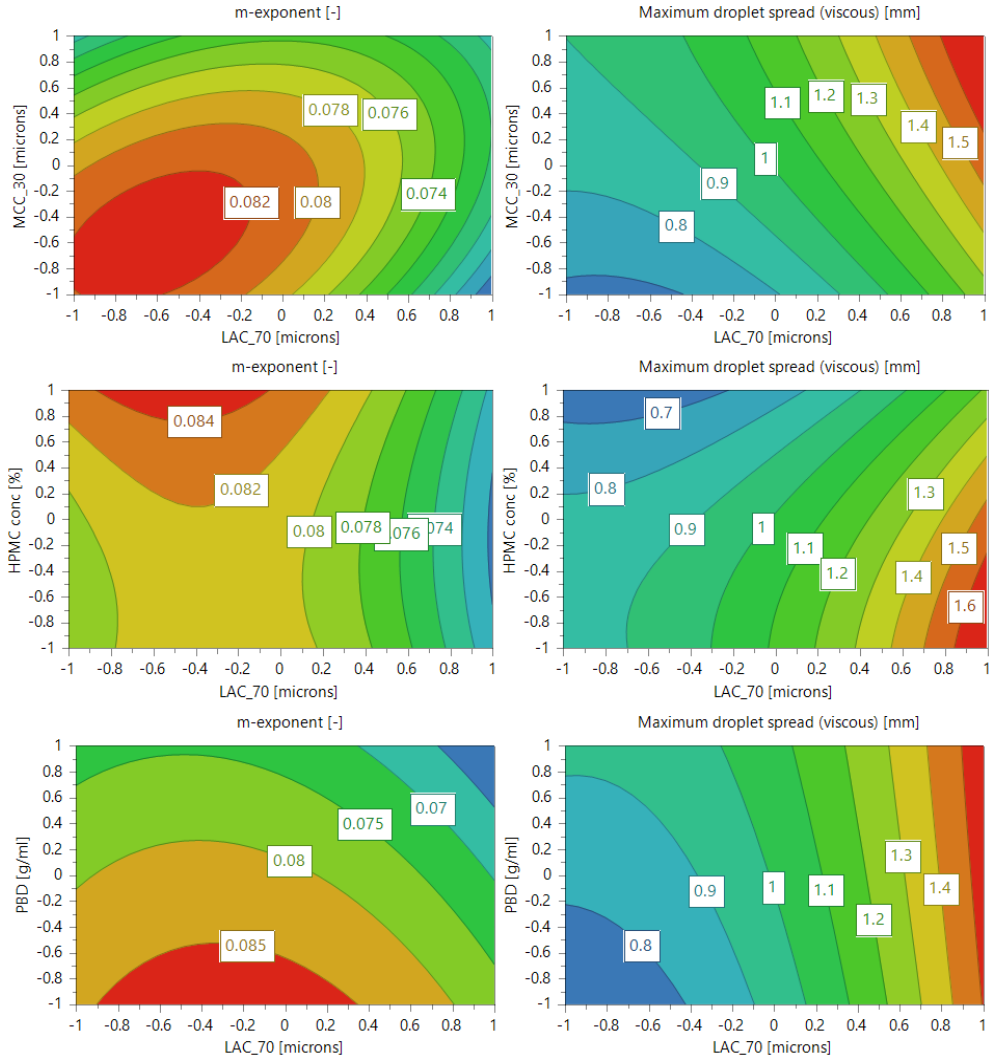

Figure 3.38 Response surfaces illustrating the MLR models pertaining to the m-exponent (left) and viscous droplet spread, dv, (right) on LAC:MCC powder beds.

3.7.6. Imbibition analysis

Figure 3.39 shows various normalised droplet measurements as functions of time. The imbibed volume and rate are normalised with respect to the droplet impingement volume, V_0; and the contact area is normalised with respect to the droplet cross sectional area, d_0^2.

Interestingly, the imbibed volume-time curve is similar to that obtained from WCR tests (Figure 2.18b), whereby the rate of absorption initially increases exponentially, followed by a linear portion before plateauing as droplet penetration approaches completion. Previously it has been reported that droplet spreading represents a rate limiting factor in imbibition, as the contact area determines the number of entry pores in the substrate's surface accessible to the imbibing liquid (Grzelakowski et al., 2009). Therefore, when comparing the time-profile of the imbibed volume to that of the contact area, it would be expected that the imbibition flow rate ($\Delta V/\Delta t$) would increase with increased contact area during viscous spreading. This does not seem to be the case as the imbibition rate (redline in Figure 3.39) remains relatively constant, albeit with a gradual decline, throughout droplet spreading despite an increase in contact area during viscous spreading – up to 35 % - leading up to d_{max}.

Additionally, the imbibition flow rate would also be expected to decrease in line with the receding contact area during the final stage of the penetration test. The droplet spreading reached d_{max} when approximately 60% of the water droplet had been absorbed, however, despite the reduction in contact area that immediately followed, the imbibition rate did not decrease until approximately 80% of the droplet had been imbibed. These discrepancies between the imbibition rate and the contact area allude to an alternative or additional rate limiting factor to contact area lone. This can be better illustrated by the Darcy adimensional imbibition rate, V_{imb}(adim) (green line in Figure 3.39).

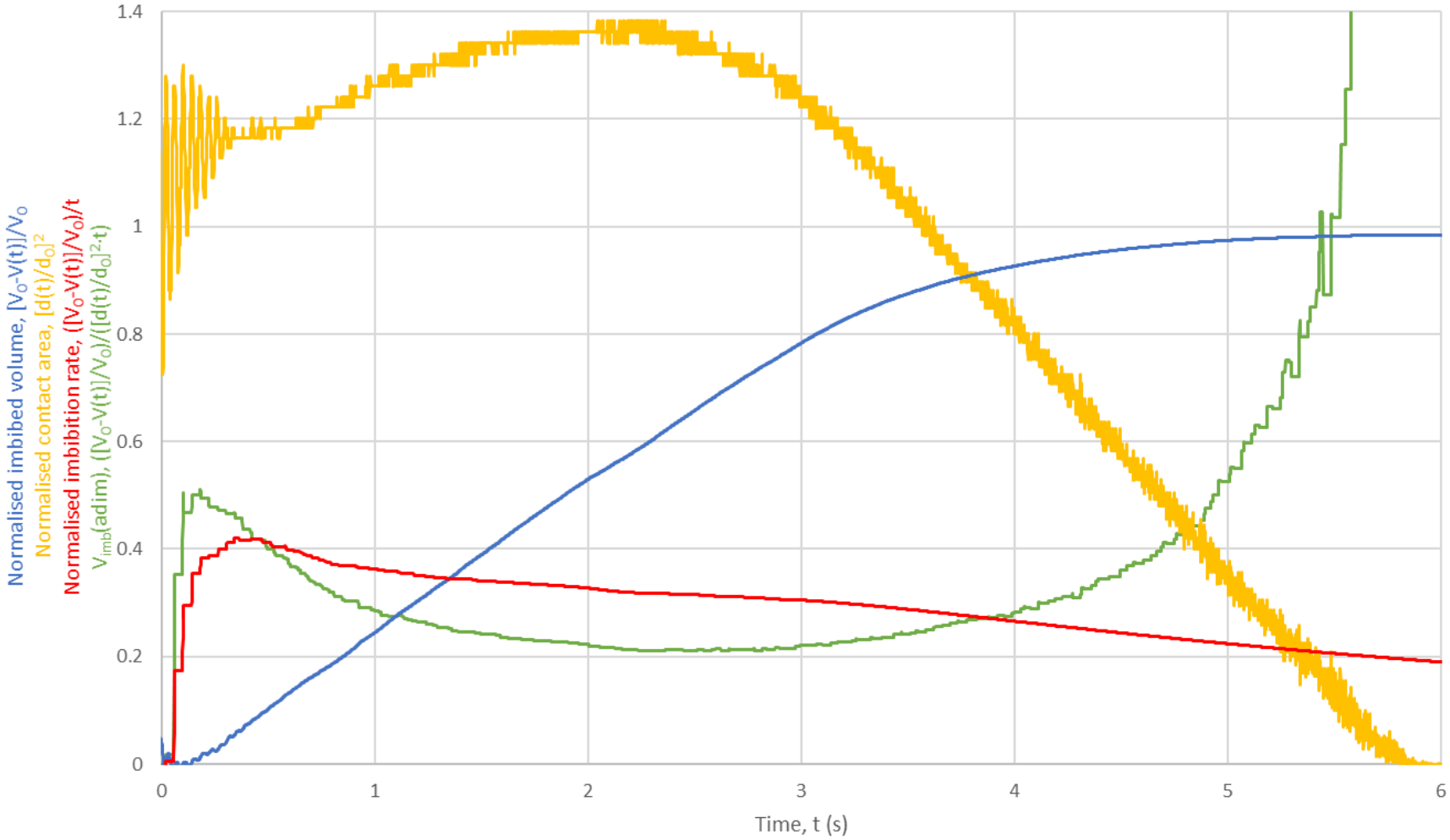

Figure 3.39 Normalised imbibed volume, $[V_0-V(t)]/V_0$ (blue line), normalised contact area, $[d(t)/d_0]^2$ (orange line), normalised imbibition rate, $([V_0-V(t)]/V_0)/t$ (red line) and Darcy's adimensional imbibition rate, $([V_0-V(t)]/V_0)/([d(t)/d_0]^2t)$ (green line) plotted concurrently as a function of time.

As can be seen, the imbibition rate per unit area decreased with the commencement of droplet viscous spreading, before reverting to an increased rate once the contact area receded below d_i. This implies the imbibition rate of the imbibing liquid per unit area decreased as the overall flow rate was relatively constant even though the contact area increased. These findings suggest very limited imbibition actually occurred through the dry entry pores located within the area that became accessible during viscous spreading, d_v. These results contrast with the conclusion drawn by Grzelakowski et al. (2009), whereby it was reported that the Darcy adimensional imbibition rate of a droplet in a nano-porous alumina membrane increased during penetration with increased spreading. One possible explanation for this is related to observations made by Hapgood et al. (2009) and Marston et al. (2013). In those studies, it was demonstrated that liquid droplets more readily and preferentially penetrated into a pre-wetted powder than a dry powder because of the deposition of the precursor film on the inside of the surface entry pores, resulting in shorter penetration times. What's more, Hapgood et al. (2009) described a phenomenon whereby if a droplet was simultaneously in contact with two adjacent regions of powder that had different moisture concentrations, i.e. one dry and one wet, then the imbalanced Laplace pressure would result in the droplet being drawn into the wetted region and not penetrate the dry region (Figure 3.40).

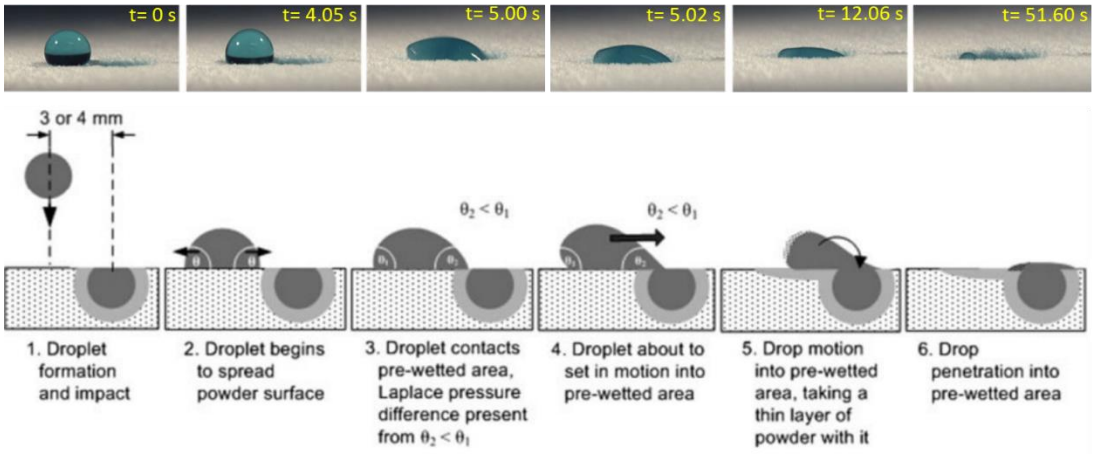

Figure 3.40 Images of a PEG400 droplet deposited adjacent to pre-wetted lactose 200 mesh powder (top) and schematic diagram (bottom) depicting lateral drop motion due to Laplace pressure imbalance (Hapgood et al., 2009).

It therefore stands to reason, that as the droplet expanded radially across the powder bed surface during the viscous spreading regime, flow through the newly accessible dry entry pores was slower (or non-existent) than flow through the already wetted pores that were available at $t=d_i$ following inertial spreading, as illustrated in Figure 3.41. Hence, the flow through the newly accessible dry pores contributed less to the overall flow rate than flow through the original entry pores. In other words, the pores resulting from viscous spreading were not observed to influence the imbibition flow rate. This is further evidenced by the flow rate during droplet recession, whereby only once the contact area had receded below the pre-viscous spreading contact diameter, $d(t)<d_i$, did the overall flow rate substantially decrease. This phenomenon may explain the conflicting results with Grzelakowski et al. (2009); in that instance, the completely wetting properties of the silicone oil droplet ($\theta_{eq}\approx0^o$) could have lessened the Laplace pressure imbalance induced by the presence of a precursor film.

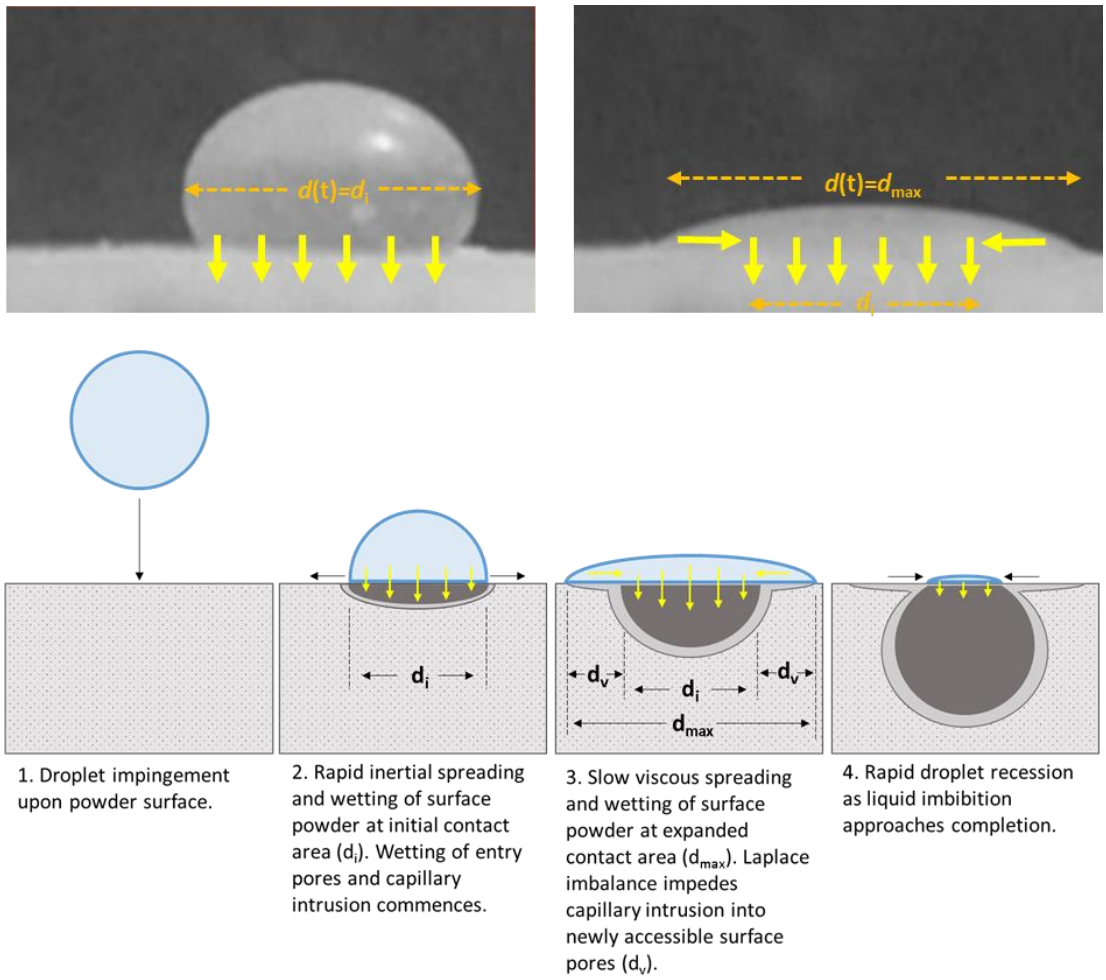

Figure 3.41 Images (top) and schematic (bottom) representing stages of droplet imbibition. Yellow arrows indicate the suspected liquid flow of penetrating droplet at the various stages of droplet penetration.

In addition to this, the hydrostatic pressure at the periphery of the droplet contact area could be lower than that at the centre of the droplet. Therefore, the pressure from the droplet at the periphery may be below a critical threshold to overcome the surface tension and force required for pore entry. This phenomenon was explored by Hosseini (2015) using a series of transparent parallel pores upon which a droplet was deposited. A representation of this is presented in Figure 3.42 and it can be clearly seen that the droplet does not penetrate the pores uniformly, as the pores towards the centre are penetrated to a greater extent than the peripheral pores.

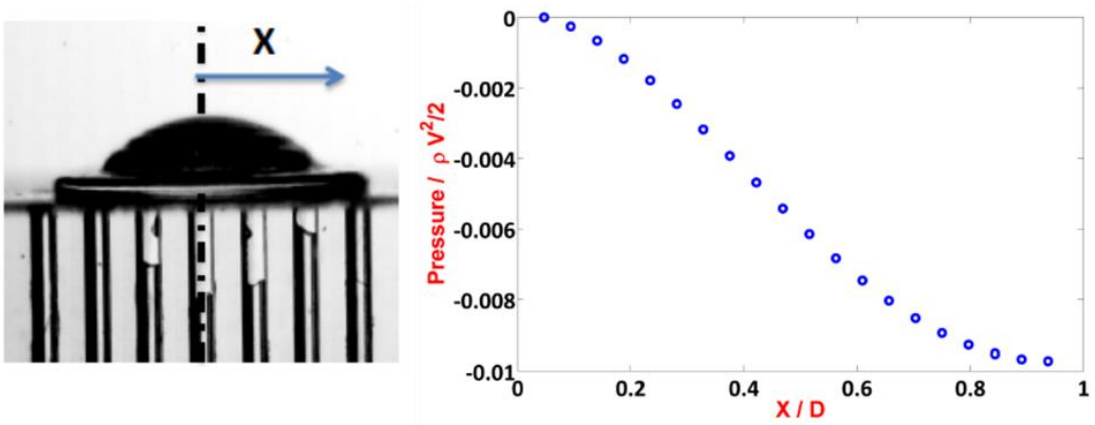

Figure 3.42 Pressure gradient on the substrate across the droplet during spreading (Hosseini, 2015).

The power law $V_{imb}(adim) \sim A' t^k$, quantified the relationship between the contact area and flow rate for the duration of viscous spreading. The *A'*-coefficient ranged from 0.066, indicating a slow rate of imbibition, to 0.483, resulting from rapid imbibition. The *k*-exponent ranged from -0.0044, indicating minimal reduction in $V_{imb}(adim)$ due to negligible spreading, and -0.371 resulting from significant viscous spreading. Hence, the negative values of the *k*-exponent indicate that in none of the experimental conditions did the pores beneath d_v contribute to imbibition proportionally. The more negative values indicate that a greater viscous spreading rate was not accompanied by an increased flow rate. These results are more in agreement with Mundozah et al. (2018) than Grzelakowski et al. (2009), as they too reported negative *k* values that decreased in magnitude with increased wettability and viscosity.

Figures 3.43 compares the main effect of each variable. The significant coefficients included in the MLR models (Figure 2.44) indicate that larger LAC_70 particles, greater HPMC concentration, increased consolidation, and the inclusion of MCC_30 decreased $V_{imb}(adim)$ at $t=d_{max}$. Increasing the bimodality of the PSD via LAC_30 also increased *k* (LAC_70*LAC_30 $p<0.05$).

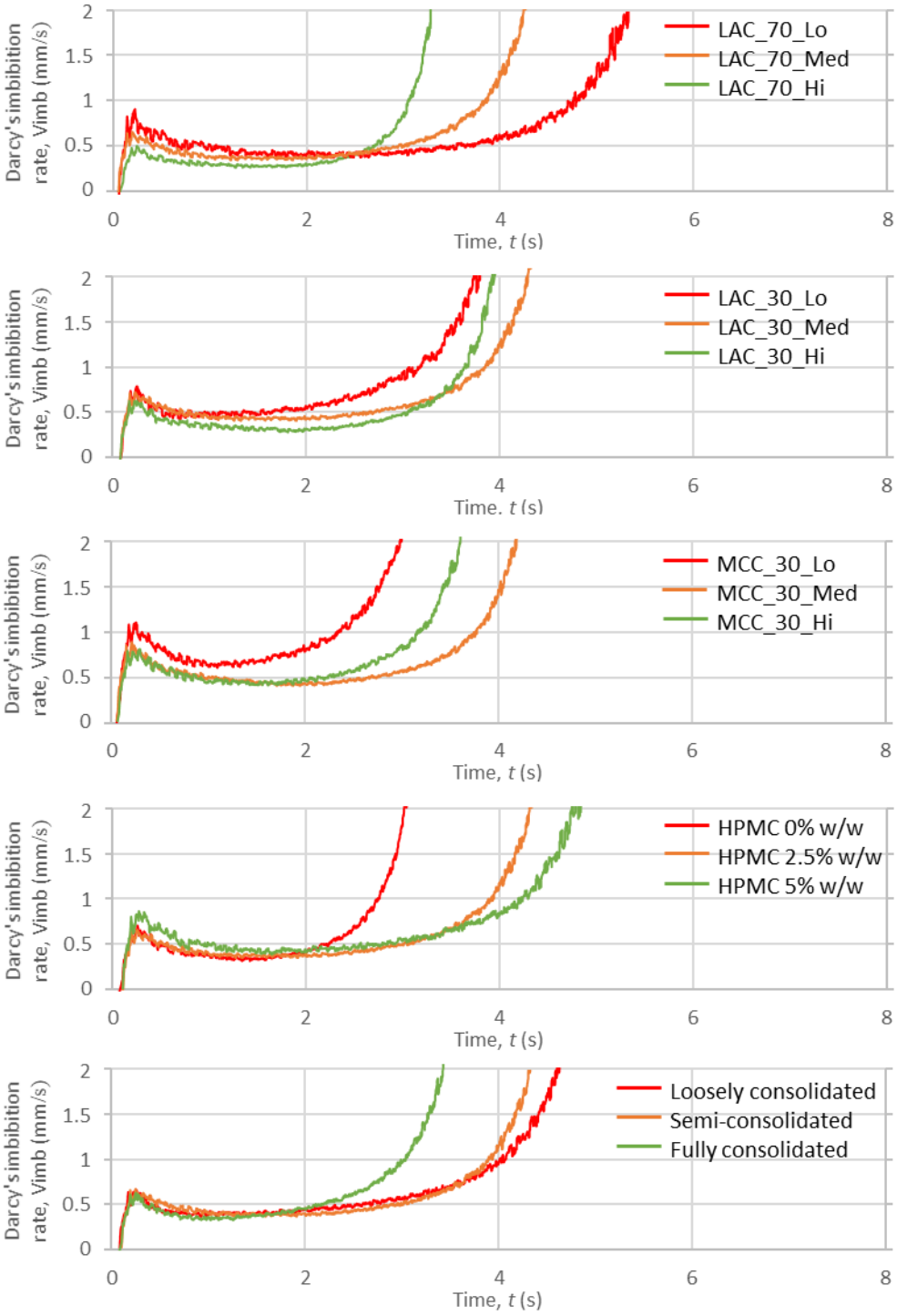

Figure 3.43 Comparison of the main effect of each variable on Darcy's imbibition rate plotted against time. All other variables were at the medium level.

Another observation related to a phenomenon identified by Charles-Williams et al. (2011), whereby the maximum spreading diameter, d_{max}, corresponded to an infiltrated volume fraction, and was viscosity dependent. This was true for this study, in that the d_{max} of water on a LAC:LAC powder bed was achieved when circa 60% of the droplet volume had been imbibed for multiple powder bed conditions. This decreased to ~45% and ~40% for the 2.5% w/w and 5% w/w HPMC droplets, respectively. These values were lower and less defined for LAC:MCC powder beds, likely due to MCC's hygroscopic properties. Charles-Williams et al. (2011) attributed this phenomenon to hydrostatic pressure in the body of the droplet pinning the three-phase contact line, and potentially increasing its sensitivity to topographical variation. Other authors have speculatively cited this pinning theory following observations of arrested spread prior to imbibition completion (Grzelakowski et al., 2009; Haidara et al., 2008; Lee et al., 2016b; Mundozah et al., 2018). However, in light of the above discussion, it is possible that hydrostatic pressure within the droplet opposed lateral expansion of the outer rim, rather than capillarity-induced forces pinning the contact line to the surface.

To determine whether the size of the contact area resulting from inertial spreading, d_i, was a limiting factor we must further consider V_{imb}(adim) and its *A'*-coefficient. The *A'*-coefficient represented the overall liquid velocity through the d_i entry pores. A low *A'*-coefficient value indicated a lack of capillary action from the powder bed and that the microstructure restricted penetration despite a large contact area resulting from significant inertial spreading (d_i/d_0>>1). Conversely, a high value was the result of strong capillary forces arising from the powder bed to promote a high imbibition rate despite a small contact area due to limited spreading (d_i/d_0≤1). Hence, similar trends to those observed for penetration times

were also evident for coefficient *A'*; decreased viscosity, increased LAC_70 pseudo-grade, increased powder bed consolidation and the inclusion of MCC_30 all elevated coefficient *A'*.

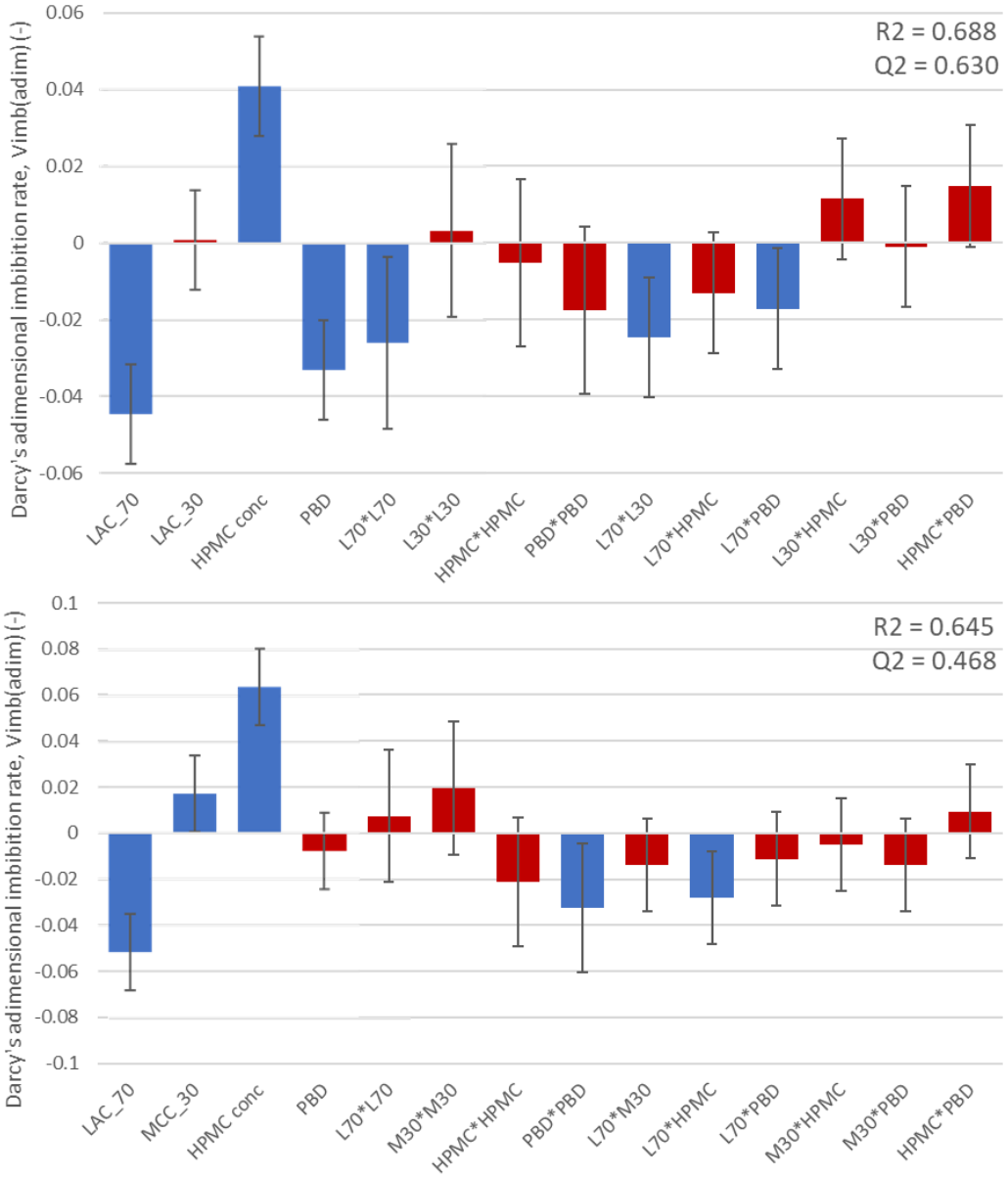

Figure 3.44 MLR coefficients pertaining to Darcy's adimensional imbibition rate for (i) LAC:LAC powder beds and (ii) LAC:MCC powder beds. Significant coefficients ($p<0.05$) are coloured blue.

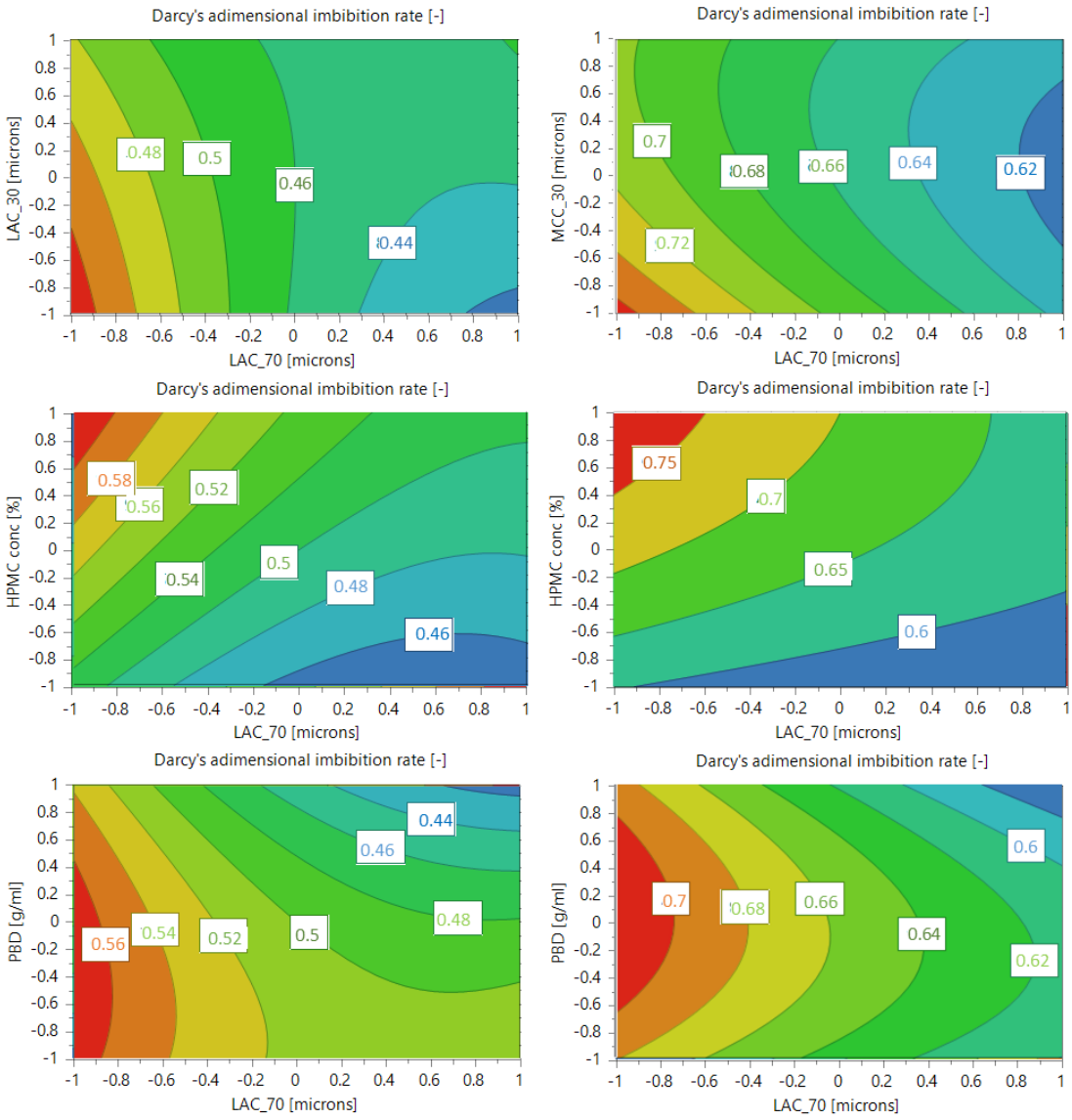

Figure 3.45 Surface response surfaces pertaining to Darcy's adimensional imbibition rate for LAC:LAC powder beds (left) and LAC:MCC powder beds (right).

3.7.7. Granule morphology

Once dried, the physical properties of the resulting nuclei were assessed. Nucleation resulted in three distinct granule morphologies, of which typical representations are shown in Figure 3.46. As can be seen, these morphologies included small spherical granules with exterior protrusions (Figure 3.46a); mushroom-shaped granules with distinctive "stalk and cap" features (Figure 3.46b); and shallow disk-like granules (Figure 3.46c).

These morphologies are in accordance with those previously described in the literature (Davis et al., 2017; Emady et al., 2011; Nguyen et al., 2009). Emady et al. (2011) attributed the formation of small spherical granules to a *tunnelling* mechanism resulting from fine and cohesive particles, whereby the surface tension driven cohesive forces exceeded the weight of the surface particles causing them to be drawn first to the droplet's surface, and then into the bulk, as observed and described in the current study (section 3.6.1). Disk-shaped granules were attributed to a *spreading* mechanism resulting from coarse, freely-flowing particles, where, as the name would suggest, the droplet extensively spreads across the powder surface resulting in shallow capillary penetration.

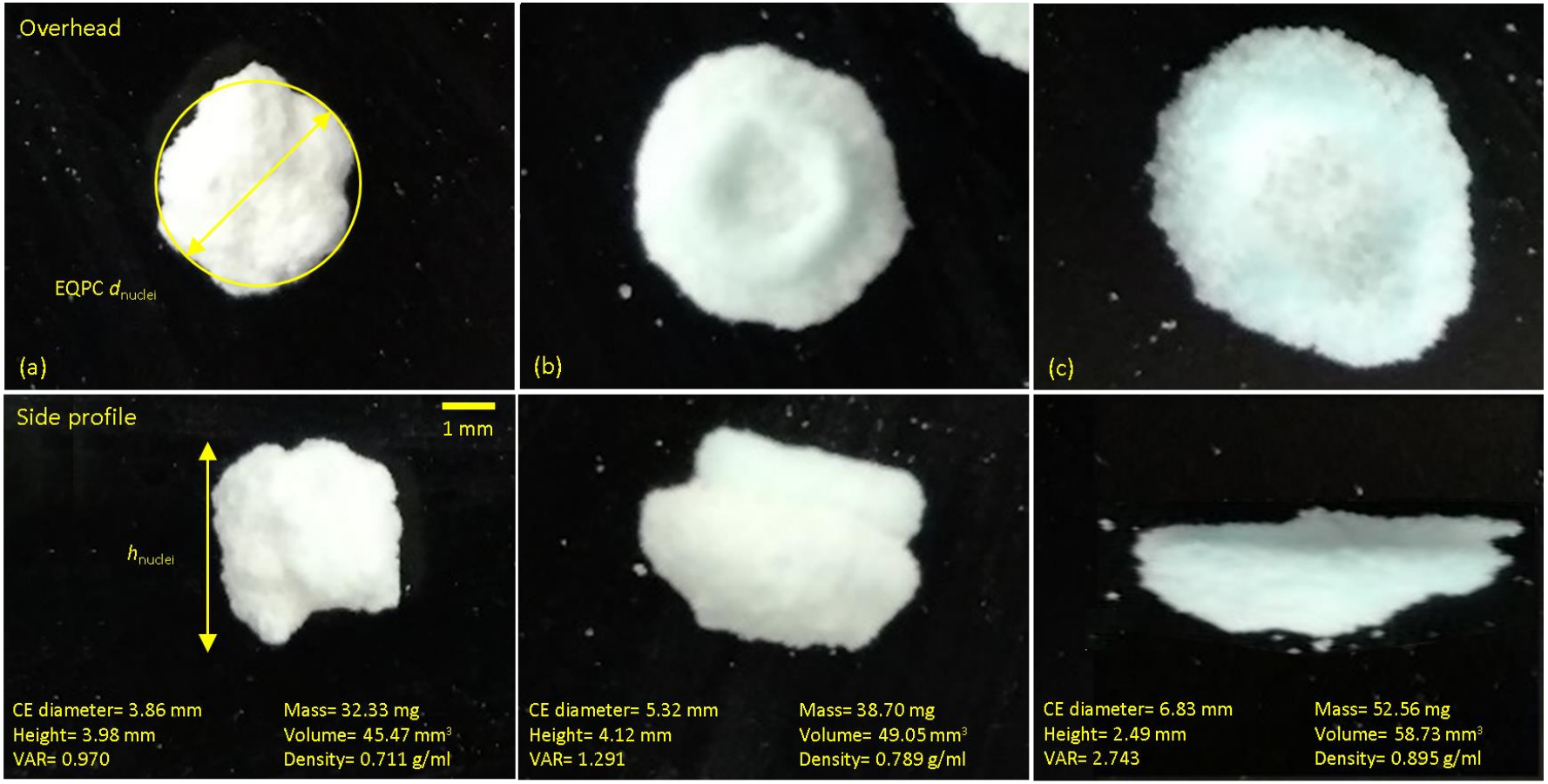

Figure 3.46 Example nuclei resulting from (a) LAC_Lo induced tunnelling, (b) LAC_Med induced late–diffusive intra-spreading and (c) LAC_Hi induced surface spreading. Measurements taken from overhead (top) and side profile (bottom) image analysis.

In a regime map outlined by Emady et al. (2013b), the determinative mechanism is predicated on the powder attributes represented by the Bond number, Bo_g*. A Bond number above 65,000 resulted in tunnelling, whereas a smaller Bond number produced spreading. True to that study, in this current work LAC_Hi, LAC_Med and LAC_Lo had respective Bond numbers of circa 34,000, 58,000 and 105,000 in relation to water. Tests involving LAC_Med confirm observations made by Emady et al. (2013b), whereby granules resulting from powders with a Bond number close to 65,000 possess transitional properties. Nguyen et al. (2009) and Mundozah et al. (2018) described how this morphology resulted from imbibition of a droplet forming a saturated core within the powder bed, followed by liquid diffusion, resulting in a mushroom-shaped morphology. This mechanism was coined *late-diffusive intra-spreading* (Mundozah et al., 2018) and both studies used 200 mesh lactose with an estimated bond number of 54,000-59,000 which is within the vicinity of the transitional threshold. This morphology was observed only for LAC_70_Med formulations in this study.

As a consequence of the random topography of the powder bed and the subsequent isotropic radial spreading and infiltration, the majority of the granules had a circular and axisymmetric overhead projection, with an aspect ratio of approximately 1. However, some of the granules resulting from the spreading mechanism were not circular, exhibiting skewed projections and aspect ratios well below 1. This is attributable to defects in the powder bed surface coercing liquid flow during droplet spreading in a particular direction. These granules were omitted from further analysis.

A correlation between d_{nuclei} and d_{max} was evident (Figure 3.47), and generally d_{nuclei} exceeded d_{max} due to late-diffuse intra-spreading taking place. However, d_{nuclei} did not exceed d_{max} in all cases. This is because, experimental conditions that involved 5% w/w HPMC or

LAC_70_Lo, intra-spreading was minimal and surface spreading was limited, and resulted in small spherical granules whereby d_{nuclei} was approximately equal to d_{max}. Mundozah et al. (2018) observed that the diameter of the nuclei, $d_{nuclei,}$ was always larger than $d_{max.}$ However, those observations resulted from a droplet release height ten-fold greater than this study. Hence, the droplet's kinetic energy and subsequent impact deformation accounted for the contact diameter with little spreading taking place. Granule morphology is indicative of the mechanism by which the imbibing liquid penetrates the powder bed. Naturally, granule height, h_{nuclei}, was inversely proportional to d_{nuclei}, as extensive droplet spreading distributed the droplet volume laterally with limited liquid available for vertical imbibition.

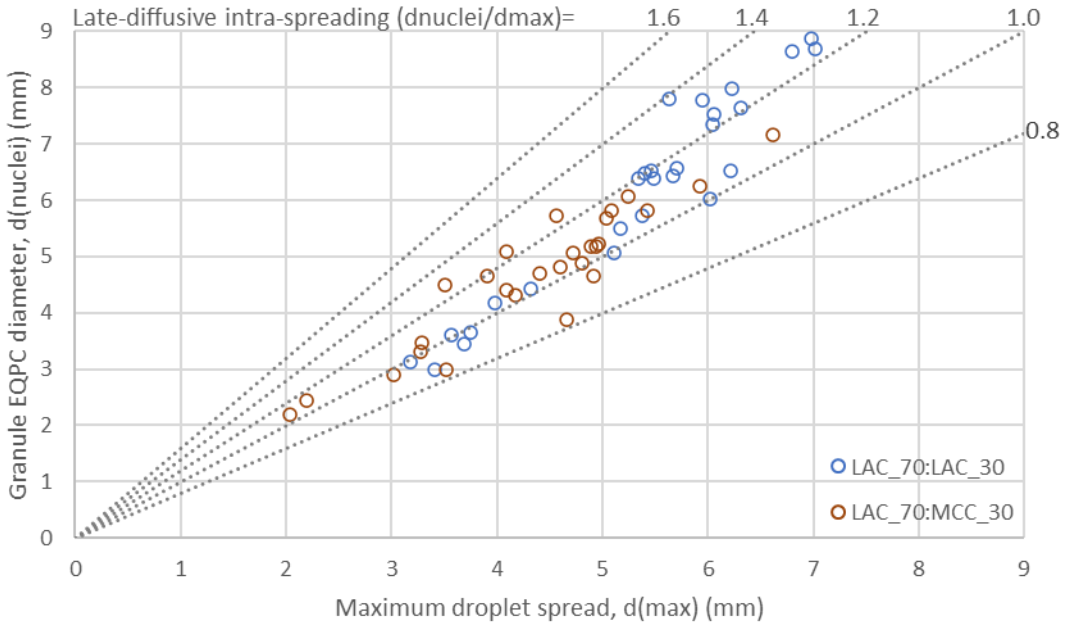

Figure 3.47 Granule diameter, d_{nuclei}, in relation to maximum droplet spread, d_{max}, for all experimental conditions. All DoE permutations are displayed but only LAC_30 and MCC_30 are visually distinguished for comparison. The dashed lines represent the extent of late-diffusive intra-spreading (d_{nuclei}/d_{max}).

The particle size distribution of LAC_70 was the most determinant factor with regards to granule morphology, with each pseudo-grade resulting almost exclusively in one of the aforementioned granule morphologies. On account of limited spreading and capillary action, LAC_70_Lo resulted in the small spherical granules with a vertical aspect ratio close

to unity, VAR≈1, and $d_{nuclei} \approx d_{max} \approx d_0$. This not only shows that very little spreading occurred at the surface, but also, negligible intra-spreading occurred beneath the surface and that the resulting granule represents the saturated core. This was likely due to low permeability arising from wide pores and limited capillary action, in addition to a high surface area and tortuosity, all of which impeded infiltration. The combination of high saturation and large surface area increased the number of liquid bridges between particles, resulting in granules that were robust and durable. The protrusions at the surface of the granules were attributable to particles and particle aggregates at the edge of the saturated core only being partially wetted, but sufficiently wetted to be incorporated into the granule structure.

The coarse particles of LAC_70_Hi resulted in the shallow disk-shaped granules with a $d_{nuclei}/d_{max}>1$ and a significantly greater VAR, than LAC_70_Lo. The combination of extensive droplet spreading, low surface area, high permeability and strong capillary action resulted in substantial radial infiltration but limited the liquid volume available for vertical penetration. Therefore, the granules presented with a level top and rounded underside. However, as a result of the limited surface area, the particles were bound by fewer liquid bridges following penetration, resulting in fewer solid bridges once dried. This manifested as fragile granules that often crumbled when handled. Therefore, particular care was taken, and handling was kept to a minimum during characterisation.

The mushroom-shaped granules resulted from LAC_70_Med. With a d_{nuclei} between LAC_Lo and LAC_Hi, LAC_Med granule morphology fittingly demonstrated characteristics of both pseudo-grades. The “stalk” feature was a result of limited surface spreading, yet reasonably fast imbibition. Once the liquid had imbibed vertically to form a saturated core, it then proceeded to infiltrate radially beneath the surface in the bulk of the powder bed resulting in the “cap”. Therefore, the diameter of the “stalk” correlated closely to the droplet surface

footprint, $d_{stalk} \approx d_{max}$, whereas the difference between the nuclei "cap" diameter and droplet spread, $d_{cap} > d_{max}$, was indicative of late-diffuse intra-spreading (Mundozah et al., 2018; Nguyen et al., 2009). Also, the granule mass was found to decrease with decreasing pseudo-grade PSD as less particle mass was incorporated into each granule by the imbibing liquid due to the reduced capillary action and resultant infiltration. The increased void volume of LAC_Lo entrapped a greater volume of liquid that did not contribute to liquid bridge formation, whereas the decreased void space of LAC_Hi enabled the liquid to increase particle surface coverage.

The influence of powder bed consolidation on granule properties was identified to be dependent on the LAC_70 pseudo grade. Increased consolidation of mixtures containing LAC_70_Lo and LAC_70_Med increased the mass and dimensions (d_{nuclei} and h_{nuclei}) of the resulting granules. This can be attributed to the increased consolidation resulting in a reduced porosity on account of the increased packing and diminished macrovoids. The resultant increase in capillary action propagated the imbibing liquid further, allowing more particles to be wetted and incorporated into the granule than their loosely consolidated counterparts. As seen above, the increased consolidation of LAC_70_Lo and LAC_70_Med increased droplet spreading due to a smaller fraction of the surface being occupied by air. Consequently, d_{nuclei} increased to a greater extent than h_{nuclei}, and therefore, the vertical aspect ratio (VAR=d_{nuclei}/h_{nuclei}) increased slightly with increased consolidation, as previously reported (Emady et al., 2013b). With regards to LAC_70_Hi, prolonged tapping had little effect on the packing efficiency, as indicated by the 10-20% compressibility index, and thus, the liquid front was not likely to advance significantly further than in the loose powder bed. Hence, the morphological properties of granules composed of LAC_70_Hi were independent

of consolidation state. It can therefore be concluded that the sensitivity of the granule morphology to powder bed consolidation increased with decreased LAC_70 pseudo grade.

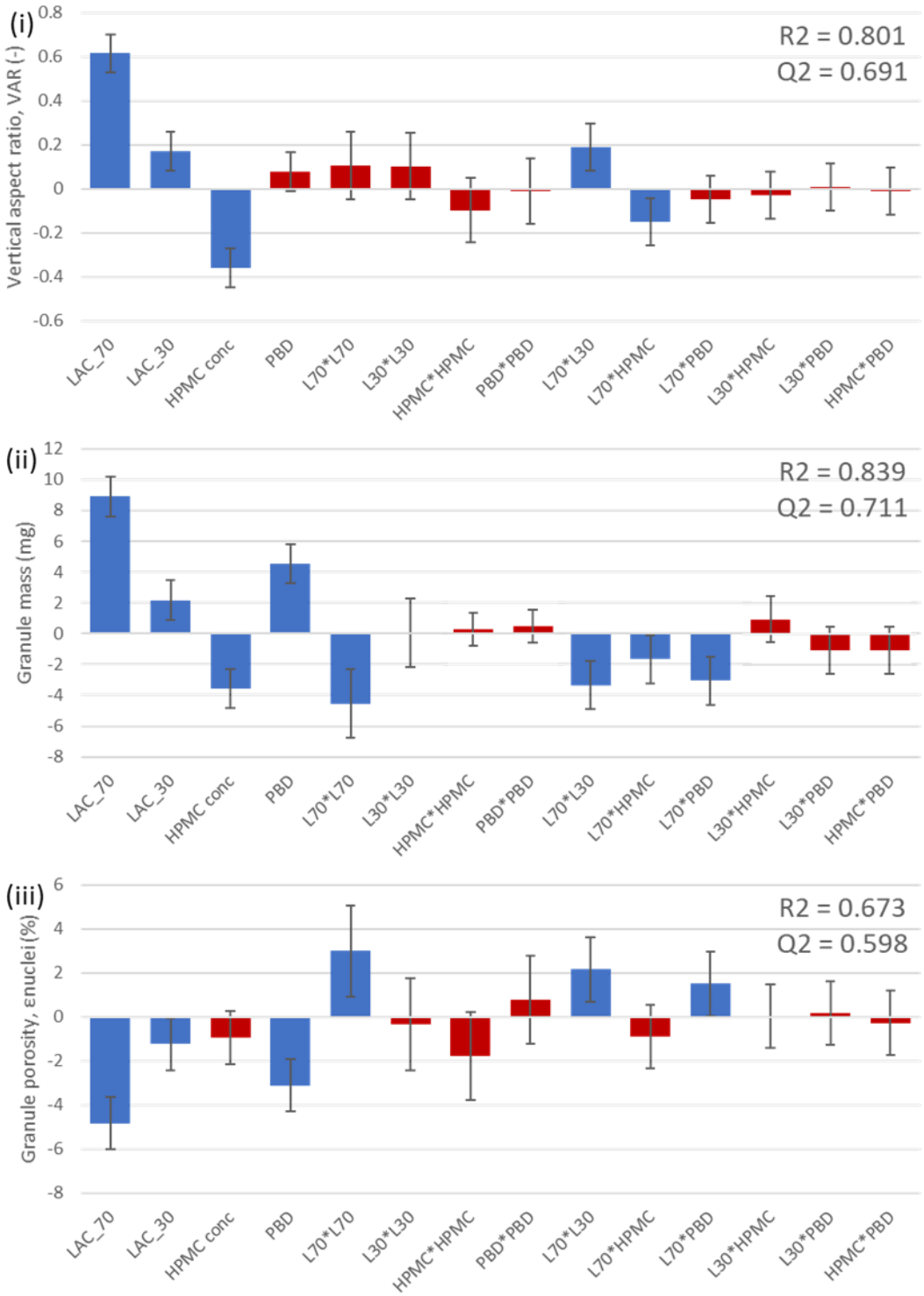

Figure 3.48 MLR coefficients pertaining to (i) vertical aspect ratio, (ii) mass and (iii) porosity of granules resulting from LAC:LAC powder beds. Significant coefficients ($p<0.05$) are coloured blue.

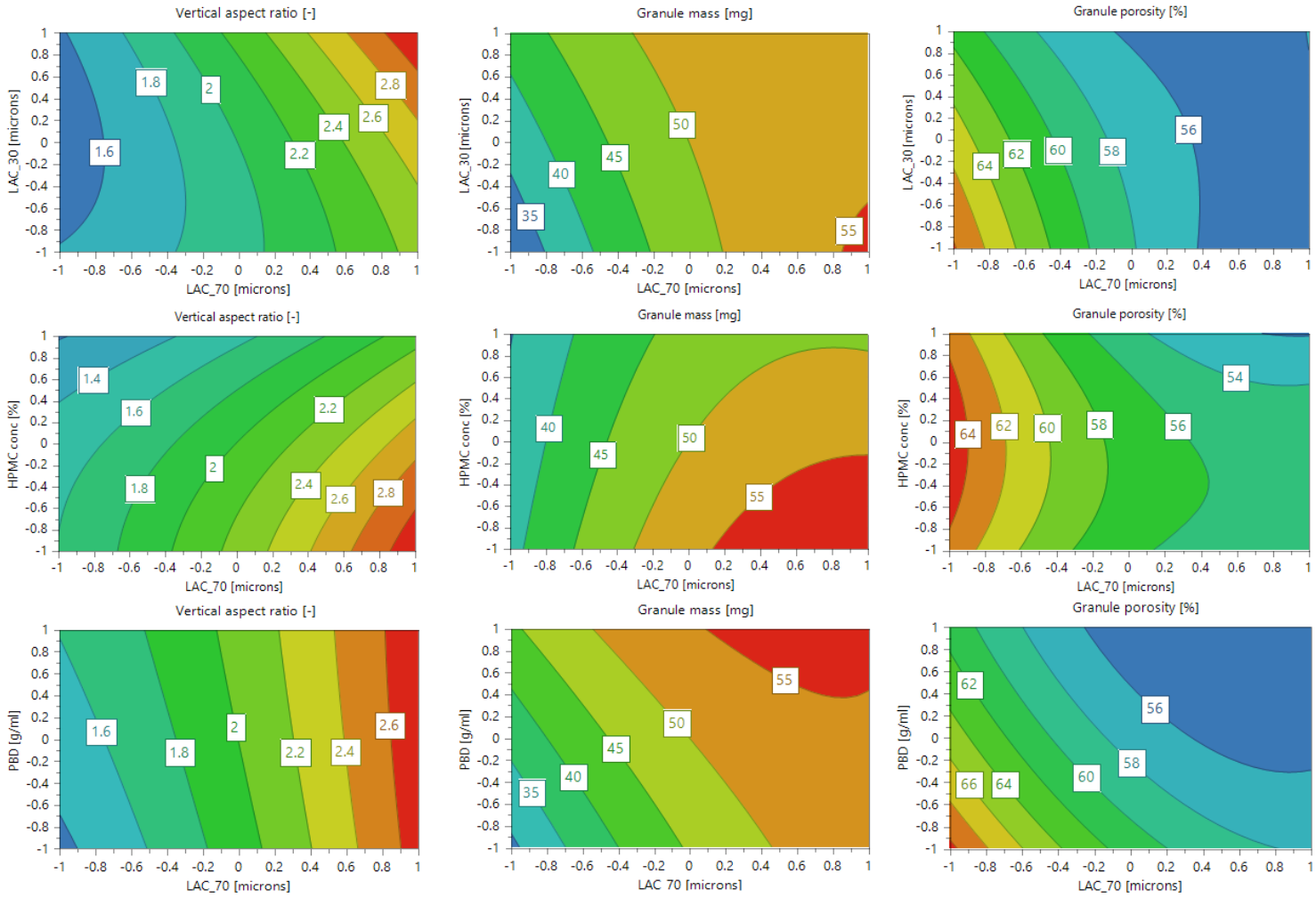

Figure 3.49 Response surfaces resulting from the MLR models for granule properties resulting from LAC:LAC powder beds; V.A.R (left), granule mass (centre), and granule porosity (right).

The concentration of HPMC also had a significant influence on the granule properties. Increasing HPMC resulted in a decrease in d_{nuclei}, which corresponded to the limited spreading. However, diameter sensitivity to HPMC concentration decreased with decreased LAC_70 particle size and in most cases d_{nuclei} of LAC_70_Lo was independent of liquid properties. In accordance with the overall reduction in wetted particles as a result of diminished infiltration, the granule mass also decreased with increased HPMC. Furthermore, it was observed that with increased HPMC, sensitivity to the microstructure of the powder bed decreased, as the effects of LAC_70 and consolidation were greatly muted for 5% w/w HPMC when compared to water. This is because the more viscous HPMC solution was less susceptible to the capillary action induced by pore width and was influenced more by viscous friction. This was most evident for LAC_70_Med, as the late-diffusive infiltration was opposed by viscous friction, and the "cap" was almost indistinguishable from the "stalk" when 5% w/w HPMC was used. This is supported by Mundozah et al. (2018), whereby the mass of the nuclei decreased with increased viscosity. Further, the h_{nuclei} generally decreased with increased viscosity, indicating decreased infiltration, and resulted in increased VAR. Although some of Emady et al. (2013b) results indicated this, the trend was less general.

The effect of the LAC_30 pseudo-grade was dependent on both LAC_70 and HPMC concentration. Increasing the bimodality of the particle size distribution of the powder bed, i.e. a combination of LAC_Lo:LAC_Hi or LAC_Hi:LAC_Lo, resulted in the infiltration of water increasing and the dimensions and mass of the granule were greater than their respective unimodal PSD. However, the reduction in porosity associated with the bimodal mixtures resulted in a small decrease in the infiltration of the 5% w/w HPMC solution, resulting in a smaller d_{nuclei} and mass than their unimodal counterparts.

The inclusion of MCC_30 as the secondary component resulted in a notable reduction in h_{nuclei} for all of the formulations, and therefore resulted in an increased VAR. This is attributable to MCC's hygroscopic properties, thereby absorbing the imbibing liquid close to the surface and impeding further penetration. Although the moisture retention capacity of MCC is dependent on the proportion of the amorphous region (Mihranyan et al., 2004), generally MCC has demonstrated an ability to retain approximately 50% of its weight in water despite exhibiting limited swelling (Desai et al., 2012; Tomer et al., 2001). This coupled with MCC's intense wicking properties (Desai et al., 2012), caused the imbibing liquid to be disproportionately concentrated in the MCC particles. This effect on h_{nuclei} was most evident for MCC_30_Lo and least pronounced for MCC_30_Hi. It is likely that the fine MCC_Lo particles were more accessible to the penetrating liquid than the coarse particles of MCC_Hi, on account of the significantly larger surface area (Koo and Heng, 2001). Overall, the dry granules that nucleated from LAC:MCC weighed less than those composed of LAC:LAC mixtures. This was because less of the imbibing liquid was available for infiltration and the formation of inter-particle liquid bridges.

3.7.8. Granule porosity

Archimedes principle was used to estimate the envelope volume of the granules, from which the average nuclei density was calculated. The data from the nuclei density correlated closely to that of the powder bed density, and hence, the pseudo-grade combination of the A:B mixture and the extent of consolidation determined the density of the granules. It can be concluded that the imbibing liquid did not significantly alter the porosity of the powder bed when binding particles together and forming the granules. However, the microstructure is likely to have reconfigured as the lactose particles partially dissolved into liquid bridges and recrystallised to form solid bridges.

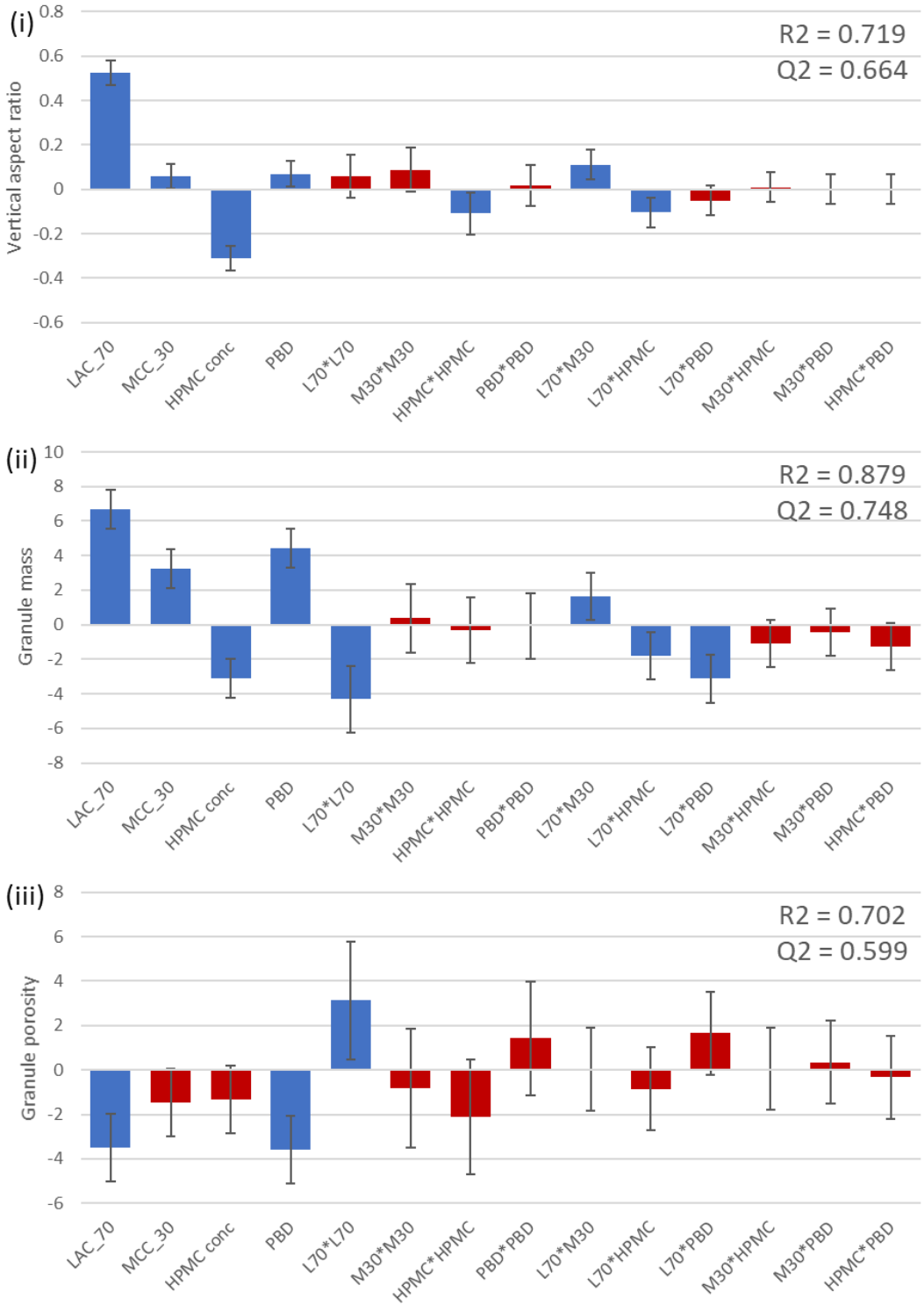

Figure 3.50 MLR coefficients pertaining to (i) vertical aspect ratio, (ii) mass and (iii) porosity of granules resulting from LAC:MCC powder beds. Significant coefficients ($p<0.05$) are coloured blue.

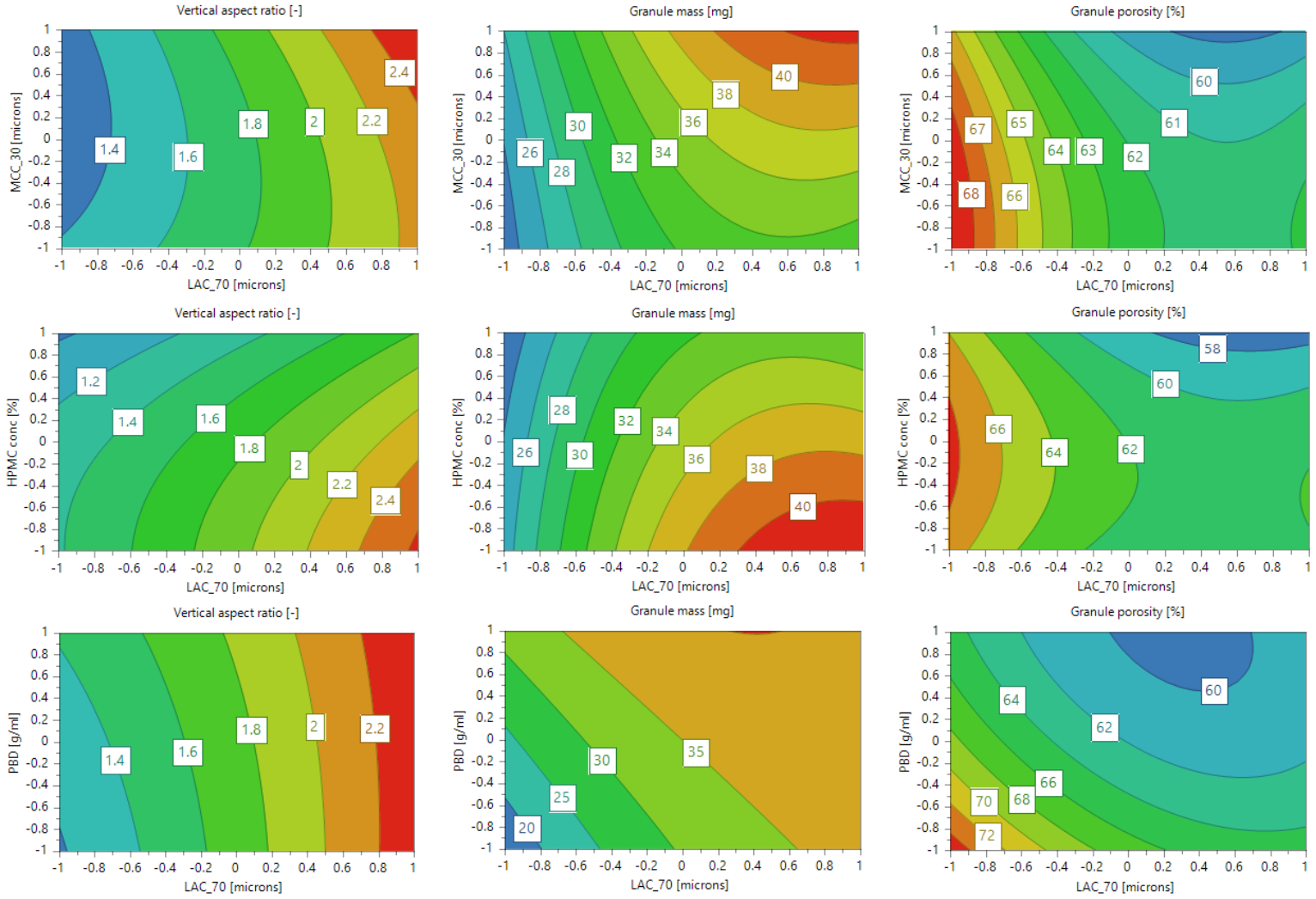

Figure 3.51 Response surfaces resulting from the MLR models for granule properties resulting from LAC:MCC powder beds; V.A.R (left), granule mass (centre), and granule porosity (right).

3.8. Conclusion

An in-depth analysis of droplet penetration tests was performed to elucidate the role of powder bed microstructure on powder wetting and granule formation. In this study, a powder's microstructure was taken to be the sum total of the particle size distribution and consolidation. Fine cohesive particles with a large surface area agglomerated to form macrovoids and a heterogenous pore distribution, contributing to an overall greater porosity. This was somewhat reduced by increasing consolidation in the form of tapping, and thus, large CI% values were obtained. Conversely, coarse particles were able to pack more efficiently, even in the absence of consolidating forces (CI%≤20), resulting in a more uniform and smaller pore size distribution, and overall lower porosity. Particle packing was further enhanced by increasing the bimodality of the PSD, as fine particles were able to percolate in between coarse particles.

The surface of the powder bed represented a cross section of the bulk. Hence, a powder possessing greater porosity resulted in a larger surface pore fraction, which in turn increased the non-wetting component, air, of the powder surface. Powder beds primarily composed of the fine LAC pseudo-grades prolonged energy dissipation and impeded surface spreading; behaviour consistent with a hydrophobic surface. The coarse LAC pseudo-grade demonstrated faster energy dissipation and greater spreading as surface pores were less prominent. Hence, despite both powders possessing the same intrinsic chemical properties, divergent wettability was observed by virtue of differing PSDs and consolidation. Additionally, these observations were evidence that inertial spreading assumed a Cassie-Baxter regime, as a greater surface area did not enhance wetting.

Further, it was shown that the inertial regime accounted for the majority of the droplet maximum footprint (>67 %), and consequently, dictated granule properties (d_{nuclei} and VAR). Due to an imbalance in Laplace pressure, the droplet liquid is believed to have preferentially imbibed via the surface pores wetted during inertial spreading rather than the surface pores acquired during viscous spreading.

Droplet penetration reflected droplet spreading, in that the presence of heterogenous macrovoids impeded liquid infiltration throughout the bulk. Therefore, it was observed that powder beds composed of fine particles resulted in prolonged imbibition and limited late-diffusive intra-spreading. These observations were attributed to increased tortuosity. A small quasi-spherical granule produced from a saturated core was demonstrative of limited liquid distribution. Extensive tapping resulted in a small increase in d_{nuclei}, a small decrease in h_{nuclei} and an increase granule mass.

Uniform and narrow pores resulting from larger particles elicited stronger capillary forces, as demonstrated by rapid penetration and extensive liquid distribution. Therefore, droplet penetration into the coarse LAC pseudo-grade manifested as large disc shaped nuclei.

The intermediate LAC pseudo-grade demonstrated limited inertial spreading but substantial viscous spreading, accompanied by an intermediate penetration time. Upon visually examining the resulting granules, it was evident that significant late-diffusive intra-spreading occurred as the saturated “stalk” was encapsulated by a diffuse “cap”. Increased consolidation emphasised the size discrepancy between these two features.

Modulating the LAC:LAC formulation to possess a bimodal PSD resulted in improved liquid distribution. However, this was only observed when the powder bed was fully consolidated.

The inclusion of MCC negated any bimodal effect on liquid distribution. Instead, MCC's hygroscopic properties resulted in an increased penetration rate but decreased liquid distribution, as evidence by smaller nuclei dimensions. This can be attributed to its hygroscopic properties, which appear to have been enhanced with particle size reduction due to an increase in surface area.

The above observations were made when the droplet was composed of an inviscid liquid. Increasing the concentration of HPMC diminished the effect of the considerations previously mentioned. This was because surface spreading and capillary action were opposed by viscous friction. As a result, all of the granules produced from HPMC 5% w/w exhibited small dimensions, indicative of restricted liquid distribution.

This in-depth study has shown the effects of varying particle size, a dominant powder property, on powder wetting. A change in particle size can influence droplet-surface interaction, penetration and infiltration, all of which can impact liquid distribution. Doping the bulk with a minority component or manipulating process parameters to vary channel fill and consolidation present options for upstream intervention during powder processing to mitigate input variability.

In HSM granulation, to obtain a narrower, and more workable, granule size distribution then drop-controlled immersion nucleation must be achieved (Hapgood et al., 2003). This nucleation regime is dependent on rapid penetration of each droplet into the powder bed (Hapgood et al., 2003). During TSG, greater liquid distribution manifests as a more uniform granule size distribution. This experimental work shows that conditions resulting in a decrease in droplet penetration time (larger particle size, greater consolidation, less viscous

liquid droplet) also resulted in greater energy dissipation and improved wettability, whereby larger nuclei - consisting of a greater number of primary particles - manifested from liquid droplets of equal volume and is indicative of greater liquid distribution. Therefore, in the following experimental work, it is to be determined if powder properties can be used to promote a more desirable granule size distribution. Further, this methodology can be replicated to inform the particle engineering process for new APIs of the preferable particle profile, as well as during formulation development to establish powders and properties that facilitate penetration and improve liquid distribution.

4. The Effects of Powder Properties and Channel Fill on Twin Screw Wet Granulation

4.1. Aims and objectives

The aim of this chapter is to determine the effects that powder properties, namely particle size distribution (PSD), and barrel fill conditions have on twin screw wet granulation (TSG) and granule properties. In turn, this study is intended to elucidate the sensitivity of TSG to raw material variability and the role of total volumetric fraction (TVF) in a risk management strategy. Additionally, the residence time will be evaluated for material diversion and lot identification considerations.

4.2. Materials

For this study, three commercial grades of α-lactose monohydrate (LAC; Granulac 70, 140 and 230, Meggle, Germany) and three commercial grades of microcrystalline cellulose (MCC; Avicel PH101, PH105 and PH200, FMC Biopolymer, USA) were used to generate three pseudo-grades - Lo, Med and Hi - using the aforementioned method (section 2.4.1).

In addition, Hypromellose (HPMC; Pharmacoat 603, Shin-Etsu, Japan) and croscarmellose sodium (CCS; Ac-Di-Sol SD-711, FMC BioPolymer, USA) were included in the formulation blend, as per Table 7. This mixture is typical of a wet granulation formulation and is similar to blends used in studies previously published in the literature (Chan Seem et al. 2016; R. M. Dhenge et al. 2011; A. El Hagrasy, Hennenkamp, et al. 2013; Gorringe et al. 2017; K. T. Lee, Ingram, and Rowson 2012; J. G. Osorio et al. 2017; Saleh et al. 2015; Sayin et al. 2015). A

75-125 µm sieve fraction of theophylline anhydrate (THP; Alfa Aesar, Thermo Fischer Scientific, USA) was included at 5% w/w concentration as a model compound for granule inhomogeneity and tablet release studies. THP belongs to Biopharmaceutical Classification System I possessing high solubility (Somani et al. 2016), and hence, any difference in dissolution is attributable to tablet properties. THP is a bronchodilator routinely used in therapy for respiratory diseases such as chronic obstructive pulmonary disorder and asthma (MHRA & EMA 2017).

Purified water (Milli-Q Water Purification System, Merck Millipore, USA) was used as the liquid binder. Patent V Blue dye (Sigma-Aldrich, Merck Group, USA) was used as a tracer to profile the residence time distribution (RTD) within the TSG. Magnesium stearate (MgSt; Parteck LUB MST, Merck Millipore, USA) was added extra-granularly prior to tableting to reduce friction between the powder compact and the punch and die wall.

Table 7 TSG formulation composition

Material	Functional category	Brand	Manufacturer	Mass (% w/w)
α-lactose monohydrate*	Diluent	Granulac 70, 140 and 230	Meggle	70
Microcrystalline cellulose*	Diluent and binder	Avicel PH200, PH101 and PH105	FMC Biopolymer	20
Theophylline anhydrate	API	-	Alfa Aesar	5
Hypromellose	Binder	Pharmacoat 603	Shin-Etsu	3.5
Croscarmellose sodium	Disintegrant	Ac-Di-Sol SD-711	FMC Biopolymer	1.5
Magnesium stearate**	Lubricant	Parteck LUB MST	Merck Millipore	0.5

*Commercial stock grades were first modified into pseudo-grades
**added extra-granularly prior to tablet compaction

4.3. Method

4.3.1. Formulation preparation and characterisation

LAC and MCC were varied across the three pseudo-grades to create three blends of distinct PSD. Three batches of 1.5 kg blends were prepared for each combination and were blended for 30 minutes in a 5 L cone vessel with a tumbling speed of 20 rpm and agitator speed of 300 rpm (AgiBlend AB-015, Pharmatech, UK).

The physical properties of each blend were then characterised. The true density was taken from ten measurements using gas displacement pycnometry (Accupyc II 1340 Pycnometer, Micromeritics, USA). The PSD of each of the formulation blends was measured using sieve analysis (FRITSCH GmbH, Germany; Titan 450 Sieve Shaker, Endecotts, UK). The conditioned bulk density and flow properties of the individual grades and the formulation powder blends were measured using a FT4 Powder Rheometer (Freeman Technology, UK). The tapped density was measured after 2000 taps (Autotap, Quantachrome, USA).

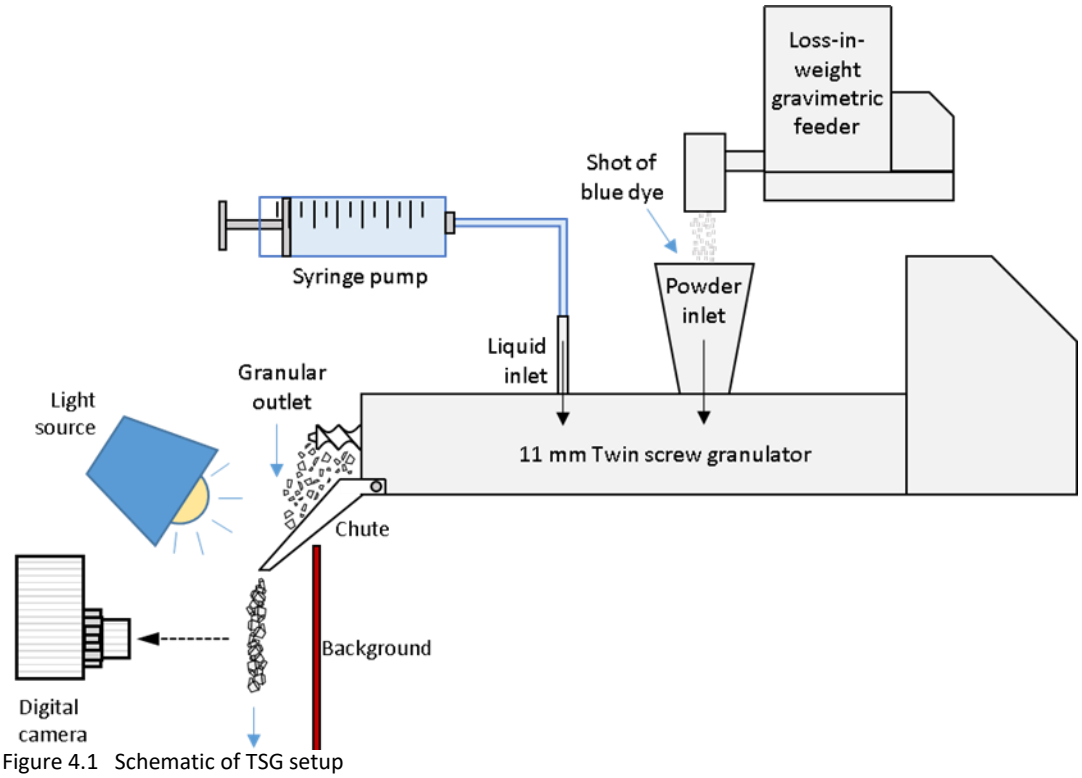

Figure 4.1 Schematic of TSG setup

4.3.2. Twin screw wet granulation

TSG was performed using a modified 11mm twin screw hot melt extruder (Process 11 Twin-screw Extruder, Thermo Fisher Scientific, USA) with a 40:1 barrel length-to-width ratio. The general setup is presented in Figure 4.1.

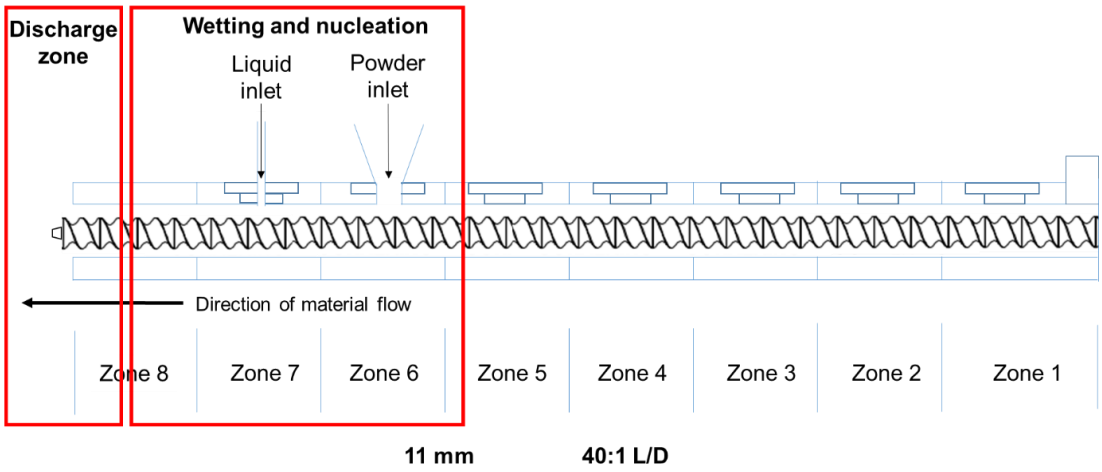

Figure 4.2 Schematic of the twin screw extruder's modified setup for nucleation studies.

To evaluate *nucleation*, the setup of the TSG was such that the dry material inlet was located at the penultimate inlet (zone 6) and the liquid inlet was fitted at the final inlet (zone 7), as shown in Figure 4.2. This was so that the material collected at the outlet resembled material that would otherwise be transported into the kneading region of a typical TSG setup following wetting and nucleation. The liquid inlet features a single nozzle located above the centre of the intermeshing region of the co-rotating screws. The configuration of the functional portion of the screw featured only helical conveying elements - 13*CE(1D) - with a 0.5D pitch.

For the *granulation* studies, the barrel was set up so that the powder inlet was located at zone 5 and the liquid inlet at zone 6 (Figure 4.3). The active screw configuration included a single block of seven bilobe kneading elements (KE) arranged at a 60° forwarding angle: 13*CE(1D)-7*KE(0.25D)60°f-3*CE(1D). The active section of the screw was preceded by 22*CE(1D) and 1*KE(0.25D) for spacer purposes. The two screw configurations are compared in Figure 4.4.

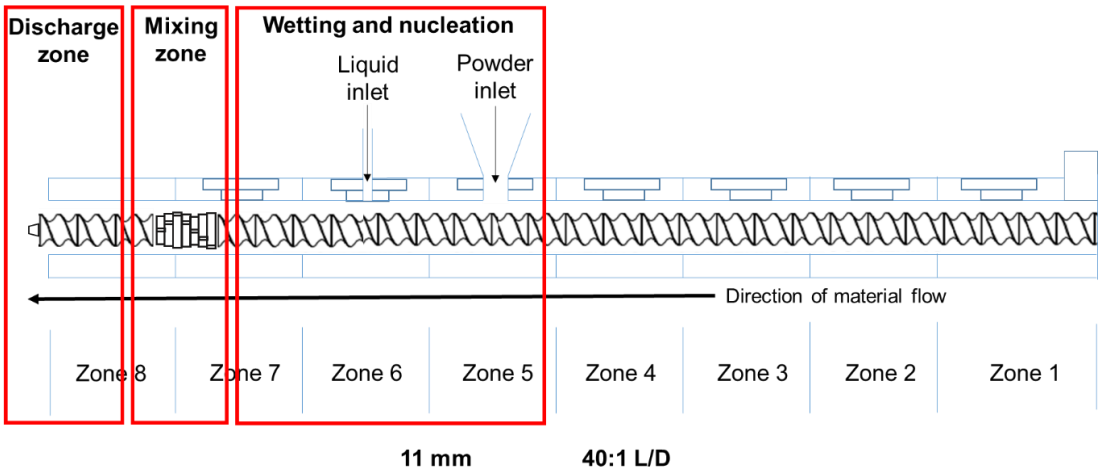

Figure 4.3 Schematic of the twin screw extruder's modified setup for granulation studies.

For both studies, the liquid-to-solid ratio (LSR) was varied between either 0.15 or 0.18 by changing the settings of the syringe pump (PHD ULTRA, Harvard Apparatus, USA). The screw speed (SS) was varied to achieve a TVF of approximately 0.2, 0.5 or 0.8 (see section 4.3.3).

To determine the effects of LSR, PSD and TVF the material feed rate (MFR) was initially maintained at 0.8 kg·hr^{-1} using a loss-in-weight gravimetric feeder (MT-S LIW, Brabender Technologie GmbH & Co. KG, Germany). The TVF was then evaluated across a larger MFR and SS operating space at LSR=0.18 (see section 4.4.9). The operating space was limited by the maximum MFR at which the gravimetric feeder was stable for each formulation, flowability permitting: 1.2, 1.8 and 2.0 kg·hr^{-1} for PSD *Lo* (-1), *Med* (-0.176) and *Hi* (+1), respectively.

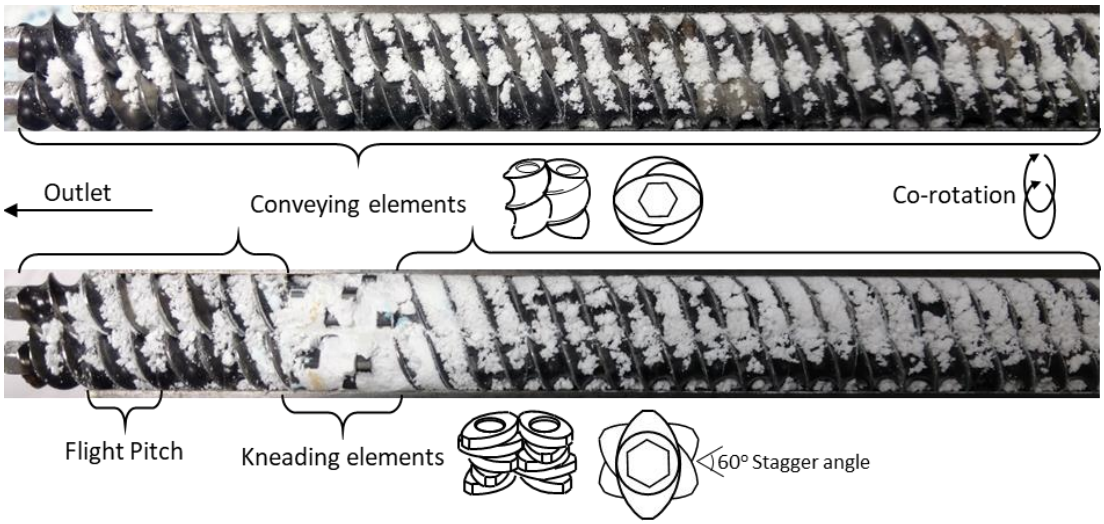

Figure 4.4 Screw configuration for nucleation (top) and granulation (bottom)

After allowing 10 minutes for the system to achieve steady state, and confirmed by stable torque, material was collected from the outlet for a further ten minutes. The collected material was dried in an open tray for 72 hours at ambient conditions before characterisation.

4.3.3. Total volumetric fraction, TVF

Various methods of measuring the barrel fill level have been presented in the literature, and include visual inspection (Thompson and Sun 2010), positron emission particle tracking (K. T. Lee, Ingram, and Rowson 2012), and volumetric calculations (Gorringe et al. 2017; Lute, Dhenge, and Salman 2018a; Robin Meier et al. 2017b; J. G. Osorio et al. 2017). TVF is a dimensionless number and is defined as the fraction of the occupied volume of the available volume within the channels of the conveying elements. In this study, TVF was considered to be a function of *volumetric efficiency* (η_v) and modified to include *conveying efficiency* (c_v).

The η_v is a dimensionless parameter equal to the ratio between the material's measured volumetric flow rate, Q_a, and the screw's theoretical volumetric flow rate, Q_t (Srivastava et al. 2006; Miao et al. 2014). The theoretical volumetric flow rate was calculated from the free conveyor volume of the screw, V_f, screw lead, S_L, screw length composed of conveying elements, L, and the screw speed, N (Equation 4.1).

In this study, the V_f was calculated by deducting the volume of the active screw configuration – determined using Archimedes principle of displacement – from the volume of the barrel – calculated geometrically. The V_f was 10.25 cm^3 and 17.34 cm^3 for the *nucleation* and *granulation* configurations, respectively.

$$Q_t(m^3/s) = V_f \cdot \left(\frac{S_L}{L}\right) \cdot N \qquad (m^3 \cdot \frac{m}{m} \cdot s^{-1}) \qquad \text{Equation 4.1}$$

In reality, powder porosity and limited consolidation reduce the volumetric throughput of the conveying screw elements. Therefore, the material's actual volumetric flow rate Q_a was estimated from the mass flow rate, $\dot{m}$ (kg s^{-1}), and the powder density, ρ (kg m^{-3}):

$$Q_a(m^3/s) = \frac{\dot{m}}{\rho} \ \frac{(kg/s)}{(kg/m^3)} \qquad \text{Equation 4.2}$$

Hence, the volumetric efficiency η_v is derived from:

$$\eta_v = \frac{\dot{m}}{\rho \cdot V_f \cdot \frac{S_L}{L} \cdot N} = \frac{Q_a}{Q_t} \frac{(m^3/s)}{(m^3/s)} \qquad \text{Equation 4.3}$$

Osorio et al. (2017) sought to evaluate a dimensionless powder feed number derived from η_v for scaling between different sized TSGs. The powder feed number was found to have minor significance on the GSD resulting from a screw configuration composed of only CEs and a distributive feed screw.

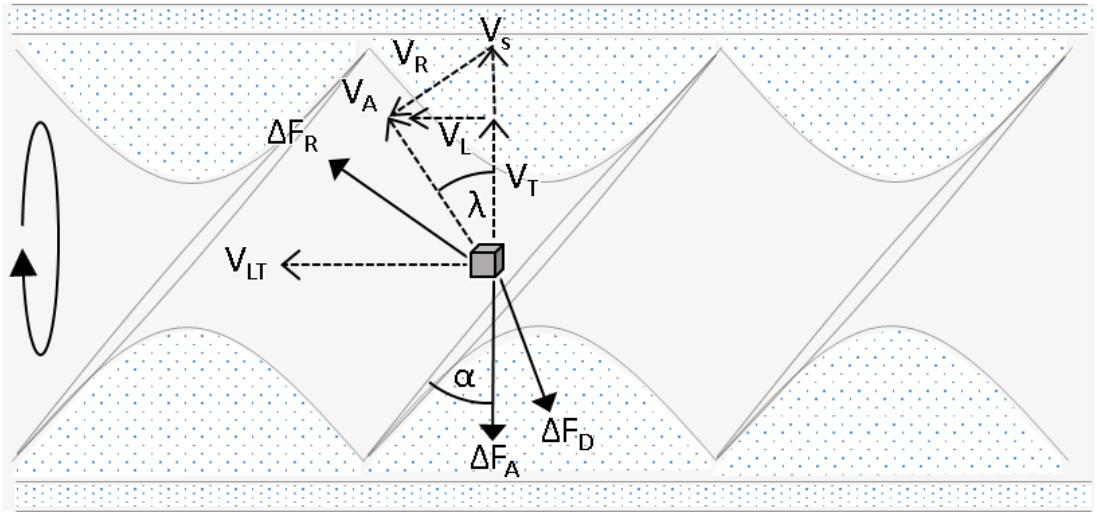

Figure 4.5 Mechanics of conveying action and forces acting on a particle in a screw conveyor (adapted from Roberts, 1999). VS is screw velocity (m/s), VA is absolute velocity (m/s), VR is relative velocity (m/s), VL is conveying velocity component (m/s), VLT is maximum theoretical conveying velocity (m/s), VT is rotating velocity component (m/s), λ is helix angle of particle (o), α is helix angle of screw (o), ΔFA is axial force due to particle weight (N), ΔFD is frictional drag force due to sliding against casing (N), and ΔFR is resultant force due to sliding on screw surface (N).

Gorringe et al. (2017) presented η_v as the total volumetric fraction of conveying element channels filled with powder. In that study the assumption that the conveying efficiency was constant and independent of screw configuration, formulation, screw speed and powder feed rate was experimentally verified. However, in that study, c_v was assumed to be 1 which might explain why the maximum value of η_v achieved was approximately half of the theoretical maximum.

Empirically, the conveying efficiency, c_v, is less than 1 as the relative velocity of particles within a twin screw granulator vary and is lower than the velocity of the conveying screw. Roberts (1999) attributed this divergence to the vortex motion of particle material. The vortex motion of grain in an auger conveyor was modelled as a function of various forces acting upon the particles including internal shear between concentric layers, frictional drag forces between the powder and screw/wall surface, and centrifugal force which determines the helical path of the particles (Figure 4.5). In TSG, particle axial velocity is further retarded by the inclusion of non-conveying elements in the kneading block as transport becomes dependent on pressure from material build up rather than screw conveyance (K. T. Lee, Ingram, and Rowson 2012). Additionally, it has been observed that particles can temporarily accumulate in an immobile layer of wetted material in the clearance between the screw and the barrel wall, as well as along the screw surface (K. T. Lee, Ingram, and Rowson 2012). Thus, the reality of a c_v being less than 1 results in axial mixing and a distribution in particle residence time (Ashish Kumar, Vercruysse, Toiviainen, et al. 2014) rather than a perfect pulse and plug flow. For these reasons, Roberts (1999) considered conveying 'fullness' to be a function of both the volumetric efficiency and the *'vortex'* conveying efficiency (Figure 4.6).

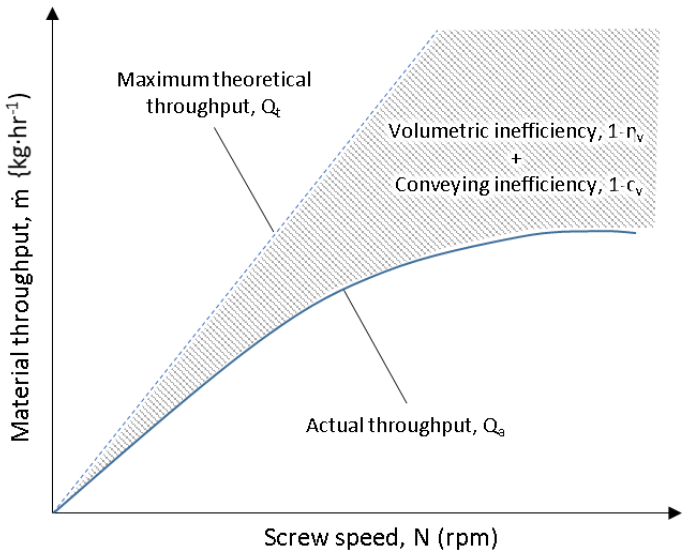

Figure 4.6 Throughput of an enclosed screw conveyor (adapted from Roberts, 1999).

In this study, c_v was determined experimentally and evaluated as a dimensionless ratio between the experimentally measured mean residence time, $\bar{t}_m$, and the theoretical residence time, $\bar{t}_t$. The theoretical residence time can be described as the time taken for the number of screw rotations to generate an axial displacement equal to the length of the barrel navigated by the material, *L*. The axial displacement of the screw surface per revolution is known as the screw lead, S_L, and is equivalent to D. Hence, $\bar{t}_t$ was calculated using

$$\bar{t}_t(s) = \frac{L}{S_L} \cdot N \quad \left(\frac{m}{m} \cdot s^{-1}\right) \qquad \text{Equation 4.4}$$

From which the conveying efficiency was derived as

$$c_v = \frac{\bar{t}_m}{\bar{t}_t} \quad \left(\frac{s}{s}\right) \qquad \text{Equation 4.5}$$

Hence, the proposed estimate for TVF in this study was deduced as

$$TVF = \frac{\eta_v}{c_v} \qquad \text{Equation 4.6}$$

The maximum achievable value of TVF was determined practically for each formulation by gradually decreasing the screw speed until a build-up of powder was observable at the powder inlet for the nucleation setup (Figure 4.7) or until the torque sharply increased and exceeded 70 % during granulation runs (Figure 4.8). From either of these observations it was inferred that the screw channels were fully occupied.

Figure 4.8 Material build-up at powder inlet due to screws becoming flooded in the *nucleation* setup.

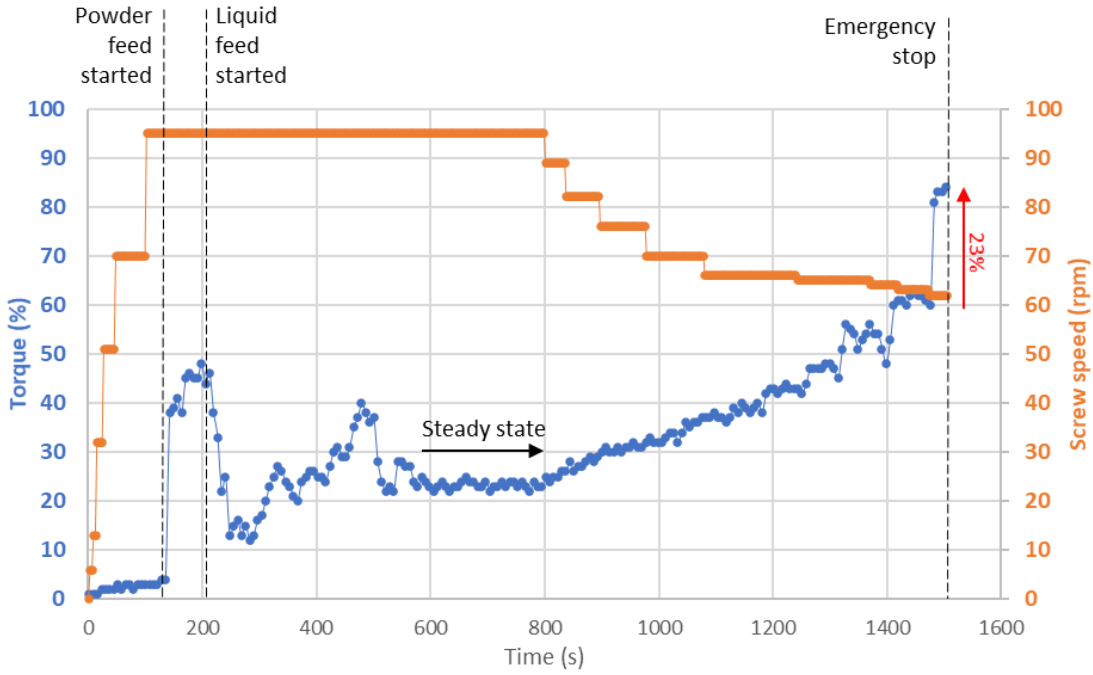

Figure 4.7 Torque (blue line) charted as a function of screw speed (orange line) and time. To determine the maximum TVF in the *granulation* setup, TSG was stopped when the torque suddenly rose above 70%. LSR=0.18, PSD=-0.176 and MFR=1.2 kg·hr^{-1}.

4.3.4. Residence time distribution, RTD

To estimate TVF, the conveying efficiency, c_v, was assessed with respect to the process parameters. To do so, residence time distribution, RTD, studies were performed over a range of screw speeds, SS, for each formulation and for both TSG setups.

The time and profile of the material to traverse the barrel of the twin-screw extruder was studied by implementing a photometric imaging technique similar to those used in previously published investigations (Fogler 2006; Ajay Kumar et al. 2006; Mu and Thompson 2012). A shot of Patent Blue V dye equivalent to 1% w/w of the material throughput per second was manually introduced into the powder inlet port mid-operation. For the purposes of this study, the input pulse was assumed to be perfect and the tracer was assumed to have no influence on the granulation process.

A video of the processed material exiting the barrel via the outlet was recorded at 25 fps for 90 seconds (Sony DSC-RX100 V, Sony Corporation, Japan), and later each frame was converted into an image (VideoPad Video Editor v4.30, NCH Software, Canberra, Australia). A chute fitted to the outlet was created in-house to concentrate the granules exiting the barrel into a narrower stream of limited depth. The chute was coloured red to better contrast the colour intensity of the blue dye. A schematic of the setup is shown in Figure 4.1.

Photometric imaging software (ImageJ, National Institute of Health, USA) was utilised to perform digital colorimetry, quantifying the colour intensity of each image (Figure 4.9), which was proportional to the concentration of dye. Hence, by plotting the colour intensity as a function of time the distribution of dye could be quantified.

The colour intensity of the chute was also recorded and analysed, and the subsequent measurements were used to cancel out background noise originating from variations in lighting and shadows, as well as vibrations of the chute.

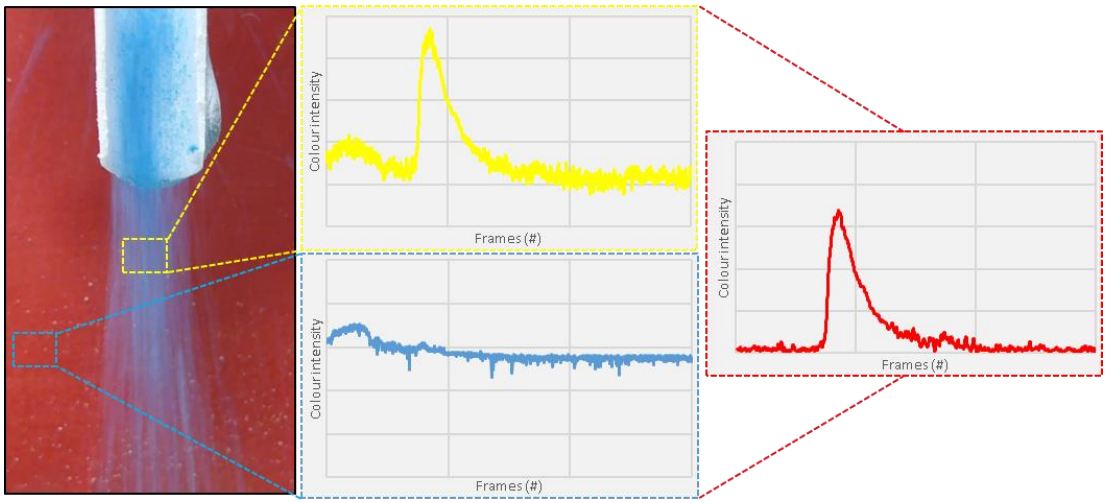

Figure 4.9 Still image from footage of granular outlet captured and analysed: noise from background region of interest (blue) was removed from concentration measurements of granular output (yellow) to produce residence time profile (red).

The resulting concentration distribution profile was normalised to the area under the curve as the residence time distribution function, *E(t)*, was calculated (Equation 4.7). From this, the residence time distribution for each blend was characterised in the form of the mean residence time, $\bar{t}_m$, and the residence time variance, σ^2, calculated using Equation 4.8 and Equation 4.9, respectively.

$$E(t) = \frac{C(t)}{\int_0^\infty C(t)\cdot\delta t} \qquad \text{Equation 4.7}$$

Where $C(t)\cdot\delta t$ is the concentration of the dye between time t and $t+\delta t$.

$$\bar{t}_m = \int_0^\infty t \cdot E(t) \cdot \delta t \qquad \text{Equation 4.8}$$

$$\sigma^2 = \int_0^\infty (t-\bar{t})^2 \cdot E(t) \cdot \delta t \qquad \text{Equation 4.9}$$

After determining $\bar{t}_m$ and σ^2, the dimensionless Péclet number, *Pe*, was calculated using Equation 4.10. *Pe* can be defined as a ratio between the mass transfer resulting from advective transport and the mass transfer resulting from diffusive transport, indicating the extent of axial mixing (Fogler 2006). Hence, powder transport increasingly approaches plug flow conditions as σ^2 approaches zero and *Pe* approaches infinity.

$$\frac{\sigma^2}{t_m^2} \approx \frac{2}{Pe} - \frac{2}{Pe^2} \cdot (1 - e^{-Pe}) \qquad \text{Equation 4.10}$$

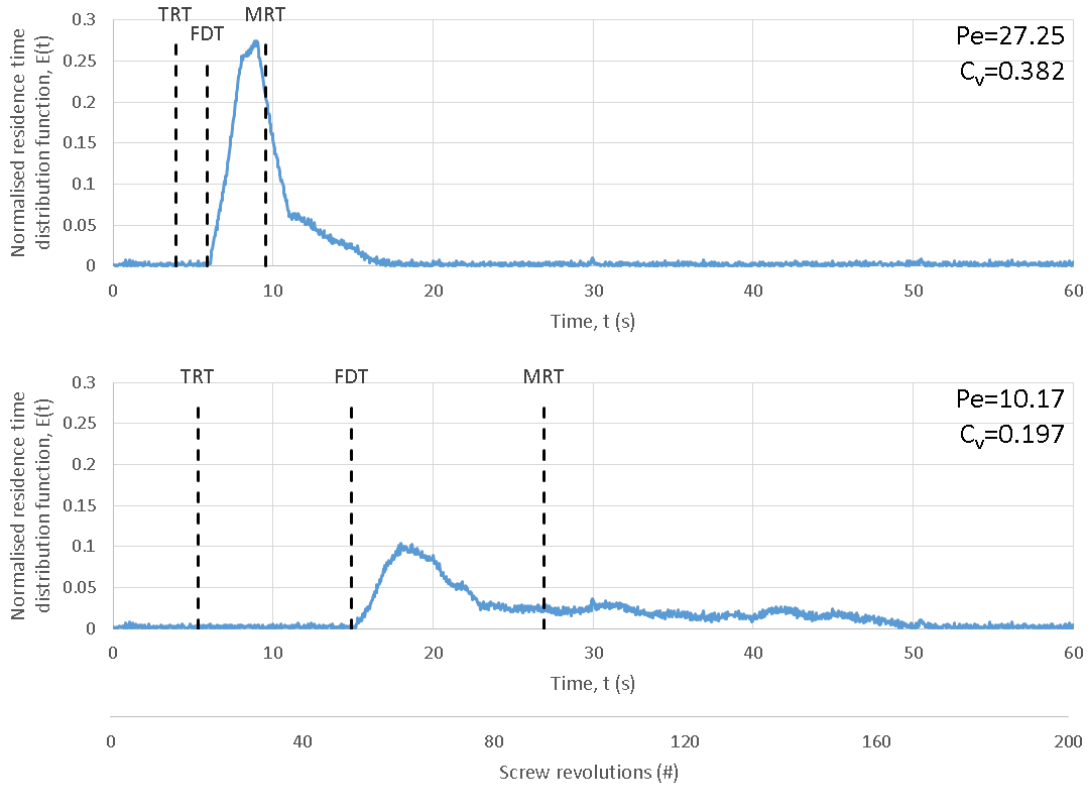

Figure 4.10 Example residence time profiles: RTD resulting from the *nucleation* setup (top) and the *granulation* setup (bottom) were captured under identical conditions: PSD=-0.176, MFR=0.8 kg·hr-1, SS=200 rpm, LSR=0.18. The theoretical residence time (TRT), first detection time (FDT) and mean residence time (MRT) are highlighted.

The time at which the blue dye was first detected (t_{fd}) was plotted against $\bar{t}_t$ and $\bar{t}_m$. t_{fd} was taken to be the time for particles to navigate the barrel with the least retention. Example RTD profiles are shown in Figure 3410 to highlight the key measurements.

Preliminary RTD experiments were conducted to calculate the conveying efficiency at various operating conditions. By estimating c_v from the RTD curves, and by calculating η_v, an operating space was produced whereby the necessary values of SS could be estimated to approximate TVF values (φ) of 0.2, 0.5 and 0.8 at variable MFR for all three formulations and both TSG setups (Figure 4.11).

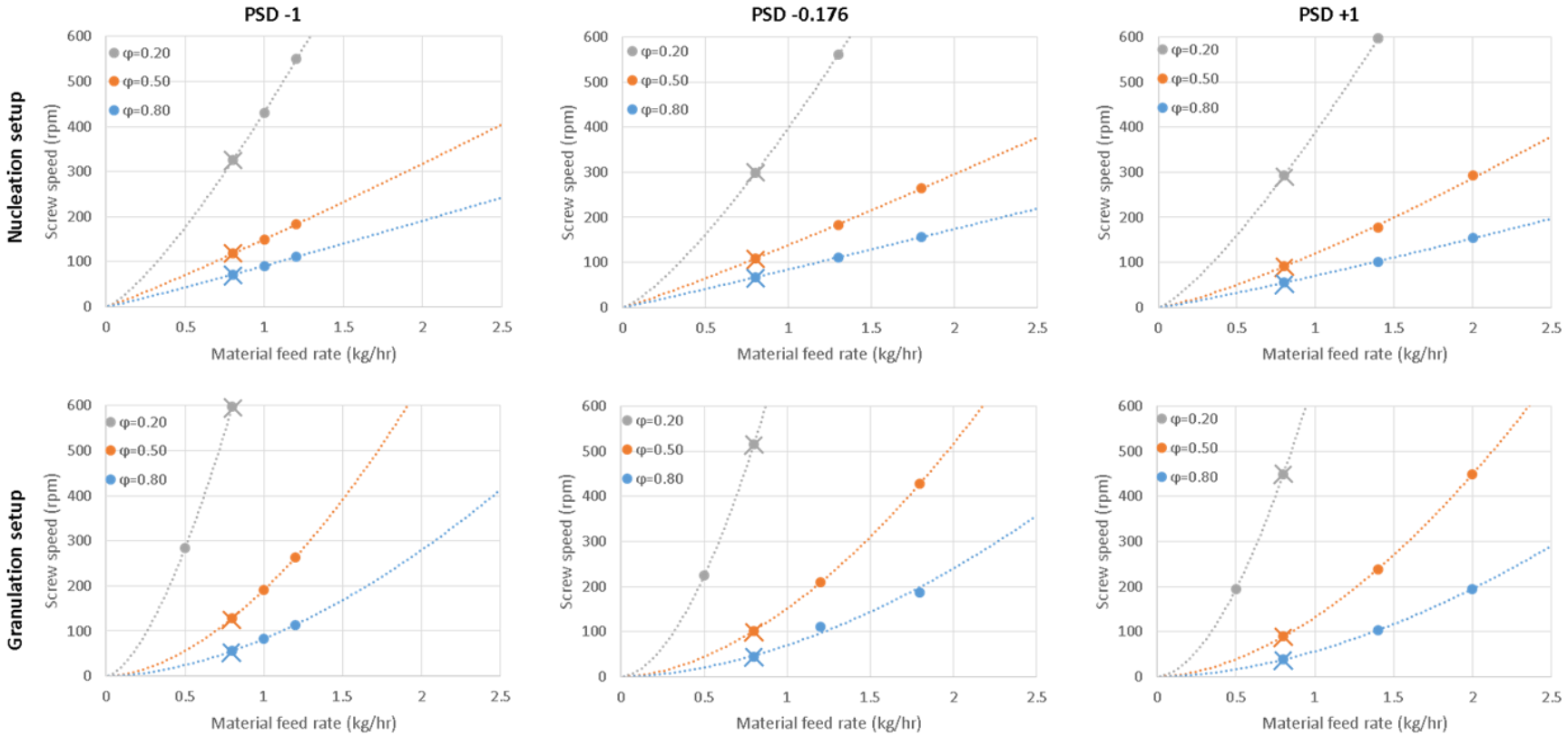

Figure 4.11 Experimental space and the dashed lines indicate the material feed rate, MFR, and screw speed, SS, process conditions to achieve the desired total volumetric fraction, TVF (φ), for both TSG setups and for each formulation (based on Equations 3.3 to Equation 3.6 using the empirically estimated mean residence time). The experimental conditions are marked as ● and are approximate to the TVF value. The initial experimental conditions used to compare the effects of TVF, liquid-solid ratio, LSR, and particle size distribution, PSD, at MFR=0.8 kg·hr^{-1} are marked with an "X".

4.3.5. Granule characterisation

Sub-samples of granular material used for characterisation were obtained using a rotary sample divider (Laborette 27, FRITSCH GmbH, Germany) to ensure accurate representation.

4.3.6. Granule size distribution, GSD

A 40±0.1 g sample of the granulated material from each experimental condition was sieved across a R20/3 nest of ten 200 mm stainless steel sieves (FRITSCH GmbH, Germany) at an amplitude of 2.5 mm in repeated 5-minute intervals until not more than 3% change in mass was observed. The mass of material retained on each mesh was recorded.

The normalised mass frequency (*f*) with respect to the logarithm of particle size was calculated using:

$$f_i(\ln x) = \frac{y_i}{\ln\left({}^{x_i}/_{x_{i-1}}\right)} \qquad \text{Equation 4.11}$$

where y_i is the mass fraction in size interval *i* and x_i is the upper limit of the size interval (Allen 2003).

4.3.7. Granule porosity distribution

Equation 4.12 was used to determine the porosity of each sieve fraction. The tapped density, ρ_{tap}, was measured from the volume of 20±0.1 g of granules after 2000 taps. The true density of the granules, ρ_{true}, was the average of 10 measurements using gas pycnometry (Accupyc II 1340, Micromeritics, USA).

$$\varepsilon\ (\%) = 100 \cdot \left(1 - \frac{\rho_{tap}}{\rho_{true}}\right) \qquad \text{Equation 4.12}$$

This method did not distinguish between *intra*-granular pores and *inter*-granular voids, and hence the intra-granular porosity of larger granules was likely to be overestimated (Verstraeten et al. 2017).

4.3.8. Theophylline,THP, distribution

To determine granule inhomogeneity, a 1±0.01 g sample from each sieve fraction was added to 500 mL of purified water and heated to 37±0.5 °C. The sample was covered and placed on a hotplate magnetic stirrer for approximately 1 hour.

UV-Vis spectrophotometry (ALS SP700 UV Spectrophotometer, Automated Lab Systems, UK) was used to measure the absorbance at a wavelength of 272 nm through a 10 mm quartz cuvette. The concentration was determined using a calibration curve previously established via serial dilution up to a THP concentration of 55 µg/ml (Figure 4.12). Linearity was observed up to 14 µg/ml.

THP distribution was expressed in terms of relative standard deviation (RSD) using:

$$RSD = \frac{\sigma}{\bar{x}} \cdot 100\% \qquad \text{Equation 4.13}$$

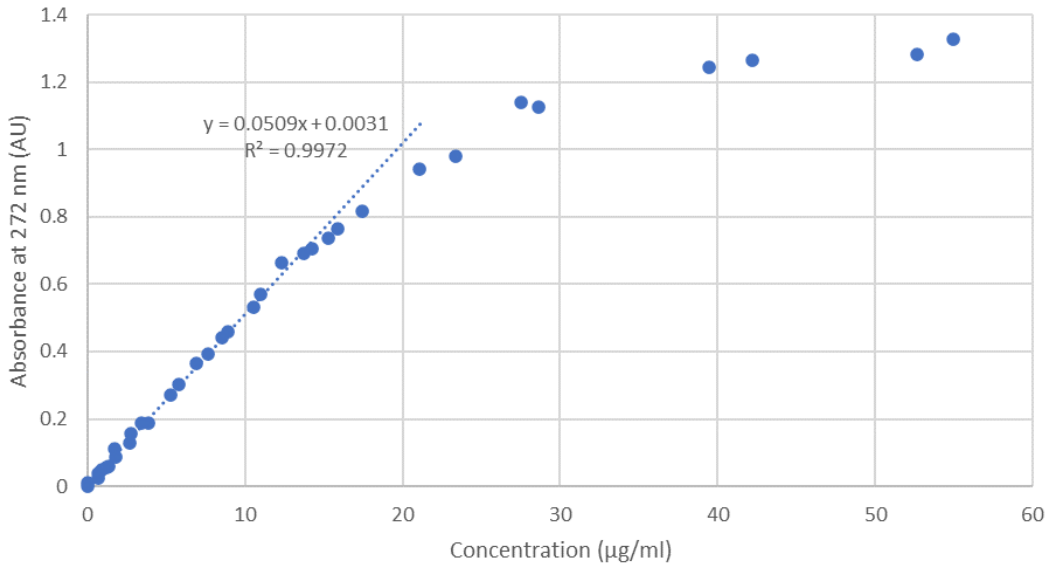

Figure 4.12 UV-Vis at 272 nm of THP absorbance correlated to concentration in demineralised water heated to 37.0 ±0.5 °C

4.3.9. Tablet production

Attempts to tablet the entire TSG output (0-1400 µm) resulted in erratic tablet production during preliminary studies due to inconsistent die filling. Hence, only the 212--850 µm sieve fractions of granular material were used for tablet production. The individual sieve fractions were reconstituted and blended with 0.5% w/w magnesium stearate for one minute at 10 rpm to gently lubricate the granules. The blend was then transferred to the hopper of a single punch tablet press (Korsch XP1, Korsch AG, Germany) to produce flat-faced bevel-edged tablets in a 9 mm diameter die at a rate of 10 min^{-1}. The fill-die position was calibrated for each blend to produce tablets with a target weight of 200±5 mg. The compression force and tablet mass were recorded following the production of each tablet.

4.3.10. Tablet strength

Tablet hardness was determined via the application of a compressive load in the form of a unidirectional stainless-steel platen across the tablet diameter (Tablet Hardness Tester HC 6.2, Kraemer Elektronik GmbH, Germany). The force at failure (*P*) was recorded.

Prior to testing but a minimum of 24 hours post compaction, the diameter (*d*), height (*h*) and wall height (*w*) of each tablet was measured (Figure 4.13), so that the tensile strength (TS) of each tablet could be calculated via Equation 3.14 (Pitt et al. 1989). The tensile strength represents an intensive property, as it normalises the failure force against the tablet dimensions, and hence, the strength of tablets of different shapes and sizes can be directly compared.

$$TS = \frac{2}{3} \cdot \left(\frac{10 \cdot P}{\pi \cdot d^2 \left(2.84 \cdot \frac{h}{d} - 0.126 \cdot \frac{h}{w} + 3.15 \cdot \frac{w}{d} + 0.01 \right)} \right) \qquad \text{Equation 4.14}$$

Twenty-five tablets were produced with compression forces ranging between 5 and 35 kN, and the corresponding tensile strength was used to produce a tabletability profile for each of the TSG conditions. A further 10 tablets at a compressive force of 25±1 kN were produced, and their hardness was subsequently tested.

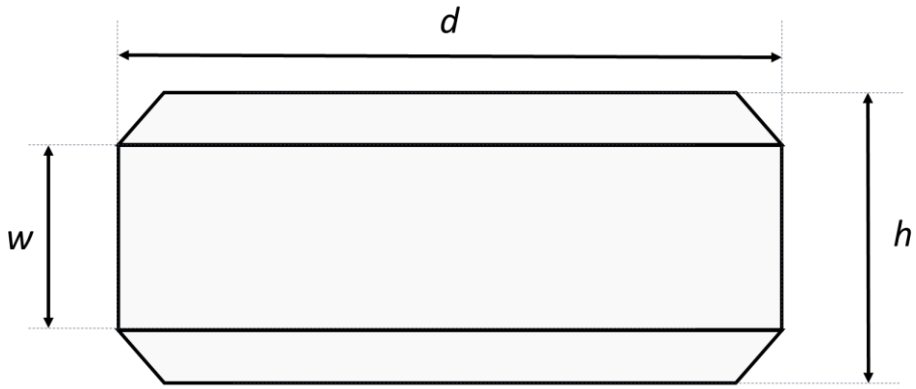

Figure 4.13 Dimensions of a flat-faced bevel-edged tablet used in Equation 3.14 to determine density and tensile strength.

The punch and die displacement during compaction were recorded and used to calculate the pre-compaction and in-die thickness (H_{min}) of each tablet, to be compared with the out-of-die thickness (H_{max}) – measured immediately after compaction, and again at least 24 hours later - to determine elastic recovery (ER%) using Equation 4.15 (Armstrong and Haines-Nutt, 1974).

$$ER\% = \frac{(H_{max} - H_{min})}{H_{min}} \cdot 100 \qquad \text{Equation 4.15}$$

Tablet porosity (ε_{tab}) was calculated from the tablet mass and dimensions, and the weighted true density of the formulation (1.578 g/cm^3).

4.3.11. Tablet drug release profile

To obtain the THP release profile, UV-Vis spectrophotometry (ALS SP700 UV Spectrophotometer, Automated Lab Systems UK) and the aforementioned absorbance-

concentration curve, were used to measure the dissolved THP as a function of time. Six tablets produced at 25±0.5 kN were evaluated for each TSG condition. Each tablet was introduced into a glass vessel filled with 900 mL of demineralised water heated to 37±0.5 °C with rotating paddles operating at 50 rpm (ADT8 Dissolution Bath, Automated Lab Systems, Wokingham, UK), in accordance with *apparatus 2* dissolution testing of the US Pharmacopeia (United States Pharmacopeial Convention 2016). Absorbance at a wavelength of 272 nm was measured through a 10 mm quartz cuvette every 2 minutes in a closed loop system for 30 minutes for each tablet.

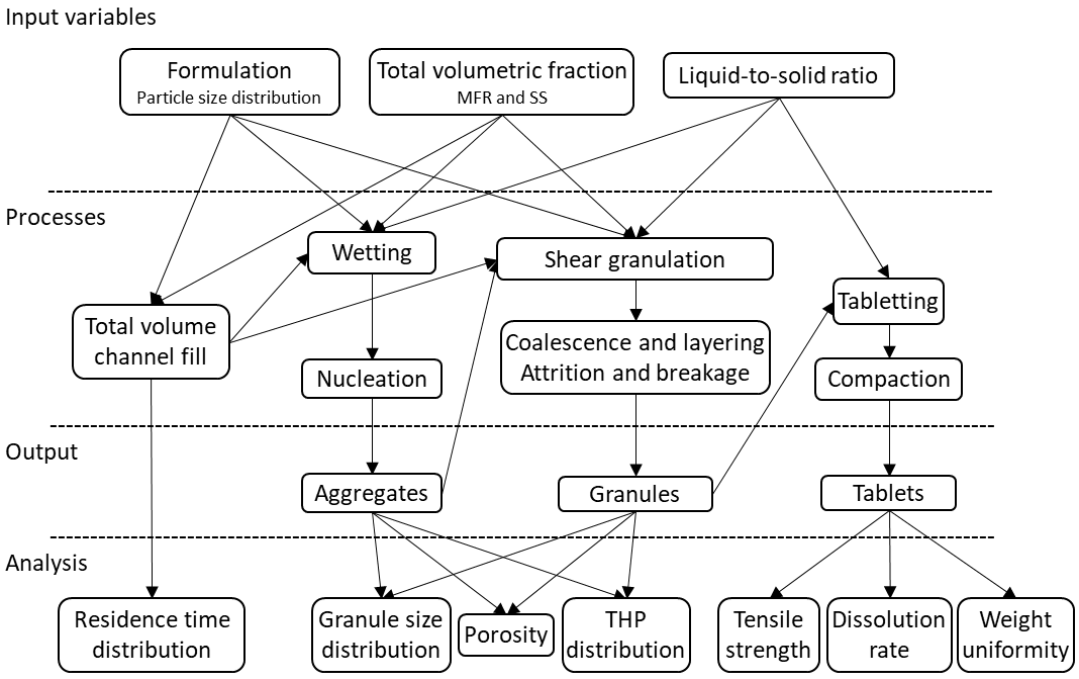

Figure 4.14 Flow diagram outlining the scope of the current study.

4.3.12. Data analysis

Figure 4.14 outlines the scope of this study. As the PSD levels of the pseudo-grades were not equidistant and the LSR was only varied between two levels, neither a fractional nor abbreviated factorial experimental design were suitable. Hence, a full factorial design of

experiments was performed for both TSG setups, shown in Table 8. The PSD of the medium blend was assigned a level of -0.176, reflecting its d_{32} value in relation to the high (PSD +1) and low (PSD -1) blends.

Table 8 Experimental design repeated for both the *nucleation* setup and the *granulation* setup. The levels for each variable correspond to the values listed beneath.

	LSR	TVF	PSD
1	+1	+1	-1
2	+1	0	-1
3	+1	-1	-1
4	+1	+1	-0.176
5	+1	0	-0.176
6	+1	-1	-0.176
7	+1	+1	+1
8	+1	0	+1
9	+1	-1	+1
10	-1	+1	-1
11	-1	0	-1
12	-1	-1	-1
13	-1	+1	-0.176
14	-1	0	-0.176
15	-1	-1	-0.176
16	-1	+1	+1
17	-1	0	+1
18	-1	-1	+1

LSR (-)		TVF, φ (-)		PSD, d_{32} (μm)	
+1	0.18	+1	0.8	+1	123.37
0	-	0	0.5	-0.176	65.53
-1	0.15	-1	0.2	-1	28.12

The measured responses were analysed using Modde 10.12 (Umetrics, Sweden). Multivariate linear regression (MLR) was used to fit the regression models resulting from the

TSG results as no covariance between variables was anticipated (L. Eriksson et al. 2008). Model terms were refined to maximise the predictive cross-validation coefficient (Q^2) and a 95% confidence level was applied in all models. Response surfaces are presented to illustrate non-linear effects and secondary interactions.

4.4. Results

4.4.1. Residence time distribution, RTD, and conveying efficiency, c_v

To establish the conveying efficiency, the RTD was assessed for a range of experimental conditions for both TSG setups. Figure 4.10 depicts typical RTD profiles both setups. Each comprises of a peak followed by a tail, a profile common to TSG (R. Dhenge, Cartwright, J. Hounslow, et al. 2012; R. M. Dhenge et al. 2011; A. El Hagrasy, Hennenkamp, et al. 2013; Ashish Kumar, Alakarjula, et al. 2016; Ashish Kumar, Vercruysse, Toiviainen, et al. 2014; K. T. Lee, Ingram, and Rowson 2012; Y. Liu et al. 2016; Mu and Thompson 2012; Shirazian et al. 2018). The peak-to-tail ratio is indicative of the extent of retention and axial mixing (Ashish

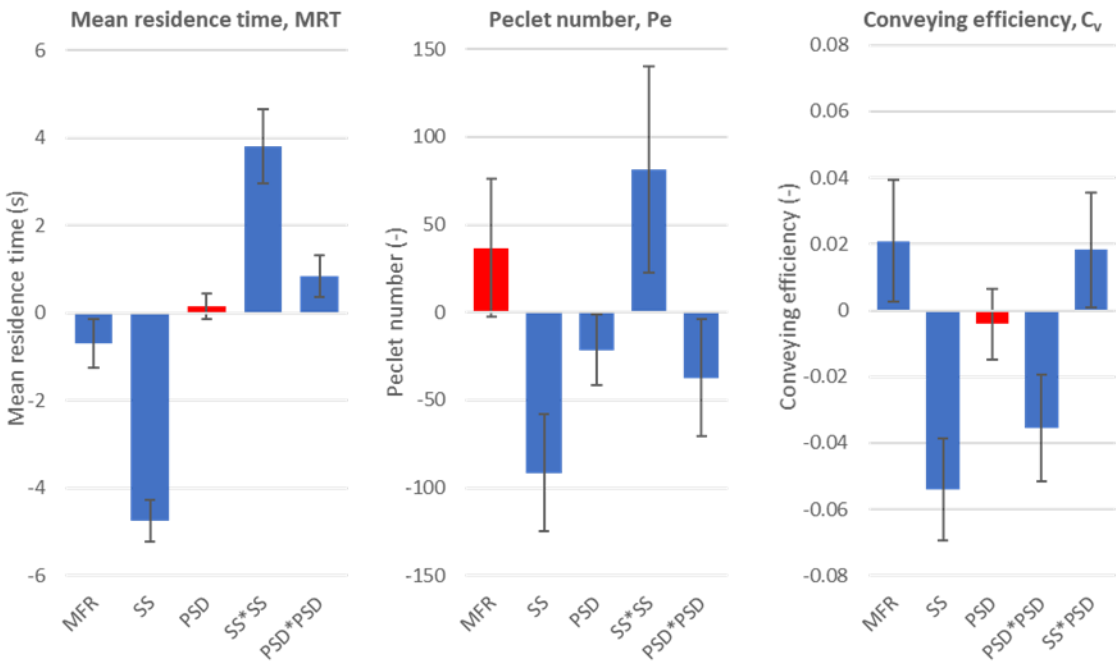

Figure 4.15 MLR coefficients pertaining to RTD from the *granulation* setup.

Kumar, Alakarjula, et al. 2016). The conveying-element-only screw configuration of the *nucleation* setup resulted in a prominent peak and a short tail, indicative of limited axial mixing. Contrastingly, the low conveying capacity of the kneading block in the *granulation* setup resulted in a smaller peak and a longer tail. This is reflected by a lower conveying efficiency and smaller Peclet number. These observations were consistent with other studies that have found RTD to lengthen and MRT to increase with the addition of kneading blocks (Ashish Kumar, Alakarjula, et al. 2016; Ashish Kumar, Vercruysse, Toiviainen, et al. 2014; Mu and Thompson 2012; Shirazian et al. 2018).

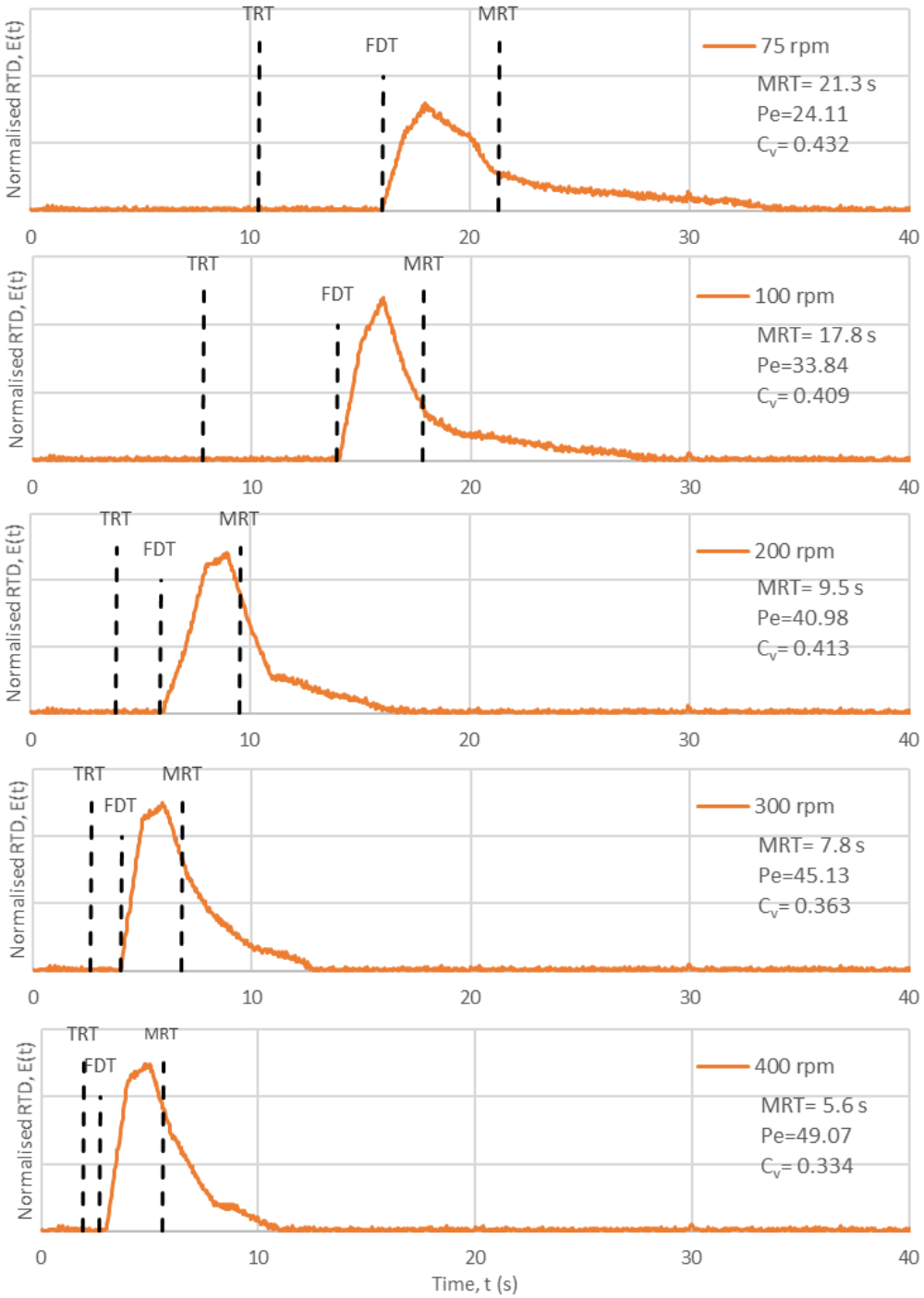

Figure 4.16 Profiles (10-point moving average) comparing the effect of SS on RTD during *nucleation*. MFR=0.8kghr-1, PSD=-0.176, LSR=0.18.

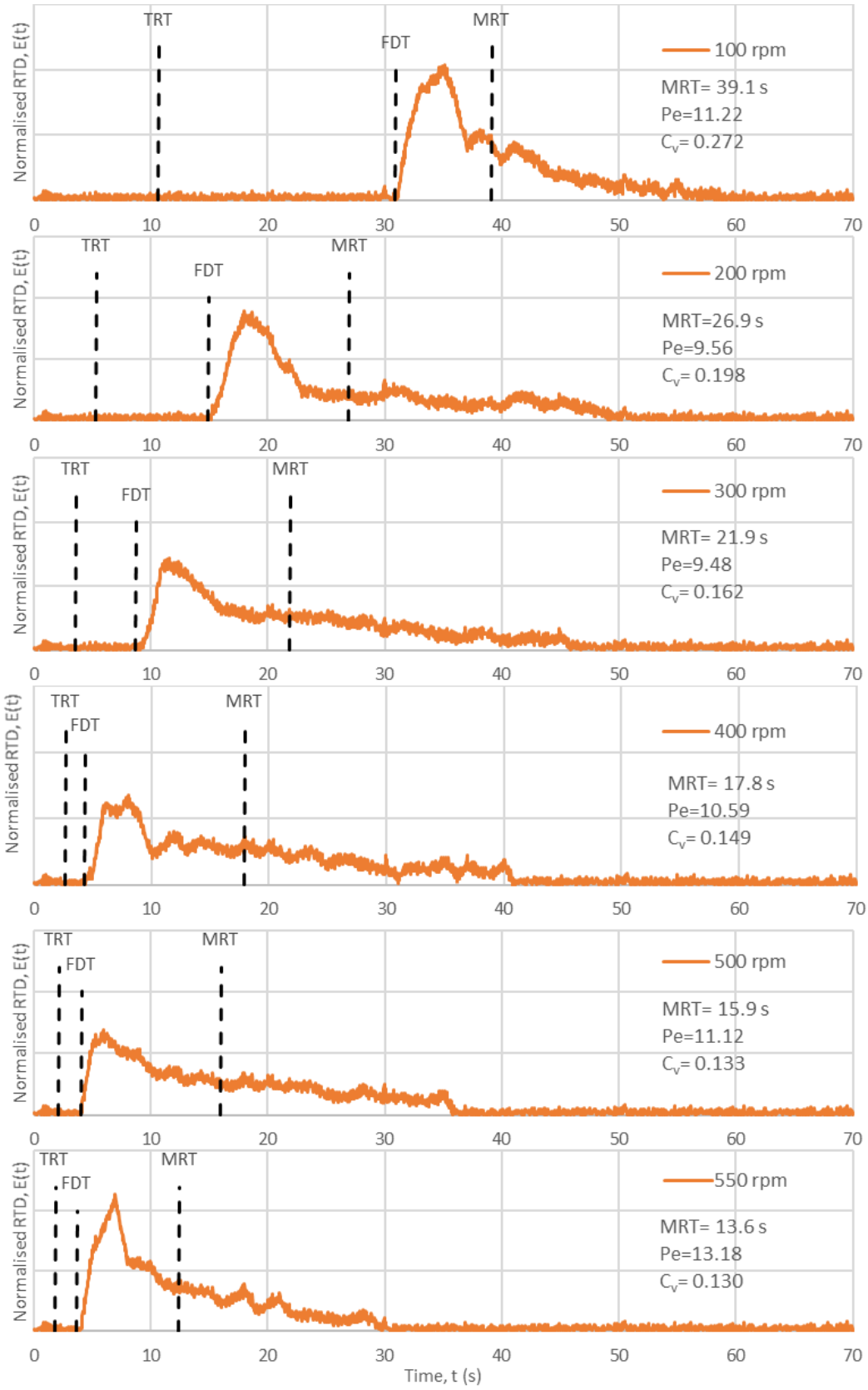

Figure 4.17 Profiles comparing the effect of SS on RTD during *granulation*. MFR=0.8kghr-1, PSD=-0.176, LSR=0.18.

From the MLR coefficients shown in Figure 4.15, it is evident the MRT was primarily determined by, and was inversely correlated to, screw speed. The effect of SS on RTD is shown in Figure 4.16 for *nucleation* and Figure 4.17 for *granulation*. The dominance of SS was to be expected as screw speed determines the rate of axial transport (Lute, Dhenge, and Salman 2018a; Shirazian et al. 2018). However, for both setups the relationship was non-linear as the MRT's rate of decrease declined with increased SS, hence the significance of the SS*SS term in the MLR model (p<0.05). Both non-linear (Lute, Dhenge, and Salman 2018a) and linear (Ashish Kumar, Alakarjula, et al. 2016; Ashish Kumar, Vercruysse, Toiviainen, et al. 2014; Robin Meier et al. 2017b) relationships have previously been reported.

The disparity between theoretical residence time, TRT, and the measured MRT was greater with the inclusion of the kneading elements (Figure 4.18) due to their near-neutral conveying geometry. However, the ratio between first detection time, FDT, and TRT was independent of screw speed for both setups indicating that a fraction of the tracer was able to traverse the kneading block largely unimpeded. For the *nucleation* setup, the conveying efficiency (c_v=TRT/MRT) decreased from 0.476 to 0.297 as the SS increased from 75 rpm to 400 rpm (Figure 4.22). For the *granulation* setup, the c_v decreased from 0.272 to 0.118 as the SS increased from 100 rpm to 550 rpm.

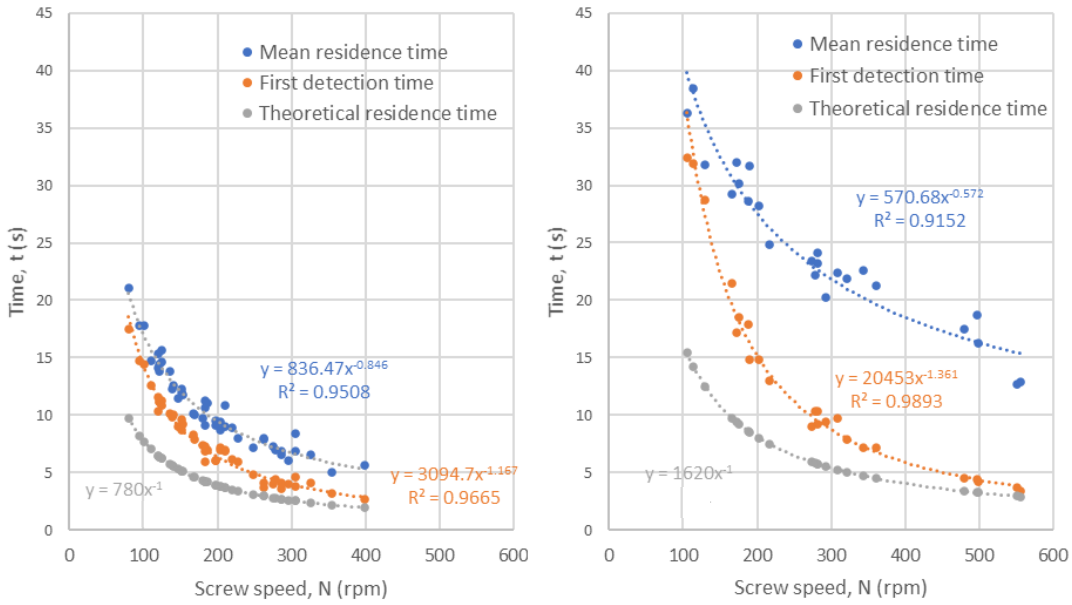

Figure 4.18 RTD measurements resulting from the *nucleation* setup (left) and the *granulation* setup (right) as a function of screw speed.

With increased SS the difference between the FDT and the MRT increased and was more evident for the granulation setup. This is indicative of increased axial mixing and correlates with the decreasing Peclet number. Additionally, the Peclet MLR model indicates that the increased axial mixing resulting from increased blend PSD was significant (p<0.05), albeit small (Figure 4.15). The flow function coefficient measured by the FT4 rotational shear tests (Figure 3.12) may explain this observation; the concentric layers of PSD+1 were able to radially shear freely (FFc>10) whereas PSD-1 exhibited restrained shearing (FFc<4) on account of cohesive forces and poor flow properties. Hence, for PSD+1 sufficient relative motion between particles produced a broader particle velocity distribution, facilitating axial mixing, as shown in Figure 4.19. It is assumed that this disparity in particle velocity occurred only between dry particles and it is difficult to determine the role of PSD and flow properties on axial mixing of wetted particles that had begun to agglomerate.

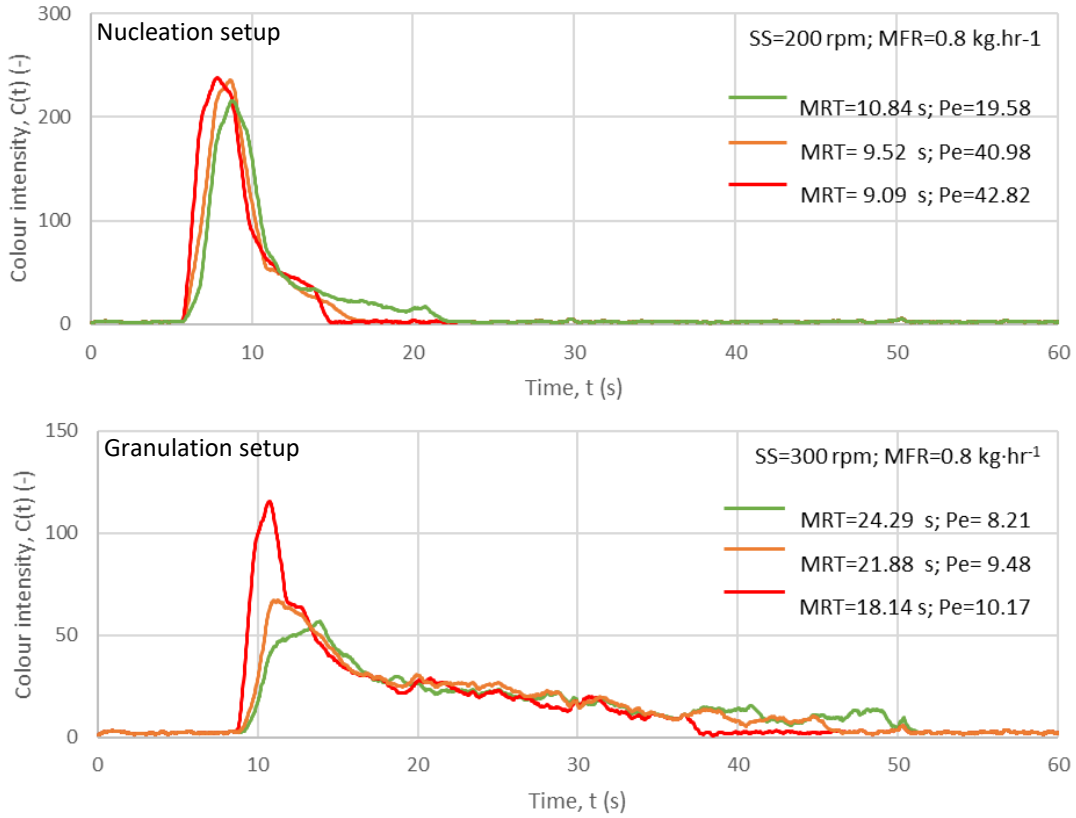

Figure 4.19 Profiles (10-point moving average) comparing the effect of PSD on RTD during *nucleation* (top) and *granulation* (bottom); PSD+1 (green), PSD-0.176 (amber) and PSD-1 (red).

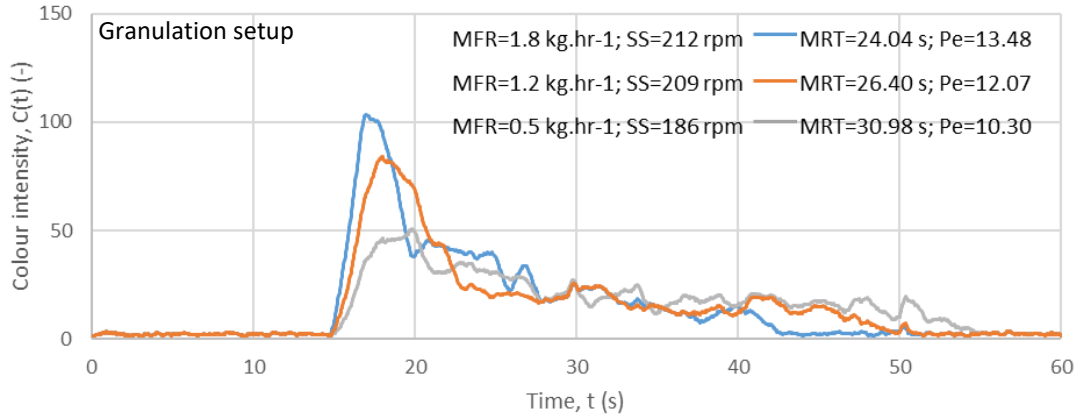

Figure 4.20 Profiles (10-point moving average) comparing the effect of TVF on RTD during granulation at comparable SS; TVF+1 (blue), TVF0 (amber) and TVF-1 (grey). Note: It was not possible to achieve all three TVF conditions at comparable SS with the nucleation setup.

By only changing the MFR, the effects of the fill level on RTD were studied at similar rotations per minute, independent of SS, as shown in Fig 4.20. As reported by Dhenge et al. (2010), a small reduction in MRT was observed with increased MFR, and was likely a result of increased TVF. Kumar et al. (2014) report lower axial mixing was observed at higher fill levels as the degree of backflow was restricted, resulting in a higher value of Pe.

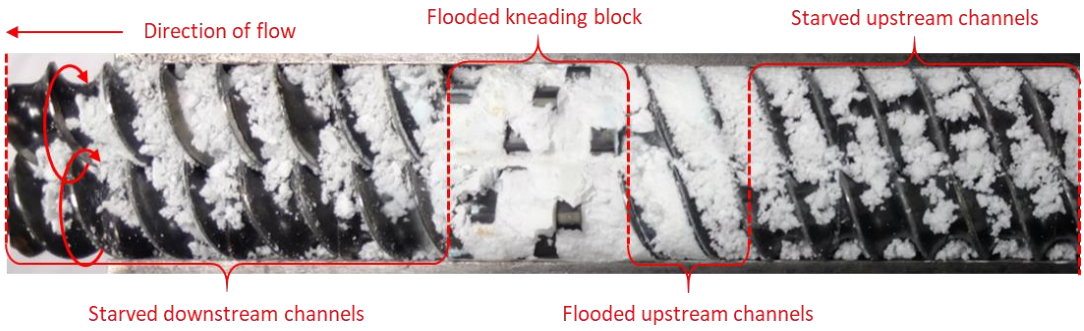

Figure 4.21 Screw and barrel conditions following emergency stop mid-operation and removing the upper barrel casing. TVF=0.204.

It can be deduced that at low SS and low PSD the material transport approached plug flow under nucleation conditions. In contrast, a low Peclet number was obtained for all the RTD resulting from the granulation setup, indicating significant axial mixing. The low conveying capacity of the successive kneading elements resulted in a dependence on the upstream conveying elements for material transport as a build-up of pressure was required to push the material through the kneading block. This created uneven flow and promoted axial mixing. This bottle neck effect was evidenced by observing flooded channels in the conveying elements immediately upstream of the kneading block, whereas the channels downstream of the kneading block were “starved”, as shown in Figure 4.21.

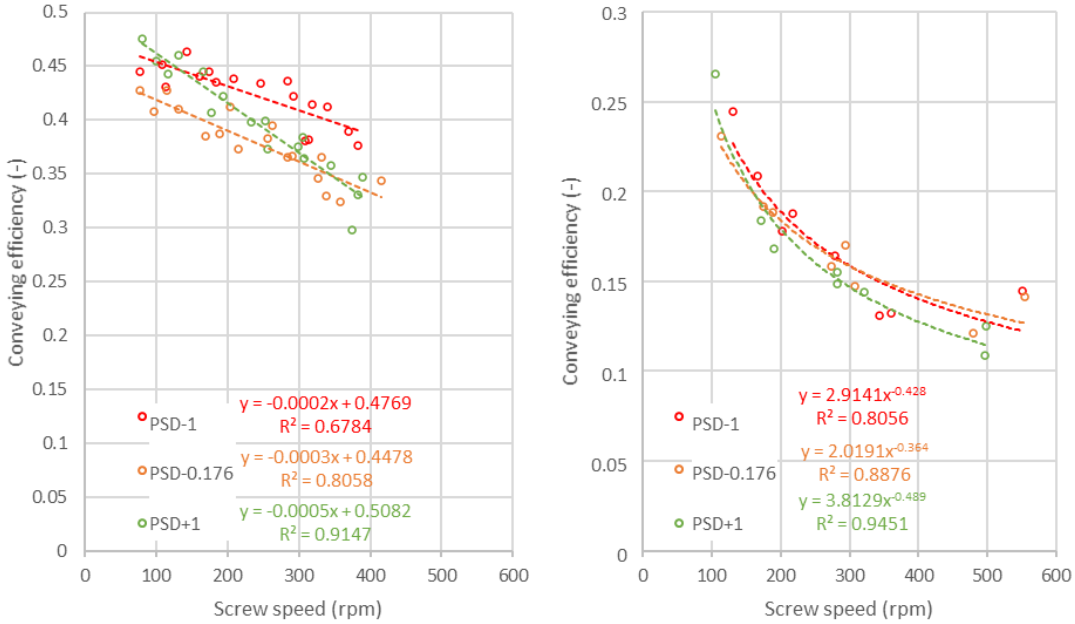

Figure 4.22 Conveying efficiency, c_v, in relation to screw speed for the *nucleation* setup (left) and the *granulation* setup (right). MFR=0.8 kg·hr^{-1}, LSR=0.18.

From the range of TRT and measured MRT the conveying efficiency trend was established as regression equations and found to decrease with increased screw speed under both setups (Figure 4.22). This endorses Roberts' findings that the disparity between particle speed and impeller speed increased at higher impeller speed (Roberts and Willis 1962). Under nucleation conditions the rate of decrease in efficiency was linear with respect to SS and the gradient increased with increased PSD. Under granulation conditions the decrease in conveying efficiency was non-linear and independent of PSD The regression equations had high R^2 values and were used to estimate the conveying efficiency as a function of screw speed, formulation PSD and TSG setup for the TVF studies.

4.4.2. Determining maximum TVF

To ascertain if the experimental maximum channel fill conditions approached TVF=1.0, the screw speed was gradually decreased at a constant MFR. With the *nucleation* setup (1.3 kg·hr^{-1}, PSD-0.176) the torque never rose sharply or above 30% despite operating at low SS. However, at 59 rpm raw formulation began to build up at the powder inlet indicating that the channels of the conveying elements directly downstream of the inlet were volumetrically fully occupied and unable to accommodate more material, resulting in a visible overflow (figure 4.7). According to Equation 4.1 to 4.6, the value of TVF at these conditions was calculated to be 0.917 (Figure 4.23).

Figure 4.23 Visual inspection of the channel fill during nucleation at various TVF values following an emergency shutdown mid-operation and removing the upper barrel casing. MFR=0.8 kg·hr^{-1}, PSD=-0.176.

With the granulation setup (1.2 kg·hr^{-1}, PSD-0.176) the torque rose sharply above 70% when the SS was decreased to 69 rpm (Figure 4.8). The value of TVF at these conditions was calculated to be 0.934. Hence, it is evident that by deriving TVF from both the calculated volumetric efficiency and the experimentally determined conveying efficiency, a more representative value of the conveying channel fill fraction can be determined than using the

volumetric efficiency equation (Equation 4.1) alone. In doing so, the maximum calculated channel fill tested by Gorringe et al. (2017) was less than 0.5.

Note the asymmetric distribution of material between the two screws shown in Figures 4.21 and 4.23. The channels of the top/right screw had a higher fill level than the bottom screw. Chan Seem et al. (2016) experimentally determined that under starved conditions the top/right screw conveys the majority of the material, as the bottom screw loads material onto the top/right driving screw. The authors attributed this asymmetry to gravity, barrel and screw dimensions, and the direction of screw rotation; the loading screw transfers material to the driving screw below the screw, whereas the driving screw transfers material above the screw, hence, gravity favours material passed to the driving screw. With increased barrel fill levels this disparity lessens as gravity becomes less of a factor and the material was more constrained (Figure 4.23).

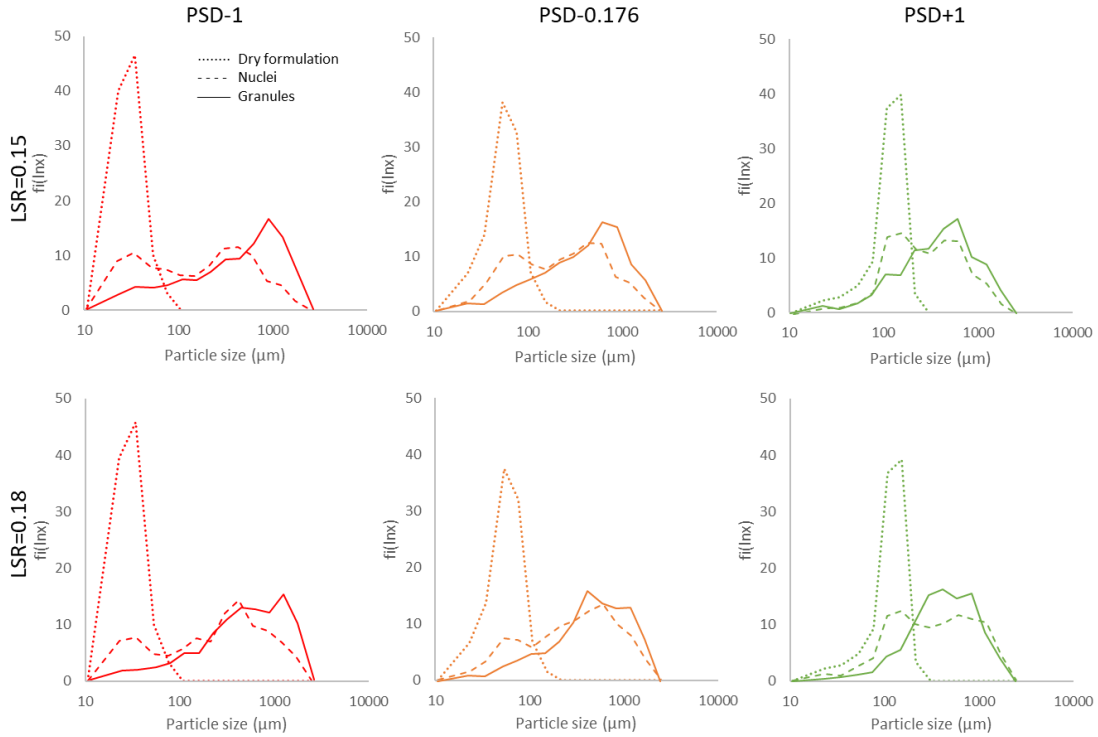

Figure 4.24 Comparison of size distribution of dry formulation (dotted line, ····), material following nucleation (dashed line,- - - -), and material following granulation (solid line, ——) of PSD-1 (left, red), PSD-0.176 (middle, amber) and PSD+1 (right, green) at LSR=0.15 (top) and LSR=0.18 (bottom). MFR and TVF were maintained at 0.8 kg·hr^{-1} and ~0.5, respectively. Each curve is a mean average, n=3.

4.4.3. Nuclei size distribution, NSD, following twin screw nucleation

To assess the influence of the twin screw granulation (TSG) setup, liquid-solid ratio (LSR), total volumetric fill (TVF) and particle size distribution (PSD) on the nuclei size distribution (NSD), the material feed rate (MFR) was initially maintained at 0.8 $kg \cdot hr^{-1}$. To simulate nucleation under *granulation* conditions, the same TVF values were targeted for both TSG setups. Screw speed (SS) was varied to achieve a TVF of circa 0.2, 0.5 and 0.8 in accordance with Equations 4.1 to 4.6. Figure 4.24 illustrates the evolution of the size distribution of the powder material during size enlargement. The narrow unimodal peak representing the dry formulation became broad and multimodal. The significant overlap between the nucleated material and dry formulation indicates that a significant portion of the powder experienced no wetting or negligible agglomeration.

The NSDs obtained from sieve analysis of the nuclei are shown in Figure 4.25 and all depict a bimodal curve. To fully evaluate the role of each factor, the processed material was classified as fines and non-wetted material (<212 µm), small agglomerates (212-850 µm) and large agglomerates (>850 µm) and displayed in Figure 4.26. The granule size distributions (GSD) resulting from *granulation* are discussed in section 4.4.4.

The proportion of non-wetted material ranged between 29.5 and 52.5% and was assumed to be inversely proportional to liquid distribution (Chan Seem et al. 2016; A. El Hagrasy, Hennenkamp, et al. 2013; J. G. Osorio et al. 2017; Sayin et al. 2015; Verstraeten et al. 2017). This high proportion of fines was a result of the limited shear forces exerted by the conveying elements to promote liquid distribution, and the brief period for liquid distribution to occur (<20 s). Expectedly, the proportion of non-wetted material decreased with increased LSR as the potential for inter-particle liquid bridges increased as a result of liquid droplets being

introduced into the barrel more frequently via the syringe pump (V. Lute, Dhenge, and J. Hounslow & Agba D. Salman 2016). Hence, LSR was the most significant factor for determining the proportion of non-wetted material (Figure 4.27). However, LSR had no statistically significant effect on proportion of small agglomerates (Figure 4.27); as well as resulting in a reduction in non-wetted material, increased LSR also manifested as an increase in large agglomerates, producing little net change in small agglomerates.

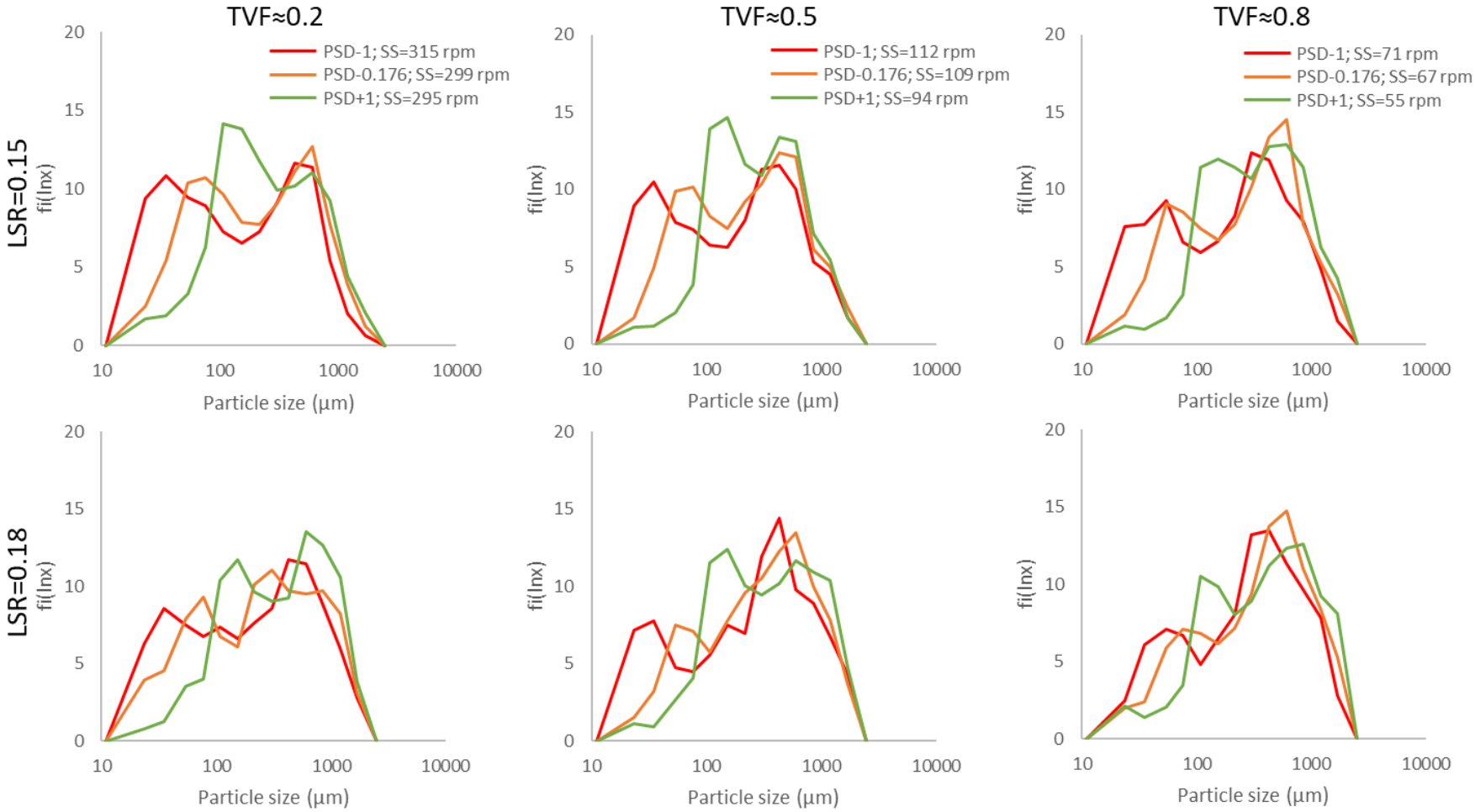

Figure 4.25 Nuclei size distribution measured by sieve analysis following nucleation of PSD-1 (red), PSD-0.176 (amber) and PSD+1 (green), at LSR=0.15 (top) and LSR=0.18 (bottom), and TVF=0.2 (left), TVF=0.5 (middle) and TVF=0.8 (right). MFR was kept constant at 0.8 kg·hr^{-1}. Each curve is a mean average, n=3.

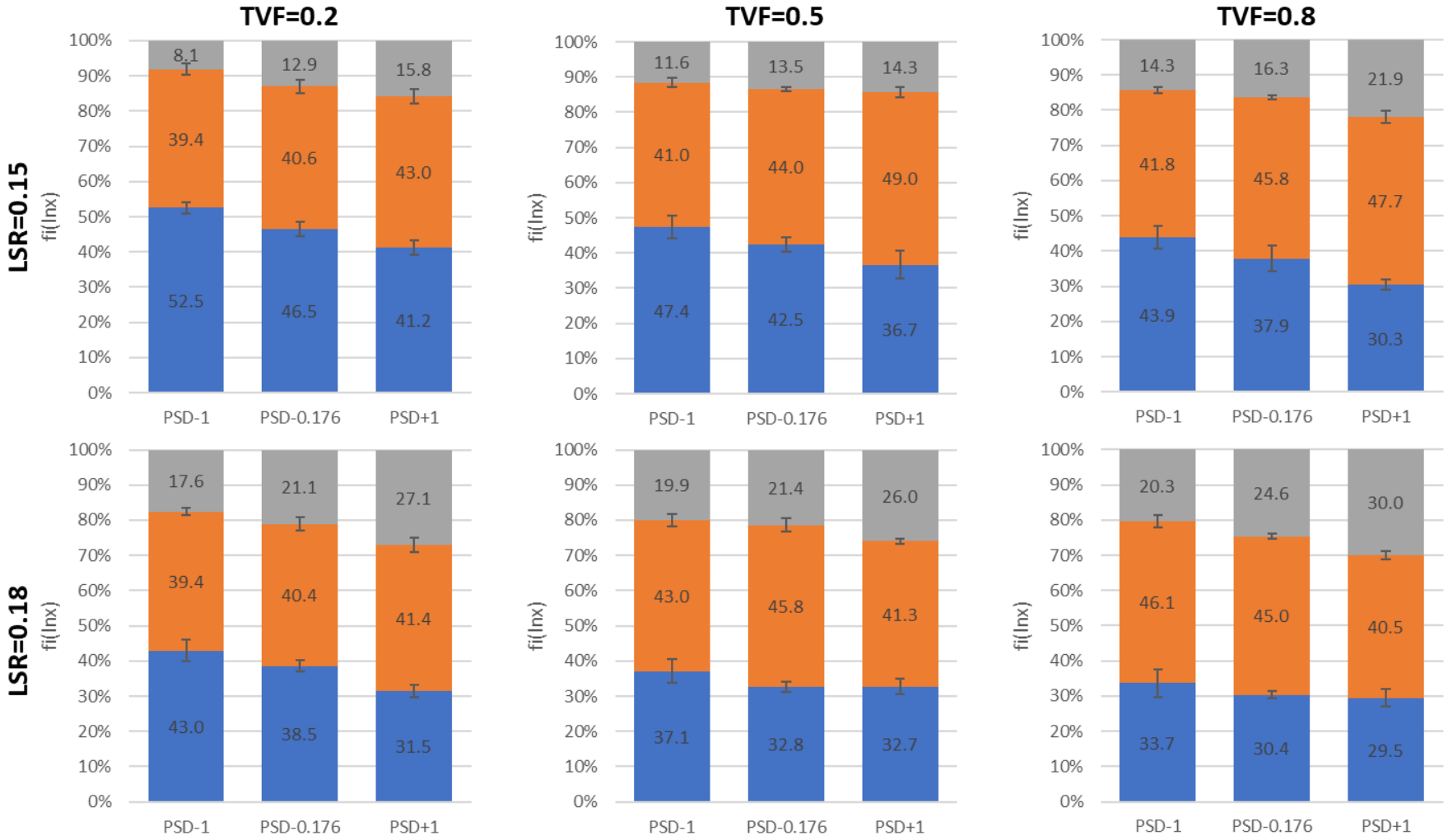

Figure 4.26 Material resulting from the *nucleation* setup categorised into non-wetted material <212 µm (blue), small agglomerates 212-850 µm (orange) and large agglomerates >850 µm (grey). Mean ±sd, n=3.

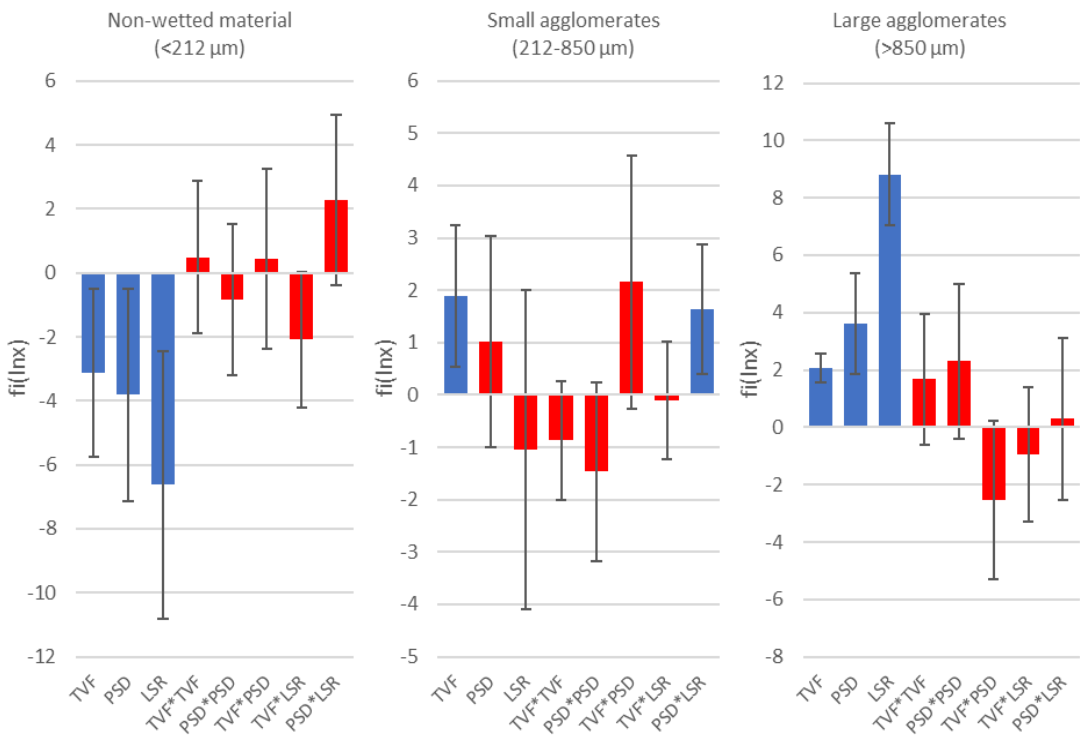

Figure 4.27 MLR model – magnitude of each significant term influencing the size distribution of material following nucleation. Statistically insignificant terms (p>0.05) are highlighted in red.

The proportion of non-wetted material decreased and large agglomerates increased with increased formulation PSD for all conditions. At LSR=0.15 the proportion of small agglomerates increased with increased PSD at all TVF conditions. However, at LSR=0.18 this trend was not evident, hence the significance of the PSD*LSR term (p<0.05) in the MLR model. Mackaplow et al. (2000) compared nucleation of coarse, medium and fine grades of lactose in a high shear granulator; two minutes after adding the granulating liquid, a significantly higher proportion of the coarse grade had nucleated into large agglomerates than the fine grade. However, when the size of the nucleated material was considered relative to the starting powder i.e. agglomerate-to-particle size ratio, Badawy and Hussain (2004) found that a fine sieve fraction of lactose anhydrous underwent greater agglomeration growth than a coarse sieve fraction. This study observed similar behaviour, as the normalised agglomeration growth (agglomerate d_{50}/primary particle d_{50}) was greatest for PSD-1 and least for PSD+1 (Figure 3.28).

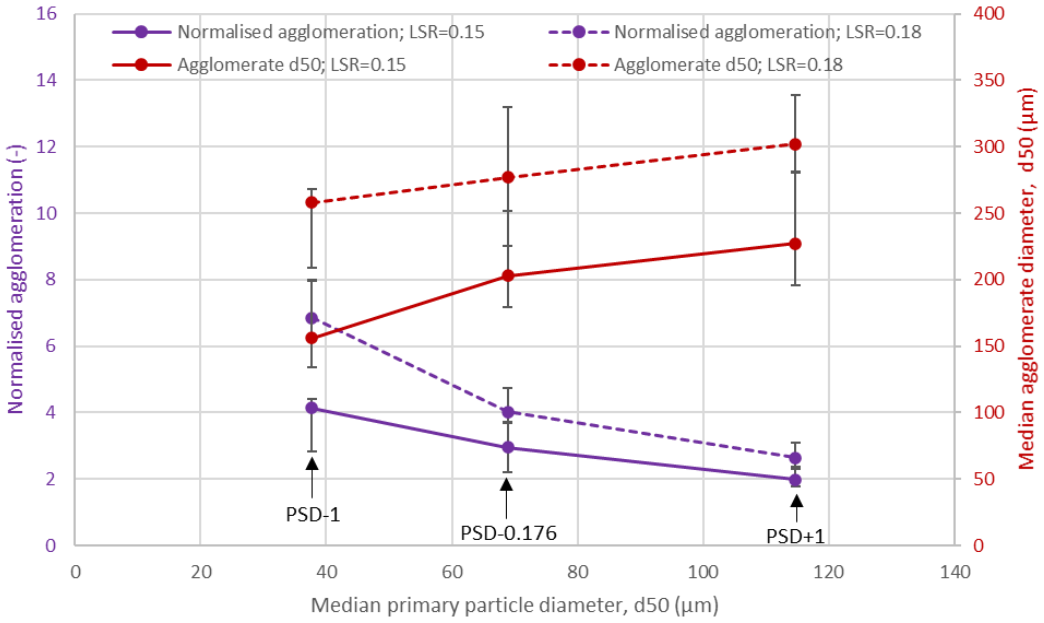

Figure 4.28 Normalised agglomeration (agglomerate d_{50}/primary particle d_{50}) as a function of formulation PSD and LSR. The line represents value obtained at TVF=0.5 and the plus and minus error bars correspond to TVF=0.8 and TVF=0.2, respectively.

In this regard, excipient PSD variation had little effect on the nucleation size distribution. The median diameter of a PSD+1 primary particle was over three times larger than that of PSD-1 but the influence on the nucleation size distribution was only modest (less than 50%). Therefore, the NSD was dominated by other factors including LSR and mechanical forces.

Increasing TVF was found to facilitate liquid distribution in most cases, as the proportion of non-wetted material decreased. Although not explicitly measuring the channel fill, Lute et al. (2016) found that by reducing the screw speed at constant feed rate, and in effect increasing channel fill, the proportion of fines decreased and agglomeration increased in a conveying only screw configuration - 2*CE(2D)-4*CE(1D). Yet, Dhenge et al. (2013) reported an increase in fines and decreased agglomeration with increased feed rate at constant screw speed. In that study, however, nucleation took place over the full length of the barrel i.e. 2*CE(2D)-16*CE(1D), and therefore, was subject to greater shear over a longer duration. Dhenge et al. (2012), too, tried to simulate nucleation and found increased feed rate at

constant screw speed to increase the median particle size of the nucleated material. As only the d_{50} value was reported, it is unclear whether more particles became wetted and underwent modest agglomeration, or whether nuclei excessively agglomerated to skew the median particle size.

TVF was the only significant coefficient in the small agglomerate MLR, as increasing TVF resulted in a greater proportion of small agglomerates between 212 and 850 µm. It is possible that the constrained conditions at higher TVF and confined barrel dimensions limited the agglomeration of large nuclei.

Within TSG, nucleation occurred by the immersion mechanism as the droplet emitted from the liquid port was significantly larger than the primary powder particles (Schæfer and Mathiesen 1996). This mechanism has been shown to result in inefficient liquid distribution and less controlled nucleation when compared to a spraying distribution mechanism (Kayrak-Talay and Litster 2011). The droplet emerging at the inlet was routinely wiped by a fresh collection of dry primary particles traversing across the intermeshing region beneath. This resulted in a saturated mass of powder, from which excess liquid infiltrated to the surrounding powder bulk. This infiltration was the function of minimal shear forces inflicted by the conveying elements and capillary action. As discussed in Chapter 3, a larger particle size and lower surface area resulted in a less tortuous pore network and a smaller effective contact angle, and ultimately, facilitated liquid intrusion within a powder bulk (Depalo and Santomaso 2013; Kiesvaara and Yliruusi 1993; Kirchberg, Abdin, and Ziegmann 2011; Y.-W. Yang, Zografi, and Miller 1988). At increased TVF, the barrel conditions were more constrained and particle packing became more consolidated, which again, was shown to improve liquid penetration in Chapter 3 and previously (Siebold et al., 1997; Hapgood et al., 2002; Galet et al., 2010; Yang and Xu, 2017). As can be seen in Figure 4.23 at TVF=0.8 the

powder within the barrel forms a continuous mass with very little of the screw channel visible. Therefore, the liquid had a less fragmented pore network to navigate, allowing more particles to be wetted. Additionally, the constrained conditions at high TVF limit pore size within which binder liquid can accumulate without contributing to wetting and nucleation. With decreasing TVF the screw channel became more visible and the powder bulk more disconnected, hence, more of the channel could be occupied by free liquid with fewer liquid-particle interactions.

Further, increased consolidation owing to higher TVF resulted in a greater proportion of large agglomerates (>850 μm). This was possibly due to a greater number of successful particle coalescence as a result of closer contact (S. Iveson et al. 2001); or due to a larger number of particles coming into contact with the initial droplet due to a greater particle density within the barrel (Schæfer and Worts 1978); or a combination of both. Another explanation for greater wetting and agglomeration at higher TVF, was because the lower screw speed resulted in a longer MRT, allowing for a greater period of time for liquid distribution to occur. Conversely, Dhenge et al. (2013) reported that at lower SS the specific mechanical energy - an indication of shear forces inflicted on the material - was lower and likely to contribute to mechanical liquid dispersion less. However, it is not possible to compare the independent magnitude or contribution each of these factors made to liquid distribution and nucleation in this present study.

Due to the zero-sum relationship between the size categories it is difficult to relate the proportion of small agglomerates directly to any of the factors. That is to say, small agglomerates can be the result of (i) limited agglomeration of primary particles or (ii) size reduction of large agglomerates via breakage. The MLR model and response surface cannot determine which mechanism was dominant.

This study has attempted to simulate nucleation in a TSG barrel in the absence of a kneading block by maintaining the channel fill. Previous studies have attempted to investigate nucleation by translocating the powder and liquid inlet towards the barrel outlet (R. Dhenge, Cartwright, J Hounslow, et al. 2012; V. Lute, Dhenge, and J. Hounslow & Agba D. Salman 2016). However, by not adjusting the MFR and SS accordingly, these studies did not account for the increased barrel fill resulting from the loss of conveyance with the inclusion of the kneading block. Therefore, the conditions did not simulate nucleation under typical TSG conditions with a screw configuration consisting of one or more kneading zones.

4.4.4. Granule size distribution, GSD, following twin screw granulation

Figure 4.29 shows a sample of granules in each sieve fraction following granulation (experiment 15). The resulting GSDs at 0.8 kg·hr^{-1} are displayed in Figure 4.30. As above, the granulated material was divided into fines (<212 μm), small granules (212-850 μm) and large granules (>850 μm) as displayed in Figure 3.31. Typically, small granules would be considered the yield, as they possess desirable properties for tablet production (Forlano and Chavkin 1960; Marks and Sciarra 1968; Šantl et al. 2012; Yajima et al. 1996). The presence of large granules and fines impede tablet production and uniformity, and are therefore, removed to be milled or reworked, respectively. Hence, a higher proportion of small granules was indicative of greater granulation efficiency.

The resulting GSDs were broad and skewed towards larger granules and possessed fewer fines than the size distributions obtained following nucleation. This was because the rotating kneading lobes promoted liquid distribution and agglomeration as the shear forces squeezed liquid from saturated voids to non-wetted regions, whereby it contributed to granule growth via coalescence and layering (A. S. El Hagrasy and Litster 2013).

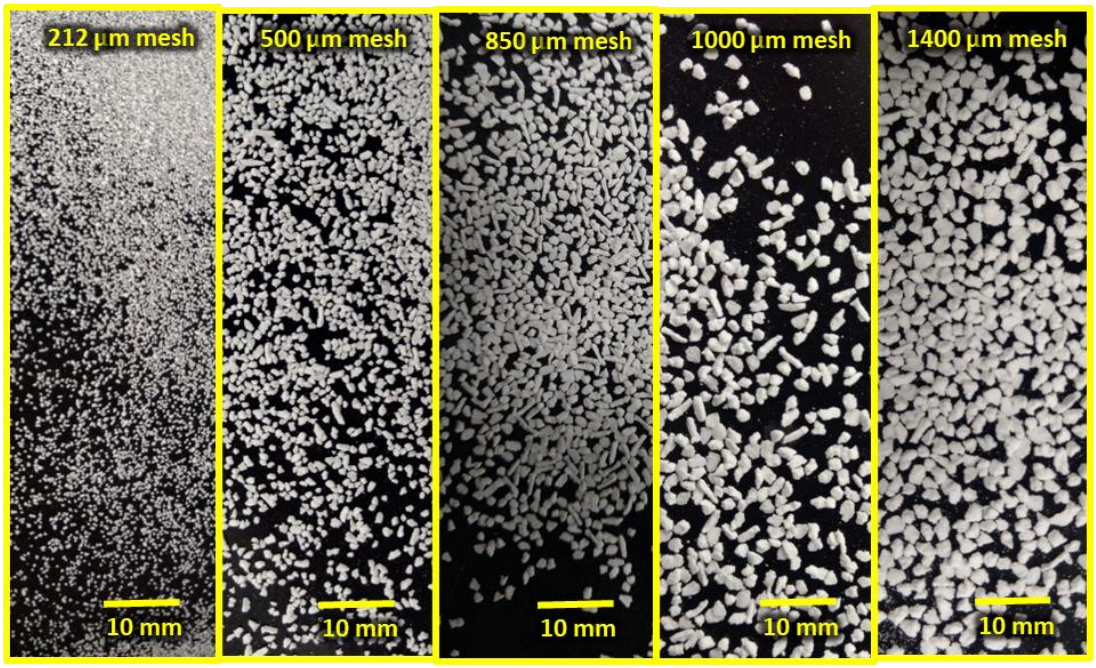

Figure 4.29 Samples of granules following granulation retained on 212-1400 µm sieve meshes (left to right) from experiment 15. No visual differences were observed between experiments.

The presence of fines indicated that granulation was incomplete under all conditions (A. El Hagrasy, Hennenkamp, et al. 2013) as a result of insufficient mechanical dispersion. Previous studies suggest that liquid distribution to non-wetted particles could have been enhanced by including an additional kneading block (Mu and Thompson 2012; Shirazian et al. 2018; Jurgen Vercruysse et al. 2015; Verstraeten et al. 2017), by increasing the stagger angle of the kneading elements, or by reversing the direction of the kneading element configuration (Dejan Djuric and Kleinebudde 2008; A. S. El Hagrasy and Litster 2013), although a smaller fraction of fine material may have still remained. As observed elsewhere, increasing LSR results in a decrease in fines (R. M. Dhenge et al. 2010; J. G. Osorio et al. 2017; Verstraeten et al. 2017), with complete granulation occurring at substantially higher LSR levels than those used in this study (A. El Hagrasy, Hennenkamp, et al. 2013; Verstraeten et al. 2017).

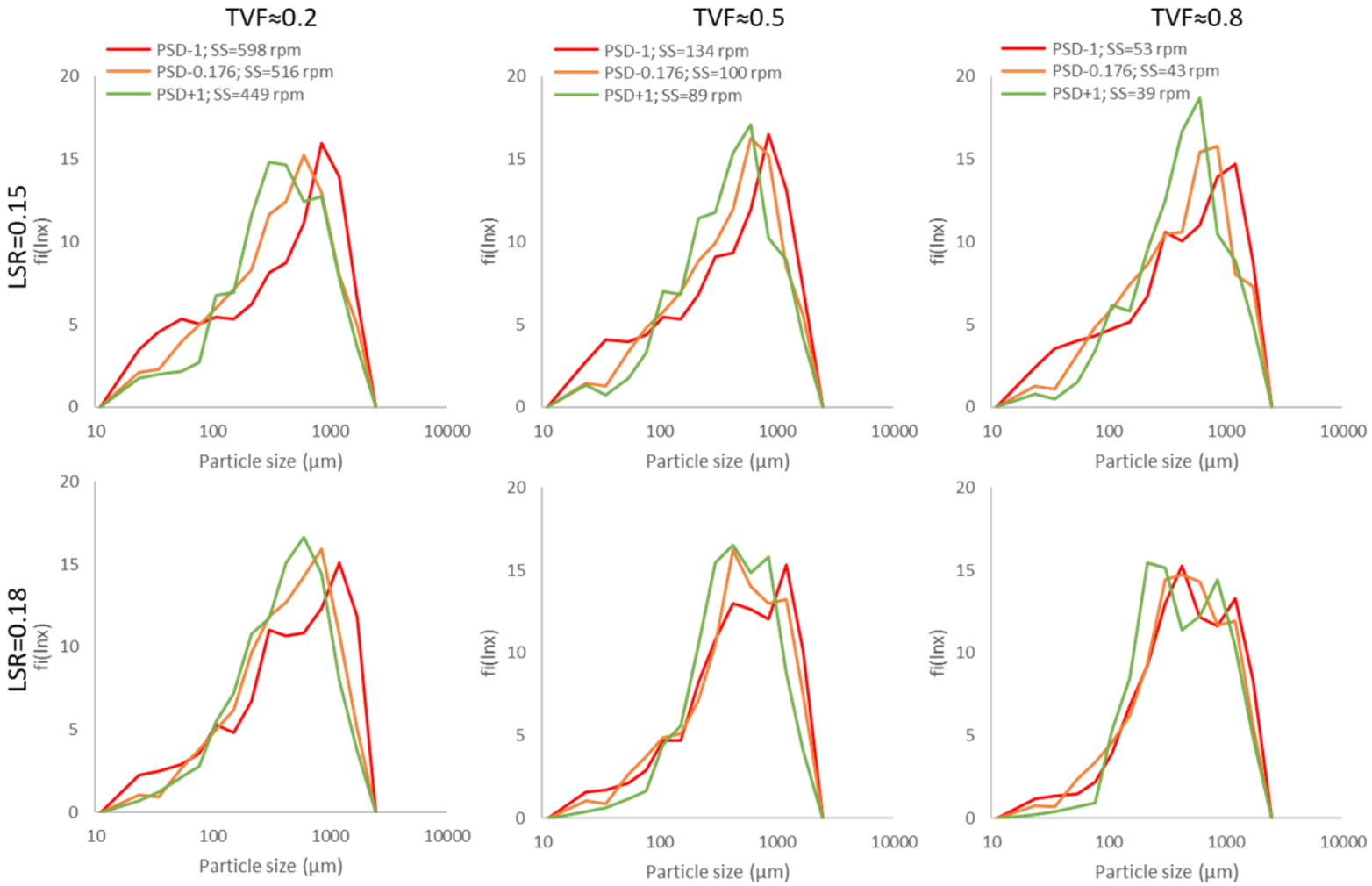

Figure 4.30 Size distribution measured by sieve analysis following granulation of PSD-1 (red), PSD-0.176 (amber) and PSD+1 (green), at LSR0.15 (top) and LSR0.18 (bottom), and TVF0.8 (left), TVF0.5 (middle) and TVF0.2 (right). MFR=0.8 kg.hr-1. Each curve is a mean average, n=3.

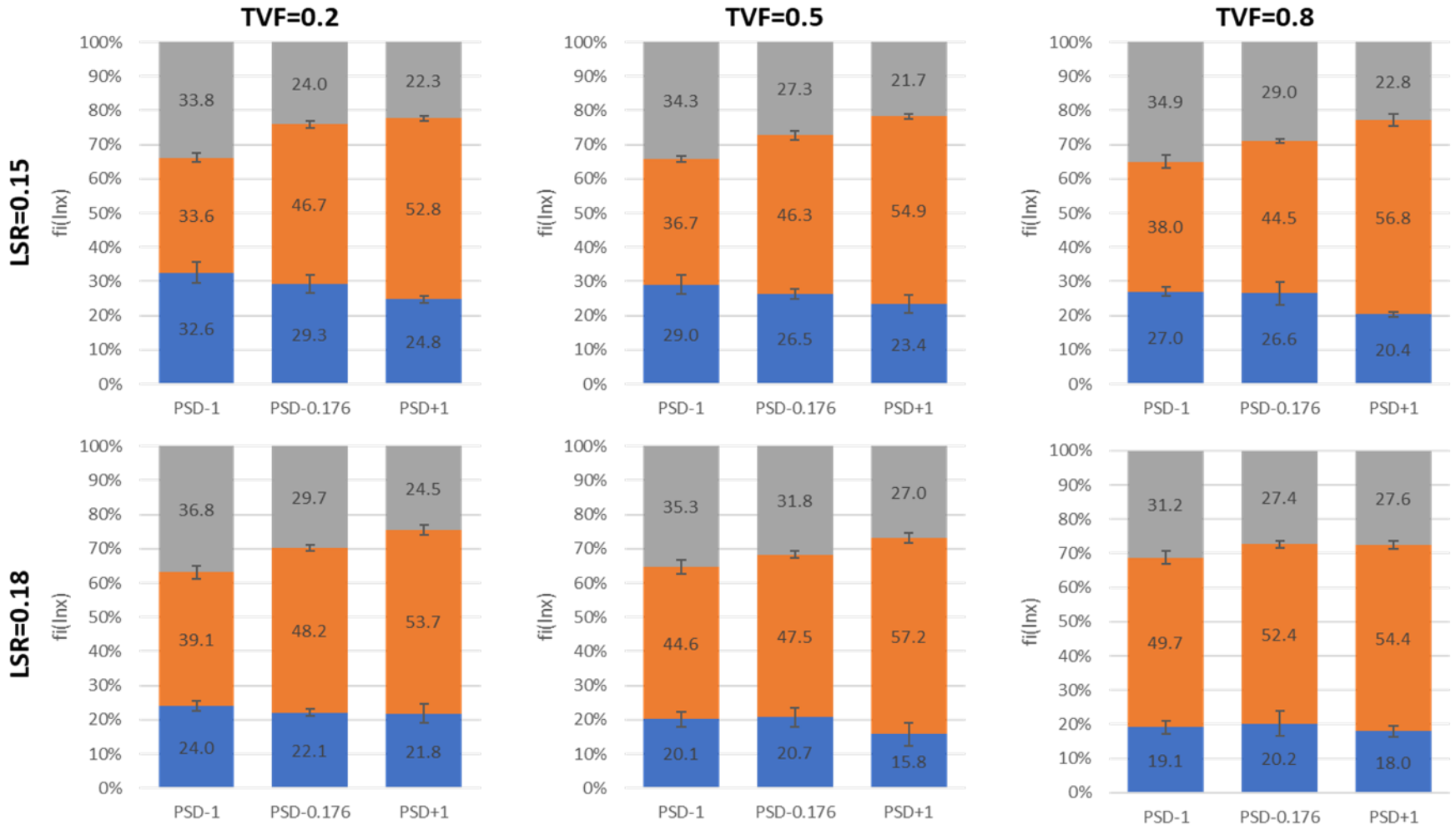

Figure 4.31 Material resulting from the granulation setup categorised into fines <212 µm (blue), small granules 212-850 µm (orange) and large granules >850 µm (grey). Mean ±sd, n=3.

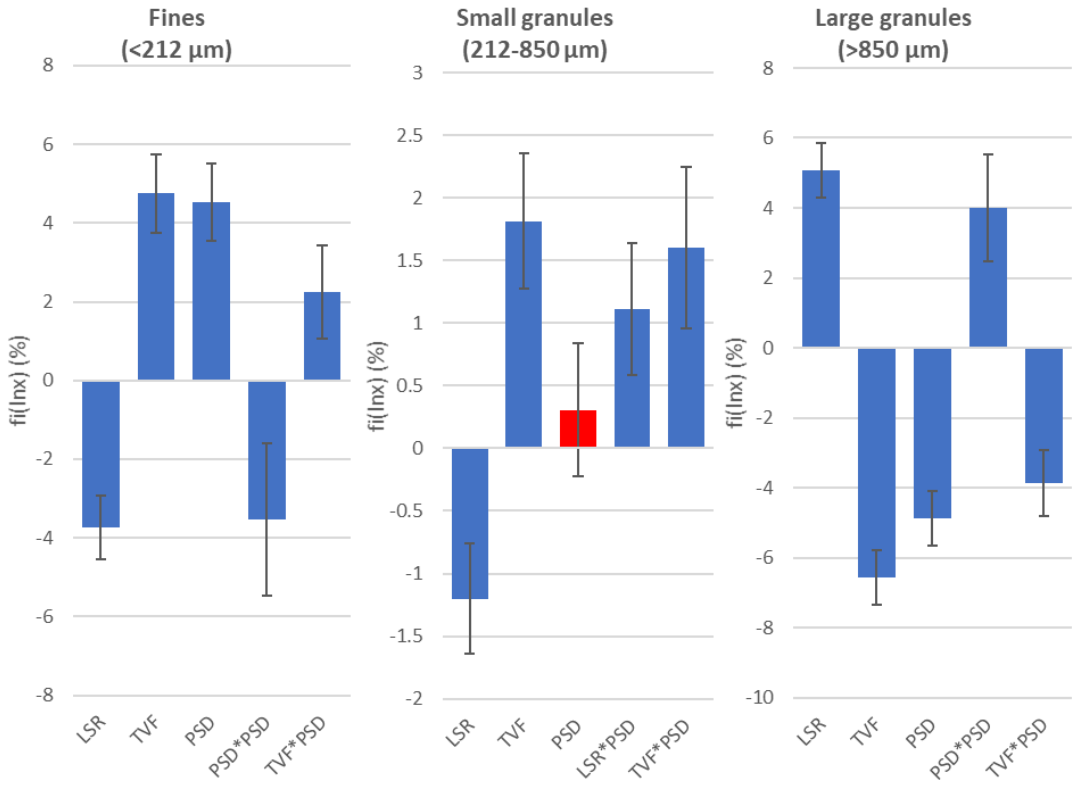

Figure 4.32 MLR model – magnitude of each significant term influencing the size distribution of material following granulation. Statistically insignificant terms (p>0.05) have mostly been excluded or coloured red.

It is well established in the literature that an increase in LSR results in an increased proportion of large granules, accompanied by a decrease in fines (A. El Hagrasy, Cruise, et al. 2013; Seem et al. 2015; Thompson 2015; Verstraeten et al. 2017). As shown in the MLR models, this too was the case in the current study (Figure 4.32). Naturally, the higher liquid concentration resulted in greater particle coverage and more liquid bridges forming. It also increased the deformability of granules facilitating successful coalescence following granule collisions.

At LSR=0.15, increasing the formulation PSD demonstrated a reduction in fines, however, this trend was not observed at LSR=0.18. This indicates that the influence of PSD on fines diminished with increased LSR - hence the significance of LSR*PSD (p<0.05). This is possibly due to elevated liquid concentration increasingly mitigating the difference in powder surface area as has been reported elsewhere (Knight et al. 1998; Schaefer, Holm, and Kristensen

1992; Schæfer 1996). However, as only two levels of LSR were tested within a limited range, then it is not possible to delineate this relationship beyond speculation.

During nucleation, PSD+1 facilitated liquid distribution and agglomeration. However, during granulation, the proportion of large granules was inversely proportional to PSD. The low surface area of PSD+1 limited the strength and number of interfacial capillary bridges between particles. Hence, large agglomerates did not possess sufficient tensile strength to withstand the compressive and shear forces inflicted by the rotating kneading elements (Vonk et al. 1997). Keningley et al. (1997) concluded that higher viscosities are required for larger primary particles to mitigate excessive breakage in HSM. Further, Lute et al. (2016) demonstrated that granule size reduction, as well as granule growth, can occur within the kneading block. Consequently, in the absence of a more viscous binder, large granules composed of PSD+1 underwent substantial breakage, and the proportion of small granules increased as the proportion of large granules decreased. However, a limitation of this study was that the extent of breakage during handling and sieving was not accounted for.

Conversely, PSD-1 produced the greatest proportion of large granules following granulation under all conditions. On account of a greater surface-to-mass ratio, and subsequent greater inter-particle contact, PSD-1 particles were more resistant to shear forces and more susceptible to cohesive capillary forces (Keningley, Knight, and Marson 1997). Therefore, granules composed of PSD-1 proved more robust and suffered less breakage, and instead, demonstrated greater overall granule growth following granulation.

These findings are consistent with HSM findings by van den Dries and Vromans (2002), whereby finer grades of lactose demonstrated steady growth, whereas granules composed of a coarse lactose grade underwent significant breakage. In another HSM study, Badawy

and Hussain (2004) showed that lactose particles within a 40-75 µm size fraction resulted in greater growth than those of a 212-250 µm sieve fraction. Likewise, Keleb et al. (2004) reported the proportion of large granules to increase with decreasing lactose grade during twin-screw extrusion granulation.

The greater growth capacity of PSD-1 resulted in a smaller proportion of small granules (34.3-49.8%) than PSD+1 (53.5-57.4%), therefore, in this respect PSD-1 reduced granulation efficiency. These fractions are similar to studies by Djuric & Kleinebudde (2008) and Vercruysse et al. (2012), in which similar screw configurations resulted in a yield fraction (125-1250 µm and 150-1400 µm, respectively) circa 50-55% from a 200M grade of lactose powder. A study by Kumar et al. (2014) yielded comparatively low proportions (<25%) of suitable granules (150-1000 µm) and high proportions (35-55%) of fines (<150 µm), however, significantly lower LSR values were used (0.045-0.07). Generally, this current study demonstrated that the broad GSD resulting from TSG produced a yield significantly lower than HSM (~80%) (K. T. Lee, Ingram, and Rowson 2013).

El Hagrasy et al. (2013; 2013) compared the granule properties resulting from three different grades of lactose. The GSD curves did vary between the grades and they demonstrated different sensitivities to high LSR levels, however, the median particle size (d_{50}) values were similar. Likewise, in the current study the effect of formulation PSD on median granule size was significant but small considering a three-fold difference in mean diameter (Figure 4.33). The combination of the liquid, mechanical and dimensional parameters permitted PSD-1 to granulate to 10-14 times the size of original primary particle, whereas PSD+1 was only able to granulate to 2-4 times on average. A further factor highlighted by Abberger et al. (2003) is that with large droplet sizes, agglomerate formation results from the immersion mechanism which minimised the effect of powder particle size, compared to the distribution

mechanism resulting from small droplets. The culmination of these considerations indicates that twin screw granulation represents a robust process in response to drastically variable raw material.

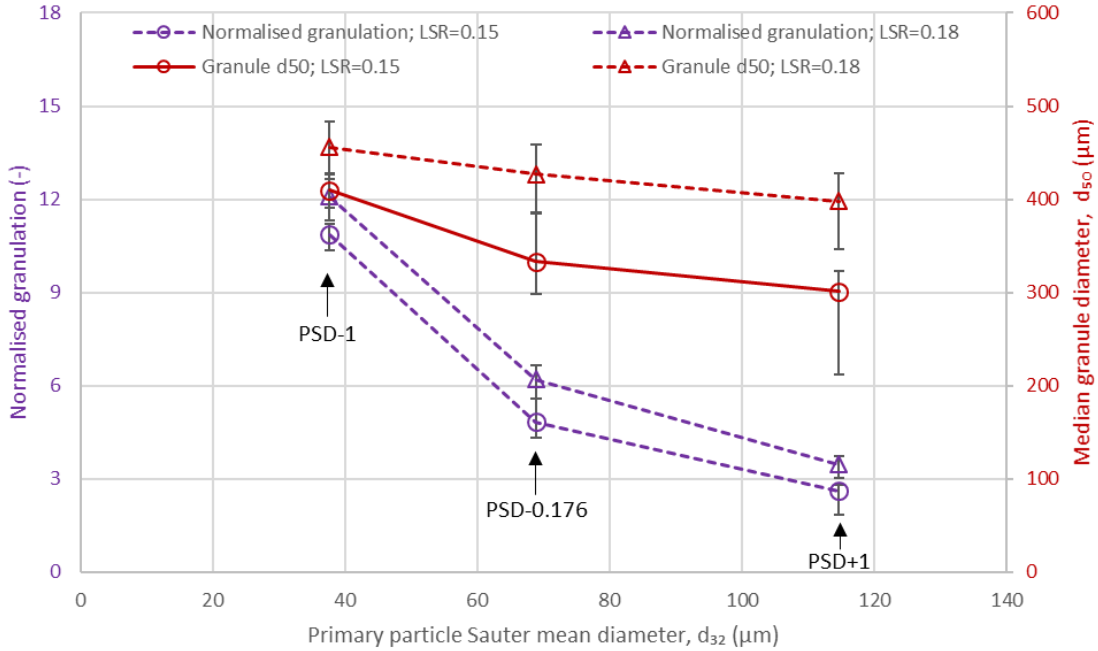

Figure 4.33 Normalised granulation (granule d_{50}/primary particle d_{50}) as a function of formulation PSD and LSR. The line represents values obtained at TVF=0.5 and the plus and minus error bars correspond to TVF=0.8 and TVF=0.2, respectively.

Increased TVF resulted in a small, yet significant, decrease in fines and large granules, and an increase in small granules. From this, it can be inferred that the binder liquid was more uniformly distributed at high TVF than at low TVF. By measuring moisture loss on drying of different sieve fractions, Chan Seem et al. (2016) reported similar findings. Visual examination of the barrel following an emergency stop showed that the kneading block and the channels of the conveying elements immediately upstream of the kneading block were nearing maximum fill under all conditions on account of its limited conveying capacity (Figure 4.4). This was confirmed experimentally by Lee et al. (2012). Hence, all material experienced the same conditions within the kneading block irrespective of TVF level, and any variation in GSD arising from changes in TVF was a result of differences in liquid distribution

during the wetting and nucleation portion of the barrel. Chan Seem et al. (2016) demonstrated size segregation occurring within the TSG at low fill level and hypothesised that large agglomerates, resulting from wetting at the site of liquid injection, may possess a separate flow stream from that of dry fines, and therefore, reduce their interaction and liquid redistribution. Hence, at high TVF segregation was minimised resulting in greater liquid distribution and a larger proportion of small granules. Additionally, at higher fill level the compaction and consolidation of agglomerates increased, and granules were restricted in size as a result of the reduced free volume and were abraded through greater shear and collisions with other granules (Chan Seem et al. 2016). Figure 4.29 further shows implications of the geometrical dimensions of the TSG; most granules are non-spherical and irregular with an aspect ratio approaching 1. However, material retained on the 850 and 1000 µm meshes show the presences of some elongated granules in contrast to the granule majority. These are likely the result of wetted material undergoing extrusion-like deformation through the kneading block but escaping or resisting the shear forces of the rotating kneading elements which normally result in granule cleavage into smaller granules. Similar granule morphology has been observed and reported elsewhere (Thompson and Sun 2010; Jurgen Vercruysse et al. 2012; R. Dhenge, Cartwright, J. Hounslow, et al. 2012; Verstraeten et al. 2017), with the inclusion of further kneading blocks or a chopper screw element reducing the presence of elongated granules (Verstraeten et al. 2017). Incorporating more kneading elements/blocks and higher levels of LSR have also been shown to increase granule smooth and sphericity as a result of greater deformability and particle layering (Thompson and Sun 2010; Verstraeten et al. 2017).

4.4.5. Granule porosity

The porosity of each sieve fraction was derived from the true and tapped density, in accordance with Equation 4.12, and are depicted in Figure 4.34 and Figure 4.36 The porosity measurements were stratified by sieve fraction in order to normalise inter-granular void volume and uncouple the influence of packing efficiency from the effects of LSR, PSD and TVF on intra-granular porosity. Stratification also mitigates the influence of the granule size distribution on granule packing, and hence, the tapped density. As seen from section 3, under consolidated conditions obtained from repeated tapping, a broader size distribution would yield a higher density due to smaller particles filling the voids between larger particles.

Expectedly, the porosity of the non-wetted material (<212 µm) was similar to the porosity of the initial blend (ca. 50-63 %). Following nucleation and granulation, porosity generally decreased with increased nuclei/granule size. This was because packing efficiency increased as particles became more free-flowing with particle enlargement and intra-agglomerate pores were compressed due to shear and compressive forces applied in the kneading block. Although these results were comparable to those reported by Dai et al. (2008) following HSM, they were in direct contradiction to Verstraeten et al. (2017), whereby porosity increased with granule size following TSG. This is possibly due to the bulk density being used to calculate porosity using Equation 4.12, as opposed to the tapped density as is the case in this study. This would have resulted in the granule porosity being overestimated further due to the inter-granular voids, particularly for larger granules. Alternative methods employed for measuring granule porosity include X-ray computed tomography (Davis et al. 2017) and X-ray microtomography ((R. M. Dhenge et al. 2013), however, these are resource intensive, and do not lend themselves to measuring a sufficient number of granules to a provide a representative sample of the output material. El Hagrasy et al. (2013) used Geopyc to

measure granule porosity which utilises a similar principle to that used in section 2 for measuring the nuclei envelope volume thereby mitigating inter-granular voids, however, its accuracy is limited to larger granules.

The effects of primary particle size on the porosity of granules resulting from TSG have previously been studied (A. El Hagrasy, Hennenkamp, et al. 2013; Lute, Dhenge, and Salman 2018b), however, in those studies the different grades possessed considerably different particle morphology as a result of their production processes – i.e. spray drying, granulated. Thus, delineating the effect of primary particle size on porosity from the effect of primary particle structure was not possible. In this study, the main components of all the grades were crystalline α-lactose monohydrate and partially crystalline MCC fibrils, and therefore, possessed the same intrinsic properties.

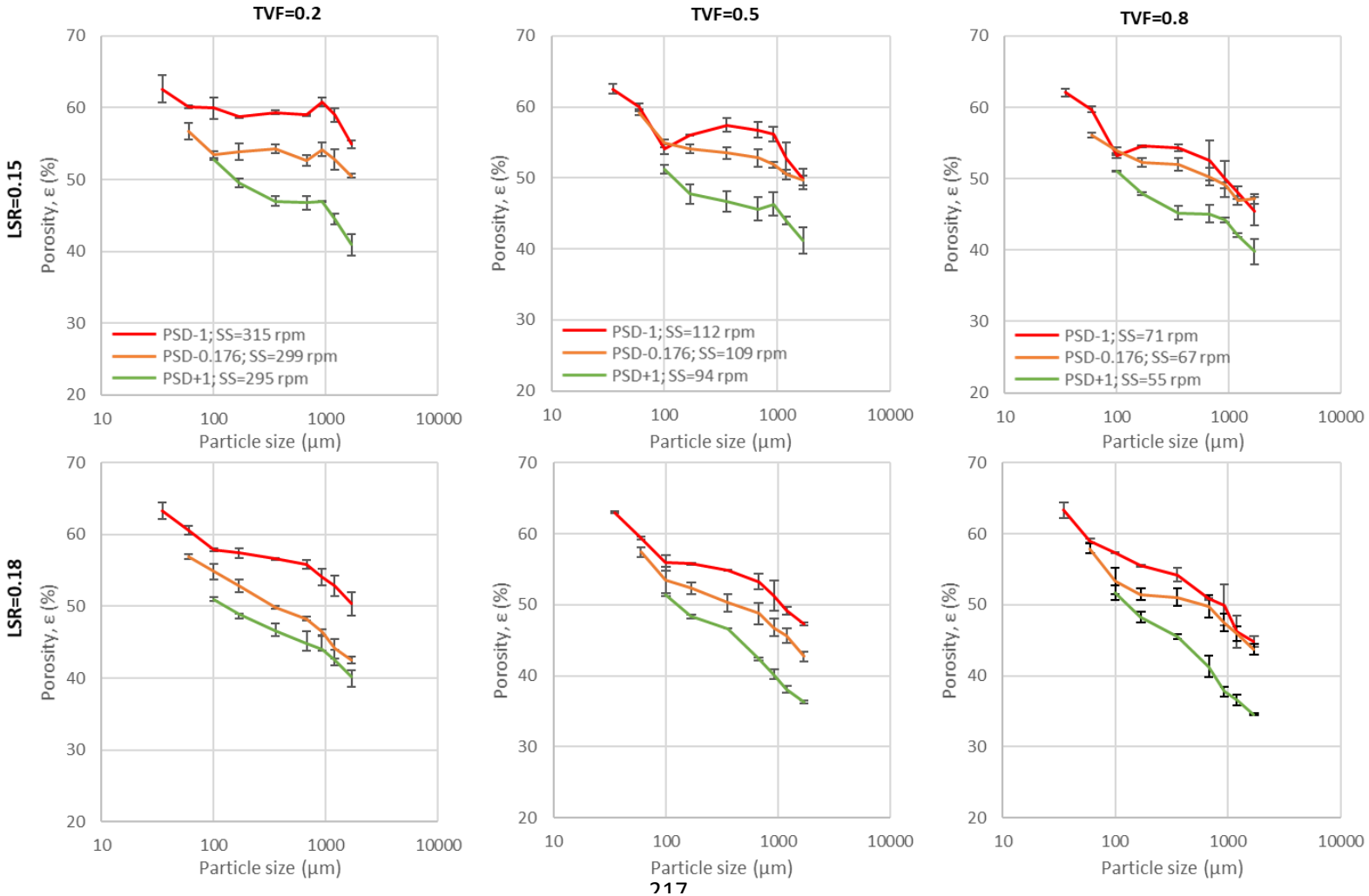

Figure 4.34 Porosity as a function of particle size following *nucleation*. MFR=0.8 kg.hr^{-1}. Mean ±range, n=3.

Following *nucleation*, blend PSD was the most determinative factor for agglomerate porosity (Figure 4.35). Agglomerates resulting from PSD-1 possessed the greatest porosity, as the primary particles were least efficient at consolidating during nucleation. Nuclei composed of PSD+1 had the lowest porosity, as a result of greater densification. This relationship is common to HSM observations (S. M. Iveson and Litster 1998b; M. B. Mackaplow, Rosen, and Michaels 2000). A lower surface area enabled greater particle mobility and allowed PSD+1 particles to come into closer contact on account of fewer electrostatic and frictional forces (S. M. Iveson and Litster 1998b). In contrast, Fonteyne et al. (2014) reported that finer grades of lactose resulted in granulated material of a higher density than coarse lactose grades. However, in that study the density was measured from the entire GSD, rather than individual sieve fractions as is the case in this study. Therefore, the density was more reflective of particle packing of a broad multimodal size distribution than the particle packing within individual granules. Under most nucleation conditions, the porosity of the nucleated PSD-0.176 was more comparable to PSD-1 and significantly dissimilar to that of PSD+1. Hence, this non-linear relationship between PSD and porosity manifested as the significance of the PSD*PSD term in the porosity MLR model (Figure 4.35).

Increased TVF facilitated consolidation and caused nuclei porosity to generally decrease (R. M. Dhenge et al. 2011; Dejan Djuric and Kleinebudde 2010). This was likely due to the increasingly constrained conditions and increased particle collisions (Keleb et al. 2004a). This response was dependent on PSD blend (TVF*PSD, $p<0.05$) as PSD-1 was most sensitive to changes in TVF, accounting for approximately 10% decrease in porosity of the agglomerated material. Conversely, varying TVF during nucleation of the PSD+1 blend yielded a negligible change in nuclei porosity.

Additionally, increasing LSR reduced porosity as the liquid layer increased the mobility of particles and enhanced plasticity and malleability of agglomerates to further facilitate densification, as previously reported (A. El Hagrasy, Hennenkamp, et al. 2013; Jiayu Li, Pradhan, and Wassgren 2019; Lute, Dhenge, and Salman 2018b; Matsui et al. 2019; J. G. Osorio et al. 2017; Pradhan et al. 2017; Sayin et al. 2015; Verstraeten et al. 2017; Jonathan B. Wade, Martin, and Long 2015). Interestingly, increasing LSR reduced PSD-1's sensitivity to TVF from approximately 10% to ~4%, whereas, PSD+1's response to TVF increased from having a negligible effect to ~6%. Lute et al. (2018b) too, found the effect of particle properties on porosity to diminish with increased LSR.

The PSD-1 nuclei produced at TVF-1 were noteworthy, as the porosity of much of the agglomerated material did not substantially decrease below that of the original powder blend. One possible explanation for this observation, is that even though the inter-agglomerate voids decreased as a result of more efficient packing, the intra-agglomerate pores may not have markedly decreased below that of the powder bed due to the presence of cohesive particle structures during nucleation.

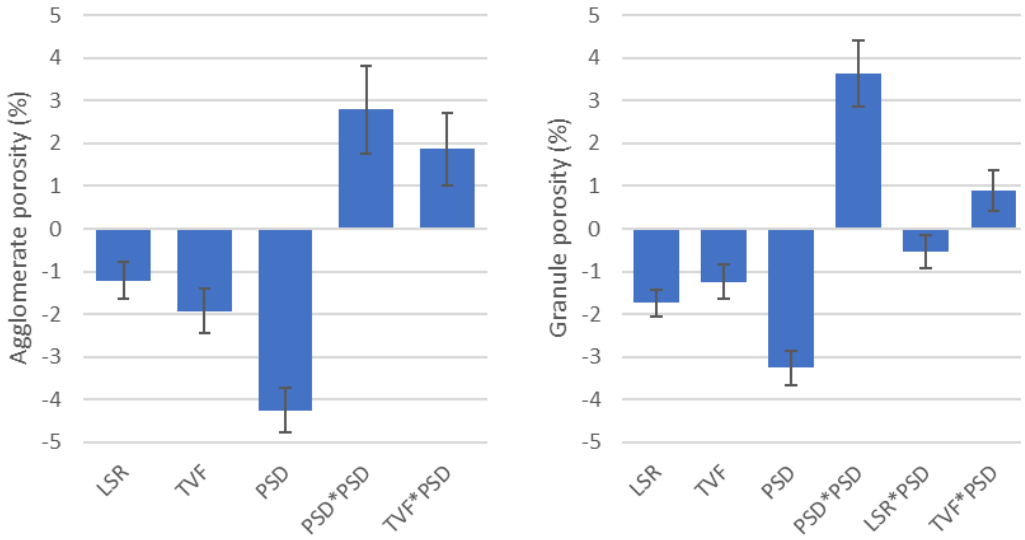

Figure 4.35 MLR coefficients depicting the effect of each factor on the porosity of nuclei following *nucleation* (left) and granules following *granulation* (right).

Following *granulation*, the average porosity of worked material decreased from 68% to 47% as a result of greater consolidation (Figure 4.36). Similar to nucleation, increased LSR, TVF and PSD resulted in denser granules on account of the increased deformability (S. M. Iveson and Litster 1998b), consolidation, and shear (Dejan Djuric and Kleinebudde 2010). The influence of PSD and TVF decreased as the shear forces became the primary driver for densification. Additionally, the influence of PSD further diminished at high TVF, as did the influence of LSR.

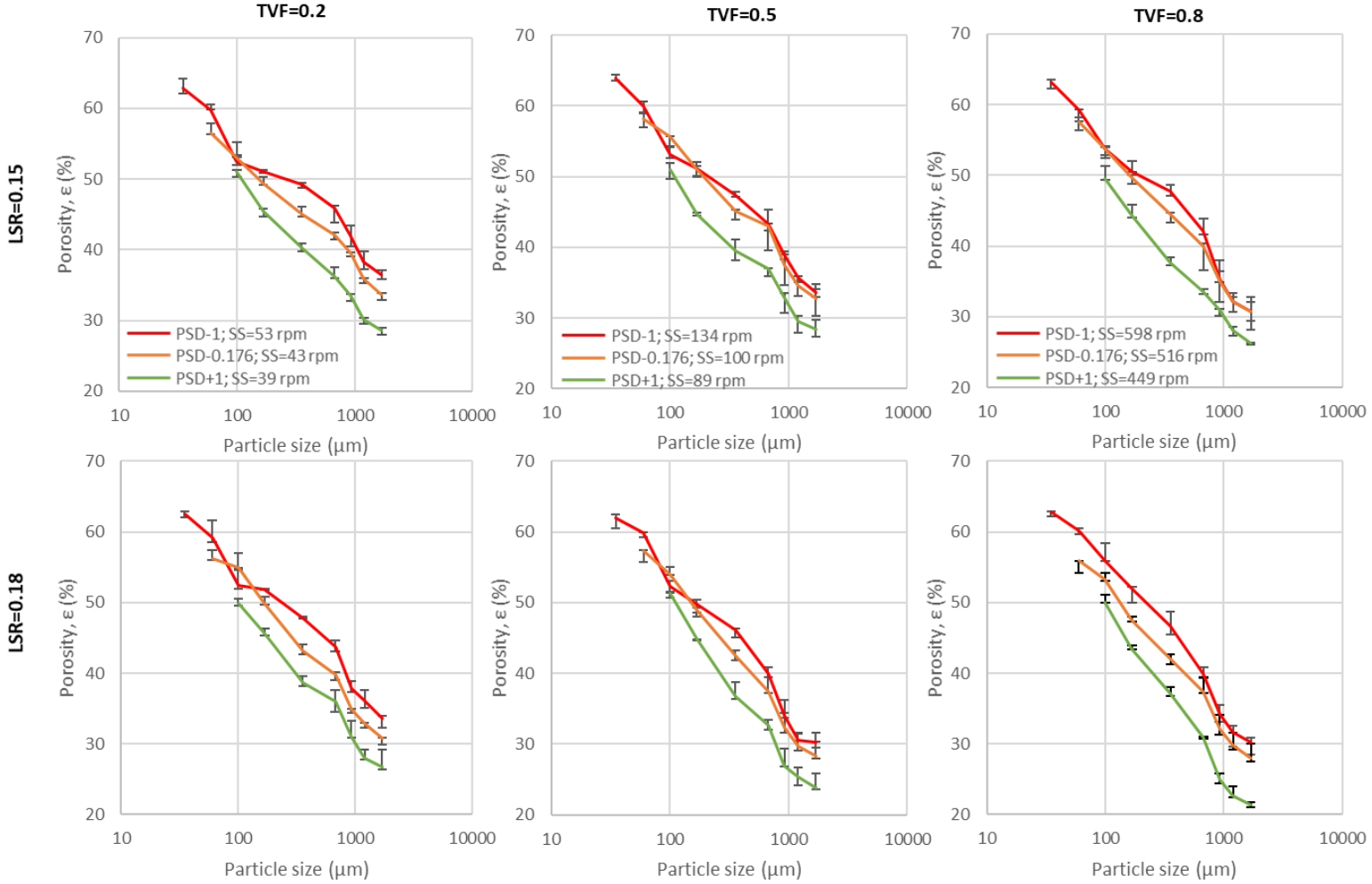

Figure 4.36 Porosity as a function of particle size following *granulation*. MFR=0.8 kg.hr^{-1}. Mean ±range, n=3.

4.4.6. Theophylline, THP, distribution

To evaluate the distribution of theophylline anhydrate, THP, the concentration in each granule size fraction was measured via UV-vis absorbance. THP was chosen as it is hydrophilic and has similar wettability to LAC (Kiesvaara, Yliruusi, and Ahomäki 1993; Kiesvaara and Yliruusi 1993). Hence, inhomogeneity can be attributed to segregation via physical properties as opposed to physicochemical properties.

To assess the overall granule inhomogeneity of each experimental condition, the demixing potential (DP%) was calculated using Equation 4.16 (Thiel and Nguyen 1982). The DP% specifies the coefficient of variation of THP in the different size fractions as a quantification of the latent ability to segregate.

$$DP\% = \frac{100}{\bar{p}} \cdot \sqrt{\sum \frac{w}{100}(p - \bar{p})^2} \qquad \text{Equation 4.16}$$

Where p is the proportion of THP in size fraction of weight w, and $\bar{p}$ is the mean average proportion of THP in all the size fraction i.e. 5% w/w. A higher DP% value indicates a less homogenous THP distribution.

Granule uniformity has been the subject of many studies, with the vast majority pertaining to HSM. From these, two mechanisms of segregation have become prevalent; Van den Dries and Vromans (K. van den Dries and Vromans 2002) postulated that granule breakage continually exposes new surfaces for coalescence to incorporate new particles. This dynamic exchange of primary particles results in a more homogenous distribution. However, when granule strength exceeds the shear forces, granules will not break, and the dynamic exchange is minimal. Instead, strong granules grow predominantly via layering, whereby densification causes liquid from voids to be squeezed to the surface for fresh particles to attach. It has

been suggested that smaller particles have a higher affinity for layering than larger particles, and hence, this preferential layering can cause granule inhomogeneity to arise from blends with a broad and multimodal size distribution.

Figure 4.37 shows the concentration of THP in each sieve fraction following *nucleation*. Segregation did occur as a function of particle size as significant discrepancies between the blend concentration of THP and granule concentration were evident. As established in the literature, small particles are more likely to nucleate into larger agglomerates than coarse particles. Due to their smaller mass, fine particles require lower saturation levels to successfully adhere than coarser particles. This is particularly important at the outer surface of agglomerates where liquid saturation is low. Further, it has also been postulated that finer particles can better access the binder liquid within surface pores, whereas asperities geometrically restrict larger primary particles (Kaspar van den Dries and Vromans 2003). Therefore, smaller particles are disproportionately represented in larger agglomerates. By considering the THP size disparity in each of the blends (Figure 4.38) it becomes apparent why the large agglomerates resulting from nucleation of PSD+1 were super-potent (>50 mg/g) and the non-wetted material was sub-potent (<50 mg/g) – the smaller THP particles preferentially nucleated than the larger excipient particles. Conversely, the finer particles of PSD-1 preferentially nucleated over THP particles to result in sub-potent agglomerates. PSD-0.176 resulted in the least inhomogeneity, as indicated by the significance of the PSD*PSD term (p<0.05). This was because PSD-0.176 had the least particle size disparity with THP. However, PSD-0.176 still resulted in non-uniform THP distribution, attributable to its broader PSD than THP's narrow 75-125 µm sieve fraction. Thus, the presence of finer excipient primary particles skewed THP particles towards non-wetted material.

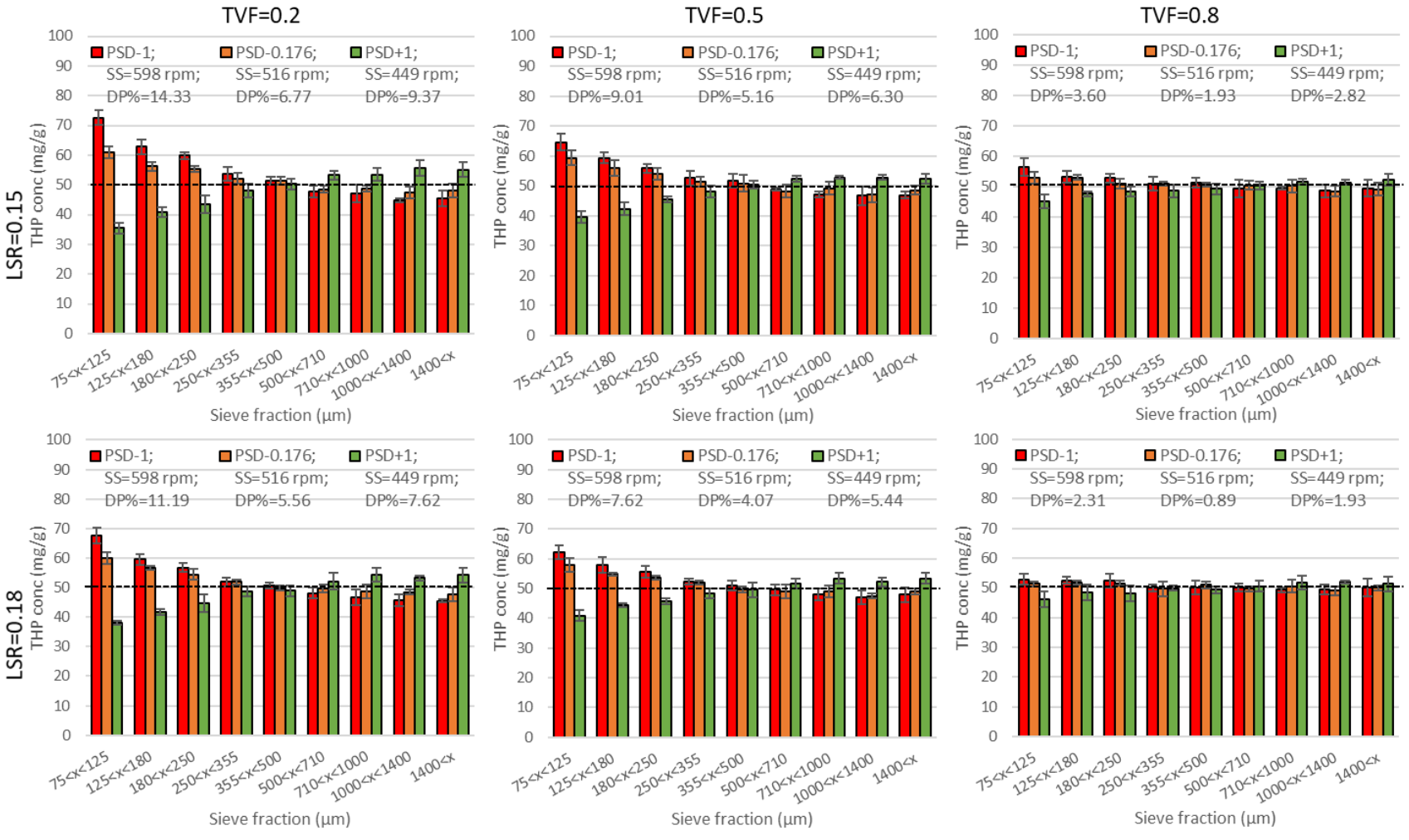

Figure 4.37 THP concentration as a function of granule size following nucleation. The horizontal dashed line at 50 mg/g represents the nominal THP concentration.

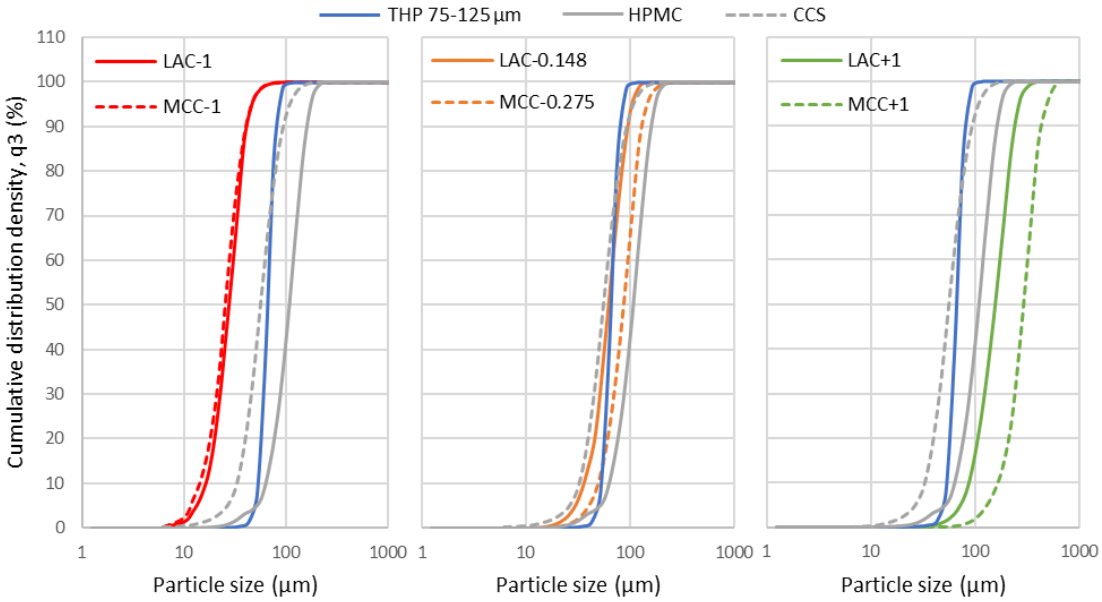

Figure 4.38 Particle size distribution of each ingredient in each blend measured via QICPIC; PSD-1 (left), PSD-0.176 (centre) and PSD+1 (right).

From Figure 4.39 it can be seen that the DP% during *nucleation* was generally low (≤14.33%) due to the limited shear and time for segregation to occur. The immersion mechanism, by which the powder was wetted, resulted in regions of high liquid saturation which nucleated under limited shear forces within a matter of seconds. The high concentration of binder liquid was enough to bind larger particles and mitigated much of the preferential agglomeration of smaller particles. Work by Pradhan et al. (Pradhan et al. 2017), showed very little breakage occurs within the channels of conveying elements in TSG. Therefore, the little segregation that did occur during nucleation could not be offset by the dynamic particle exchange that occurs during breakage and coalescence.

From the MLR model (Figure 4.40), both the LSR and TVF were significant factors and inversely correlated to DP%. As it is believed that preferential particle adhesion is the product of contact surfaces with low liquid concentration binding smaller particles but incapable of binding larger particles, it stands to reason that increased LSR improved content uniformity. Further, increasing TVF further reduced granule inhomogeneity as the powder

matrix within the channels was more restricted in concentric movement and hence, the flux of smaller particles contacting the outer region of the wetted area was reduced, limiting the potential for preferential layering.

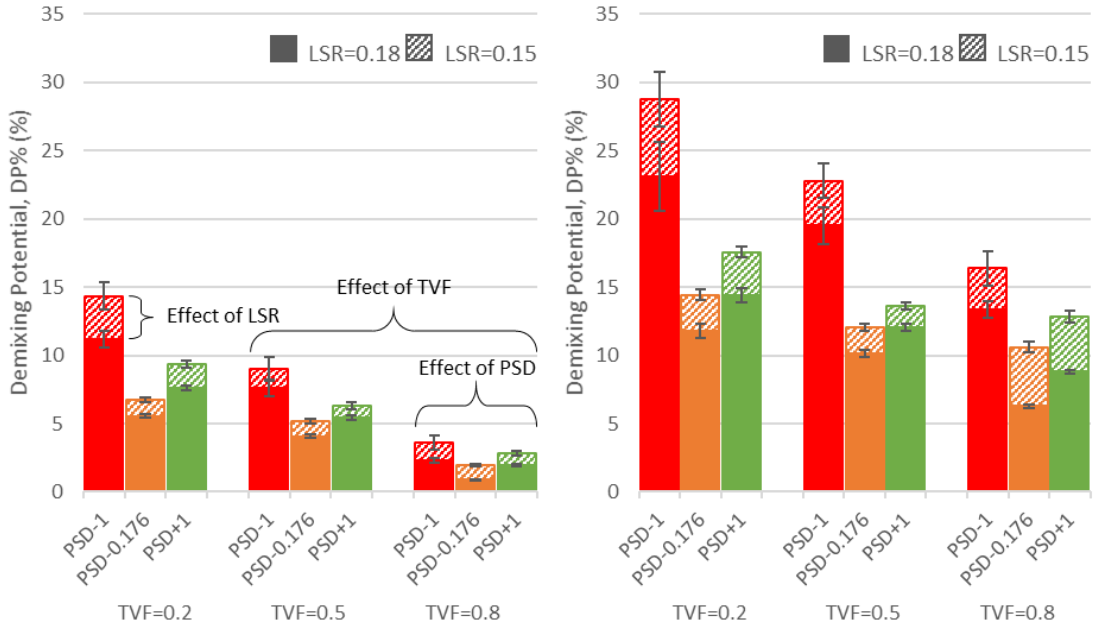

Figure 4.39 Comparison of the effects of LSR, TVF and PSD on the demixing potential of THP during *nucleation* (left) and *granulation* (right). MFR=0.18 kg·hr^{-1}. Mean ±sd, n=3.

Following *granulation*, the DP% significantly increased up to 28.73% (Figure 4.39) despite the mixing and distributive capability of the kneading block. The THP concentration in each sieve fraction is shown in Figure 4.41, with greater divergence from the nominal concentration than *nucleation*. The significant terms in the MLR model for DP% are the same as those resulting from *nucleation*, albeit, the magnitude of each term is greater (Figure 4.40). Additionally, the relationship between PSD and THP concentration is similar, in that PSD+1 resulted in large granules that were super-potent, and PSD-1 and PSD-0.176 resulted in sub-potent large granules, although PSD-0.176 resulted in the lowest values of DP% (6.26-14.43%). This is because the combination of the kneading block's shear forces and retentive flow capacity, promoted liquid distribution resulting in greater areas of low liquid saturation.

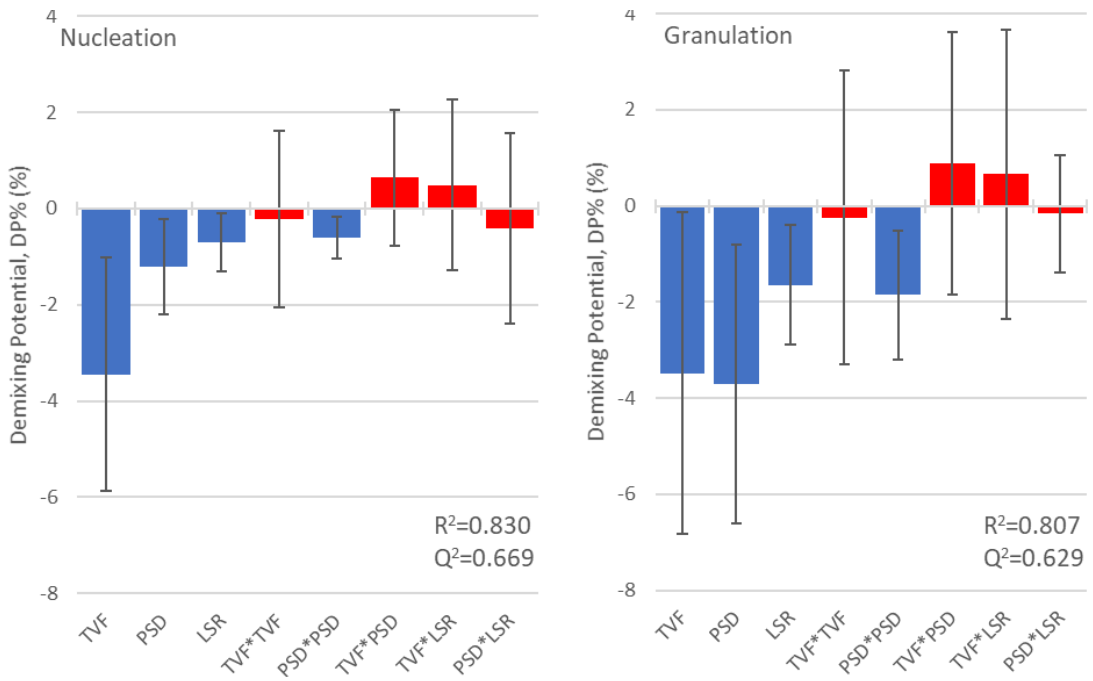

Figure 4.40 MLR model coefficients for the demixing potential for *nucleation* (left) and *granulation* (right). The statistically insignificant coefficients (p>0.05) are coloured red.

As discussed, areas of low liquid saturation disproportionately bind finer particles rather than coarse particles, due to lower capillary force requirements. As a result, preferential layering occurred to a greater extent during *granulation* than *nucleation*; the fine excipient particles of PSD-1 and PSD-0.176 preferentially granulated into large granules, whereas THP particles were disproportionately represented in large granules when included in the PSD+1 blend.

Although the PSD-1 and PSD+1 excipient blends had similar size disparity ratios with THP particles (PSD-1/THP=0.38 and THP/PSD+1=0.36, respectively), PSD-1 resulted in greater values of DP%. This was likely to be because as the size of the primary particles becomes larger, then the effect of preferential layering diminishes as overall adherence becomes less favourable. Additionally, the granules composed of PSD+1 were weaker and underwent significant breakage (Kaspar van den Dries and Vromans 2003), resulting in the aforementioned dynamic particle exchange as surfaces of higher liquid saturation were exposed, further improving granule uniformity.

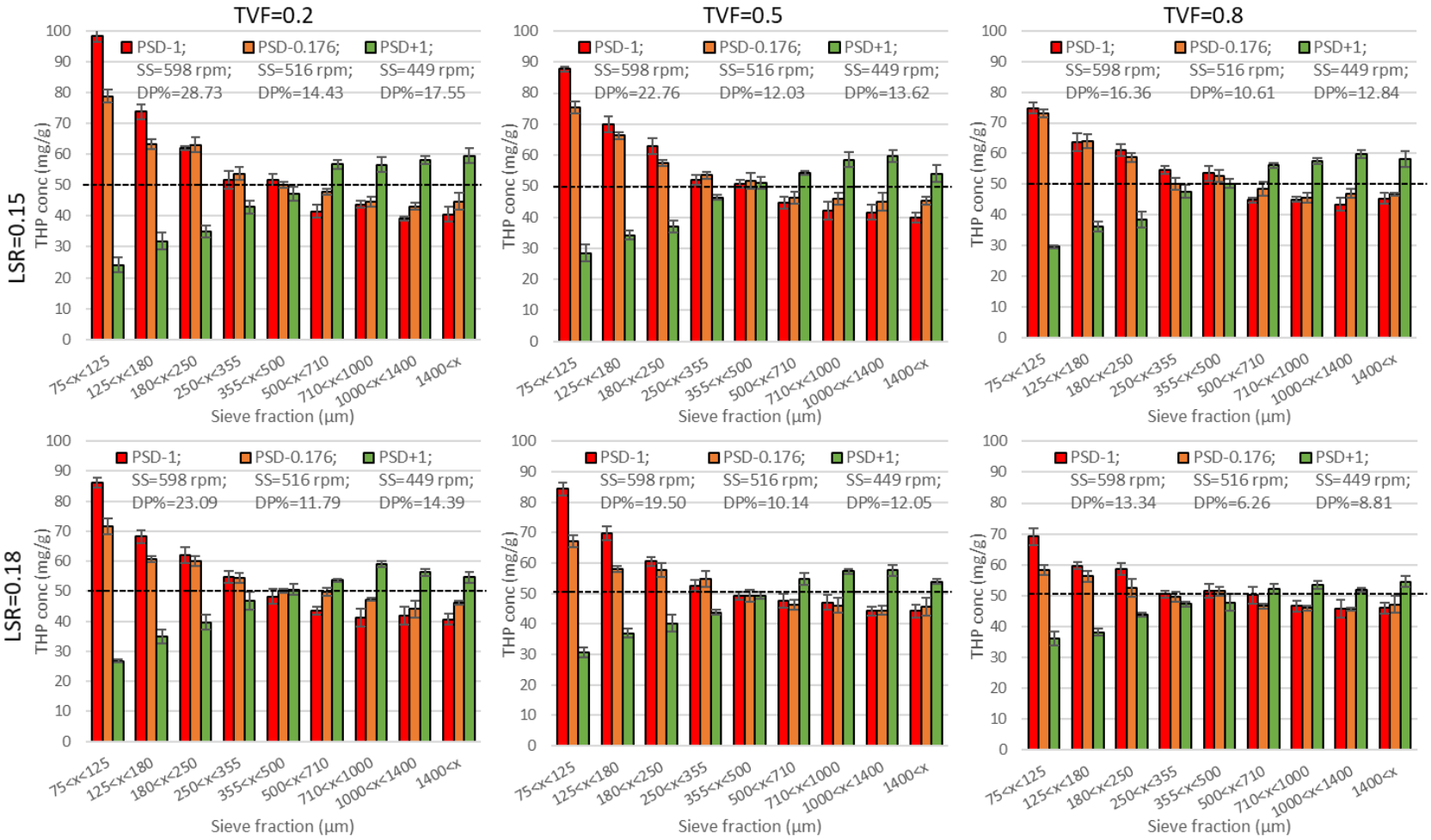

Figure 4.41 THP concentration as a function of granule size following *granulation*. The horizontal dashed line at 50 mg/g represents the nominal THP concentration. MFR=0.8 kg·hr^{-1}. Mean ±sd, *n*=3.

This relationship between PSD and API homogeneity conflicts with observations by Fonteyne et al. (Fonteyne, Wickström, et al. 2014), whereby paracetamol was found in higher concentration in larger granules irrespective of whether the coinciding lactose grade consisted of smaller or larger particles. This is possibly due to paracetamol possessing greater wetting properties than lactose monohydrate (Heng and Williams, 2006; Heng et al. 2006).

It is worth noting that, as Figure 4.38 suggests, THP is not the only ingredient to possess a size disparity within the blend. Therefore, it is plausible that granule inhomogeneity not only pertains to the API but other excipients, but unfortunately, this was not within the scope of this current investigation. Although non-uniform excipient distribution is likely to effect

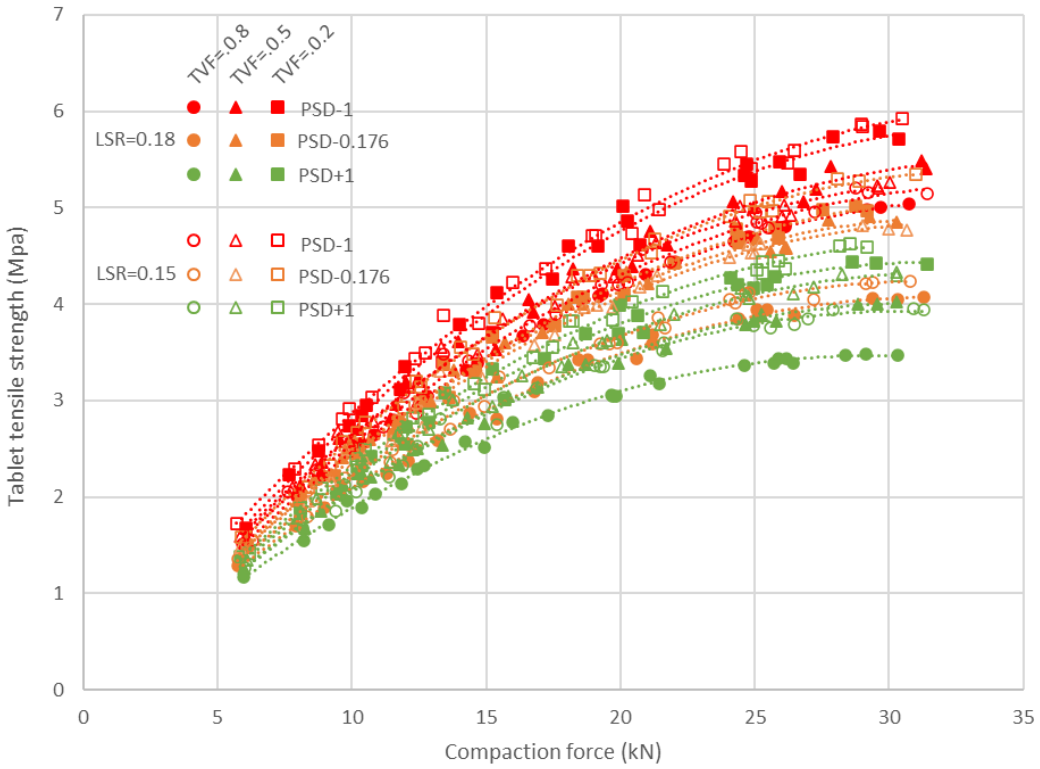

Figure 4.42 Tabletability profiles comparing the effects of formulation PSD, TVF, and LSR on tablet tensile strength. Refer to Figure 3.43 for direct comparison following 25±0.5 kN compaction.

granule properties, few studies have been performed to determine the possible influence on the final dosage form, and therefore, if excipient inhomogeneity could be considered a CQA.

4.4.7. Tablet tensile strength

Following *granulation*, the granules within the 210-850 µm sieve fractions were lubricated with MgSt and compacted to produce 200±5 mg tablets. Fines and large granules were excluded from tableting as their respective cohesive and bulky physical properties impeded homogenous packing and die fill uniformity (Ewsuk 2001; Zakhvatayeva et al. 2018). Additionally, sieving the GSD normalised the influence of MgSt, as fines are less sensitive to lubrication than large granules on account of a larger surface area (Almaya and Aburub 2008; Bos, Vromans, and Lerk 1991). MgSt's physicochemical properties are known to disrupt interparticle bonding (Cabiscol et al. 2018), facilitate elastic recovery (Zuurman, Van der Voort Maarschalk, and Bolhuis 1999) and impede wetting (M. E. Johansson and Nicklasson

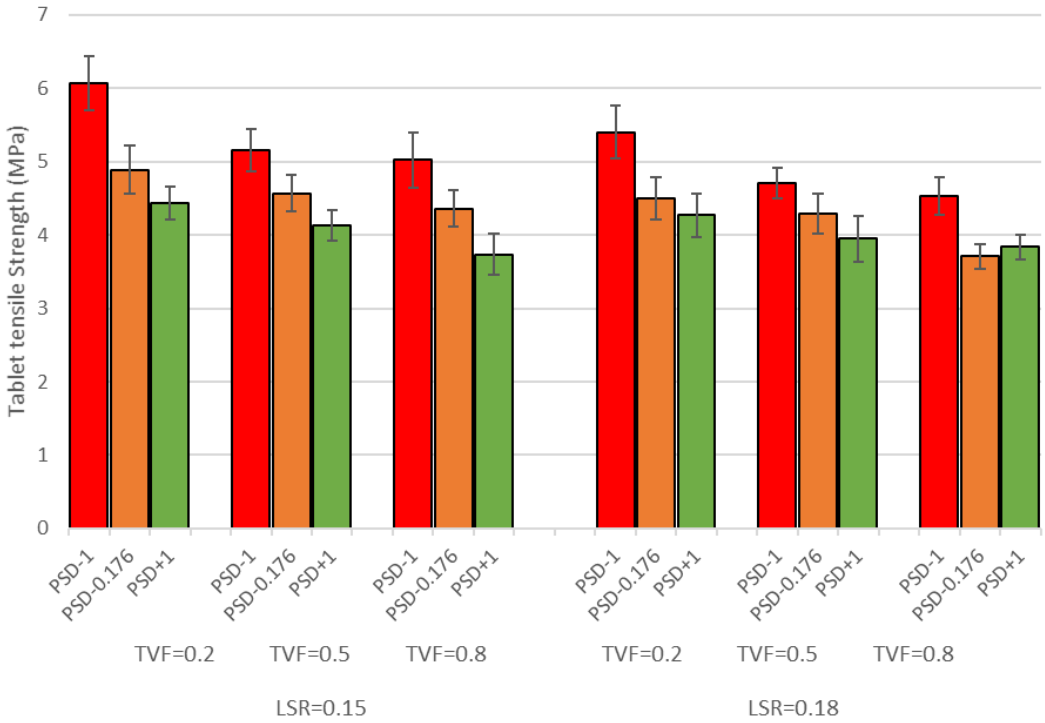

Figure 4.43 Tensile strength of 200±5 mg tablets following 25±0.5 kN compaction produced from each TSG condition and formulation. Mean ±sd, n=10.

1986; Keleb et al. 2004b), resulting in weaker and less soluble tablets (Vromans et al. 1987; Jennifer Wang, Wen, and Desai 2010). Further, normalising the GSD between the experiments was important as granule size has been shown to directly influence tablet performance (Sherif I.F. Badawy et al. 2012; Šantl et al. 2012).

The tabletability plot in Figure 4.42 depicts tablet tensile strength as a function of increasing compaction force. To compare the effects of granulation conditions on granule compaction, the tensile strength was derived from the dimensions and hardness of 10 tablets produced at 25±0.5 kN. The range of tensile strengths achieved within the design space was between 3.52 and 6.17 MPa (Figure 4.43). Although pharmacopeial standards for *Tablet Breaking Force* set no limits for tensile strength (The United States Pharmacopeial Convention 2011a), tablets should be sufficiently strong to maintain their dosage integrity during packaging, transport and handling, for which friability testing is a more representative assessment. It has been shown that tablet friability and tensile strength are closely correlated (Osei-Yeboah and Sun 2015) and tablets with a tensile strength greater than 2 MPa exhibit friability weight loss of less than 1% (Paul and Sun 2017). Hence, the physical robustness of all the tablets

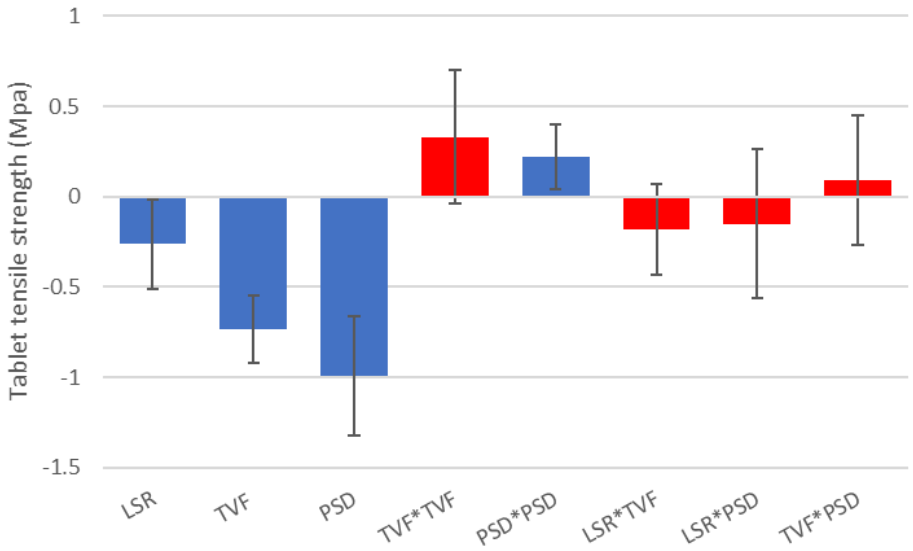

Figure 4.44 MLR coefficients for tablet tensile strength. Insignificant terms are coloured red.

produced was considered acceptable. Based on this, an operating range of 15 to 20 kN compaction force within a design space would yield sufficiently strong tablets whilst minimising energy wastage and wear & tear to the tablet press.

From the MLR (Figure 4.44), it is evident that primary particle size has the greatest influence on tablet strength, followed by TVF and LSR. Tablet tensile strength was inversely influenced by PSD, TVF and LSR, and directly correlated with granule porosity (R^2=0.848), as shown in Figure 4.45. It is widely reported that more porous granules improve compactability, whilst stronger granules compromise tablet tensile strength (Arndt et al. 2018; S. Badawy and Hussain 2004; Sherif I. Farag Badawy et al. 2000; Horisawa, Danjo, and Sunada 2000; H. Liu et al. 2017b; T. H. Nguyen, Morton, and Hapgood 2015; Nordström and Alderborn 2015; Wikberg and Alderborn 1991). As discussed in section 4.4.5, granule densification increased with LSR, due to greater granule deformability and lubricated particle mobility during HSM (Sherif I.F. Badawy et al. 2012; Matsui et al. 2019; T. H. Nguyen, Morton, and Hapgood 2015; Salman et al. 2007) and TSG (Robin Meier et al. 2017a; R. Meier et al. 2015). Contrary to this, however, Liu et al. (H. Liu et al. 2017b) found increasing LSR during TSG to result in stronger tablets. The authors suggested that the existence of high liquid bridges produced more porous granules but this conflicts with the findings of this current study and others (A. El Hagrasy, Hennenkamp, et al. 2013; Jiayu Li, Pradhan, and Wassgren 2019; Lute, Dhenge, and Salman 2018a; Matsui et al. 2019; J. G. Osorio et al. 2017; Pradhan et al. 2017; Sayin et al. 2015; Verstraeten et al. 2017; J. B. Wade, Martin, and Long 2015).

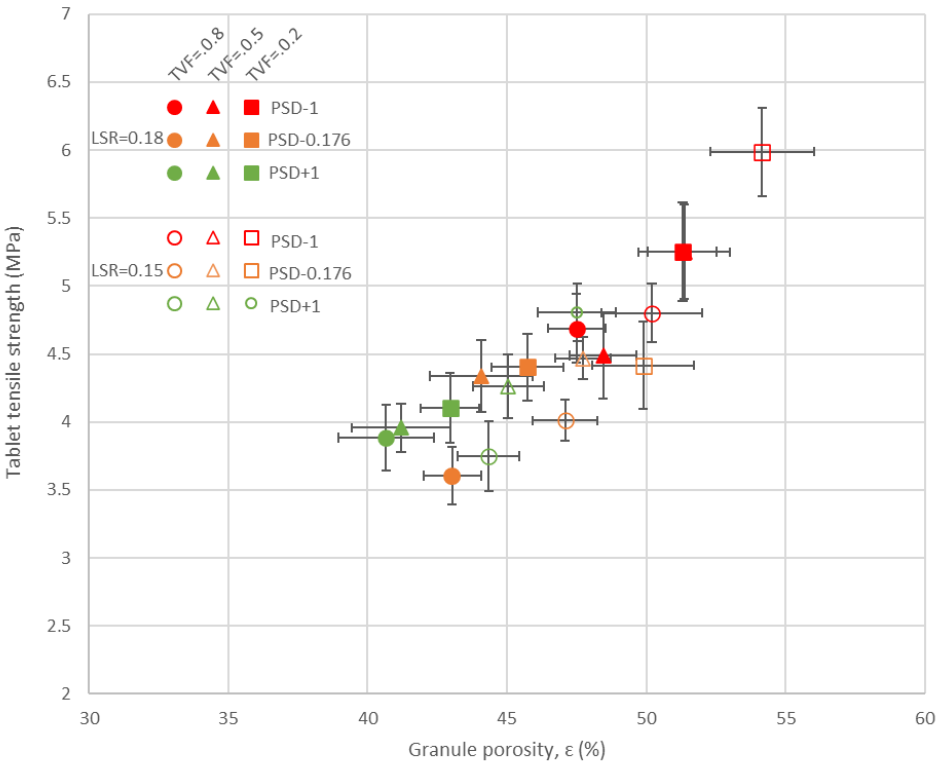

Figure 4.45 Tablet tensile strength plotted as a function of granule porosity. Mean ±sd, n=10 and n=3, respectively. Note X- and Y-axes do not start at zero. R^2=0.848, p<0.05.

In accordance with Dhenge et al. (2011), Liu et al. (2017b) and Lute et al. (2018b), greater channel fill resulted in lower granule porosity on account of increased shear forces from constrained conditions. Dhenge et al. (2010) showed that increasing the MFR, of a formulation similar to this study, resulted in stronger granules. Similarly, increasing the shear intensity by increasing the impeller speed (Sherif I.F. Badawy et al. 2012; Sherif I. Farag Badawy, Gray, and Hussain 2006) and prolonging the wet massing time in HSM (Sherif I.F. Badawy et al. 2012; Sherif I. Farag Badawy, Gray, and Hussain 2006; Sherif I. Farag Badawy et al. 2000; T. H. Nguyen, Morton, and Hapgood 2015) or increasing the number of kneading elements in TSG (Dejan Djuric and Kleinebudde 2008; Jurgen Vercruysse et al. 2012) resulted in denser and stronger granules that hindered tablet strength. Yet, conflictingly, Thapa et al. (2019) found that denser granules resulting from increased impeller speed and increased wet massing time during HSM resulted in stronger tablets. Also, Lute et al. (2018a) reported

barrel fill level during TSG had no significant impact on the tensile strength of granules produced from LAC and MCC in contrast to this study.

The larger particles of PSD+1 resulted in less porous granules, as they were more mobile and less hindered by cohesive forces acting across a smaller surface area, and so could agglomerate more closely to produce denser granules and weaker tablets, as reported following similar investigations (Sherif I. Farag Badawy et al. 2000; H. G. Kristensen, Holm, and Schaefer 1985). Additionally, granules first fracture along the solid bridges resulting from granulation, before the fragmentation of the original primary particles (Nordström and Alderborn 2015). Hence, PSD-1 granules collapsed into a larger surface area for contact bonding. The relationship between surface area and tablet tensile strength is well established in the literature (A. Adolfsson, Gustafsson, and Nyström 1999). Yet, Lute et al. (2018b) reported that the primary particle size of LAC and mannitol had little influence on tablet strength as they both undergo extensive fragmentation. Further considerations specific to the excipient material properties may have played a role on granule compaction. MCC's intrinsic porosity has been shown to diminish following wet granulation (Sherif I. Farag Badawy, Gray, and Hussain 2006; Westermarck et al. 1999) and negatively impact tensile strength (B. Johansson, Nicklasson, and Alderborn 1998; Staniforth et al. 1988; Sun 2008). Balaxi et al. (2009) reported that MCC particles increased in plasticity during granulation in the presence of higher liquid concentrations, resulting in less porous granules that resisted deformation during tablet compaction. Also, Sun et al. (2008) and Badawy et al. (2006) showed MCC increasingly loses its ability to deform once dried following wetting. These effects are further compounded as MCC has a greater contribution to tablet tensile strength than LAC (A. Adolfsson, Gustafsson, and Nyström 1999; Cabiscol et al. 2018), and MCC's binding functionality is derived from its ability to plastically deform and interlock particles.

Furthermore, Horisawa et al. (2000) concluded that due to LAC's propensity to undergo brittle fracture, tablet tensile strength was largely unaffected by the porosity of lactose granules. Although some studies have shown that MCC's binding ability is unaffected by primary particle size (A. Adolfsson, Gustafsson, and Nyström 1999; Mckenna and Mccafferty 1982; 1982), it is likely that the plastic deformation of larger MCC particles was restricted and limited as they were included in denser and stronger granules that were more resistant to compaction.

As observed by Van den Ban and Goodwin (2017) following an in-depth analysis of the effects of granule density on tablet properties following HSM, more porous granules produced less porous and stronger tablets. Nordstrom et al. (2013) arrived at a similar conclusion, following the tableting of high porosity pellets and low porosity pellets. Lee et al. (2013) showed that granules produced via HSM were less porous and stronger than TSG granules, resulting in a significantly lower tablet tensile strength. More porous granules resisted compaction to a lesser extent to reveal a larger surface area for inter-particle bonding (Nordström and Alderborn 2015). Dense granules with low porosity were more resistant to compaction, hence weakening inter-particle bonds (van den Ban and Goodwin 2017). Moreover, greater resistance to compaction limited deformation of binder particles, resulting in less particle interlocking and further weakening tablets (Wikberg and Alderborn 1990b; Zuurman et al. 1994). Additionally, as more porous granules had a higher propensity to fragment, they would more readily reveal clean surfaces not compromised by MgSt (M. Eriksson and Alderborn 1995). Furthermore, Riepma et al. (1991) showed that dense and intimate contact between particles, as was the case in the least porous granules, resisted compaction as there was limited free volume for particles to deform or fragment into.

As with granules, tablet strength is largely a function of porosity (Dejan Djuric and Kleinebudde 2008; Riippi et al. 1998), and is plotted as a compactability profile (not shown). Porosity depends on the area of intimate contact between particles and the attractive forces over the entire contacting area (Esezobo and Pilpel 1976; Kurup and Pilpel 1977). These attractive forces are exponentially dependent on distance. During tableting, the compaction

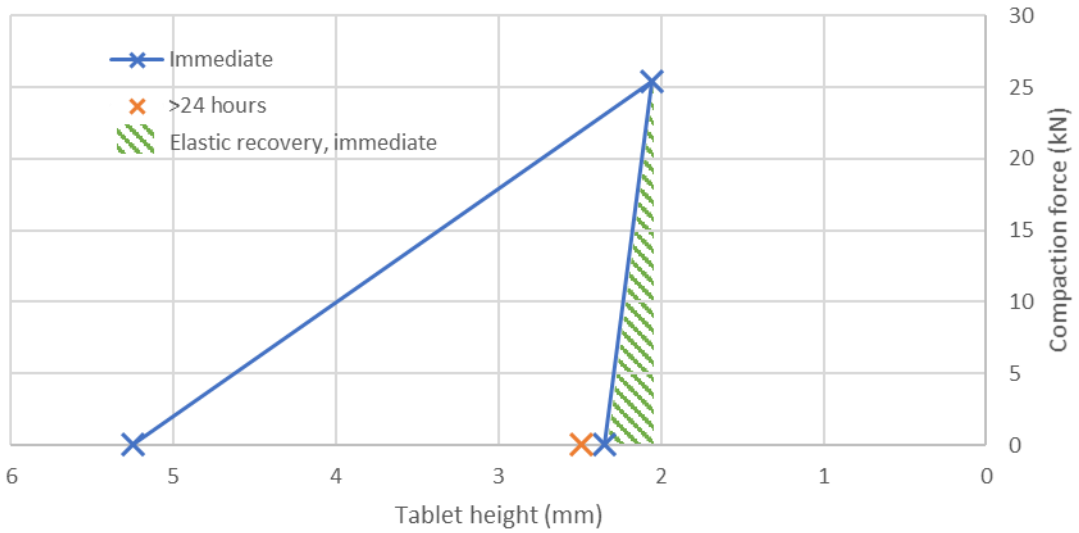

Figure 4.46 An example profile of tablet thickness as a function of 25.4 kN compaction force taken from experiment 12 (PSD-1, TVF=0.2, LSR=0.15). The ER% immediately post-compaction is highlighted green.

force brings particles into closer proximity to one another, and the reduced distance facilitates the creation and strength of intermolecular forces, mechanical interlocking and solid bridges (Olsson and Nyström 2001). The relationship between tablet porosity and compaction pressure is known as the compressibility profile and can be presented graphically (not shown).

Paradoxically, less porous granules resulted in more porous tablets, and vice versa. Elastic recovery, ER%, following decompression was a prominent contributor to tablet porosity and weaker tablets. Figure 4.46 shows a typical elastic recovery curve. ER% was the result of excess compaction energy that did not contribute to particle fragmentation or plastic

deformation, and thus was stored as elastic energy (Å. Adolfsson and Nyström 1996). As denser granules were less likely to yield under compaction forces, a greater proportion of the compaction energy was stored as elastic energy. As the compaction load was removed, compressed powder particles and air pockets relaxed to occupy a greater volume and increase porosity, subsequently weakening inter-particle bonds.

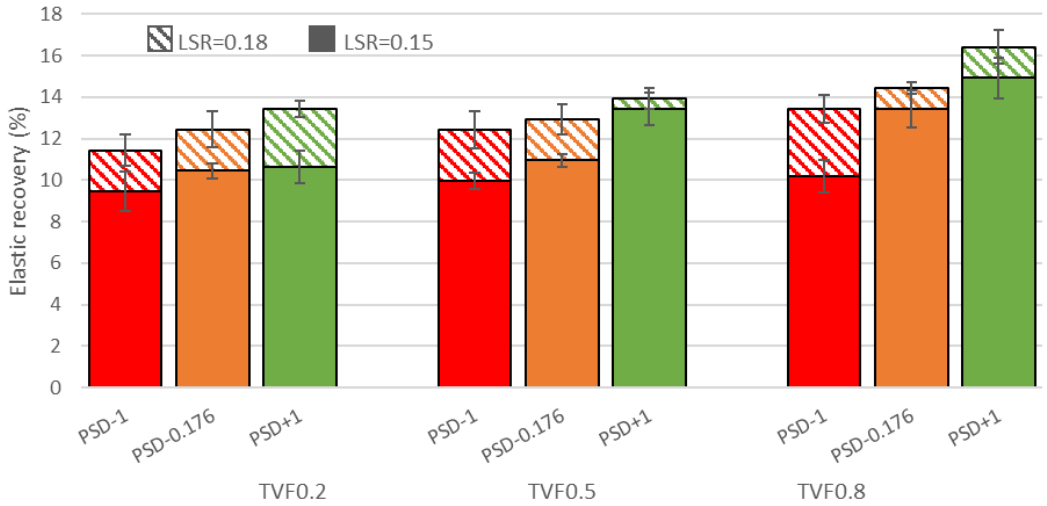

Figure 4.47 Comparison of ER% for 200±5 mg tablets compacted at 25±1 kN resulting from each granulation condition. Mean ±sd, n=10.

The majority of ER% occurred immediately following decompression, however, further relaxation occurred over the following 24 hours (Haware, Tho, and Bauer-Brandl 2010). Studies by Kachrimanis and Malamataris (2004) and Haware et al. (2010) showed that particle size of plastically deforming MCC to positively correlate with elastic recovery, whereas the elastic recovery of a brittle excipient (calcium hydrogen phosphate dihydrate) was independent of particle size. Hence, it is likely that the role of PSD on elastic recovery, and its hinderance on tablet strength, was predominantly the product of MCC, rather than LAC. The extent of ER% ranged from 9.3 to 16.2% (Figure 4.47) with greater ER% resulting from denser granules and resulting in weaker tablets, and vice versa.

4.4.8. Tablet content uniformity and dissolution

Pharmacopoeial chapters outline requirements for manufacturers to sample and assay at least ten, and up to 30, individual dosage units from each batch (The United States Pharmacopeial Convention 2011b). The acceptance value (AV) for the active ingredient, calculated from Equation 4.17, must be within 15% of the claimed dosage and the range of all dosage units must be within 25%. This corresponds to 8.5-11.5 mg and 7.5-12.5 mg of THP, respectively.

$$AV = [M - \bar{X}] + k \cdot sd \qquad \text{Equation 4.17}$$

Where *M* is the dosage claim, $\bar{X}$ is the mean dosage of the individual dosage units, *k* is the acceptability constant - equal to 2.4 when the sample size is 10, and 2 when the sample size is 30 - and *sd* is the sample standard deviation.

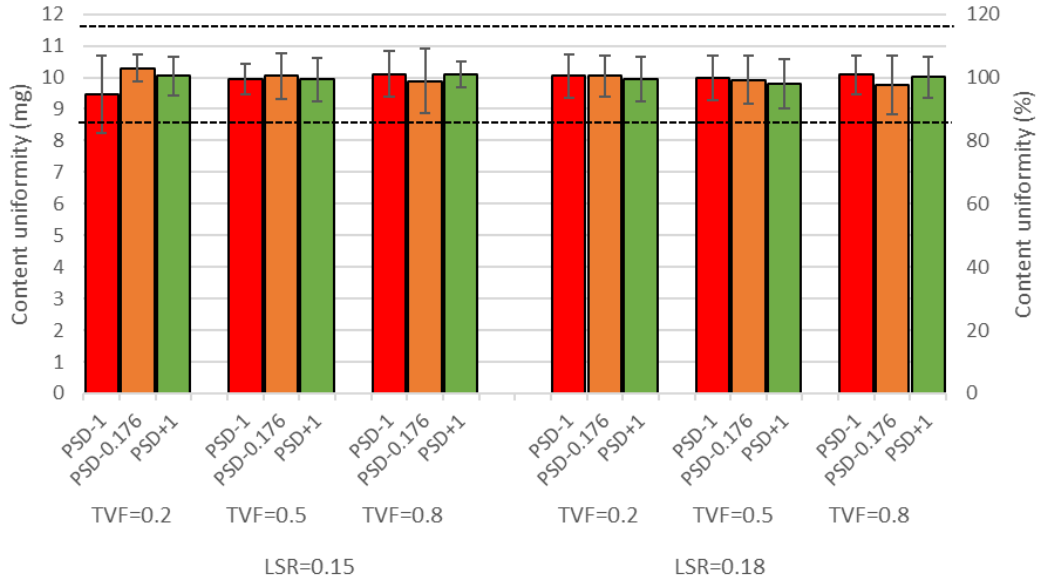

Figure 4.48 Content uniformity of 200±5 mg tablets produced under each TSG condition and formulation. The dashed lines represent the acceptance limit (<15%) of the claimed dose (10 mg). Mean ±AV, n=10.

The assay showed all but one (Exp 12) of the experimental conditions to result in tablets within the acceptance limit (Figure 4.48). This uniformity can be attributed to the exclusion of fines and large granules that were most affected by inhomogeneous THP distribution, as detailed in section 4.4.6. In a commercial manufacturing environment, excluding a

substantial portion of granulated material only to be reworked would demonstrate an inefficient and convoluted process. Despite the potential advantages of continuous granulation, traditional HSM would present a more feasible option unless the bimodal granule size distribution is resolved into a more uniform composition that can be directly tableted.

It should be noted that the acceptance value of experiment 12 (PSD-1, TVF=0.2, LSR=0.15) exceeded the acceptance limit as four of the 10 assayed tablets possessed dosages below 8.5 mg. This can be attributed to the higher demixing potential of the conditions that experiment 12 created.

Figure 4.49 presents the dissolution profiles resulting from every TSG experiment. The time for 80% of the total THP to be released (t_{80}) was used to compare the dissolution profiles of tablets resulting from each experimental condition. Despite a hydrophilic formulation and inclusion of a super-disintegrant (croscarmellose sodium), varying the LSR, TVF and PSD within the design space resulted in t_{80} ranging from 5:14 to 17:26 mm:ss. These times are well within the FDA's *Guidance for Industry*, advising that 80% of highly soluble API formulated into an immediate release dosage form dissolve within 60 minutes or less (Food and Drug Administration 1997).

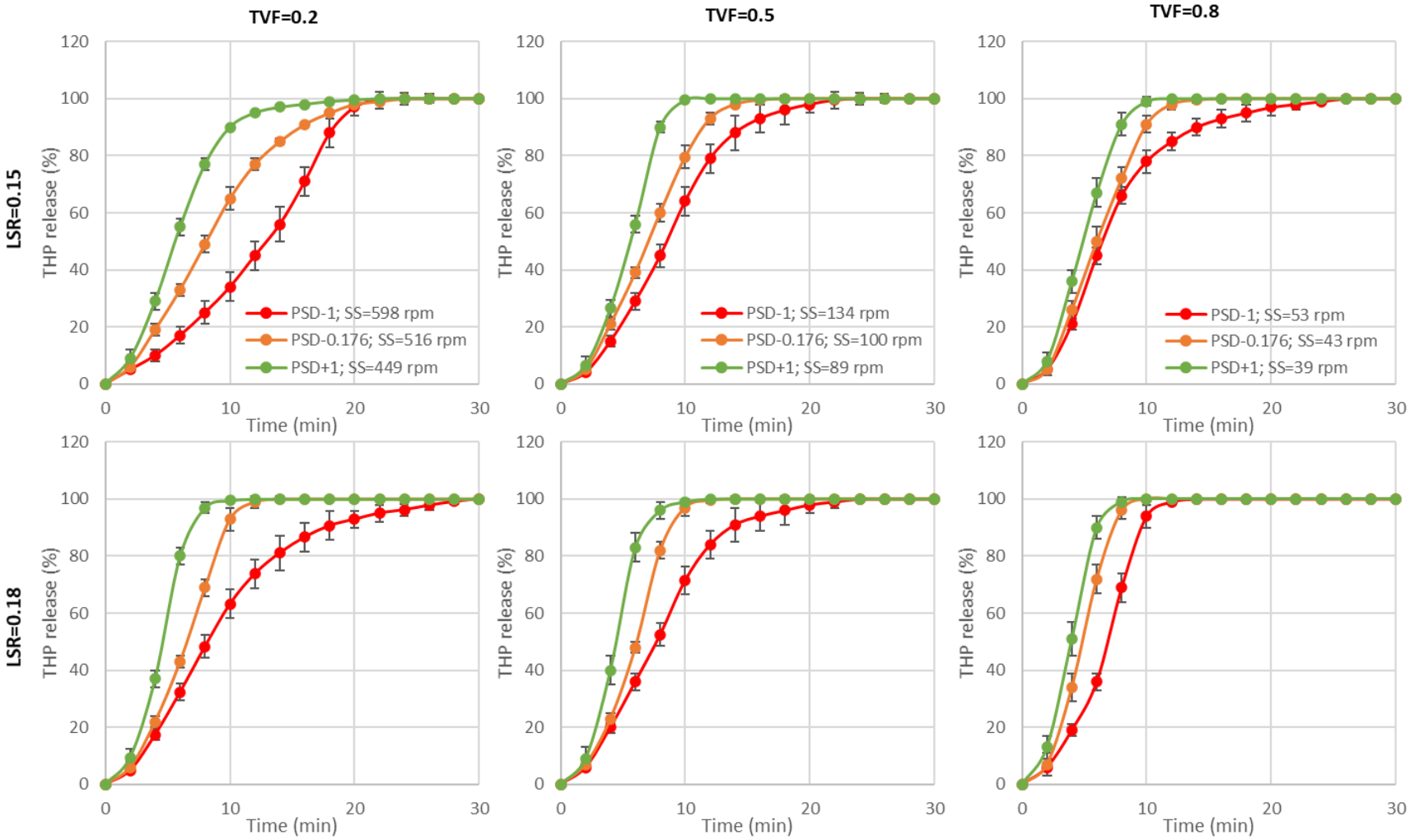

Figure 4.49 Comparison of THP release profiles during tablet dissolution in 37.5 °C purified water. Mean ±sd, n=6.

With that said, substantial differences in dissolution profiles manifest when varying formulation PSD, TVF and LSR. These are highlighted by using a model independent approach to compare dissolution profiles (Food and Drug Administration 1997; Stevens et al. 2015).

The difference factor, f_1, calculates the percentage difference between curves at each time point and is the measurement of the relative error between the two curves:

$$f_1 = \{[\Sigma_{t=1}^{n}|A_t - B_t|]/[\Sigma_{t=1}^{n}A_t]\} \cdot 100 \qquad \text{Equation 4.18}$$

where *n* is the number of time points, A_t is the dissolution value of experiment A at time *t* and B_t is the dissolution value of experiment B at time *t*.

The similarity factor, f_2, is a logarithmic reciprocal square root transformation of the sum of squared error and is a measurement of the similarity in the percent (%) dissolution between the two curves:

$$f_2 = 50 \cdot \left\{\left[1 + \left({}^{1}/_{n}\right)\Sigma_{t=1}^{n}(A_t - B_t)^2\right]^{-0.5} \cdot 100\right\} \qquad \text{Equation 4.19}$$

For curves to be considered sufficiently similar to support a SUPAC-IR application f_1 should be close to zero and f_2 should be close to 100. Generally, f_1 values up to 15 and f_2 values greater than 50 ensure equivalence of the two curves.

The f_1 and f_2 values were calculated for curves resulting from experimental conditions that differ by a single factor and single level step change e.g. PSD-1 to PSD-0.176 or TVF=0.5 to TVF=0.8. Of the 33 comparisons shown in Table 9, only 8 demonstrated equivalence as defined by the aforementioned criteria. This demonstrates that each parameter can introduce variability that is beyond what regulators consider acceptable. Further, this

variability could be amplified for a less soluble drug of BCS class II or IV and cause it to take longer than 60 minutes for 80% of the dose to dissolve.

Table 9 Difference factor, f1, and similarity factor, f2, calculated from the dissolution profiles for each single variable single level step change. Values coloured green, amber and red indicate equivalence (f_1<15, f_2>50), borderline equivalence (15<f_1<20, 45>f_2>50) and non-equivalence (f_1>20, f_2<45), respectively.

	LSR=0.15 TVF=0.2	LSR=0.15 TVF=0.2	LSR=0.15 TVF=0.5	LSR=0.15 TVF=0.5	LSR=0.15 TVF=0.8	LSR=0.15 TVF=0.8
Step change	PSD-1 PSD-0.176	PSD-0.176 PSD+1	PSD-1 PSD-0.176	PSD-0.176 PSD+1	PSD-1 PSD-0.176	PSD-0.176 PSD+1
f1	60.8	24.1	33.8	42.9	14.0	32.9
f2	32.5	47.3	45.9	37.4	56.6	42.0

	LSR=0.18 TVF=0.2	LSR=0.18 TVF=0.2	LSR=0.18 TVF=0.5	LSR=0.18 TVF=0.5	LSR=0.18 TVF=0.8	LSR=0.18 TVF=0.8
Step change	PSD-1 PSD-0.176	PSD-0.176 PSD+1	PSD-1 PSD-0.176	PSD-0.176 PSD+1	PSD-1 PSD-0.176	PSD-0.176 PSD+1
f1	40.9	62.8	39.3	44.6	62.0	36.6
f2	38.0	30.0	36.6	34.0	31.2	41.9

	LSR=0.15 PSD-1	LSR=0.15 PSD-1	LSR=0.15 PSD-0.176	LSR=0.15 PSD-0.176	LSR=0.15 PSD+1	LSR=0.15 PSD+1
Step change	TVF=0.2 TVF=0.5	TVF=0.5 TVF=0.8	TVF=0.2 TVF=0.5	TVF=0.5 TVF=0.8	TVF=0.2 TVF=0.5	TVF=0.5 TVF=0.8
f1	66.3	19.9	20.1	18.4	22.4	12.2
f2	32.9	45.5	49.2	51.8	42.5	57.1

	LSR=0.18 PSD-1	LSR=0.18 PSD-1	LSR=0.18 PSD-0.176	LSR=0.18 PSD-0.176	LSR=0.18 PSD+1	LSR=0.18 PSD+1
Step change	TVF=0.2 TVF=0.5	TVF=0.5 TVF=0.8	TVF=0.2 TVF=0.5	TVF=0.5 TVF=0.8	TVF=0.2 TVF=0.5	TVF=0.5 TVF=0.8
f1	12.9	21.9	10.4	33.1	1.8	17.7
f2	57.7	44.4	59.7	40.0	83.7	54.2

	TVF=0.2 PSD-1	TVF=0.2 PSD-0.176	TVF=0.2 PSD+1	TVF=0.5 PSD-1	TVF=0.5 PSD-0.176	TVF=0.5 PSD+1	TVF=0.8 PSD-1	TVF=0.8 PSD-0.176	TVF=0.8 PSD+1
Step change	LSR=0.15 LSR=0.18	LSR=0.15 LSR=0.18	LSR=0.15 LSR=0.18	LSR=0.15 LSR=0.18	LSR=0.15 LSR=0.18	LSR=0.15 LSR=0.18	LSR=0.15 LSR=0.18	LSR=0.15 LSR=0.18	LSR=0.15 LSR=0.18
f1	54.0	35.1	51.7	11.8	23.8	26.1	4.2	37.5	40.4
f2	34.7	39.0	31.5	60.3	44.4	41.6	55.8	38.2	39.4

The time for tablet dissolution was strongly positively correlated with tablet tensile strength (Figure 4.50), and inversely correlated to granule porosity. As the LSR, TVF and PSD decreased, granule porosity increased to yield stronger tablets, and the time for THP release

increased (Figure 4.51). It is widely accepted in the literature that stronger tablets prolong disintegration and drug release (Kurup and Pilpel 1977; Riippi et al. 1998). The stronger tablets possessed fewer and smaller pores (Esezobo and Pilpel 1976), and the reduced distance between particles increased the attractive interfacial forces. Water was able to permeate through the body of the weaker and more porous tablet microstructure more efficiently to hydrate the croscarmellose particles in the bulk. The croscarmellose particles rapidly swelled to rupture the tablet into fragments, increasing the available surface area for dissolution, and in turn the rate of THP release. This correlation is consistent with the hypothesis that granule porosity controls dissolution (Sherif I.F. Badawy et al. 2012), however, contrastingly, Badawy et al. (2012) found that the porosity of granules resulting from HSM was reflected in tablet porosity i.e. more porous granules resulted in more porous tablets that exhibited faster dissolution, despite being weaker tablets.

Interestingly, as the TVF increased the effect of formulation PSD on dissolution decreased (PSD*TVF, $p<0.05$). This may be a result of the greater consolidation at the higher channel fill resulting in denser and less compactible granules, more porous tablets, and ultimately, comparatively faster dissolution.

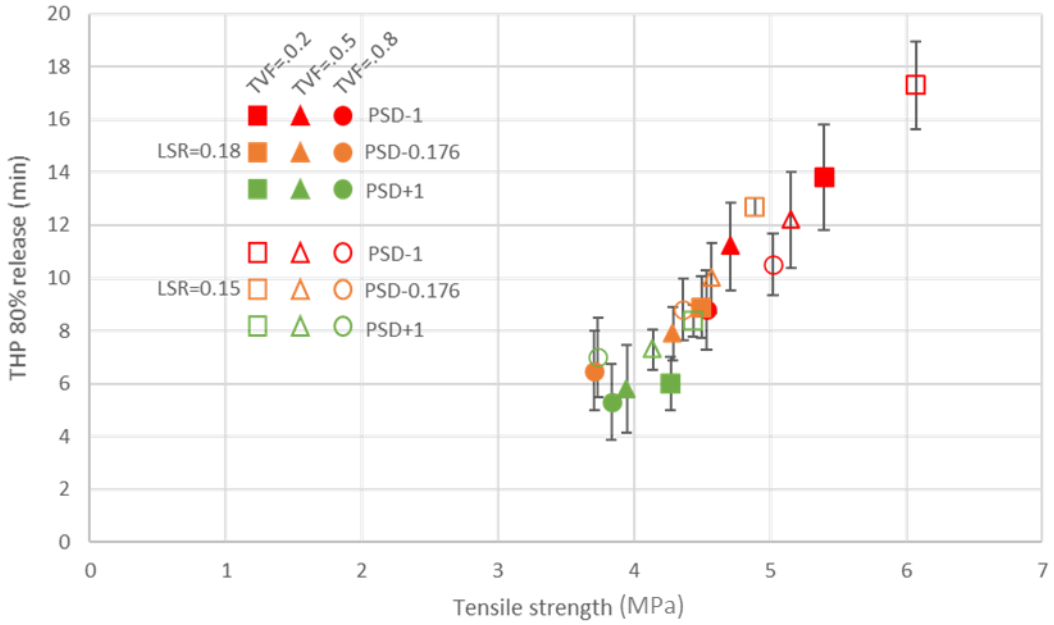

Figure 4.50 Time taken for 80% of THP to dissolve plotted as a function of estimated tablet tensile strength. Mean ±sd, n=6. R^2=0.901, p<0.05.

I

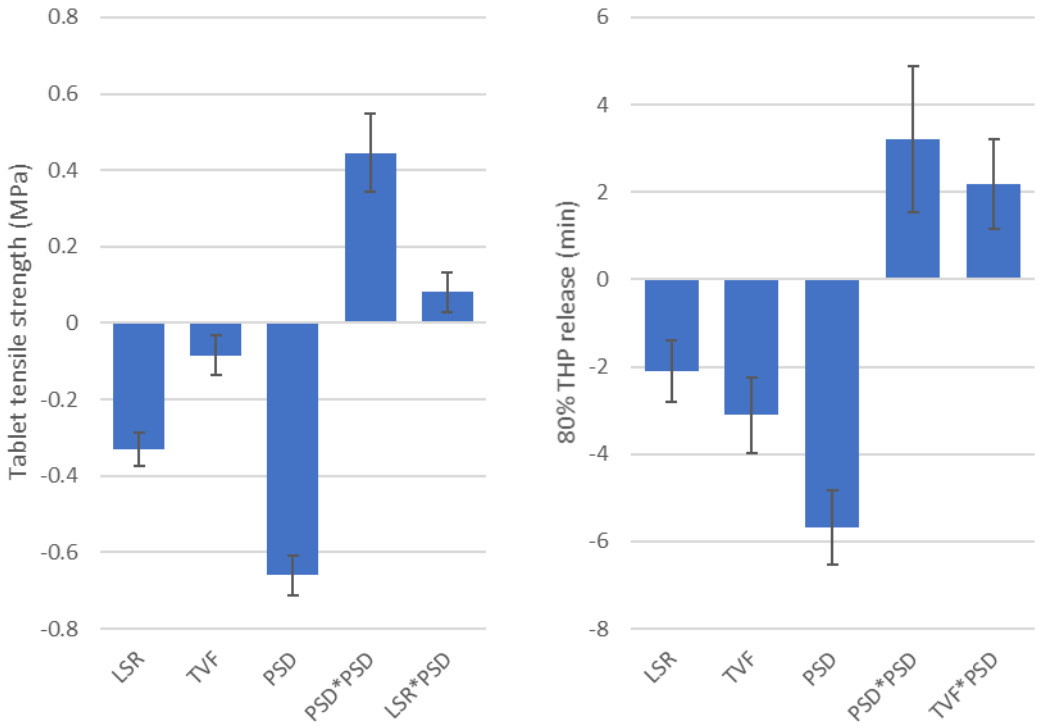

Figure 4.51 MLR coefficients pertaining to tablet performance; tablet tensile strength (left) and 80% THP release (right).

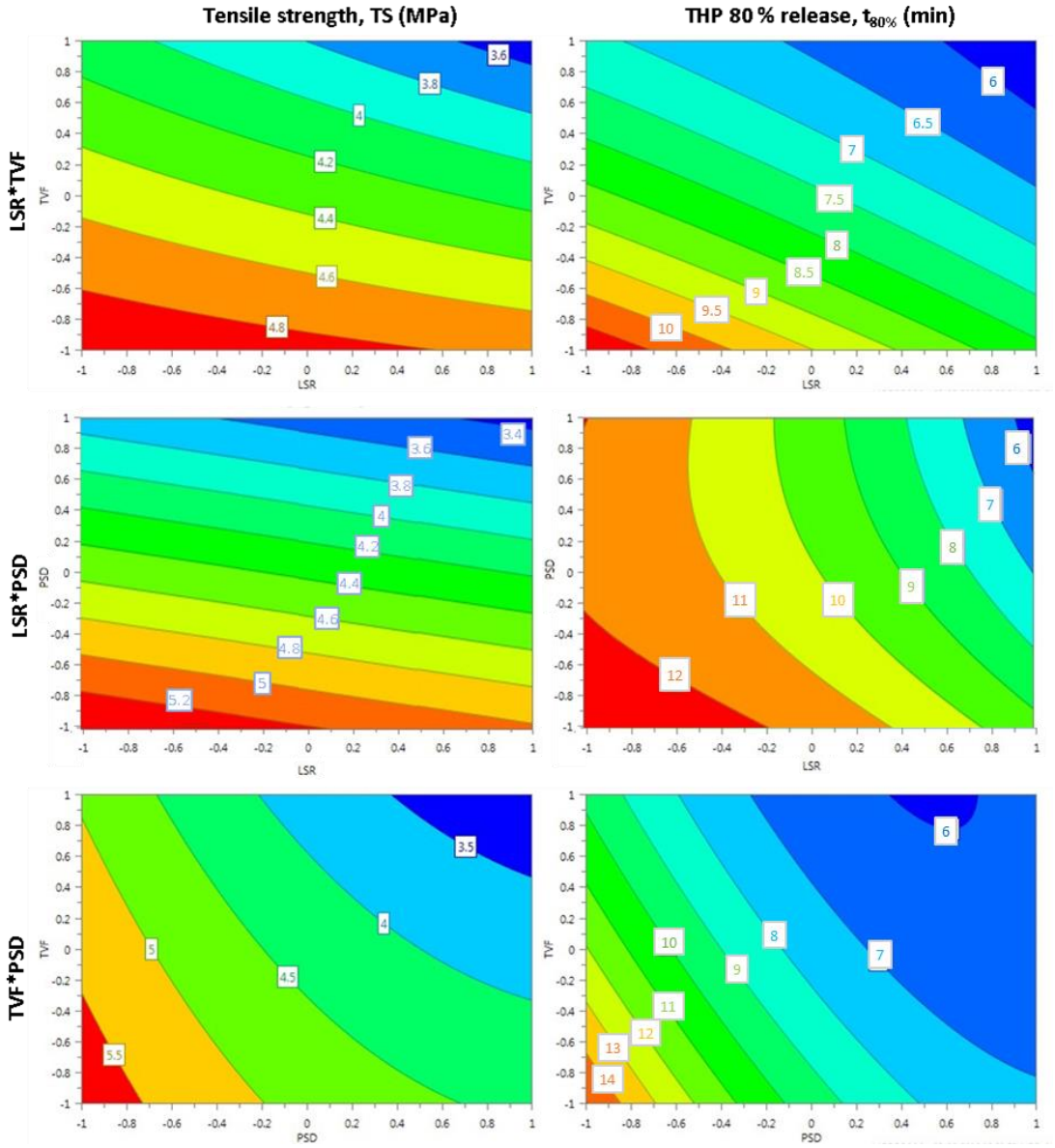

Figure 4.52 Response surfaces illustrating the effect of each variable on tablet tensile strength (left) and 80% THP release (right).

4.4.9. Evaluation of TVF

As a potential scale-up option, channel fill can be kept constant whilst increasing the TSG throughput by calculating and maintaining the TVF. To evaluate TVF as a dimensionless parameter, the *nucleation* and *granulation* experiments were repeated two more times at increased MFR for each TVF value. The SS necessary to maintain TVF was calculated using Equation 4.4 and the process maps are displayed in Figure 4.53. For TVF=0.2 repetitions at elevated MFR, the process conditions exceeded the design space (>600 rpm), therefore the MFR was decreased to 0.5 $kg.hr^{-1}$ and only repeated once. All repetitions were performed at LSR=0.18 only. The relative standard deviation, RSD (Equation 4.18), was calculated for key granule and tablet properties: median granule diameter, d_{50}; granulation yield i.e. 250-810 µm granule fraction; mean porosity of yield granules, ε_{yield}; tablet tensile strength following compaction at 25 kN,; and time for tablet dissolution and 80% THP release, THP80%.

Figures 4.54 and 4.55 compare the size distributions obtained at constant TVF. The GSD profiles are comparable but do display differences that result in a d_{50} RSD between 10.8 and 14.4% following nucleation, but this reduced to 8.3-12.5% following granulation. The d_{50} generally increased with higher throughput despite maintaining a constant TVF and LSR. This can be attributed to greater shear forces promoting greater granule growth, as the number of revolutions inflicted upon the material per residence time increased. The RSD for granulation yield ranged from 6.2-17.1%, but there was no general trend with respect to throughput. Figure 4.56 shows the porosity of the granules following granulation at a higher throughput to be, overall, slightly less porous (RSD 6.7-14.8%) than their 0.8 kg/hr counterpart.

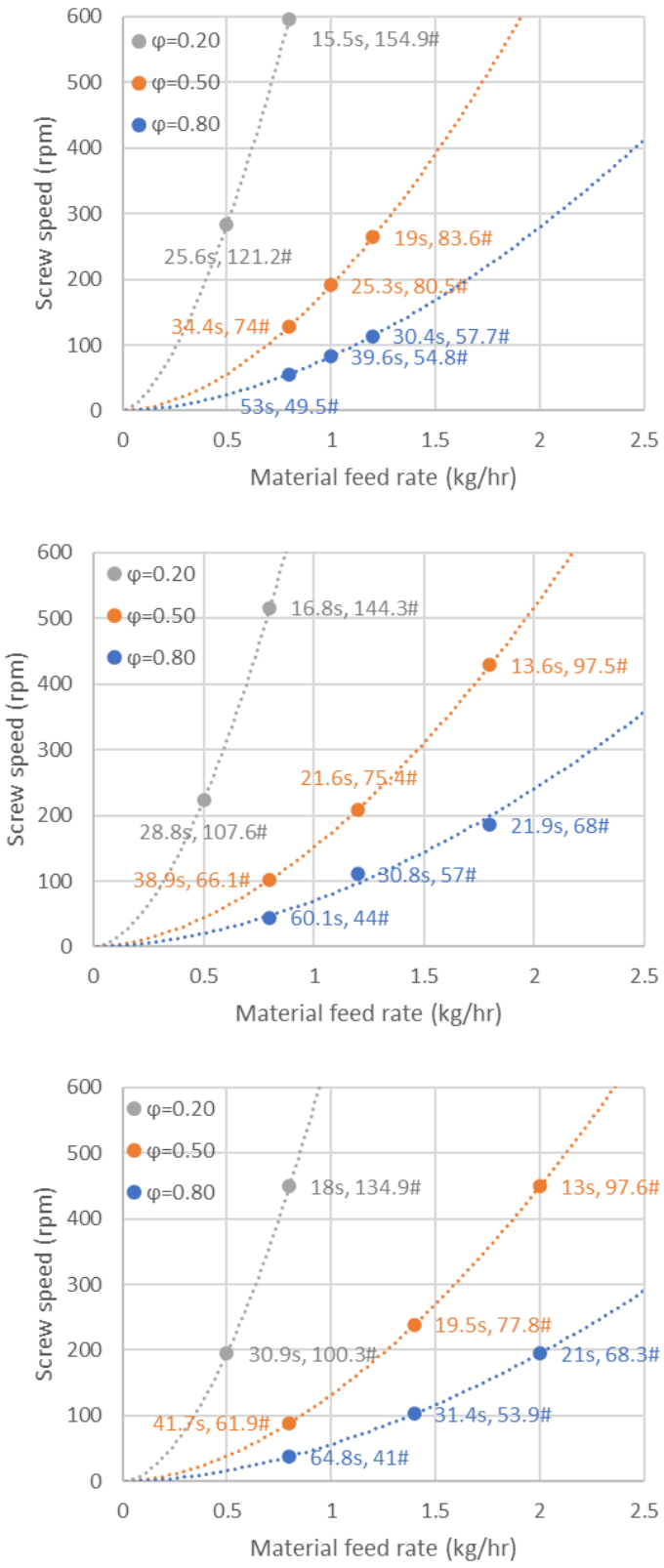

Figure 4.53 Process map to evaluate TVF (φ) for each formulation – PSD-1 (top), PSD-0.176 (middle) and PSD+1 (bottom) - and the various throughput conditions. Each operating condition is labelled with the MRT, followed by the number of screw revolutions per MRT.

These findings show that granule properties correlate with TVF, and concur with conclusions drawn by Gorringe et al. (2017), that MFR and SS should not be considered in isolation, as it is their combined effect that determine the barrel conditions that influence granule properties. Gorringe et al. (2017) also observed that granule properties were more sensitive to throughput changes at flooded conditions than at starved conditions. Similarly, in this study, TVF=0.8 yielded greater RSD values than TVF=0.2. Curiously, flooded conditions at TVF=0.8 were least sensitive to changes in formulation PSD but most sensitive to increased throughput.

As can be seen from Figures 4.57 and 4.58, and with the exception of experiment 3 (LSR=0.18, TVF=0.2 and PSD-1), the differences in granule properties did not result in a significant difference in tablet performance; tablet tensile strength had low RSD values of 2.8-8.1%, and 80% THP release resulted in RSDs between 3.4 and 12.5%. The higher throughput conditions did result in slightly weaker tablets and faster dissolution. Again, this can be attributed to the greater shear forces contributing to granule consolidation and densification from the greater number of screw revolutions per MRT, yielding denser granules that were less compactable. From the smaller RSD values it appears that compaction reduced tablet variability arising from granule variability. However, the tablets resulting from experiment 3 had markedly higher RSD values of 10.9% for tensile strength and 19.0% for THP release. The reason for this is not clear as the RSD values for the median granule size and granule porosity were relatively small when compared to the other experimental conditions. Despite this anomaly, the tablet properties were still well within the range accepted for immediate-release dosage forms. Hence, this study has shown that scaling up via increasing material throughput whilst maintaining the channel fill level is potentially an effective method of increasing production output.

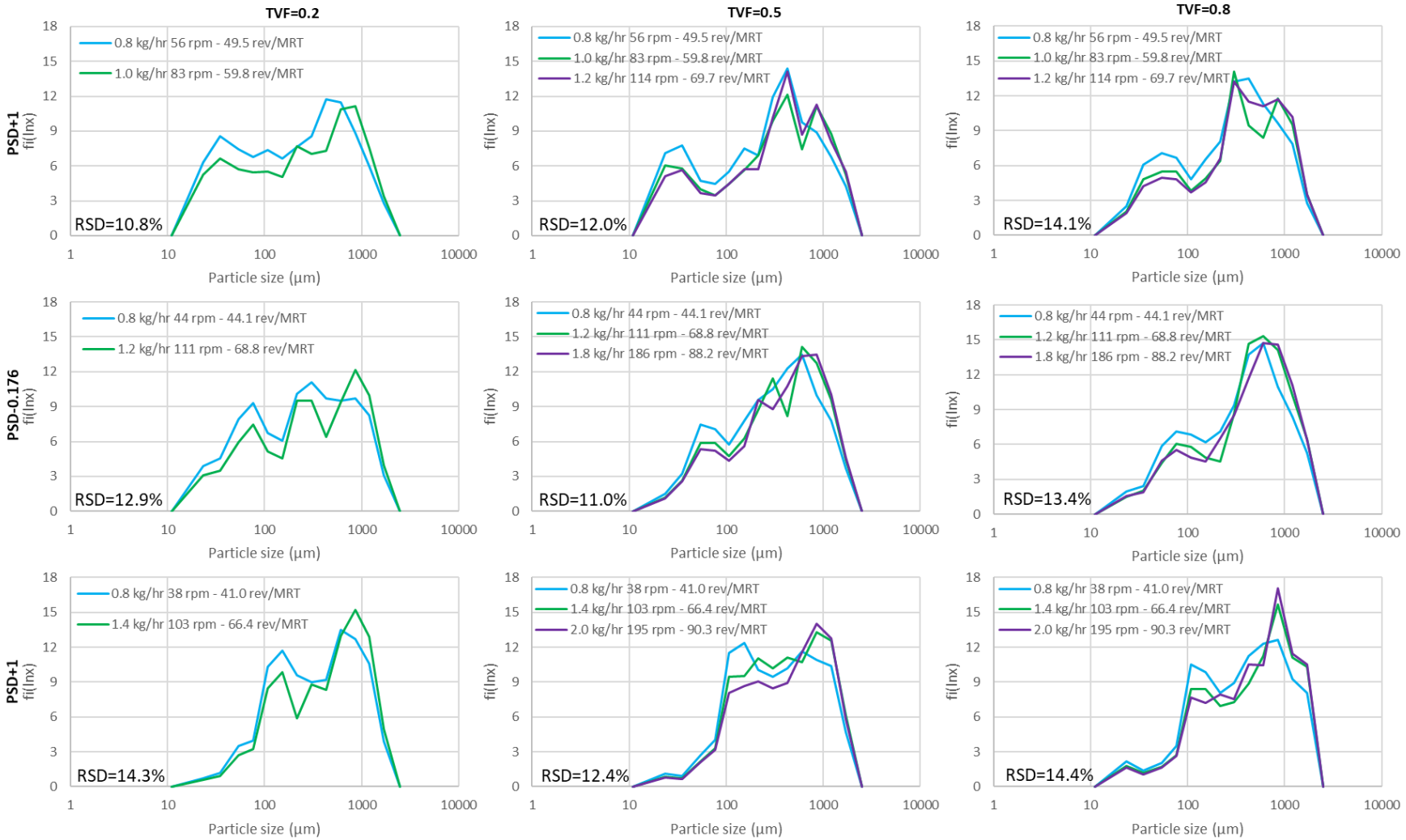

Figure 4.54 Particle size (µm) vs Normalised mass frequency, $f_i(lnx)$: nuclei size distributions comparing effects of throughput at consistent channel fill and LSR=0.18. Mean measurement, n=3.

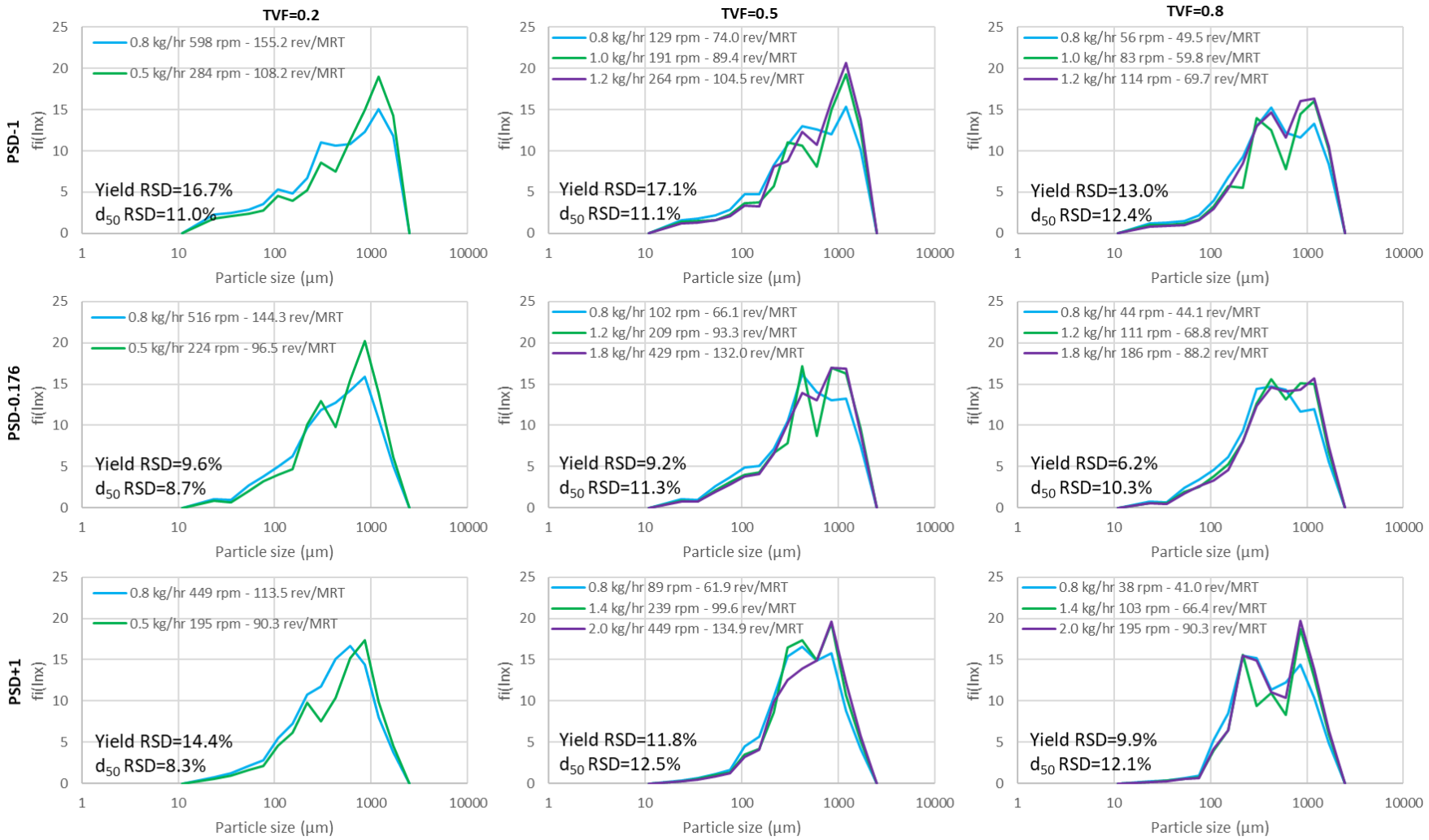

Figure 4.55 Particle size (µm) vs Normalised mass frequency, fi(lnx): granule size distributions comparing effects of throughput at consistent channel fill and LSR=0.18. Mean measurement, n=3.

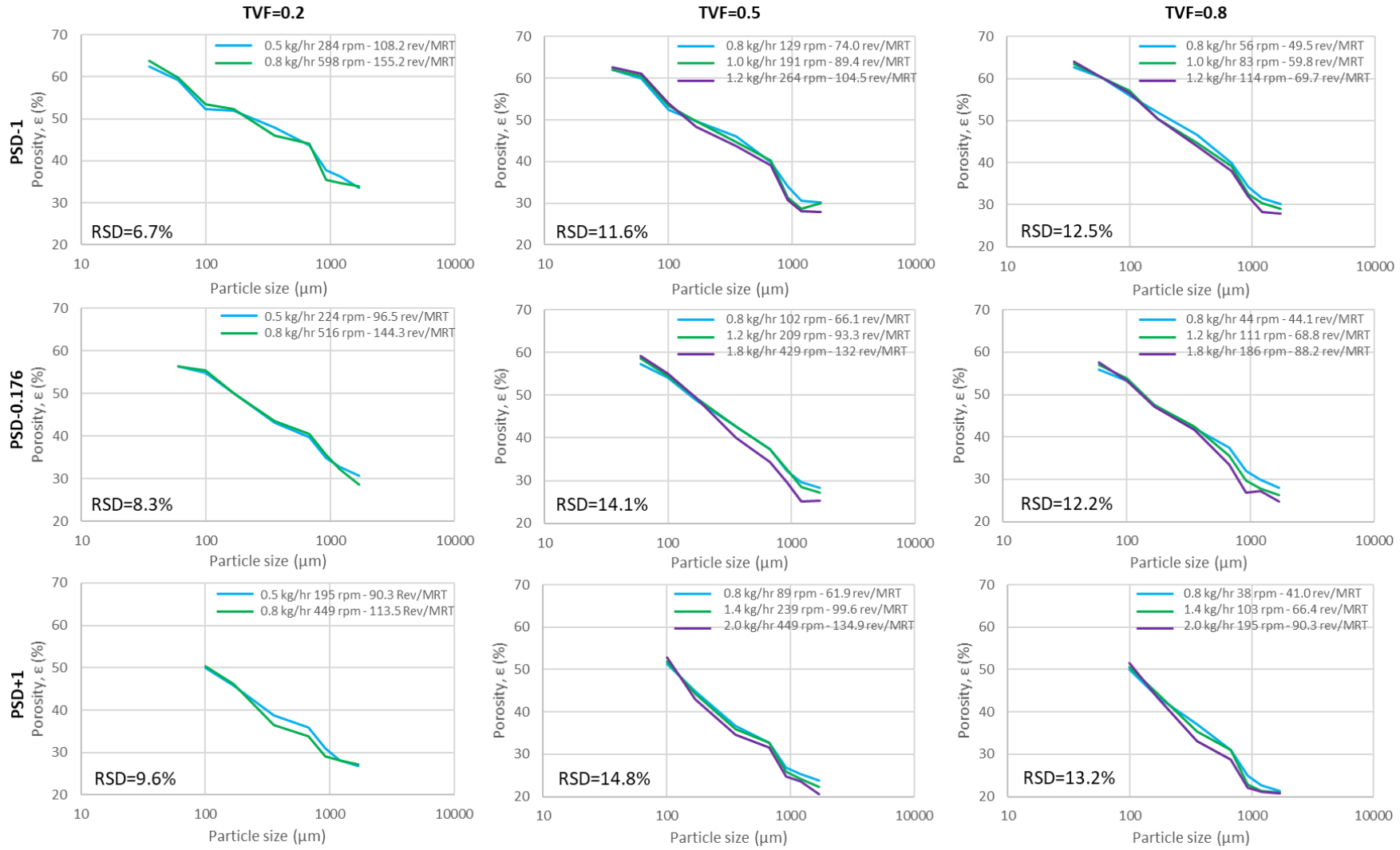

Figure 4.56 Particle size (µm) vs Porosity, ε (%): comparison of effects of throughput on porosity at consistent channel fill and LSR=0.18. Mean measurement, n=3.

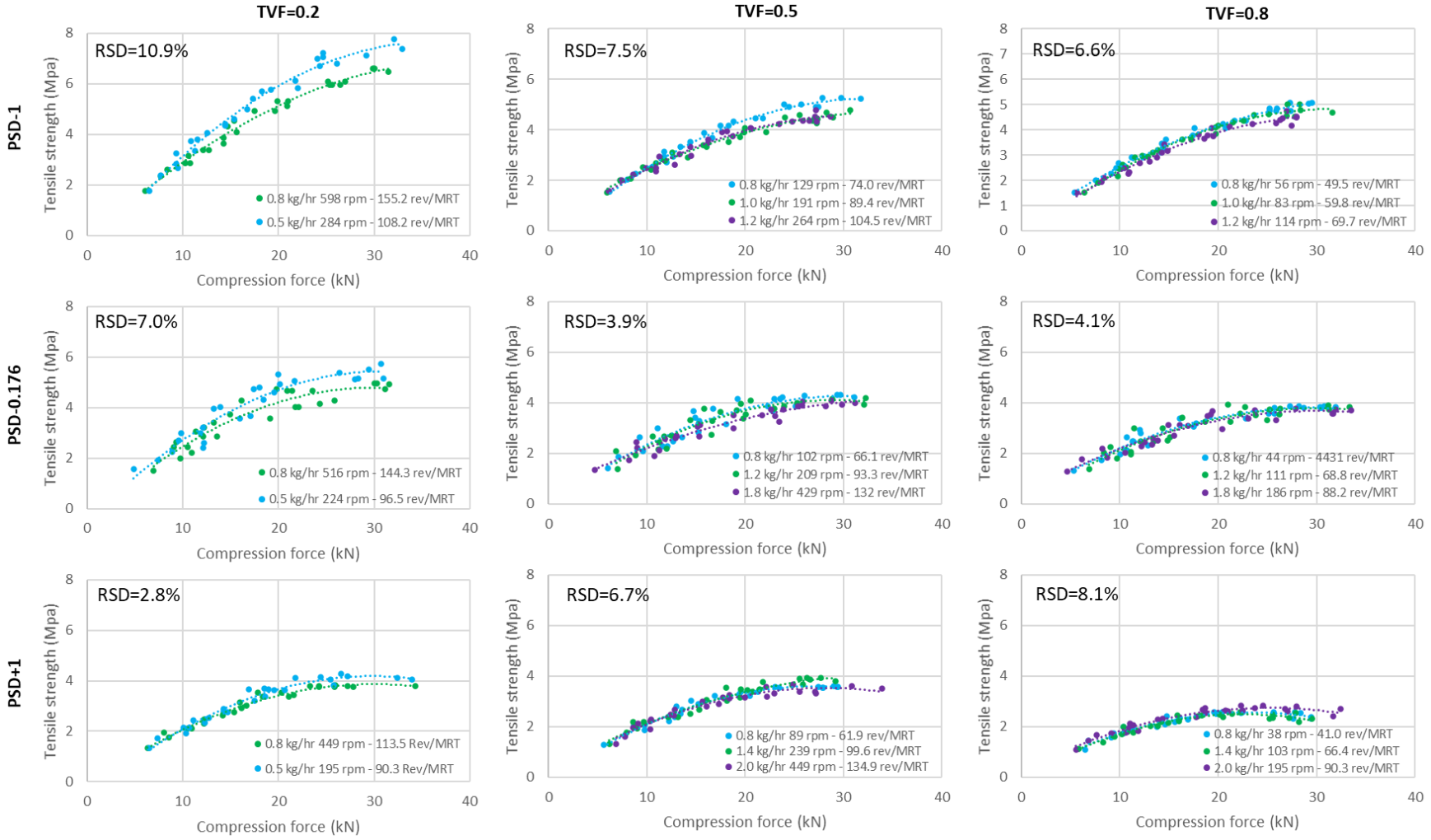

Figure 4.57 Compaction force (kN) vs Tensile strength (MPa): comparing effects of throughput at consistent channel fill and LSR=0.18. Mean measurement, n=3.

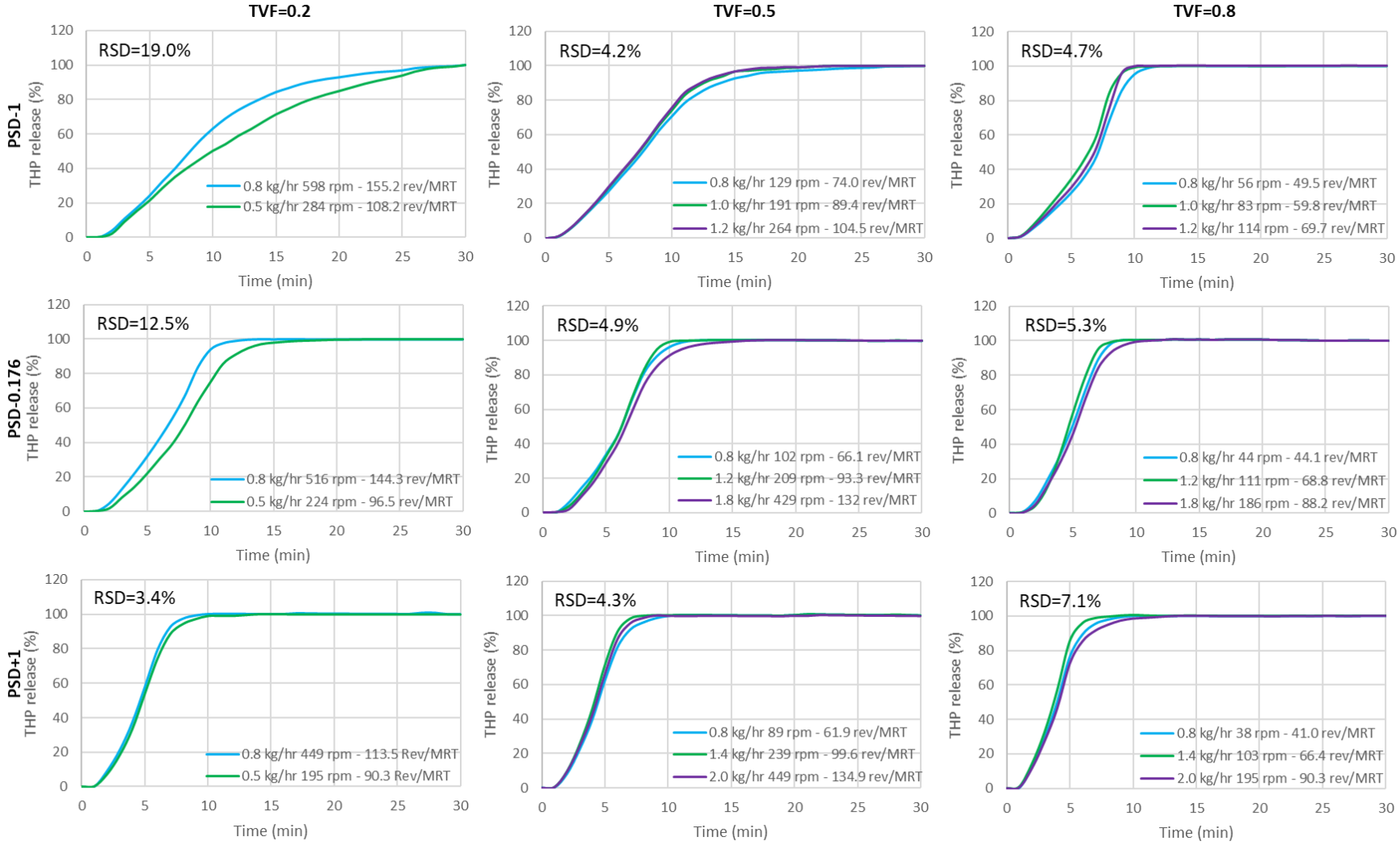

Figure 4.58 Time (min) vs THP release (%): THP release profiles comparing effects of throughput at consistent channel fill and LSR=0.18. Mean measurement, n=3.

4.5. Conclusion

An in-depth analysis of the effects of powder properties and operating parameters on TSG was conducted. Each of the variables studied proved to have a statistically significant, albeit small, effect on tablet performance, as indicated by the multiple linear regression models; <0.7 MPa on tablet tensile strength and <6 minutes on THP dissolution.

Likewise, the main effect coefficient for each variable was statistically significant for each of the granule physical properties measured. The granule physical properties were found to be proportionally influenced by the liquid concentration as an increase from LSR=0.15 to LSR=0.18 (20%) caused the granule d_{50} to increase by 26.6 ±15.5% (mean ±sd, *n*=9) and the yield granule porosity to decrease by 7.1±3.4% (mean ±sd, *n*=9). Whereas, drastically increasing the channel fill from TVF=0.2 to TVF=0.8 (300%) caused the granule d_{50} to increase modestly by 24.3±14.3% (mean ±sd, *n*=6) and granule porosity to decrease by 7.7±2.5% (mean ±sd, *n*=6). Likewise, increasing the primary particle size of the formulation by 204.2% from PSD-1 to PSD+1 resulted in granule d_{50} decreasing by only 23.2±11.4% (mean ±sd, *n*=6) and granule porosity decreased by 12.0±3.9% (mean ±sd, *n*=6). This shows that for this TSG setup, wet granulation was particularly sensitive to LSR but comparatively insensitive to barrel conditions and formulation changes. In the absence of dramatic process perturbations, it is unlikely that channel fill and formulation PSD would vary to the extremes of this study's design space. Hence, this combination of the formulation and the TSG setup used presents a forgiving process that can accommodate relatively large throughput and excipient variability. This was evident from the TVF evaluation studies, whereby granule properties were comparable despite scaling-up the output by 60-150%. Variance was further decreased by compaction to yield immediate-release tablets acceptable by

pharmacopeial standards with respect to content uniformity, tensile strength and drug release. Only at the extreme edge of the design space (experiment 12: LSR=0.15, TVF=0.2, PSD-1) did the production appear to falter with inadequate content uniformity.

However, in this study TSG was shown to be inefficient with maximum yields of only 57.4% being considered suitable for tableting. Reviews by Thompson (2015) and Seem et al. (2015) highlight the prevalence of broad bimodal granule size distribution throughout the literature, emanating from inhomogeneous liquid distribution at moderate liquid concentrations. Whilst, increasing TVF and PSD improved liquid distribution, at least 42.6% and up to 65.7% of the granulated material was either under- or over-sized. Hence, current continuous tableting lines, such as ConsiGma®, include a milling module to homogenous granule PSD. This workaround is inelegant, negates advantageous aspects of continuous processing and demonstrates a lack of control.

5. General Conclusions and Future Work

This thesis has sought to shed further light on the consequences of excipient variability on continuous wet granulation by artificially manipulating the physical properties of commonly used excipient grades.

In chapter 3 it was observed that varying the particle size distribution and bulk properties of a static powder bed composed of commonly used excipients had a drastic effect on powder wetting, including droplet oscillation and energy dissipation, spreading, and penetration time. Additionally, varying the excipients across the three pseudo grades resulted in the formation of three distinct nuclei morphologies and was dependent on the powder bed's ability to induce capillary action on the liquid at the surface of the powder bed and in the powder bulk following imbibition. However, the limitations of making these observations in vitro on a static powder bed became evident when equally significant effects on TSG granulation did not manifest in chapter 4. Whilst capillary-driven wetting was the prominent means of liquid distribution in a static powder bed, capillary action was not indicative of liquid distribution within a dynamic twin-screw environment whereby liquid distribution is driven by mechanical dispersion modulated by process parameters and screw configuration rather than excipient properties. Further, the consolidation of the static powder bed did not correspond to the constrained conditions of the barrel controlled via the TVF. Therefore, the results of the drop penetration tests and conclusions drawn in chapter 3 are meaningful only as far as characterising the powders themselves. The findings in chapter 4 pertaining to TSG indicated that process parameters, rather than formulation parameters, were most determinative. This can be explained by considering the concurrent mechanism during

granulation and understanding that the drop penetration tests only simulated wetting and nucleation. Granule growth, consolidation and breakage mechanisms were not explored in chapter 3 but featured significantly in chapter 4 and were attributable to the compressive and shear forces inflicted in the dynamic conditions in the barrel. Hence, the findings in chapter 4 were not informed or explained by powder-orientated observations made in chapter 3 and demonstrate the inability to extrapolate findings from the in vitro tests to TSG. Therefore the null hypothesis was proven true, in that wetting and nucleation did not play a more significant role in TSG than in HSM due to the shorter period for mechanical dispersion to occur.

Based on the robust ability of TSG to yield similar granular output and adequately performing tablets independently of the input materials tested in chapter 4, the particle size distributions of LAC and MCC would not be considered critical material attributes in a comparable formulation for a low dose product. Furthermore, attempts to mitigate excipient variability by "doping" the majority formulation component with a minority component to manipulate granule and tablet properties proved inconsequential.

A less forgiving formulation involving a high dose formulation comprised of a less wettable and workable API may form the basis of a more exploratory investigation, whereby the limits of TSG can manifest. However, from this study and assuming a similar formulation, it can be seen that manufacturers utilising a QbD framework could incorporate a broad excipient PSD specification into the design space, and rationally utilise numerous suppliers rather than being dependent on the sole vendor stipulated in the CTD submission. Applying this approach to assess and incorporate other material attributes has the potential to liberate pharmaceutical supply chains and mitigate drug shortages.

To-date no adequate method of producing a monomodal narrow granule size distribution via TSG has been presented in the literature. The addition of a milling stage post-granulation has been used in continuous lines (GEA-Siemens 2020) but does not present an elegant solution. Broad and bimodal granule size distributions are the result of inhomogeneous liquid distribution, for which the underlying cause is the liquid addition method. TSG's dependence on *immersion nucleation* originates from the limited number of liquid inlets introducing large droplets onto the powder mass and reliance on mechanical dispersion. A TSG redesign involving a greater number of liquid inlets of narrower aperture arranged radially around the barrel and screw shaft may result in a more even liquid distribution method approaching the drop controlled *spraying nucleation* common to HSM. By considering LSR, MRT, aperture diameter and geometric distribution of the liquid inlets, the number of droplets introduced to a cross-section of powder mass as a function of time could be calculated and may meaningfully relate to liquid distribution and GSD.

This study and the literature are unanimous in showing that LSR is the most critical process parameter in TSG. LSR is a relatively easy parameter to control as it is a function of the material feed rate via a loss-in-weight feeder and the liquid addition rate via a pump. However, it is still worth considering the segregation process if perturbations in LSR were to arise. In this study, the RTD of the material was extensively profiled as the tracer powder traversed the barrel length. Yet, it is unknown if this correlates directly with the granulating liquid and hence, profiling of a liquid tracer would be of value.

By incorporating the disparity between the experimentally determined mean residence time and theoretical residence time into volumetric fill calculations, the channel fill level could be estimated. Increasing throughput whilst maintaining granule properties was satisfactorily

achieved, however, whether this is also the case in larger industrial units (16 mm and above), where higher shear forces are achieved, and for less forgiving formulations is yet to be determined.

In summary, an in-depth investigation of formulation and process parameters has been conducted with a direct through line to the quality and performance of the end product. However, seeking to evaluate the influence of excipient properties on TSG in vitro proved to be arbitrary and of limited value. However, applying a QbD approach by following a DoE and RSM enabled for a vast quantity of data to be gathered, which can further be utilised in the development of computational modelling.

6. References

Abberger, Thomas, Anette Seo, and Torben Schaefer. 2003. 'The Effect of Droplet Size and Powder Particle Size on the Mechanisms of Nucleation and Growth in Fluid Melt Agglomeration'. *International Journal of Pharmaceutics* 249 (January): 185–97. https://doi.org/10.1016/S0378-5173(02)00530-6.

Adolfsson, A., C. Gustafsson, and C. Nyström. 1999. 'Use of Tablet Tensile Strength Adjusted for Surface Area and Mean Interparticulate Distance to Evaluate Dominating Bonding Mechanisms'. *Drug Development and Industrial Pharmacy* 25 (6): 753–64. https://doi.org/10.1081/ddc-100102235.

Adolfsson, Åsa, and Christer Nyström. 1996. 'Tablet Strength, Porosity, Elasticity and Solid State Structure of Tablets Compressed at High Loads'. *International Journal of Pharmaceutics* 132 (1–2): 95–106. https://doi.org/10.1016/0378-5173(95)04336-5.

Aghajan, Mohammad Hossein, Seyed Mostaffa Hosseini, and Mehdi Razzaghi-Kashani. 2019. 'Particle Packing in Bimodal Size Carbon Black Mixtures and Its Effect on the Properties of Styrene-Butadiene Rubber Compounds'. *Polymer Testing* 78 (September): 106002. https://doi.org/10.1016/j.polymertesting.2019.106002.

Agrawal, Anjali M., and Preetanshu Pandey. 2015. 'Scale Up of Pan Coating Process Using Quality by Design Principles'. *Journal of Pharmaceutical Sciences* 104 (11): 3589–3611. https://doi.org/10.1002/jps.24582.

Ahmed, Bilal, Cameron J. Brown, Thomas McGlone, Deborah L. Bowering, Jan Sefcik, and Alastair J. Florence. 2019. 'Engineering of Acetaminophen Particle Attributes Using a Wet Milling Crystallisation Platform'. *International Journal of Pharmaceutics* 554 (January): 201–11. https://doi.org/10.1016/j.ijpharm.2018.10.073.

Alava, Mikko, Martin Dubé, and Martin Rost. 2004. 'Imbibition in Disordered Media'. *Advances in Physics* 53 (2): 83–175. https://doi.org/10.1080/00018730410001687363.

Alghunaim, Abdullah, Suchata Kirdponpattara, and Bi-min Zhang Newby. 2016. 'Techniques for Determining Contact Angle and Wettability of Powders'. *Powder Technology* 287 (January): 201–15. https://doi.org/10.1016/j.powtec.2015.10.002.

Al-Ibraheemi, Zahraa A.Mousa, M. S. Anuar, F. S. Taip, M. C. I. Amin, S. M. Tahir, and Ali Basim Mahdi. 2013. 'Deformation and Mechanical Characteristics of Compacted Binary Mixtures of Plastic (Microcrystalline Cellulose), Elastic (Sodium Starch Glycolate), and Brittle (Lactose Monohydrate)'. *Particulate Science and Technology* 31 (6): 561–67. https://doi.org/doi:10.1080/02726351.2013.785451.

Alkhatib, Aveen. 2015. 'The Study of Mixing and Initial Granule Formation During High Shear Granulation of Pharmaceutical Powders'. PhD Thesis. University of Western Ontario. https://ir.lib.uwo.ca/etd/2720.

Allen, Terence. 2003. *Powder Sampling and Particle Size Determination*. Elsevier. https://doi.org/10.1016/B978-0-444-51564-3.X5000-1.

Allison, Gretchen, Yanxi Tan Cain, Charles Cooney, Tom Garcia, Tara Gooen Bizjak, Oyvind Holte, Nirdosh Jagota, et al. 2015. 'Regulatory and Quality Considerations for Continuous Manufacturing May 20–21, 2014 Continuous Manufacturing Symposium'. *Journal of Pharmaceutical Sciences* 104 (3): 803–12. https://doi.org/10.1002/jps.24324.

Almaya, Ahmad, and Aktham Aburub. 2008. 'Effect of Particle Size on Compaction of Materials with Different Deformation Mechanisms with and without Lubricants'. *AAPS PharmSciTech* 9 (2): 414–18. https://doi.org/10.1208/s12249-008-9059-3.

Alvarez, L, Angel Concheiro, Jose Gomez, Consuelo Souto, and R Martínez-Pacheco. 2002. 'Effect of Microcrystalline Cellulose Grade and Process Variables on Pellets Prepared by Extrusion–Spheronization*'. *Drug Development and Industrial Pharmacy* 28 (May): 451–56. https://doi.org/10.1081/DDC-120003006.

Antonini, Carlo, Alidad Amirfazli, and Marco Marengo. 2012. 'Drop Impact and Wettability: From Hydrophilic to Superhydrophobic Surfaces'. *Physics of Fluids* 24 (10). https://doi.org/10.1063/1.4757122.

Apel-Paz, Meirav, and Abraham Marmur. 1999. 'Spreading of Liquids on Rough Surfaces'. *Colloids and Surfaces A: Physicochemical and Engineering Aspects* 146 (1): 273–79. https://doi.org/10.1016/S0927-7757(98)00778-X.

Arlington, Steve. 2011. 'Pharma 2020: From Vision to Decision'. Pharma 2020. Pricewaterhouse Cooper. https://www.pwc.com/gx/en/industries/pharmaceuticals-life-sciences/publications/pharma-2020.html.

Arndt, Oscar-Rupert, Roberto Baggio, Anna Kira Adam, Julia Harting, Erica Franceschinis, and Peter Kleinebudde. 2018. 'Impact of Different Dry and Wet Granulation Techniques on Granule and Tablet Properties: A Comparative Study'. *Journal of Pharmaceutical Sciences* 107 (12): 3143–52. https://doi.org/10.1016/j.xphs.2018.09.006.

Arns, Christoph H., Mark A. Knackstedt, and Nicos S. Martys. 2005. 'Cross-Property Correlations and Permeability Estimation in Sandstone'. *Physical Review. E, Statistical, Nonlinear, and Soft Matter Physics* 72 (4 Pt 2): 046304. https://doi.org/10.1103/PhysRevE.72.046304.

Arora, Deepak, Abhijit P. Deshpande, and S. R. Chakravarthy. 2006. 'Experimental Investigation of Fluid Drop Spreading on Heterogeneous and Anisotropic Porous Media'. *Journal of Colloid and Interface Science* 293 (2): 496–99. https://doi.org/10.1016/j.jcis.2005.06.055.

Badawy, Sherif, and Munir Hussain. 2004. 'Effect of Starting Material Particle Size on Its Agglomeration Behavior in High Shear Wet Granulation'. *AAPS PharmSciTech* 5 (June): e38. https://doi.org/10.1208/pt050338.

Badawy, Sherif I. Farag, David B. Gray, and Munir A. Hussain. 2006. 'A Study on the Effect of Wet Granulation on Microcrystalline Cellulose Particle Structure and Performance'. *Pharmaceutical Research* 23 (3): 634–40. https://doi.org/10.1007/s11095-005-9555-z.

Badawy, Sherif I. Farag, Mark M. Menning, Mary Ann Gorko, and Donna L. Gilbert. 2000. 'Effect of Process Parameters on Compressibility of Granulation Manufactured in a High-Shear Mixer'. *International Journal of Pharmaceutics* 198 (1): 51–61. https://doi.org/10.1016/S0378-5173(99)00445-7.

Badawy, Sherif I.F., Ajit S. Narang, Keirnan LaMarche, Ganeshkumar Subramanian, and Sailesh A. Varia. 2012. 'Mechanistic Basis for the Effects of Process Parameters on Quality Attributes in High Shear Wet Granulation'. *International Journal of Pharmaceutics* 439 (1–2): 324–33. https://doi.org/10.1016/j.ijpharm.2012.09.011.

Badawy, Sherif, Tara J. Lee, and Michael Menning. 2000. 'Effect of Drug Substance Particle Size on the Characteristics of Granulation Manufactured in a High-Shear Mixer'. *AAPS PharmSciTech* 1 (February): E33. https://doi.org/10.1208/pt010433.

Bai, Yun, Grady Wagner, and Christopher B. Williams. 2017. 'Effect of Particle Size Distribution on Powder Packing and Sintering in Binder Jetting Additive Manufacturing of Metals'. *Journal of Manufacturing Science and Engineering* 139 (8). https://doi.org/10.1115/1.4036640.

Balaxi, Maria, Ioannis Nikolakakis, Kyriakos Kachrimanis, and Stavros Malamataris. 2009. 'Combined Effects of Wetting, Drying, and Microcrystalline Cellulose Type on the Mechanical Strength and Disintegration of Pellets'. *Journal of Pharmaceutical Sciences* 98 (2): 676–89. https://doi.org/10.1002/jps.21454.

Ban, Sander van den, and Daniel J. Goodwin. 2017. 'The Impact of Granule Density on Tabletting and Pharmaceutical Product Performance'. *Pharmaceutical Research* 34 (5): 1002–11. https://doi.org/10.1007/s11095-017-2115-5.

Banks, Darren, Cynthia Ajawara, Rafael Sanchez, Hamza Surti, and Guillermo Aguilar. 2014. 'Effect of Liquid and Surface Characteristics on Oscillation Behaviour of Droplets upon Impact'. *Atomization and Sprays* 24 (10). https://doi.org/10.1615/AtomizSpr.2014007590.

Barjat, H., S. Checkley, T. Chitu, N. Dawson, A. Farshchi, A. Ferreira, J. Gamble, et al. 2020. 'Demonstration of the Feasibility of Predicting the Flow of Pharmaceutically Relevant Powders from Particle and Bulk Physical Properties'. *Journal of Pharmaceutical Innovation*, February. https://eprints.whiterose.ac.uk/158693/.

Bauer, Hans H., and Marc Fischer. 2000. 'Product Life Cycle Patterns for Pharmaceuticals and Their Impact on R&D Profitability of Late Mover Products'. *International Business Review* 9 (6): 703–25. https://doi.org/10.1016/S0969-5931(00)00028-7.

Beer, Paul, David Wilson, Zhenyu Huang, and Marcel Matas. 2014. 'Transfer from High-Shear Batch to Continuous Twin Screw Wet Granulation: A Case Study in Understanding the Relationship Between Process Parameters and Product Quality Attributes'. *Journal of Pharmaceutical Sciences* 103 (October). https://doi.org/10.1002/jps.24078.

Bell, J. M., and F. K. Cameron. 1906. 'The Flow of Liquids through Capillary Spaces'. *The Journal of Physical Chemistry* 10 (8): 658–74. https://doi.org/10.1021/j150080a005.

Bernadiner, Mark G. 1998. 'A Capillary Microstructure of the Wetting Front'. *Transport in Porous Media* 30 (3): 251–65. https://doi.org/10.1023/A:1006571720867.

Berthier, Jean. 2013. 'Chapter 3 - The Physics of Droplets'. In *Micro-Drops and Digital Microfluidics*, edited by Jean Berthier, 2nd ed., 75–160. Micro and Nano Technologies. William Andrew Publishing. https://doi.org/10.1016/B978-1-4557-2550-2.00003-1.

Biance, Anne-Laure, Christophe Clanet, and David Quere. 2004. 'First Steps in the Spreading of a Liquid Droplet'. *Physical Review E* 69 (1). https://doi.org/10.1103/PhysRevE.69.016301.

Bico, J., C. Tordeux, and D. Quéré. 2001. 'Rough Wetting'. *EPL (Europhysics Letters)* 55 (2): 214. https://doi.org/10.1209/epl/i2001-00402-x.

Bird, James, Shreyas Mandre, and Howard A Stone. 2008. 'Short-Time Dynamics of Partial Wetting'. *Physical Review Letters* 100 (June): 234501. https://doi.org/10.1103/PhysRevLett.100.234501.

Blackburn, Timothy D., Thomas A. Mazzuchi, and Shahram Sarkani. 2011. 'Overcoming Inherent Limits to Pharmaceutical Manufacturing Quality Performance with QbD (Quality by Design)'. *Journal of Pharmaceutical Innovation* 6 (2): 69–76. https://doi.org/10.1007/s12247-011-9102-x.

Blagden, N., M. de Matas, P. T. Gavan, and P. York. 2007. 'Crystal Engineering of Active Pharmaceutical Ingredients to Improve Solubility and Dissolution Rates'. *Advanced Drug Delivery Reviews*, Drug Solubility: How to Measure it, How to Improve it, 59 (7): 617–30. https://doi.org/10.1016/j.addr.2007.05.011.

Boinovich, L B, and A M Emelyanenko. 2008. 'Hydrophobic Materials and Coatings: Principles of Design, Properties and Applications'. *Russian Chemical Reviews* 77 (7): 583–600. https://doi.org/10.1070/RC2008v077n07ABEH003775.

Bonn, Daniel, Jens Eggers, Joseph Indekeu, Jacques Meunier, and Etienne Rolley. 2009. 'Wetting and Spreading'. *Reviews of Modern Physics* 81 (2): 739–805. https://doi.org/10.1103/RevModPhys.81.739.

Börjesson, Erik, Fredrik Innings, Christian Trägårdh, Björn Bergenståhl, and Marie Paulsson. 2014. 'Evaluation of Particle Measures Relevant for Powder Bed Porosity—A Study of Spray Dried Dairy Powders'. *Powder Technology* 253 (February): 453–63. https://doi.org/10.1016/j.powtec.2013.11.050.

Börjesson, Erik, Jonathan Karlsson, Fredrik Innings, Christian Trägårdh, Björn Bergenståhl, and Marie Paulsson. 2017. 'Entrapment of Air during Imbibition of Agglomerated Powder Beds'. *Journal of Food Engineering* 201 (May): 26–35. https://doi.org/10.1016/j.jfoodeng.2017.01.004.

Bos, C.E., H. Vromans, and C.F. Lerk. 1991. 'Lubricant Sensitivity in Relation to Bulk Density for Granulations Based on Starch or Cellulose'. *International Journal of Pharmaceutics* 67 (1): 39–49. https://doi.org/10.1016/0378-5173(91)90263-N.

Bosanquet, C. H. 1923. 'LV. On the Flow of Liquids into Capillary Tubes'. *The London, Edinburgh, and Dublin Philosophical Magazine and Journal of Science*, 6, 45 (267): 525–31. https://doi.org/10.1080/14786442308634144.

Brown, Cameron, Thomas McGlone, Stephanie Yerdelen, Vijay Srirambhatla, Fraser Mabbott, Rajesh Gurung, Maria L. Briuglia, et al. 2018. 'Enabling Precision Manufacturing of Active Pharmaceutical Ingredients: Workflow for Seeded Cooling Continuous Crystallisations'. *Molecular Systems Design & Engineering* 3 (3): 518–49. https://doi.org/10.1039/C7ME00096K.

Bruil, H. G., and J. J. van Aartsen. 1974. 'The Determination of Contact Angles of Aqueous Surfactant Solutions on Powders'. *Colloid and Polymer Science* 252 (1): 32–38. https://doi.org/10.1007/BF01381692.

Bruttin, Frances, and Doug Dean. 2005. 'The Metamorphosis of Manufacturing: From Art to Science'. IBM Business Consulting Services. http://www-935.ibm.com/services/us/imc/pdf/ge510-4034-metamorphosis-of-manufacturing.pdf.

Buckton, G. 1990. 'Contact Angle, Adsorption and Wettability — a Review with Respect to Powders'. *Powder Technology* 61 (3): 237–49. https://doi.org/10.1016/0032-5910(90)80090-L.

Buckton, G., and J. M. Newton. 1985. 'Assessment of the Wettability and Surface Energy of a Pharmaceutical Powder by Liquid Penetration'. *The Journal of Pharmacy and Pharmacology* 37 (9): 605–9. https://doi.org/10.1111/j.2042-7158.1985.tb05094.x.

———. 1986. 'Assessment of the Wettability of Powders by Use of Compressed Powder Discs'. *Powder Technology* 46 (2): 201–8. https://doi.org/10.1016/0032-5910(86)80027-4.

Cabiscol, Ramon, Jan Henrik Finke, Harald Zetzener, and Arno Kwade. 2018. 'Characterization of Mechanical Property Distributions on Tablet Surfaces'. *Pharmaceutics* 10 (4). https://doi.org/10.3390/pharmaceutics10040184.

Calabrese, Gary S., and Sergio Pissavini. 2011. 'From Batch to Continuous Flow Processing in Chemicals Manufacturing'. *AIChE Journal* 57 (4): 828–34. https://doi.org/10.1002/aic.12598.

Carlin, Brian. 2009. 'Workshop IV: Understanding Drug-Excipient Interactions'. Powerpoint presented at the ExcipientFest. https://www.pharmaexcipients.com/wp-content/uploads/attachments/CarlinSlides_web.pdf?t=1494572190.

Carlson, Andreas, Gabriele Bellani, and Gustav Amberg. 2012. 'Universality in Dynamic Wetting Dominated by Contact-Line Friction'. *Physical Review. E, Statistical, Nonlinear, and Soft Matter Physics* 85 (4 Pt 2): 045302. https://doi.org/10.1103/PhysRevE.85.045302.

Carlson, Glenn, and Bruno Hancock. 2006. 'Physical and Mechanical Properties of Common Tableting Diluents'. In *Excipient Development for Pharmaceutical, Biotechnology, and Drug Delivery Systems*, 1st ed., 127–53. New York, USA: Informa healthcare. https://books.google.co.uk/books?id=_QVIS81xti8C&pg=PA150&lpg=PA150&dq=excipient+size+distribution+overlap&source=bl&ots=JcaNVn7zkK&sig=ACfU3U0ShOqJGES1wqTx0s-BhsQWPeeLRw&hl=en&sa=X&ved=2ahUKEwj35eL-x5znAhWmRhUIHd6iBDQQ6AEwAnoECAgQAQ#v=onepage&q=excipient%20size%20distribution%20overlap&f=false.

Carman, P. C. 1937. 'Fluid Flow through Granular Beds'. *American Institute of Chemical Engineers* 15 (May): 155–66. https://doi.org/10.1016/S0263-8762(97)80003-2.

Cassie, A. B. D., and S. Baxter. 1944. 'Wettability of Porous Surfaces'. *Transactions of the Faraday Society* 40 (0): 546–51. https://doi.org/10.1039/TF9444000546.

Cazabat, A. M., and M. A. Cohen-Stuart. 1986. 'Dynamics of Wetting: Effects of Surface Roughness'. *The Journal of Physical Chemistry* 90 (22): 5845–49. https://doi.org/10.1021/j100280a075.

CDER. 1995. 'Scale-up and Post Approval Changes Guidance for Immediate-Release Solid Oral Dosage Forms'. FDA. http://www.fda.gov/regulatory-information/search-fda-guidance-documents/supac-ir-immediate-release-solid-oral-dosage-forms-scale-and-post-approval-changes-chemistry.

———. 2004. 'Guidance for Industry PAT - A Framework for Innovative Pharmaceutical Development, Manufacturing, and Quality Assurance'. FDA. https://www.fda.gov/media/71012/download.

———. 2019. 'Quality Considerations for Continuous Manufacturing - Guidance for Industry (Draft Guidance)'. CDER. http://www.fda.gov/regulatory-information/search-fda-guidance-documents/quality-considerations-continuous-manufacturing.

Center for Drug Evaluation and Research and US Food & Drug Administration. 2017. 'Advancement of Emerging Technology Applications for Pharmaceutical Innovation and Modernization Guidance for Industry'. FDA-2015-D-4644. http://www.fda.gov/regulatory-information/search-fda-guidance-documents/advancement-emerging-technology-applications-pharmaceutical-innovation-and-modernization-guidance.

Chamakos, Nikolaos T., Michail E. Kavousanakis, Andreas G. Boudouvis, and Athanasios G. Papathanasiou. 2016. 'Droplet Spreading on Rough Surfaces: Tackling the Contact Line Boundary Condition'. *Physics of Fluids* 28 (2): 022105. https://doi.org/10.1063/1.4941577.

Chamarthy, Sai P., Rodolfo Pinal, and M. Teresa Carvajal. 2009. 'Elucidating Raw Material Variability—Importance of Surface Properties and Functionality in Pharmaceutical Powders'. *AAPS PharmSciTech* 10 (3). https://doi.org/10.1208/s12249-009-9267-5.

Chan Seem, Tim, Neil A. Rowson, Ian Gabbott, Marcel de Matas, Gavin K. Reynolds, and Andy Ingram. 2016. 'Asymmetric Distribution in Twin Screw Granulation'. *European Journal of Pharmaceutics and Biopharmaceutics*, 7th International Granulation Workshop: Granulation across the Length Scales, 106 (September): 50–58. https://doi.org/10.1016/j.ejpb.2016.01.013.

Charles-Williams, Heledd R., Robert Wengeler, Karin Flore, Herman Feise, Michael J. Hounslow, and Agba D. Salman. 2011. 'Granule Nucleation and Growth: Competing Drop Spreading and Infiltration Processes'. *Powder Technology*, 9th International Symposium on Agglomeration and 4th International Granulation Workshop, 2009, 206 (1): 63–71. https://doi.org/10.1016/j.powtec.2010.06.013.

Chatzis, I, and F. A. L Dullien. 1983. 'Dynamic Immiscible Displacement Mechanisms in Pore Doublets: Theory versus Experiment'. *Journal of Colloid and Interface Science* 91 (1): 199–222. https://doi.org/10.1016/0021-9797(83)90326-0.

Chen, Longquan, Günter K. Auernhammer, and Elmar Bonaccurso. 2011. 'Short Time Wetting Dynamics on Soft Surfaces'. *Soft Matter* 7 (19): 9084–89. https://doi.org/10.1039/C1SM05967J.

Chen, Longquan, and Elmar Bonaccurso. 2014a. 'Electrowetting — From Statics to Dynamics'. *Advances in Colloid and Interface Science*, Thin liquid films in wetting, spreading and surface interactions: a collection of papers presented at 6th Australian Colloid & Interface Symposium, 210 (August): 2–12. https://doi.org/10.1016/j.cis.2013.09.007.

———. 2014b. 'Effects of Surface Wettability and Liquid Viscosity on the Dynamic Wetting of Individual Drops'. *Physical Review E* 90 (2): 022401. https://doi.org/10.1103/PhysRevE.90.022401.

Chen, Longquan, Elmar Bonaccurso, Peigang Deng, and Haibo Zhang. 2016. 'Droplet Impact on Soft Viscoelastic Surfaces'. *Physical Review E* 94 (6): 063117. https://doi.org/10.1103/PhysRevE.94.063117.

Chen, Xue, Jiannan Chen, Xiaolong Ouyang, Yu Song, Ruina Xu, and Peixue Jiang. 2017. 'Water Droplet Spreading and Wicking on Nanostructured Surfaces'. *Langmuir* 33 (27): 6701–7. https://doi.org/10.1021/acs.langmuir.7b01223.

Chitu, T. M., D. Oulahna, and M. Hemati. 2011. 'Wet Granulation in Laboratory Scale High Shear Mixers: Effect of Binder Properties'. *Powder Technology*, 9th International Symposium on Agglomeration and 4th International Granulation Workshop, 2009, 206 (1): 25–33. https://doi.org/10.1016/j.powtec.2010.07.012.

Clarke, A., T. D. Blake, K. Carruthers, and A. Woodward. 2002. 'Spreading and Imbibition of Liquid Droplets on Porous Surfaces'. *Langmuir* 18 (8): 2980–84. https://doi.org/10.1021/la0117810.

CMAC. 2018. 'CMAC - Annual Review 2018'. CMAC. 2018. https://www.cmac.ac.uk/annual_reviews.htm.

Colón, Yleana M., Jenny Vargas, Eric Sánchez, Gilfredo Navarro, and Rodolfo J. Romañach. 2017. 'Assessment of Robustness for a Near-Infrared Concentration Model for Real-Time Release Testing in a Continuous Manufacturing Process'. *Journal of Pharmaceutical Innovation* 12 (1): 14–25. https://doi.org/10.1007/s12247-016-9265-6.

Conway, Barbara R., and Shayne Cox Gad. 2007. 'Section 8.1 - Solid Dosage Forms'. In *Pharmaceutical Manufacturing Handbook: Production and Processes*, 223–65. https://onlinelibrary.wiley.com/doi/book/10.1002/9780470259818.

Crick, Colin R., and Ivan P. Parkin. 2010. 'Preparation and Characterisation of Super-Hydrophobic Surfaces'. *Chemistry – A European Journal* 16 (12): 3568–88. https://doi.org/10.1002/chem.200903335.

C-SOPS. 2017. 'C-SOPS Brochure 2017'. C-SOPS. 2017. https://simplebooklet.com/csopsbrochure2017.

Dai, Shu-hua, Feng-man Shen, and Ai-bing Yu. 2008. 'Granule Size Distribution and Porosity of Granule Packing'. *Journal of Iron and Steel Research International* 15 (5): 1–5. https://doi.org/10.1016/S1006-706X(08)60238-1.

Dang-Vu, T., and J. Hupka. 2005. 'Characterization of Porous Materials by Capillary Rise Method'. *Physicochemical Problems of Mineral Processing* Vol. 39: 47–65.

Das, Saurish, H. V. Patel, E. Milacic, N. G. Deen, and J. A. M. Kuipers. 2018. 'Droplet Spreading and Capillary Imbibition in a Porous Medium: A Coupled IB-VOF Method Based Numerical Study'. *Physics of Fluids* 30 (1): 012112. https://doi.org/10.1063/1.5010716.

Datta, Sharmistha, and David J. W. Grant. 2004. 'Crystal Structures of Drugs: Advances in Determination, Prediction and Engineering'. *Nature Reviews Drug Discovery* 3 (1): 42–57. https://doi.org/10.1038/nrd1280.

Dave, Rutesh H., Stephen H. Wu, and Labdhi D. Contractor. 2012. 'To Determine the End Point of Wet Granulation by Measuring Powder Energies and Thermal Properties'. *Drug Development and Industrial Pharmacy* 38 (4): 439–46. https://doi.org/10.3109/03639045.2011.609561.

Dave, Vivek, Suprit Saoji, Nishikant Raut, and Rahul Haware. 2015. 'Excipient Variability and Its Impact on Dosage Form Functionality'. *Journal of Pharmaceutical Sciences* 104 (3): 906–15. https://doi.org/10.1002/jps.24299.

Davio, Kelly. 2018. 'FDA Approves Symdeko to Treat the Underlying Cause of Cystic Fibrosis'. AJMC. 18 February 2018. https://www.ajmc.com/newsroom/fda-approves-symdeko-to-treat-the-underlying-cause-of-cystic-fibrosis.

Davis, Nathan B., Karis Waibel, Kelly Wang, and James D. Litster. 2017. 'Microstructure of Single-Droplet Granules Formed from Ultra-Fine Powders'. *Powder Technology* 305 (January): 19–26. https://doi.org/10.1016/j.powtec.2016.09.033.

Debnath, N., L.Q. Al-Mawsawi, and N. Neamati. 2010. 'Are We Living in the End of the Blockbuster Drug Era?' *Drug News & Perspectives* 23 (10): 670. https://doi.org/10.1358/dnp.2010.23.10.1506088.

Denesuk, M., G. L. Smith, B. J. J. Zelinski, N. J. Kreidl, and Donald R. Uhlmann. 1993. 'Capillary Penetration of Liquid Droplets into Porous Materials'. *Journal of Colloid and Interface Science* 158 (1): 114–20. https://doi.org/10.1006/jcis.1993.1235.

Depalo, Andrea, and Andrea C. Santomaso. 2013. 'Wetting Dynamics and Contact Angles of Powders Studied through Capillary Rise Experiments'. *Colloids and Surfaces A: Physicochemical and Engineering Aspects* 436 (September): 371–79. https://doi.org/10.1016/j.colsurfa.2013.06.040.

Desai, Parind Mahendrakumar, Patrick Xuan Hua Er, Celine Valeria Liew, and Paul Wan Sia Heng. 2014. 'Functionality of Disintegrants and Their Mixtures in Enabling Fast Disintegration of Tablets by a Quality by Design Approach'. *AAPS PharmSciTech* 15 (5): 1093–1104. https://doi.org/10.1208/s12249-014-0137-4.

Desai, Parind Mahendrakumar, Celine Valeria Liew, and Paul Wan Sia Heng. 2012. 'Understanding Disintegrant Action by Visualization'. *Journal of Pharmaceutical Sciences* 101 (6): 2155–64. https://doi.org/10.1002/jps.23119.

Dhenge, Ranjit, James Cartwright, Michael J Hounslow, and Agba D Salman. 2012. 'Twin Screw Granulation: Steps in Granule Growth'. *International Journal of Pharmaceutics* 438 (September): 20–32. https://doi.org/10.1016/j.ijpharm.2012.08.049.

Dhenge, Ranjit, James Cartwright, Michael J. Hounslow, and Agba D. Salman. 2012. 'Twin Screw Wet Granulation: Effects of Properties of Granulation Liquid'. *Powder Technology* 229 (October): 126–36. https://doi.org/10.1016/j.powtec.2012.06.019.

Dhenge, Ranjit M., James J. Cartwright, David G. Doughty, Michael J. Hounslow, and Agba D. Salman. 2011. 'Twin Screw Wet Granulation: Effect of Powder Feed Rate'. *Advanced Powder Technology*, Special issue of the 6th World Congress on Particle Technology, 22 (2): 162–66. https://doi.org/10.1016/j.apt.2010.09.004.

Dhenge, Ranjit M., Richard S. Fyles, James J. Cartwright, David G. Doughty, Michael J. Hounslow, and Agba D. Salman. 2010. 'Twin Screw Wet Granulation: Granule Properties'. *Chemical Engineering Journal*, Pharmaceutical Granulation and Processing, 164 (2): 322–29. https://doi.org/10.1016/j.cej.2010.05.023.

Dhenge, Ranjit M., Kimiaki Washino, James J. Cartwright, Michael J. Hounslow, and Agba D. Salman. 2013. 'Twin Screw Granulation Using Conveying Screws: Effects of Viscosity of Granulation Liquids and Flow of Powders'. *Powder Technology*, Special Issue: 5th International Granulation Workshop Granulation across the length scale 2011, 238 (April): 77–90. https://doi.org/10.1016/j.powtec.2012.05.045.

Djuric, D., B. Van Melkebeke, P. Kleinebudde, J. P. Remon, and C. Vervaet. 2009. 'Comparison of Two Twin-Screw Extruders for Continuous Granulation'. *European Journal of Pharmaceutics and Biopharmaceutics: Official Journal of Arbeitsgemeinschaft Fur Pharmazeutische Verfahrenstechnik e.V* 71 (1): 155–60. https://doi.org/10.1016/j.ejpb.2008.06.033.

Djuric, Dejan, and Peter Kleinebudde. 2008. 'Impact of Screw Elements on Continuous Granulation with a Twin-Screw Extruder'. *Journal of Pharmaceutical Sciences* 97 (11): 4934–42. https://doi.org/10.1002/jps.21339.

———. 2010. 'Continuous Granulation with a Twin-Screw Extruder: Impact of Material Throughput'. *Pharmaceutical Development and Technology* 15 (5): 518–25. https://doi.org/10.3109/10837450903397578.

Doelker, E. 1993. 'Comparative Compaction Properties of Various Microcrystalline Cellulose Types and Generic Products'. *Drug Development and Industrial Pharmacy* 19 (17–18): 2399–2471. https://doi.org/10.3109/03639049309047196.

Dream, Robert. 2017. 'Continuous Manufacturing Progress and the Bio/Pharmaceutical Industry "Reality or Fad"'. *American Pharmaceutical Review* 20 (5). http://www.americanpharmaceuticalreview.com/Featured-Articles/341193-Continuous-Manufacturing-Progress-and-the-Bio-Pharmaceutical-Industry-Reality-or-Fad/.

Dries, K. van den, and H. Vromans. 2002. 'Relationship between Inhomogeneity Phenomena and Granule Growth Mechanisms in a High-Shear Mixer'. *International Journal of Pharmaceutics* 247 (1–2): 167–77. https://doi.org/10.1016/s0378-5173(02)00419-2.

Dries, Kaspar van den, and Herman Vromans. 2003. 'Experimental and Modelistic Approach to Explain Granulate Inhomogeneity through Preferential Growth'. *European Journal of Pharmaceutical Sciences: Official Journal of the European Federation for Pharmaceutical Sciences* 20 (4–5): 409–17. https://doi.org/10.1016/j.ejps.2003.09.002.

Eddi, A., K. G. Winkels, and J. H. Snoeijer. 2013. 'Short Time Dynamics of Viscous Drop Spreading'. *Physics of Fluids* 25 (1): 013102. https://doi.org/10.1063/1.4788693.

Edge, S, A Kibbe, and K Kussendrager. 2006. 'Lactose, Monohydrate'. In *Handbook of Pharmaceutical Excipients*, edited by R. C. Rowe, P. J. Sheskey, and S. C. Owen, 5th ed., 18:389–95. Pharmaceutical Press. https://doi.org/10.3109/10837450.2012.751408.

efpia. 2018. '2018: The Pharmaceutical Industry in Figures - The Pharmaceutical Industry: A Key Asset to Scientific and Medical Progress'. Europen Federation of Pharmaceutical Industries and Associations. https://efpia.eu/publications/downloads/efpia/2018-the-pharmaceutical-industry-in-figures/.

El Hagrasy, A. S., and J. D. Litster. 2013. 'Granulation Rate Processes in the Kneading Elements of a Twin Screw Granulator'. *AIChE Journal* 59 (11): 4100–4115. https://doi.org/10.1002/aic.14180.

El Hagrasy, Arwa, P Cruise, I Jones, and J Litster. 2013. 'In-Line Size Monitoring of a Twin Screw Granulation Process Using High-Speed Imaging'. *Journal of Pharmaceutical Innovation* 8 (June). https://doi.org/10.1007/s12247-013-9149-y.

El Hagrasy, Arwa, Jeff Hennenkamp, Matthew Burke, James Cartwright, and J Litster. 2013. 'Twin Screw Wet Granulation: Influence of Formulation Parameters on Granule Properties and Growth Behavior'. *Powder Technology* 238 (April): 108–15. https://doi.org/10.1016/j.powtec.2012.04.035.

El Hagrasy, Arwa, and J Litster. 2013. 'Granulation Rate Processes in the Kneading Elements of a Twin Screw Granulator'. *AIChE Journal* 59 (November). https://doi.org/10.1002/aic.14180.

El-Zhry El-Yafi, Abdul Khaliq, and Hind El-Zein. 2015. 'Technical Crystallization for Application in Pharmaceutical Material Engineering: Review Article'. *Asian Journal of Pharmaceutical Sciences* 10 (4): 283–91. https://doi.org/10.1016/j.ajps.2015.03.003.

Emady, Heather, Defne Kayrak-Talay, William C. Schwerin, and James D. Litster. 2011. 'Granule Formation Mechanisms and Morphology from Single Drop Impact on Powder Beds'. *Powder Technology* 212 (1): 69–79. https://doi.org/10.1016/j.powtec.2011.04.030.

Emady, Heather N., Defne Kayrak-Talay, and James D. Litster. 2013. 'A Regime Map for Granule Formation by Drop Impact on Powder Beds'. *AIChE Journal* 59 (1): 96–107. https://doi.org/10.1002/aic.13952.

Emady, Heather N., Defne Kayrak-Talay, and James D. Litster. 2013. 'Modeling the Granule Formation Mechanism from Single Drop Impact on a Powder Bed'. *Journal of Colloid and Interface Science* 393 (March): 369–76. https://doi.org/10.1016/j.jcis.2012.10.038.

Eriksson, L, E Johansson, N Kettaneh-Wold, C WikstrÄom, and S Wold. 2008. *Design of Experiments: Principles and Applications*. 3rd ed. Umetrics AB.

Eriksson, M., and G. Alderborn. 1995. 'The Effect of Particle Fragmentation and Deformation on the Interparticulate Bond Formation Process during Powder Compaction'. *Pharmaceutical Research* 12 (7): 1031–39. https://doi.org/10.1023/a:1016214616042.

Esezobo, S., and N. Pilpel. 1976. 'Some Formulation Factors Affecting the Tensile Strength, Disintegration and Dissolution of Uncoated Oxytetracycline Tablets'. *Journal of*

Pharmacy and Pharmacology 28 (1): 8–16. https://doi.org/10.1111/j.2042-7158.1976.tb04015.x.

Eshtiaghi, Nicky, Jacques S. Liu, Wei Shen, and Karen P. Hapgood. 2009. 'Liquid Marble Formation: Spreading Coefficients or Kinetic Energy?' *Powder Technology* 196 (2): 126–32. https://doi.org/10.1016/j.powtec.2009.07.002.

EudraLex. 2011. 'Chapter 4 - Good Manufacturing Practice (GMP) Guidelines'. European Commission. Volume 4. The Rules Governing Medicinal Products in the European Union. https://ec.europa.eu/health/documents/eudralex/vol-4_en.

European Commission, and Bayer Tehnology Services GmBH. 2013. 'Final Report Summary - F^3 Factory (Flexible, Fast and Future Production Processes)'. European Community's Seventh Framework Programme. https://cordis.europa.eu/project/id/228867/reporting.

EvaluatePharma. 2018. 'EvaluatePharma World Preview 2018, Outlook to 2024'. 11th Edition. Evaluate. https://www.evaluate.com/thought-leadership/pharma/evaluatepharma-world-preview-2018-outlook-2024.

Ewsuk, K. G. 2001. 'Powder Granulation and Compaction'. In *Encyclopedia of Materials: Science and Technology*, edited by K. H. Jürgen Buschow, Robert W. Cahn, Merton C. Flemings, Bernhard Ilschner, Edward J. Kramer, Subhash Mahajan, and Patrick Veyssière, 7788–7800. Oxford: Elsevier. https://doi.org/10.1016/B0-08-043152-6/01401-7.

Faqih, AbdulMobeen, Bodhisattwa Chaudhuri, Fernando J. Muzzio, M. Silvina Tomassone, Albert Alexander, and Steve Hammond. 2006. 'Flow-Induced Dilation of Cohesive Granular Materials'. *AIChE Journal* 52 (12): 4124–32. https://doi.org/10.1002/aic.11014.

Faure, A, P York, and R C Rowe. 2001. 'Process Control and Scale-up of Pharmaceutical Wet Granulation Processes: A Review'. *European Journal of Pharmaceutics and Biopharmaceutics* 52 (3): 269–77. https://doi.org/10.1016/S0939-6411(01)00184-9.

Fedors, R.F., and R.F. Landel. 1979. 'An Empirical Method of Estimating the Void Fraction in Mixtures of Uniform Particles of Different Size'. *Powder Technology* 23 (2): 225–31. https://doi.org/10.1016/0032-5910(79)87011-4.

Florence, Alastair. 2017. 'CMAC: A Partnership Approach to Precompetitive Collaboration for Pharmaceutical Manufacturing Research'. In . Minneapolis. https://www.aiche.org/conferences/aiche-annual-meeting/2017/proceeding/paper/500d-cmac-partnership-approach-precompetitive-collaboration-pharmaceutical-manufacturing-research.

Fogler, H. Scott. 2006. 'Chapter 16 - Distribution of Residence Time'. In *Elements of Chemical Reaction Engineering*, 4th ed. Prentice-Hall International Series in the Physical and Chemical Engineering Sciences. Boston: Pearson.

Fonteyne, Margot, Ana Correia, Sofie De Plecker, Jurgen Vercruysse, Ilija Ilić, Qi Zhou, Chris Vervaet, et al. 2014. 'Impact of Microcrystalline Cellulose Material Attributes: A Case Study on Continuous Twin Screw Granulation'. *International Journal of Pharmaceutics* 478 (December). https://doi.org/10.1016/j.ijpharm.2014.11.070.

Fonteyne, Margot, Sandra Soares, Jurgen Vercruysse, Elisabeth Peeters, Anneleen Burggraeve, Chris Vervaet, Jean Remon, Niklas Sandler, and Thomas De Beer. 2012. 'Prediction of Quality Attributes of Continuously Produced Granules Using Complementary Pat Tools'. *European Journal of Pharmaceutics and Biopharmaceutics : Official Journal of Arbeitsgemeinschaft Für Pharmazeutische*

Verfahrenstechnik e.V 82 (August): 429–36. https://doi.org/10.1016/j.ejpb.2012.07.017.

Fonteyne, Margot, Jurgen Vercruysse, Damián Córdoba Díaz, Delphine Gildemyn, Chris Vervaet, Jean Paul Remon, and Thomas De Beer. 2013. 'Real-Time Assessment of Critical Quality Attributes of a Continuous Granulation Process'. *Pharmaceutical Development and Technology* 18 (1): 85–97. https://doi.org/10.3109/10837450.2011.627869.

Fonteyne, Margot, Henrika Wickström, Elisabeth Peeters, Jurgen Vercruysse, Henrik Ehlers, Björn-Hendrik Peters, Jean Paul Remon, et al. 2014. 'Influence of Raw Material Properties upon Critical Quality Attributes of Continuously Produced Granules and Tablets'. *European Journal of Pharmaceutics and Biopharmaceutics* 87 (2): 252–63. https://doi.org/10.1016/j.ejpb.2014.02.011.

Food and Drug Administration. 1997. 'Guidance for Industry: Dissolution Testing of Immediate Release Solid Oral Dosage Forms'. Centre for Drug Evaluation and Research.

Forlano, Albert J., and Leonard Chavkin. 1960. 'The Effect of Granule Size Upon Disintegration Time and Capping in Compressed Tablets**Received June 30, 1958 from the Ohio State University, Columbus 10.' *Journal of the American Pharmaceutical Association (Scientific Ed.)* 49 (2): 67–69. https://doi.org/10.1002/jps.3030490203.

Frank, Xavier, Patrick Perre, and Huai Li. 2015. 'Lattice Boltzmann Investigation of Droplet Inertial Spreading on Various Porous Surfaces'. *Phys. Rev. E* 91 (May): 052405. https://doi.org/10.1103/PhysRevE.91.052405.

Fu, Xiaowei, Deborah Huck, Lisa Makein, Brian Armstrong, Ulf Willen, and Tim Freeman. 2012. 'Effect of Particle Shape and Size on Flow Properties of Lactose Powders'. *Particuology*, Advances in Characterization and Modeling of Particulate Processes, 10 (2): 203–8. https://doi.org/10.1016/j.partic.2011.11.003.

Fulchini, Fabio, Umair Zafar, Colin Hare, Mojtaba Ghadiri, Hossam Tantawy, Hossein Ahmadian, and Massimo Poletto. 2017. 'Relationship between Surface Area Coverage of Flow-Aids and Flowability of Cohesive Particles'. *Powder Technology* 322 (December): 417–27. https://doi.org/10.1016/j.powtec.2017.09.013.

Furnas, C. C. 1931. 'Grading Aggregates - I. - Mathematical Relations for Beds of Broken Solids of Maximum Density'. *Industrial & Engineering Chemistry* 23 (9): 1052–58. https://doi.org/10.1021/ie50261a017.

Furnas, Clifford C. 1930. 'Flow of Gases through Beds of Broken Solids'. *Journal of the Franklin Institute* 209 (2): 269–70. https://doi.org/10.1016/S0016-0032(30)91076-9.

Gaffney, Alexander. 2014. 'Number of Drug Recalls Surges at FDA'. Regulatory Affairs Professionals Service. https://www.raps.org/regulatory-focus™/news-articles/2014/8/number-of-drug-recalls-surges-at-fda,-led-by-mid-level-concerns.

Galet, Laurence, Severine Patry, and John Dodds. 2010. 'Determination of the Wettability of Powders by the Washburn Capillary Rise Method with Bed Preparation by a Centrifugal Packing Technique'. *Journal of Colloid and Interface Science* 346 (2): 470–75. https://doi.org/10.1016/j.jcis.2010.02.051.

Galichet, L. Y. 2006. 'Cellulose, Microcrystalline'. In *Handbook of Pharmaceutical Excipients*, edited by R. C. Rowe, P. J. Sheskey, and S. C. Owen, 5th ed., 132–35. Pharmaceutical Press. https://doi.org/10.3109/10837450.2012.751408.

Gamble, John, Wing Sin Chiu, Vivienne Gray, Helen Toale, Mike Tobyn, and Y. M. Wu. 2010. 'Investigation into the Degree of Variability in the Solid-State Properties of Common Pharmaceutical Excipients—Anhydrous Lactose'. *AAPS PharmSciTech* 11 (October): 1552–57. https://doi.org/10.1208/s12249-010-9527-4.

Gamble, John, Andrew Dennis, and Mike Tobyn. 2009. 'Monitoring and End-Point Prediction of a Small Scale Wet Granulation Process Using Acoustic Emission'. *Pharmaceutical Development and Technology* 14 (February): 299–304. https://doi.org/10.1080/10837450802603618.

Gamble, John F., Wing-Sin Chiu, and Mike Tobyn. 2011. 'Investigation into the Impact of Sub-Populations of Agglomerates on the Particle Size Distribution and Flow Properties of Conventional Microcrystalline Cellulose Grades'. *Pharmaceutical Development and Technology* 16 (5): 542–48. https://doi.org/10.3109/10837450.2010.495395.

Gamlen, M. J., and C. Eardley. 1986. 'Continuous Extrusion Using a Raker Perkins MP50 (Multipurpose) Extruder'. *Drug Development and Industrial Pharmacy* 12 (11–13): 1701–13. https://doi.org/10.3109/03639048609042604.

Gauss, C.F. 1831. 'Besprechung des Buchs von L. A. Seeber: Intersuchungen über die Eigenschaften der positiven ternären quadratischen Formen usw'. *Göttingsche Gelehrte Anzeigen* 2 (July): 188–96.

GEA-Siemens. 2020. 'ConsiGma™ Continuous Tableting Line'. GEA Engineering for a Better World. 2020. http://www.gea.com/en/products/consigma-ctl.jsp.

Gennes, P. G. de. 1985. 'Wetting: Statics and Dynamics'. *Reviews of Modern Physics* 57 (3): 827–63. https://doi.org/10.1103/RevModPhys.57.827.

Gibson, Shannon, Hamid R Raziee, and Trudo Lemmens. 2015. 'Why the Shift? Taking a Closer Look at the Growing Interest in Niche Markets and Personalized Medicine'. *World Medical & Health Policy* 7 (1): 3–27. https://doi.org/10.1002/wmh3.131.

Gilbert, J, P Henske, and A Singh. 2003. 'Rebuilding Big Pharma's Business Model'. *In Vivo: The Business & Medicine Report* 21 (10): 1–10.

Goh, Hui Ping, Paul Wan Sia Heng, and Celine Valeria Liew. 2018. 'Comparative Evaluation of Powder Flow Parameters with Reference to Particle Size and Shape'. *International Journal of Pharmaceutics* 547 (1–2): 133–41. https://doi.org/10.1016/j.ijpharm.2018.05.059.

Gold, Gerald, Ronald N. Duvall, Blaze T. Palermo, and James G. Slater. 1966. 'Powder Flow Studies II: Effect of Glidants on Flow Rate and Angle of Repose'. *Journal of Pharmaceutical Sciences* 55 (11): 1291–95. https://doi.org/10.1002/jps.2600551125.

Gorringe, L.J., G.S. Kee, M.F. Saleh, N.H. Fa, and R.G. Elkes. 2017. 'Use of the Channel Fill Level in Defining a Design Space for Twin Screw Wet Granulation'. *International Journal of Pharmaceutics* 519 (January). https://doi.org/10.1016/j.ijpharm.2017.01.029.

Gorsek, A, and P Glavic. 1997. 'Design of Batch Versus Continuous Processes Chemical Engineering Research and Design, 75(7), 709–717 | 10.1205/026387697524209'. *Chemical Engineering Research and Design* 75 (7): 709–17.

Gottlieb, Scott, and Janet Woodcock. 2019. 'FDA Statement on FDA's Modern Approach to Advanced Pharmaceutical Manufacturing', 26 February 2019. http://www.fda.gov/news-events/press-announcements/fda-statement-fdas-modern-approach-advanced-pharmaceutical-manufacturing.

Grewal, H. S., Hong Nam Kim, Il-Joo Cho, and Eui-Sung Yoon. 2015. 'Role of Viscous Dissipative Processes on the Wetting of Textured Surfaces'. *Scientific Reports* 5 (September): 14159. https://doi.org/10.1038/srep14159.

Grzelakowski, C., D. Ben Jazia, B. Lebeau, L. Vonna, D. Dupuis, and H. Haidara. 2009. 'On the Influence of Pore Structure on the Free-Imbibition of Sessile Drops into Nanoporous Substrates'. *Langmuir* 25 (10): 5855–60. https://doi.org/10.1021/la803465u.

Gutmann, Bernhard, David Cantillo, and C. Oliver Kappe. 2015. 'Continuous-Flow Technology-A Tool for the Safe Manufacturing of Active Pharmaceutical Ingredients'. *Angewandte Chemie International Edition* 54 (23): 6688–6728. https://doi.org/10.1002/anie.201409318.

Haidara, H., B. Lebeau, C. Grzelakowski, L. Vonna, F. Biguenet, and L. Vidal. 2008. 'Competitive Spreading versus Imbibition of Polymer Liquid Drops in Nanoporous Membranes: Scaling Behavior with Viscosity'. *Langmuir* 24 (8): 4209–14. https://doi.org/10.1021/la703538g.

Hamaker, H. C. 1937. 'The London—van Der Waals Attraction between Spherical Particles'. *Physica* 4 (10): 1058–72. https://doi.org/10.1016/S0031-8914(37)80203-7.

Han, Yu. 2017. 'Droplet Penetration Method as a Wettability Test for Pharmaceutical Powders'. Master of Science, New Jersey: Rutgers, The State University of New Jersey.

Hapgood, Karen, Ria Amelia, Mohammad B. Zaman, Bryan K. Merrett, and Philip Leslie. 2010. 'Improving Liquid Distribution by Reducing Dimensionless Spray Flux in Wet Granulation—A Pharmaceutical Manufacturing Case Study'. *Chemical Engineering Journal* 164 (November): 340–49. https://doi.org/10.1016/j.cej.2010.05.007.

Hapgood, Karen P. 2000. 'Nucleation and Binder Dispersion in Wet Granulation'. PhD Thesis. University of Queensland.

Hapgood, Karen P., and Batool Khanmohammadi. 2009. 'Granulation of Hydrophobic Powders'. *Powder Technology*, Special Issue: 3rd International Workshop on Granulation: Granulation across the Length Scales, 189 (2): 253–62. https://doi.org/10.1016/j.powtec.2008.04.033.

Hapgood, Karen P., James D. Litster, Simon R. Biggs, and Tony Howes. 2002. 'Drop Penetration into Porous Powder Beds'. *Journal of Colloid and Interface Science* 253 (2): 353–66. https://doi.org/10.1006/jcis.2002.8527.

Hapgood, Karen P., James D. Litster, and Rachel Smith. 2003. 'Nucleation Regime Map for Liquid Bound Granules'. *AIChE Journal* 49 (2): 350–61. https://doi.org/10.1002/aic.690490207.

Hapgood, Karen P., Thanh H. Nguyen, Sunarko Hauw, Simon M. Iveson, and Wei Shen. 2009. 'Rewetting Effects and Droplet Motion on Partially Wetted Powder Surfaces'. *AIChE Journal* 55 (6): 1402–15. https://doi.org/10.1002/aic.11772.

Harrington, Tomás S., Mark A. Phillips, and Jagjit Singh Srai. 2017. 'Reconfiguring Global Pharmaceutical Value Networks through Targeted Technology Interventions'. *International Journal of Production Research* 55 (5): 1471–87. https://doi.org/10.1080/00207543.2016.1221541.

Harrison, Richard P., Steven Ruck, Qasim A. Rafiq, and Nicholas Medcalf. 2018. 'Decentralised Manufacturing of Cell and Gene Therapy Products: Learning from Other Healthcare Sectors'. *Biotechnology Advances* 36 (2): 345–57. https://doi.org/10.1016/j.biotechadv.2017.12.013.

Haware, Rahul V., Ingunn Tho, and Annette Bauer-Brandl. 2010. 'Evaluation of a Rapid Approximation Method for the Elastic Recovery of Tablets'. *Powder Technology* 202 (1–3): 71–77. https://doi.org/10.1016/j.powtec.2010.04.012.

Hilpert, Markus, and Avishai Ben-David. 2009. 'Infiltration of Liquid Droplets into Porous Media: Effects of Dynamic Contact Angle and Contact Angle Hysteresis'. *International Journal of Multiphase Flow* 35 (3): 205–18. https://doi.org/10.1016/j.ijmultiphaseflow.2008.11.007.

Holm, Per, Torben Schaefer, and Crilles Larsen. 2001. 'End-Point Detection in a Wet Granulation Process'. *Pharmaceutical Development and Technology* 6 (2): 181–92. https://doi.org/10.1081/PDT-100000739.

Holm, René, Simon Borkenfelt, Morten Allesø, Jens Enevold Thaulov Andersen, Stefania Beato, and Per Holm. 2016. 'Investigation of Surface Porosity Measurements and Compaction Pressure as Means to Ensure Consistent Contact Angle Determinations'. *International Journal of Pharmaceutics* 498 (1–2): 355–61. https://doi.org/10.1016/j.ijpharm.2015.12.022.

Holman, Richard K., Michael J. Cima, Scott A. Uhland, and Emanuel Sachs. 2002. 'Spreading and Infiltration of Inkjet-Printed Polymer Solution Droplets on a Porous Substrate'. *Journal of Colloid and Interface Science* 249 (2): 432–40. https://doi.org/10.1006/jcis.2002.8225.

Horisawa, E., K. Danjo, and H. Sunada. 2000. 'Influence of Granulating Method on Physical and Mechanical Properties, Compression Behavior, and Compactibility of Lactose and Microcrystalline Cellulose Granules'. *Drug Development and Industrial Pharmacy* 26 (6): 583–93. https://doi.org/10.1081/ddc-100101273.

Horsthuis, G. J. B., J. A. H. van Laarhoven, R. C. B. M. van Rooij, and H. Vromans. 1993. 'Studies on Upscaling Parameters of the Gral High Shear Granulation Process'. *International Journal of Pharmaceutics* 92 (1): 143–50. https://doi.org/10.1016/0378-5173(93)90273-I.

Hosseini, Saman. 2015. 'Droplet Impact and Penetration onto Structured Pore Network Geometries'. PhD, Toronto, Canada: University of Toronto.

Hughes, Helen, Michael M. Leane, Michael Tobyn, John F. Gamble, Santiago Munoz, and Pauline Musembi. 2014. 'Development of a Material Sparing Bulk Density Test Comparable to a Standard USP Method for Use in Early Development of API's'. *AAPS PharmSciTech* 16 (1): 165–70. https://doi.org/10.1208/s12249-014-0215-7.

ICH. 2003. 'M4Q Common Technical Document for the Registration of Pharmaceuticals Human Use - Quality'. European Medicines Agency. https://www.ema.europa.eu/en/ich-m4q-common-technical-document-registration-pharmaceuticals-human-use-quality.

———. 2005. 'Q9: Quality Risk Management'. Quality Guideline Q9. International Conference on Harmonisation. https://www.ich.org/products/guidelines/quality/article/quality-guidelines.html.

———. 2008. 'Q10: Pharmaceutical Quality System'. Quality Guideline Q10. International Conference on Harmonisation.

———. 2009. 'Q8(R2): Pharmaceutical Development'. Quality Guideline Q8(R2). International Conference on Harmonisation. https://www.ich.org/products/guidelines/quality/quality-single/article/pharmaceutical-development.html.

———. 2012. 'Q11: Development and Manufacture of Drug Substances'. Quality Guideline Q11. International Conference on Harmonisation.

———. 2018. ‘Q13: Continuous Manufacturing of Drug Substances and Drug Products’. Quality Guideline 13. International Conference on Harmonisation. https://www.ich.org/products/guidelines/quality/quality-single/article/technical-and-regulatory-considerations-for-pharmaceutical-product-lifecycle-management-copy-1.html.

International Conference on Harmonisation. 2009. ‘Q8(R2): Pharmaceutical Development’. Quality Guideline Q8(R2). International Conference on Harmonisation. https://www.ich.org/products/guidelines/quality/quality-single/article/pharmaceutical-development.html.

IPEC. 2008. ‘Qualification of Excipients for Use in Pharmaceuticals’. International Pharmaceutical Excipients Council.

Ishino, C., M. Reyssat, E. Reyssat, K. Okumura, and D. Quéré. 2007. ‘Wicking within Forests of Micropillars’. *Europhysics Letters (EPL)* 79 (5): 56005. https://doi.org/10.1209/0295-5075/79/56005.

Israelachvili, Jacob N. 1989. *Intermolecular and Surface Forces*. 1st ed. Elsevier. https://doi.org/10.1016/C2011-0-05119-0.

Iveson, S. M., and J. D. Litster. 1998a. ‘Growth Regime Map for Liquid-Bound Granules’. *AIChE Journal* 44 (7): 1510–18. https://doi.org/10.1002/aic.690440705.

———. 1998b. ‘Fundamental Studies of Granule Consolidation Part 2: Quantifying the Effects of Particle and Binder Properties’. *Powder Technology* 99 (3): 243–50. https://doi.org/10.1016/S0032-5910(98)00116-8.

Iveson, Simon, J Litster, Karen Hapgood, and Bryan J. Ennis. 2001. ‘Nucleation, Growth and Breakage Phenomena in Agitated Wet Granulation Processes: A Review’. *Powder Technology* 117 (1–2). https://doi.org/10.1016/S0032-5910(01)00313-8.

Järnström, J., M. Väisänen, R. Lehto, A. Jäsberg, J. Timonen, and J. Peltonen. 2010. ‘Effect of Latex on Surface Structure and Wetting of Pigment Coatings’. *Colloids and Surfaces A: Physicochemical and Engineering Aspects* 353 (2): 104–16. https://doi.org/10.1016/j.colsurfa.2009.11.001.

Johansson, Barbro, Fredrik Nicklasson, and Göran Alderborn. 1998. ‘Effect of Pellet Size on Degree of Deformation and Densification during Compression and on Compactability of Microcrystalline Cellulose Pellets’. *International Journal of Pharmaceutics* 163 (1): 35–48. https://doi.org/10.1016/S0378-5173(97)00355-4.

Johansson, Mats E., and Martin Nicklasson. 1986. ‘Investigation of the Film Formation of Magnesium Stearate by Applying a Flow-through Dissolution Technique’. *Journal of Pharmacy and Pharmacology* 38 (1): 51–54. https://doi.org/10.1111/j.2042-7158.1986.tb04466.x.

Jopp, Jürgen, Holger Grüll, and Rachel Yerushalmi-Rozen. 2004. ‘Wetting Behavior of Water Droplets on Hydrophobic Microtextures of Comparable Size’. *Langmuir* 20 (23): 10015–19. https://doi.org/10.1021/la0497651.

Jurin, James. 1719. ‘II. An Account of Some Experiments Shown before the Royal Society; with an Enquiry into the Cause of the Ascent and Suspension of Water in Capillary Tubes.’ *Philosophical Transactions of the Royal Society of London* 30 (355): 739–47. https://doi.org/10.1098/rstl.1717.0026.

Kachrimanis, Kyriakos, and Stavros Malamataris. 2004. ‘“Apparent” Young’s Elastic Modulus and Radial Recovery for Some Tableted Pharmaceutical Excipients’. *European Journal of Pharmaceutical Sciences: Official Journal of the European Federation for Pharmaceutical Sciences* 21 (2–3): 197–207. https://doi.org/10.1016/j.ejps.2003.10.014.

Kaerger, J. Sebastian, Stephen Edge, and Robert Price. 2004. 'Influence of Particle Size and Shape on Flowability and Compactibility of Binary Mixtures of Paracetamol and Microcrystalline Cellulose'. *European Journal of Pharmaceutical Sciences: Official Journal of the European Federation for Pharmaceutical Sciences* 22 (2–3): 173–79. https://doi.org/10.1016/j.ejps.2004.03.005.

Kaplan, Warren. 2004. 'Benefit, Risk and Innovation in Pharmaceutical Research and Development: Opportunities and Issues'. World Health Organization. http://archives.who.int/prioritymeds/report/background/barriers.doc.

Karde, Vikram, and Chinmay Ghoroi. 2014. 'Influence of Surface Modification on Wettability and Surface Energy Characteristics of Pharmaceutical Excipient Powders'. *International Journal of Pharmaceutics* 475 (1): 351–63. https://doi.org/10.1016/j.ijpharm.2014.09.002.

Kashaninejad, Navid, Weng Kong Chan, and Nam-Trung Nguyen. 2012. 'Eccentricity Effect of Micropatterned Surface on Contact Angle'. *Langmuir* 28 (10): 4793–99. https://doi.org/10.1021/la300416x.

Kato, H., Y. Ono, Y. Yonezawa, and H. Sunada. 2006. 'The Effect of Binder Particle Size on Granule and Tablet Properties in High Shear and Extrusion Granulation'. *Journal of Drug Delivery Science and Technology* 16 (6): 461–66. https://doi.org/10.1016/S1773-2247(06)50088-7.

Katsuragi, Hiroaki. 2011. 'Length and Time Scales of a Liquid Drop Impact and Penetration into a Granular Layer'. *Journal of Fluid Mechanics* 675 (May): 552–73. https://doi.org/10.1017/jfm.2011.31.

Kaye, Brian H. 1998. *Characterization of Powders and Aerosols*. Verlag, Germany: Wiley.

Kayrak-Talay, D., and J. D. Litster. 2011. 'A Priori Performance Prediction in Pharmaceutical Wet Granulation: Testing the Applicability of the Nucleation Regime Map to a Formulation with a Broad Size Distribution and Dry Binder Addition.' *International Journal of Pharmaceutics* 418 (2): 254–64. https://doi.org/10.1016/j.ijpharm.2011.04.019.

Keleb, E. I, A Vermeire, C Vervaet, and J. P Remon. 2002. 'Continuous Twin Screw Extrusion for the Wet Granulation of Lactose'. *International Journal of Pharmaceutics* 239 (1): 69–80. https://doi.org/10.1016/S0378-5173(02)00052-2.

Keleb, E. I., A. Vermeire, C. Vervaet, and J. P. Remon. 2004a. 'Twin Screw Granulation as a Simple and Efficient Tool for Continuous Wet Granulation'. *International Journal of Pharmaceutics* 273 (1–2): 183–94. https://doi.org/10.1016/j.ijpharm.2004.01.001.

Keleb, E.I., A. Vermeire, C. Vervaet, and J.P. Remon. 2004b. 'Single-Step Granulation/Tabletting of Different Grades of Lactose: A Comparison with High Shear Granulation and Compression'. *European Journal of Pharmaceutics and Biopharmaceutics* 58 (1): 77–82. https://doi.org/10.1016/j.ejpb.2004.03.007.

Keningley, S.T., P.C. Knight, and A.D. Marson. 1997. 'An Investigation into the Effects of Binder Viscosity on Agglomeration Behaviour'. *Powder Technology* 91 (2): 95–103. https://doi.org/10.1016/S0032-5910(96)03230-5.

Khinast, Johannes. 2016. 'Continuous Manufacturing - Critical Steps and Possible Solutions'. Presented at the PPB World Meeting, Glasgow, UK.

Kiesvaara, Juha, and Jouko Yliruusi. 1993. 'The Use of the Washburn Method in Determining the Contact Angles of Lactose Powder'. *International Journal of Pharmaceutics* 92 (1): 81–88. https://doi.org/10.1016/0378-5173(93)90266-I.

Kiesvaara, Juha, Jouko Yliruusi, and Elina Ahomäki. 1993. 'Contact Angles and Surface Free Energies of Theophylline and Salicylic Acid Powders Determined by the Washburn

Method'. *International Journal of Pharmaceutics* 97 (1): 101–9. https://doi.org/10.1016/0378-5173(93)90130-8.
Kim, Yearnmin, and Jinjoo Lee. 1993. 'Manufacturing Strategy and Production Systems: An Integrated Framework'. *Journal of Operations Management* 11 (1): 3–15. https://doi.org/10.1016/0272-6963(93)90029-O.
Kirchberg, S., Y. Abdin, and G. Ziegmann. 2011. 'Influence of Particle Shape and Size on the Wetting Behavior of Soft Magnetic Micropowders'. *Powder Technology* 207 (1): 311–17. https://doi.org/10.1016/j.powtec.2010.11.012.
Kirdponpattara, Suchata, Muenduen Phisalaphong, and Bi-min Zhang Newby. 2013. 'Applicability of Washburn Capillary Rise for Determining Contact Angles of Powders/Porous Materials'. *Journal of Colloid and Interface Science* 397 (May): 169–76. https://doi.org/10.1016/j.jcis.2013.01.033.
Knight, P. C., T. Instone, J. M. K. Pearson, and M. J. Hounslow. 1998. 'An Investigation into the Kinetics of Liquid Distribution and Growth in High Shear Mixer Agglomeration'. *Powder Technology* 97 (3): 246–57. https://doi.org/10.1016/S0032-5910(98)00031-X.
Kockmann, N., and D. M. Roberge. 2009. 'Harsh Reaction Conditions in Continuous-Flow Microreactors for Pharmaceutical Production'. *Chemical Engineering & Technology* 32 (11): 1682–94. https://doi.org/10.1002/ceat.200900355.
Kockmann, Norbert, Michael Gottsponer, Bertin Zimmermann, and Dominique M. Roberge. 2008. 'Enabling Continuous-Flow Chemistry in Microstructured Devices for Pharmaceutical and Fine-Chemical Production'. *Chemistry – A European Journal* 14 (25): 7470–77. https://doi.org/10.1002/chem.200800707.
Köhler, Thomas, and Heinrich Schubert. 1991. 'Influence of the Particle Size Distribution on the Flow Behaviour of Fine Powders'. *Particle & Particle Systems Characterization* 8 (1–4): 101–4. https://doi.org/10.1002/ppsc.19910080119.
Koo, Otilia May Yue, and Paul Wan Sia Heng. 2001. 'The Influence of Microcrystalline Cellulose Grade on Shape and Shape Distributions of Pellets Produced by Extrusion-Spheronization'. *Chemical and Pharmaceutical Bulletin* 49 (11): 1383–87. https://doi.org/10.1248/cpb.49.1383.
Kouraytem, N., S. T. Thoroddsen, and J. O. Marston. 2016. 'Penetration in Bimodal, Polydisperse Granular Material'. *Physical Review E* 94 (5): 052902. https://doi.org/10.1103/PhysRevE.94.052902.
Kozeny, J. 1927. 'Ueber Kapillare Leitung Des Wassers Im Boden'. *Sitzungsberichte Akademie Der Wissenschaften in Wien* 136 (2a): 271–306.
Kristensen, H. G., P. Holm, and T. Schaefer. 1985. 'Mechanical Properties of Moist Agglomerates in Relation to Granulation Mechanisms Part II. Effects of Particle Size Distribution'. *Powder Technology* 44 (3): 239–47. https://doi.org/10.1016/0032-5910(85)85005-1.
Kristensen, H. Gjelstrup, and T. Schaefer. 1987. 'Granulation: A Review on Pharmaceutical Wet-Granulation: Drug Development and Industrial Pharmacy: Vol 13, No 4-5'. *Drug Development and Industrial Pharmacy* 13 (4–5): 803–72. https://doi.org/10.3109/03639048709105217.
Kudo, Yozo, Masatoshi Yasuda, and Shuji Matsusaka. 2019. 'Effect of Particle Size Distribution on Flowability of Granulated Lactose'. *Advanced Powder Technology*, October. https://doi.org/10.1016/j.apt.2019.10.004.
Kumar, Ajay, Girish M. Ganjyal, David D. Jones, and Milford A. Hanna. 2006. 'Digital Image Processing for Measurement of Residence Time Distribution in a Laboratory

Extruder'. *Journal of Food Engineering* 75 (2): 237–44. https://doi.org/10.1016/j.jfoodeng.2005.04.025.

Kumar, Ashish, Maija Alakarjula, Valérie Vanhoorne, Maunu Toiviainen, Fien De Leersnyder, Jurgen Vercruysse, Mikko Juuti, et al. 2015. 'Linking Granulation Performance with Residence Time and Granulation Liquid Distributions in Twin-Screw Granulation: An Experimental Investigation'. *European Journal of Pharmaceutical Sciences : Official Journal of the European Federation for Pharmaceutical Sciences* 90 (December). https://doi.org/10.1016/j.ejps.2015.12.021.

———. 2016. 'Linking Granulation Performance with Residence Time and Granulation Liquid Distributions in Twin-Screw Granulation: An Experimental Investigation'. *European Journal of Pharmaceutical Sciences*, EuPAT 7 Special Issue - Inventing Tomorrow's Development and Manufacturing, 90 (July): 25–37. https://doi.org/10.1016/j.ejps.2015.12.021.

Kumar, Ashish, Jurgen Vercruysse, Giacomo Bellandi, Krist Gernaey, Chris Vervaet, Jean Remon, Thomas De Beer, and Ingmar Nopens. 2014. 'Experimental Investigation of Granule Size and Shape Dynamics in Twin-Screw Granulation'. *International Journal of Pharmaceutics* 475 (September). https://doi.org/10.1016/j.ijpharm.2014.09.020.

Kumar, Ashish, Jurgen Vercruysse, Séverine Mortier, Chris Vervaet, jp Remon, Krist Gernaey, Thomas De Beer, and Ingmar Nopens. 2016. 'Model-Based Analysis of a Twin-Screw Wet Granulation System for Continuous Solid Dosage Manufacturing'. *Computers & Chemical Engineering* 89 (March). https://doi.org/10.1016/j.compchemeng.2016.03.007.

Kumar, Ashish, Jurgen Vercruysse, Maunu Toiviainen, Pierre-Emmanuel Panouillot, Mikko Juuti, Valérie Vanhoorne, Chris Vervaet, et al. 2014. 'Mixing and Transport during Pharmaceutical Twin-Screw Wet Granulation: Experimental Analysis via Chemical Imaging'. *European Journal of Pharmaceutics and Biopharmaceutics: Official Journal of Arbeitsgemeinschaft Fur Pharmazeutische Verfahrenstechnik e.V* 87 (2): 279–89. https://doi.org/10.1016/j.ejpb.2014.04.004.

Kurup, T.R.R., and N. Pilpel. 1977. 'The Tensile Strength and Disintegration of Griseofulvin Tablets'. *Powder Technology* 16 (2): 179–88. https://doi.org/10.1016/0032-5910(77)87004-6.

Kurz, H.P., and G. Münz. 1975. 'The Influence of Particle Size Distribution on the Flow Properties of Limestone Powders'. *Powder Technology* 11 (1): 37–40. https://doi.org/10.1016/0032-5910(75)80020-9.

Kushner, Joseph. 2013. 'Utilizing Quantitative Certificate of Analysis Data to Assess the Amount of Excipient Lot-to-Lot Variability Sampled during Drug Product Development'. *Pharmaceutical Development and Technology* 18 (2): 333–42. https://doi.org/10.3109/10837450.2011.604784.

Kushner, Joseph, Beth A. Langdon, Ian Hicks, Daniel Song, Fasheng Li, Lalji Kathiria, Anil Kane, Gautam Ranade, and Kam Agarwal. 2014. 'A Quality-by-Design Study for an Immediate-Release Tablet Platform: Examining the Relative Impact of Active Pharmaceutical Ingredient Properties, Processing Methods, and Excipient Variability on Drug Product Quality Attributes'. *Journal of Pharmaceutical Sciences* 103 (2): 527–38. https://doi.org/10.1002/jps.23810.

Kushner, Joseph, Beth A. Langdon, Jon I. Hiller, and Glenn T. Carlson. 2011. 'Examining the Impact of Excipient Material Property Variation on Drug Product Quality Attributes: A Quality-By-Design Study for a Roller Compacted, Immediate Release Tablet'.

Journal of Pharmaceutical Sciences 100 (6): 2222–39. https://doi.org/10.1002/jps.22455.
Lahdenpää, Esa, Mervi Niskanen, and Jouko Yliruusi. 1997. 'Crushing Strength, Disintegration Time and Weight Variation of Tablets Compressed from Three Avicel® PH Grades and Their Mixtures'. *European Journal of Pharmaceutics and Biopharmaceutics* 43 (3): 315–22. https://doi.org/10.1016/S0939-6411(97)00053-2.
Lam, David C. C., and Mitsuo Nakagawa. 1994. 'Packing of Particles - Part 3 - Effect of Particle Size Distribution Shape on Composite Packing Density of Bimodal Mixtures'. *Journal of Ceramic Society of Japan* 102 (2): 133–38.
Lamb, Sir Horace. 1945. *Hydrodynamics*. Courier Corporation.
Landín, M., R. Martínez-Pacheco, J. L. Gómez-Amoza, C. Souto, A. Concheiro, and R. C. Rowe. 1993. 'Effect of Batch Variation and Source of Pulp on the Properties of Microcrystalline Cellulose'. *International Journal of Pharmaceutics* 91 (2): 133–41. https://doi.org/10.1016/0378-5173(93)90332-A.
Laplace, Pierre Simon marquis de. 1805. 'Traité de Mécanique Céleste'. In *Traite de Mechanique Celeste*. Vol. 4. Traite de Mechanique Celeste. Paris: Gauthier-Villars.
LaPorte, Thomas L., and Chenchi Wang. 2007. 'Continuous Processes for the Production of Pharmaceutical Intermediates and Active Pharmaceutical Ingredients'. *Current Opinion in Drug Discovery & Development* 10 (6): 738–45.
Law, Yuk Yu, Donald L. Feke, and Ica Manas-Zloczower. 2013. 'Method for Probing the Microstructure of Particle Beds Using Infiltration Behavior'. *Powder Technology* 237 (March): 427–31. https://doi.org/10.1016/j.powtec.2012.12.034.
Lazghab, Mariem, Khashayar Saleh, Isabelle Pezron, Pierre Guigon, and Ljepsa Komunjer. 2005. 'Wettability Assessment of Finely Divided Solids'. *Powder Technology*, 4th French Meeting on Powder Science and Technology, 157 (1): 79–91. https://doi.org/10.1016/j.powtec.2005.05.014.
Le, V.N.P., E. Robins, and M.P. Flament. 2010. 'Air Permeability of Powder: A Potential Tool for Dry Powder Inhaler Formulation Development'. *European Journal of Pharmaceutics and Biopharmaceutics* 76 (3): 464–69. https://doi.org/10.1016/j.ejpb.2010.09.003.
Leblanc, G. E., R. A. Secco, and M. Kostic. 1999. 'Viscosity Measurement'. In *The Measurement, Instrumentation, and Sensors Handbook*, edited by John G. Webster, 889–912. Boca Raton, FL, USA: CRC Press LLC.
Lee, Andrew C. S., and Paul E. Sojka. 2012. 'Drop Impact and Agglomeration under Static Powder Bed Conditions'. *AIChE Journal* 58 (1): 79–86. https://doi.org/10.1002/aic.12575.
Lee, J. B., D. Derome, and J. Carmeliet. 2016. 'Drop Impact on Natural Porous Stones'. *Journal of Colloid and Interface Science* 469 (May): 147–56. https://doi.org/10.1016/j.jcis.2016.02.008.
Lee, J. B., A. I. Radu, P. Vontobel, D. Derome, and J. Carmeliet. 2016. 'Absorption of Impinging Water Droplet in Porous Stones'. *Journal of Colloid and Interface Science* 471 (June): 59–70. https://doi.org/10.1016/j.jcis.2016.03.002.
Lee, Kai T., Andy Ingram, and Neil A. Rowson. 2012. 'Twin Screw Wet Granulation: The Study of a Continuous Twin Screw Granulator Using Positron Emission Particle Tracking (PEPT) Technique'. *European Journal of Pharmaceutics and Biopharmaceutics* 81 (3): 666–73. https://doi.org/10.1016/j.ejpb.2012.04.011.
———. 2013. 'Comparison of Granule Properties Produced Using Twin Screw Extruder and High Shear Mixer: A Step towards Understanding the Mechanism of Twin Screw

Wet Granulation'. *Powder Technology*, Special Issue: 5th International Granulation Workshop Granulation across the length scale 2011, 238 (April): 91–98. https://doi.org/10.1016/j.powtec.2012.05.031.

Lee, Sau. 2017. 'Impact Story: Regulatory Science Is Strengthening U.S. Drug Product Manufacturing'. *FDA*. http://www.fda.gov/drugs/science-research-drugs/impact-story-regulatory-science-strengthening-us-drug-product-manufacturing.

Lee, Sau L., Thomas F. O'Connor, Xiaochuan Yang, Celia N. Cruz, Sharmista Chatterjee, Rapti D. Madurawe, Christine M. V. Moore, Lawrence X. Yu, and Janet Woodcock. 2015. 'Modernizing Pharmaceutical Manufacturing: From Batch to Continuous Production'. *Journal of Pharmaceutical Innovation* 10 (3): 191–99. https://doi.org/10.1007/s12247-015-9215-8.

Leese, Hannah, Vivek Bhurtun, Kah Peng Lee, and Davide Mattia. 2013. 'Wetting Behaviour of Hydrophilic and Hydrophobic Nanostructured Porous Anodic Alumina'. *Colloids and Surfaces A: Physicochemical and Engineering Aspects* 420 (March): 53–58. https://doi.org/10.1016/j.colsurfa.2012.12.010.

Leonard, Matt. 2019. 'Sanofi Reduces Chemical, Water Use More than 90% with Continuous Manufacturing'. *Supply Chain Dive* (blog). 12 November 2019. https://www.supplychaindive.com/news/sanofi-chemical-water-use-continuous-manufacturing/566971/.

Lerk, C.F., G.K. Bolhuis, and A.H. de Boer. 1979. 'Effect of Microcrystalline Cellulose on Liquid Penetration in and Disintegration of Directly Compressed Tablets'. *Journal of Pharmaceutical Sciences* 68 (2): 205–11. https://doi.org/10.1002/jps.2600680222.

Leuenberger, Hans. 2001. 'New Trends in the Production of Pharmaceutical Granules: Batch versus Continuous Processing'. *European Journal of Pharmaceutics and Biopharmaceutics* 52 (3): 289–96. https://doi.org/10.1016/S0939-6411(01)00199-0.

Levin, Michael. 2001. *Pharmaceutical Process Scale-Up*. New York: Marcel Dekker, Inc. https://gmpua.com/Process/ProcessScale-Up.pdf.

Leyva, Norma, and Matthew P. Mullarney. 2009. 'Modeling Pharmaceutical Powder-Flow Performance Using Particle-Size Distribution Data'. *Pharmaceutical Technology* 33 (3). http://www.pharmtech.com/modeling-pharmaceutical-powder-flow-performance-using-particle-size-distribution-data?date=&id=&pageID=1&sk=.

Li, Jiaqian, Xiaofeng Zhou, Jing Li, Lufeng Che, Jun Yao, Glen McHale, Manoj K. Chaudhury, and Zuankai Wang. 2017. 'Topological Liquid Diode'. *Science Advances* 3 (10): eaao3530. https://doi.org/10.1126/sciadv.aao3530.

Li, Jiayu, Shankali U. Pradhan, and Carl R. Wassgren. 2019. 'Granule Transformation in a Twin Screw Granulator: Effects of Conveying, Kneading, and Distributive Mixing Elements'. *Powder Technology* 346 (March): 363–72. https://doi.org/10.1016/j.powtec.2018.11.099.

Li, Xiying, Liqun Mao, and Xuehu Ma. 2013. 'Dynamic Behavior of Water Droplet Impact on Microtextured Surfaces: The Effect of Geometrical Parameters on Anisotropic Wetting and the Maximum Spreading Diameter'. *Langmuir* 29 (4): 1129–38. https://doi.org/10.1021/la304567s.

Lichtenberg, Frank R., and Tomas J. Philipson. 2002. 'The Dual Effects of Intellectual Property Regulations: Within- and Between-Patent Competition in the U.S. Pharmaceuticals Industry'. *The Journal of Law and Economics* 45 (S2): 643–72. https://doi.org/10.1086/374703.

Lin, Shiji, Binyu Zhao, Song Zou, Jianwei Guo, Zheng Wei, and Longquan Chen. 2018. 'Impact of Viscous Droplets on Different Wettable Surfaces: Impact Phenomena, the

Maximum Spreading Factor, Spreading Time and Post-Impact Oscillation'. *Journal of Colloid and Interface Science* 516 (April): 86–97. https://doi.org/10.1016/j.jcis.2017.12.086.

Lindberg, N.-O., M. Myrenas, C. Tufvesson, and L. Olbjer. 1988. 'Extrusion of An Effervescent Granulation with a Twin Screw Extruder, Baker Perkins MPF 50D. Determination of Mean Residence Time'. *Drug Development and Industrial Pharmacy* 14 (5): 649–55. https://doi.org/10.3109/03639048809151891.

Lindberg, N.-O., C. Tufvesson, P. Holm, and L. Olbjer. 1988. 'Extrusion of an Effervescent Granulation with a Twin Screw Extruder, Baker Perkins MPF 50 D. Influence on Intragranular Porosity and Liquid Saturation'. *Drug Development and Industrial Pharmacy* 14 (13): 1791–98. https://doi.org/10.3109/03639048809151987.

Lindberg, N.-O., C. Tufvesson, and L. Olbjer. 1987. 'Extrusion of an Effervescent Granulation with a Twin Screw Extruder, Baker Perkins MPF 50 D'. *Drug Development and Industrial Pharmacy* 13 (9–11): 1891–1913. https://doi.org/10.3109/03639048709068698.

Link, Kersten Christoph, and Ernst-Ulrich Schlünder. 1996. 'A New Method for the Characterisation of the Wettability of Powders'. *Chemical Engineering & Technology* 19 (5): 432–37. https://doi.org/10.1002/ceat.270190508.

Liu, Huolong, S. C. Galbraith, Brendon Ricart, Courtney Stanton, Brandye Smith-Goettler, Luke Verdi, Thomas O'Connor, Sau Lee, and Seongkyu Yoon. 2017a. 'Optimization of Critical Quality Attributes in Continuous Twin-Screw Wet Granulation via Design Space Validated with Pilot Scale Experimental Data'. *International Journal of Pharmaceutics* 525 (1): 249–63. https://doi.org/10.1016/j.ijpharm.2017.04.055.

———. 2017b. 'Optimization of Critical Quality Attributes in Continuous Twin-Screw Wet Granulation via Design Space Validated with Pilot Scale Experimental Data'. *International Journal of Pharmaceutics* 525 (1): 249–63. https://doi.org/10.1016/j.ijpharm.2017.04.055.

Liu, L.X., I. Marziano, A.C. Bentham, J.D. Litster, E.T.White, and T. Howes. 2008. 'Effect of Particle Properties on the Flowability of Ibuprofen Powders'. *International Journal of Pharmaceutics* 362 (1–2): 109–17. https://doi.org/10.1016/j.ijpharm.2008.06.023.

Liu, Y., M. R. Thompson, K. P. O'Donnell, and N. S. Grasman. 2016. 'Effect of Temperature on the Wetting Behavior of Hydroxypropyl Methylcellulose in a Twin-Screw Granulator'. *Powder Technology* 302 (November): 63–74. https://doi.org/10.1016/j.powtec.2016.08.032.

Liu, Yi, Xiaolei Guo, Haifeng Lu, and Xin Gong. 2015. 'An Investigation of the Effect of Particle Size on the Flow Behavior of Pulverized Coal'. *Procedia Engineering*, New Paradigm of Particle Science and Technology Proceedings of The 7th World Congress on Particle Technology, 102 (January): 698–713. https://doi.org/10.1016/j.proeng.2015.01.170.

Liu, Zhanjie, Yifan Wang, Fernando J. Muzzio, Gerardo Callegari, and German Drazer. 2017. 'Capillary Drop Penetration Method to Characterize the Liquid Wetting of Powders'. *Langmuir: The ACS Journal of Surfaces and Colloids* 33 (1): 56–65. https://doi.org/10.1021/acs.langmuir.6b03589.

Lopez, Jaime, Clarence A Miller, and Eli Ruckenstein. 1976. 'Spreading Kinetics of Liquid Drops on Solids'. *Journal of Colloid and Interface Science* 56 (3): 460–68. https://doi.org/10.1016/0021-9797(76)90111-9.

Lowell, Seymour, and Joan E. Shields. 1991. *Powder Surface Area and Porosity*. 3rd ed. Vol. 2. Particle Technology Series. Springer Netherlands. https://doi.org/10.1007/978-94-015-7955-1.

Lute, Sushma V., Ranjit M. Dhenge, and Agba D. Salman. 2018a. 'Twin Screw Granulation: An Investigation of the Effect of Barrel Fill Level'. *Pharmaceutics* 10 (2): 67. https://doi.org/10.3390/pharmaceutics10020067.

———. 2018b. 'Twin Screw Granulation: Effects of Properties of Primary Powders'. *Pharmaceutics* 10 (2): 68. https://doi.org/10.3390/pharmaceutics10020068.

Macher, Jeffrey, and Jackson Nickerson. 2006. 'Pharmaceutical Manufacturing Research Project: Final Benchmarking Report'. *Olin School of Business*, 1–475.

Mackaplow, Dr M. B., Dr L. A. Rosen, and Dr J. N. Michaels. 1997. 'Effect of Primary Particle Size on Granule Growth and Endpoint Determination in High Shear Granulators'. *Particulate Science and Technology* 15 (2): 162–162. https://doi.org/10.1080/02726359708906754.

Mackaplow, Michael B., Lawrence A. Rosen, and James N. Michaels. 2000. 'Effect of Primary Particle Size on Granule Growth and Endpoint Determination in High-Shear Wet Granulation'. *Powder Technology* 108 (1): 32–45. https://doi.org/10.1016/S0032-5910(99)00203-X.

Maguire, Jennifer, and Daniel Peng. 2015. 'How to Identify Critical Quality Attributes and Critical Process Parameters'. Slide show presented at the FDA/PQRI 2nd Conference, North Bethesda, Maryland, October 6. http://pqri.org/wp-content/uploads/2015/10/01-How-to-identify-CQA-CPP-CMA-Final.pdf.

Mangili, S., C. Antonini, M. Marengo, and A. Amirfazli. 2012. 'Understanding the Drop Impact Phenomenon on Soft PDMS Substrates'. *Soft Matter* 8 (39): 10045–54. https://doi.org/10.1039/C2SM26049B.

Manglik, Raj M., Milind A. Jog, Sandeep K. Gande, and Vishaul Ravi. 2013. 'Damped Harmonic System Modeling of Post-Impact Drop-Spread Dynamics on a Hydrophobic Surface'. *Physics of Fluids* 25 (8): 082112. https://doi.org/10.1063/1.4819243.

Mangwandi, Chirangano, Liu JiangTao, Ahmad B. Albadarin, Ranjit M. Dhenge, and Gavin M. Walker. 2015. 'High Shear Granulation of Binary Mixtures: Effect of Powder Composition on Granule Properties'. *Powder Technology*, 6th International Workshop on Granulation: Granulation across the length scales, 270 (January): 424–34. https://doi.org/10.1016/j.powtec.2014.06.021.

Marks, Alan M., and John J. Sciarra. 1968. 'Effect of Size on Other Physical Properties of Granules and Their Corresponding Tablets'. *Journal of Pharmaceutical Sciences* 57 (3): 497–504. https://doi.org/10.1002/jps.2600570330.

Marmur, Abraham. 1988. 'The Radial Capillary'. *Journal of Colloid and Interface Science* 124 (1): 301–8. https://doi.org/10.1016/0021-9797(88)90351-7.

Marriott, Niamh. 2017. 'EMA Approves Janssen's Prezista Continuous Manufacturing Line'. *European Pharmaceutical Review* (blog). 27 June 2017. https://www.europeanpharmaceuticalreview.com/news/62587/ema-continuous-manufacturing/.

Marston, J. O., J. E. Sprittles, Y. Zhu, E. Q. Li, I. U. Vakarelski, and S. T. Thoroddsen. 2013. 'Drop Spreading and Penetration into Pre-Wetted Powders'. *Powder Technology* 239 (May): 128–36. https://doi.org/10.1016/j.powtec.2013.01.062.

Marston, J. O., S. T. Thoroddsen, W. K. Ng, and R. B. H. Tan. 2010. 'Experimental Study of Liquid Drop Impact onto a Powder Surface'. *Powder Technology* 203 (2): 223–36. https://doi.org/10.1016/j.powtec.2010.05.012.

Mascia, Salvatore, Patrick L. Heider, Haitao Zhang, Richard Lakerveld, Brahim Benyahia, Paul I. Barton, Richard D. Braatz, et al. 2013. 'End-to-End Continuous Manufacturing of Pharmaceuticals: Integrated Synthesis, Purification, and Final Dosage Formation'. *Angewandte Chemie International Edition* 52 (47): 12359–63. https://doi.org/10.1002/anie.201305429.

Mathers, Colin D., and Dejan Loncar. 2006. 'Projections of Global Mortality and Burden of Disease from 2002 to 2030'. *PLoS Medicine* 3 (11): e442. https://doi.org/10.1371/journal.pmed.0030442.

Matsui, Yasuhiro, Yuta Ando, Koji Yamamoto, and Satoru Watano. 2019. 'Analysis of Microstructure of Granules Prepared by Continuous Twin Screw Granulator Using X-Ray Micro-Computed Tomography'. *Chemical and Pharmaceutical Bulletin* 67 (8): 801–9. https://doi.org/10.1248/cpb.c19-00076.

Matyka, Maciej, Arzhang Khalili, and Zbigniew Koza. 2008. 'Tortuosity-Porosity Relation in Porous Media Flow'. *Physical Review E* 78 (2): 026306. https://doi.org/10.1103/PhysRevE.78.026306.

Mazumder, M. K., J. R. Mountain, T. Chasser, and P. Pettit. 1997. 'Fluidity and Flow Properties of Fine Powders'. *Particulate Science and Technology* 15 (2): 106–106. https://doi.org/10.1080/02726359708906726.

McEleney, P., G. M. Walker, I. A. Larmour, and S. E. J. Bell. 2009. 'Liquid Marble Formation Using Hydrophobic Powders'. *Chemical Engineering Journal* 147 (2): 373–82. https://doi.org/10.1016/j.cej.2008.11.026.

McGeary, R. K. 1961. 'Mechanical Packing of Spherical Particles'. *Journal of the American Ceramic Society* 44 (10): 513–22. https://doi.org/10.1111/j.1151-2916.1961.tb13716.x.

McHale, G., N. J. Shirtcliffe, S. Aqil, C. C. Perry, and M. I. Newton. 2004. 'Topography Driven Spreading'. *Physical Review Letters* 93 (3): 036102. https://doi.org/10.1103/PhysRevLett.93.036102.

Mckenna, A., and D. F. Mccafferty. 1982. 'Effect of Particle Size on the Compaction Mechanism and Tensile Strength of Tablets'. *Journal of Pharmacy and Pharmacology* 34 (6): 347–51. https://doi.org/10.1111/j.2042-7158.1982.tb04727.x.

McLaughlin, Patrick, Jonathan Nelson, and Oliver Sherhouse. 2017. 'Regulatory Accumulation in the Manufacturing Sector'. https://www.mercatus.org/publications/regulation/regulatory-accumulation-manufacturing-sector.

Meier, R., M. Thommes, N. Rasenack, M. Krumme, K.-P. Moll, and P. Kleinebudde. 2015. 'Simplified Formulations with High Drug Loads for Continuous Twin-Screw Granulation'. *International Journal of Pharmaceutics* 496 (1): 12–23. https://doi.org/10.1016/j.ijpharm.2015.05.060.

Meier, Robin, Klaus-Peter Moll, Markus Krumme, and Peter Kleinebudde. 2017a. 'Simplified, High Drug-Loaded Formulations Containing Hydrochlorothiazide for Twin-Screw Granulation'. *Chemie Ingenieur Technik* 89 (8): 1025–33. https://doi.org/10.1002/cite.201600134.

———. 2017b. ‘Impact of Fill-Level in Twin-Screw Granulation on Critical Quality Attributes of Granules and Tablets’. *European Journal of Pharmaceutics and Biopharmaceutics* 115 (June): 102–12. https://doi.org/10.1016/j.ejpb.2017.02.010.

MHRA & EMA. 2017. ‘Uniphyllin Continus 200 Mg Prolonged Release Tablets - Summary of Product Characteristics’. ..Org. Electronic Medicines Compendium. 13 April 2017. https://www.medicines.org.uk/emc/product/7719/smpc.

Miao, Zewei, Tony E. Grift, Alan C. Hansen, and K. C. Ting. 2014. ‘Flow Performance of Ground Biomass in a Commercial Auger’. *Powder Technology* 267 (November): 354–61. https://doi.org/10.1016/j.powtec.2014.07.038.

Middleman, Stanley. 1995. *Modeling Axisymmetric Flows: Dynamics of Films, Jets, and Drops*. 1st ed. Academic Press. https://www.elsevier.com/books/modeling-axisymmetric-flows/middleman/978-0-12-494950-8.

Mihranyan, Albert, Assumpcio Piñas Llagostera, Richard Karmhag, Maria Strømme, and Ragnar Ek. 2004. ‘Moisture Sorption by Cellulose Powders of Varying Crystallinity’. *International Journal of Pharmaceutics* 269 (2): 433–42. https://doi.org/10.1016/j.ijpharm.2003.09.030.

Milacic, E., M. W. Baltussen, and J. A. M. Kuipers. 2019. ‘Direct Numerical Simulation Study of Droplet Spreading on Spherical Particles’. *Powder Technology* 354 (September): 11–18. https://doi.org/10.1016/j.powtec.2019.05.064.

Mirza, Sabiruddin, Inna Miroshnyk, Jyrki Heinämäki, Osmo Antikainen, Jukka Rantanen, Pia Vuorela, Heikki Vuorela, and Jouko Yliruusi. 2009. ‘Crystal Morphology Engineering of Pharmaceutical Solids: Tabletting Performance Enhancement’. *AAPS PharmSciTech* 10 (1): 113–19. https://doi.org/10.1208/s12249-009-9187-4.

Mitra, Surjyasish, and Sushanta K. Mitra. 2016. ‘Understanding the Early Regime of Drop Spreading’. *Langmuir* 32 (35): 8843–48. https://doi.org/10.1021/acs.langmuir.6b02189.

Miwa, A., T. Yajima, and S. Itai. 2000. ‘Prediction of Suitable Amount of Water Addition for Wet Granulation’. *International Journal of Pharmaceutics* 195 (1–2): 81–92.

Moreton, C. 2009. ‘Functionality and Performance of Excipients in Quality-by-Design World’. *American Pharmaceutical Review* 12 (4): 28–33.

Mu, B., and M. R. Thompson. 2012. ‘Examining the Mechanics of Granulation with a Hot Melt Binder in a Twin-Screw Extruder’. *Chemical Engineering Science* 81 (October): 46–56. https://doi.org/10.1016/j.ces.2012.06.057.

Muller, F. L., and J. M. Latimer. 2009. ‘Anticipation of Scale up Issues in Pharmaceutical Development’. *Computers & Chemical Engineering*, Chemical Products: From conceptualization to commercialization, 33 (5): 1051–55. https://doi.org/10.1016/j.compchemeng.2008.09.015.

Mundozah, Aquino L., James J. Cartwright, Claire C. Tridon, Michael J. Hounslow, and Agba D. Salman. 2018. ‘Hydrophobic/Hydrophilic Static Powder Beds: Competing Horizontal Spreading and Vertical Imbibition Mechanisms of a Single Droplet’. *Powder Technology* 330 (May): 275–83. https://doi.org/10.1016/j.powtec.2018.02.032.

Murakami, Daiki, Hiroshi Jinnai, and Atsushi Takahara. 2014. ‘Wetting Transition from the Cassie–Baxter State to the Wenzel State on Textured Polymer Surfaces’. *Langmuir* 30 (8): 2061–67. https://doi.org/10.1021/la4049067.

Muster, Tim H., and Clive A. Prestidge. 2002. ‘Application of Time-Dependent Sessile Drop Contact Angles on Compacts to Characterise the Surface Energetics of Sulfathiazole

Crystals'. *International Journal of Pharmaceutics* 234 (1–2): 43–54. https://doi.org/10.1016/s0378-5173(01)00949-8.
———. 2005. 'Water Adsorption Kinetics and Contact Angles of Pharmaceutical Powders'. *Journal of Pharmaceutical Sciences* 94 (4): 861–72. https://doi.org/10.1002/jps.20296.
Narang, Ajit S. 2015. 'Addressing Excipient Variability in Formulation Design and Drug Development'. In *Excipient Applications in Formulation Design and Drug Delivery*, edited by Ajit S Narang and Sai H S. Boddu, 541–67. Switzerland: Springer International Publishing. https://doi.org/10.1007/978-3-319-20206-8_18.
Nasr, Moheb M., Markus Krumme, Yoshihiro Matsuda, Bernhardt L. Trout, Clive Badman, Salvatore Mascia, Charles L. Cooney, et al. 2017. 'Regulatory Perspectives on Continuous Pharmaceutical Manufacturing: Moving From Theory to Practice: September 26-27, 2016, International Symposium on the Continuous Manufacturing of Pharmaceuticals'. *Journal of Pharmaceutical Sciences* 106 (11): 3199–3206. https://doi.org/10.1016/j.xphs.2017.06.015.
National Academies of Sciences, Engineering and Medicine, Division on Earth and Life Studies, and Board on Chemical Sciences and Technology. 2019. *CONTINUOUS MANUFACTURING FOR THE MODERNIZATION OF PHARMACEUTICAL PRODUCTION: PROCEEDINGS OF A WORKSHOP*. Washington (DC): National Academies Press (US). https://www.ncbi.nlm.nih.gov/books/NBK540224/.
Nguyen, Thanh H., David A. V. Morton, and Karen P. Hapgood. 2015. 'Predicting Tablet Strength from the Wet Granulation Conditions via the Unified Compaction Curve'. *Procedia Engineering*, New Paradigm of Particle Science and Technology Proceedings of The 7th World Congress on Particle Technology, 102 (January): 517–26. https://doi.org/10.1016/j.proeng.2015.01.203.
Nguyen, Thanh M., Syed A. Muhammad, Sara Ibrahim, Lin Ma, Jinlei Guo, Baogang Bai, and Bixin Zeng. 2018. 'DeCoST: A New Approach in Drug Repurposing From Control System Theory'. *Frontiers in Pharmacology* 9. https://doi.org/10.3389/fphar.2018.00583.
Nguyen, Thanh, Wei Shen, and Karen Hapgood. 2009. 'Drop Penetration Time in Heterogeneous Powder Beds'. *Chemical Engineering Science* 64 (24): 5210–21. https://doi.org/10.1016/j.ces.2009.08.038.
Niazi, Sarfaraz K. 2009. *Handbook of Pharmaceutical Manufacturing Formulations: Compressed Solid Products*. 2nd ed. Vol. 1. Informa healthcare. https://www.crcpress.com/Handbook-of-Pharmaceutical-Manufacturing-Formulations-Volume-One-Compressed/Niazi/p/book/9781420081169.
Nordström, Josefina, and Göran Alderborn. 2015. 'The Granule Porosity Controls the Loss of Compactibility for Both Dry- and Wet-Processed Cellulose Granules but at Different Rate'. *Journal of Pharmaceutical Sciences* 104 (6): 2029–39. https://doi.org/10.1002/jps.24439.
Nordström, Josefina, Göran Alderborn, and Göran Frenning. 2018. 'Compressibility and Tablet Forming Ability of Bimodal Granule Mixtures: Experiments and DEM Simulations'. *International Journal of Pharmaceutics* 540 (1–2): 120–31. https://doi.org/10.1016/j.ijpharm.2018.02.006.
Nordström, Josefina, Ann-Sofie Persson, Lucia Lazorova, Göran Frenning, and Göran Alderborn. 2013. 'The Degree of Compression of Spherical Granular Solids Controls the Evolution of Microstructure and Bond Probability during Compaction'.

International Journal of Pharmaceutics 442 (1–2): 3–12. https://doi.org/10.1016/j.ijpharm.2012.08.011.

Novartis-MIT Center for Continuous Manufacturing. 2017. 'Novartis-MIT Center for Continuous Manufacturing'. 2017. https://novartis-mit.mit.edu/.

Oldshue, James Y. 1985. 'Transport Phenomena, Reactor Design and Scale-Up'. *Biotechnology Advances* 3 (2): 219–37. https://doi.org/10.1016/0734-9750(85)90293-9.

Olsson, Helena, and Christer Nyström. 2001. 'Assessing Tablet Bond Types from Structural Features That Affect Tablet Tensile Strength'. *Pharmaceutical Research* 18 (2): 203–10. https://doi.org/10.1023/A:1011036603006.

Onda, T., S. Shibuichi, N. Satoh, and K. Tsujii. 1996. 'Super-Water-Repellent Fractal Surfaces'. *Langmuir* 12 (9): 2125–27. https://doi.org/10.1021/la950418o.

Oostveen, Merel L.M., Gabrie M.H. Meesters, and J. Ruud van Ommen. 2015. 'Quantification of Powder Wetting by Drop Penetration Time'. *Powder Technology* 274 (April): 62–66. https://doi.org/10.1016/j.powtec.2014.09.021.

Oprea, Tudor I., Julie E. Bauman, Cristian G. Bologa, Tione Buranda, Alexandre Chigaev, Bruce S. Edwards, Jonathan W. Jarvik, et al. 2011. 'Drug Repurposing from an Academic Perspective'. *Drug Discovery Today. Therapeutic Strategies* 8 (3–4): 61–69. https://doi.org/10.1016/j.ddstr.2011.10.002.

Osei-Yeboah, Frederick, and Changquan Calvin Sun. 2015. 'Validation and Applications of an Expedited Tablet Friability Method'. *International Journal of Pharmaceutics* 484 (1–2): 146–55. https://doi.org/10.1016/j.ijpharm.2015.02.061.

Osorio, Juan Esteban García, Ridade Sayin, Arjun Vivek Kalbag, James D. Litster, Laura Martinez-Marcos, Dimitrios A. Lamprou, and Gavin Halbert. 2017. 'Scaling of Continuous Twin Screw Wet Granulation'. In . https://doi.org/10.1002/aic.15459.

Osorio, Juan G., Ridade Sayin, Arjun V. Kalbag, James D. Litster, Laura Martinez-Marcos, Dimitrios A. Lamprou, and Gavin W. Halbert. 2017. 'Scaling of Continuous Twin Screw Wet Granulation'. *AIChE Journal* 63 (3): 921–32. https://doi.org/10.1002/aic.15459.

Otsuka, Makoto, Yoshifumi Mouri, and Yoshihisa Matsuda. 2003. 'Chemometric Evaluation of Pharmaceutical Properties of Antipyrine Granules by Near-Infrared Spectroscopy'. *AAPS PharmSciTech* 4 (3): E47. https://doi.org/10.1208/pt040347.

Ouchiyama, Norio, and Tatsuo Tanaka. 1986. 'Porosity Estimation from Particle Size Distribution'. *Industrial & Engineering Chemistry Fundamentals* 25 (1): 125–29. https://doi.org/10.1021/i100021a019.

Pagnoux, Cécile, Nicolas Tessier-Doyen, Antoine Pringuet, Manuella Cerbelaud, and Pascual Garcia-Perez. 2009. 'Influence of the Suspension Flocculated State on the Microstructure of Alumina Spheres Elaborated by Colloidal Granulation'. *Journal of the European Ceramic Society* 29 (8): 1379–85. https://doi.org/10.1016/j.jeurceramsoc.2008.09.007.

Pandey, Preetanshu, and Sherif Badawy. 2016. 'A Quality by Design Approach to Scale-up of High-Shear Wet Granulation Process'. *Drug Development and Industrial Pharmacy* 42 (2): 175–89. https://doi.org/10.3109/03639045.2015.1100199.

Paul, Shubhajit, and Changquan Calvin Sun. 2017. 'Dependence of Friability on Tablet Mechanical Properties and a Predictive Approach for Binary Mixtures'. *Pharmaceutical Research* 34 (12): 2901–9. https://doi.org/10.1007/s11095-017-2273-5.

Pingali, Kalyana, Rafael Mendez, Daniel Lewis, Bozena Michniak-Kohn, Alberto Cuitino, and Fernando Muzzio. 2011. 'Mixing Order of Glidant and Lubricant – Influence on Powder and Tablet Properties'. *International Journal of Pharmaceutics* 409 (0): 269–77. https://doi.org/10.1016/j.ijpharm.2011.02.032.

Pitt, K. G., J. M. Newton, R. Richardson, and P. Stanley. 1989. 'The Material Tensile Strength of Convex-Faced Aspirin Tablets'. *The Journal of Pharmacy and Pharmacology* 41 (5): 289–92. https://doi.org/10.1111/j.2042-7158.1989.tb06458.x.

Podczeck, Fridrun. 1998. 'Particle Adhesion in Powder Assemblies'. In *Particle-Particle Adhesion in Pharmaceutical Powder Handling*, 95–140. Imperial College Press. https://www.worldscientific.com/worldscibooks/10.1142/p095.

Pohlman, Daniel A., and James D. Litster. 2015. 'Coalescence Model for Induction Growth Behavior in High Shear Granulation'. *Powder Technology*, 6th International Workshop on Granulation: Granulation across the length scales, 270 (January): 435–44. https://doi.org/10.1016/j.powtec.2014.07.016.

Pollack, Andrew. 2015. 'Orkambi, a New Cystic Fibrosis Drug, Wins F.D.A. Approval'. *The New York Times*, 2 July 2015, sec. Business. https://www.nytimes.com/2015/07/03/business/orkambi-a-new-cystic-fibrosis-drug-wins-fda-approval.html.

Popovich, Laura L, Donald L Feke, and Ica Manas-Zloczower. 1999. 'Influence of Physical and Interfacial Characteristics on the Wetting and Spreading of Fluids on Powders'. *Powder Technology* 104 (1): 68–74. https://doi.org/10.1016/S0032-5910(99)00030-3.

Porath, Daniel. 2018. 'Size and Dynamics of Order-of-Entry Effects in Pharmaceutical Markets'. *International Journal of Market Research* 60 (1): 50–66. https://doi.org/10.1177/1470785317744669.

Potter, Chris. 2009. 'PQLI Application of Science- and Risk-Based Approaches (ICH Q8, Q9, and Q10) to Existing Products'. *Journal of Pharmaceutical Innovation* 4 (1): 4–23. https://doi.org/10.1007/s12247-009-9051-9.

Pradhan, Shankali U., Maitraye Sen, Jiayu Li, James D. Litster, and Carl R. Wassgren. 2017. 'Granule Breakage in Twin Screw Granulation: Effect of Material Properties and Screw Element Geometry'. *Powder Technology* 315 (June): 290–99. https://doi.org/10.1016/j.powtec.2017.04.011.

Prestidge, Clive A., and George Tsatouhas. 2000. 'Wettability Studies of Morphine Sulfate Powders'. *International Journal of Pharmaceutics* 198 (2): 201–12. https://doi.org/10.1016/S0378-5173(00)00341-0.

Quéré, David. 2005. 'Non-Sticking Drops'. *Reports on Progress in Physics* 68 (11): 2495–2532. https://doi.org/10.1088/0034-4885/68/11/R01.

Rassouly, S.M.K. 1999. 'The Packing Density of `perfect' Binary Mixtures'. *Powder Technology* 103 (2): 145–50. https://doi.org/10.1016/S0032-5910(98)00223-X.

RCPE. 2018. 'RCPE'. RCPE. 2018. http://www.rcpe.at/en/about/.

Rekhi, Gurvinder Singh, Ralph Caricofe, Dilip Parikh, and Larry Augsburger. 1996. 'A New Approach to Scale-up of a High Shear Granulation Process Used in the Manufacture of Metoprolol Tartrate Tablet Formulations'. *Pharmaceutical Technology* 20 (58–66). https://www.researchgate.net/publication/237073248_A_new_approach_to_scale-up_of_a_high_shear_granulation_process_used_in_the_manufacture_of_metoprolol_tartrate_tablet_formulations.

Reynolds, Osborne. 1885. 'On the Dilatancy of Media Composed of Rigid Particles in Contact'. *Philosophical Magazine and Journal of Science*, 5th, 20 (127): 469–81. https://doi.org/10.1080/14786448508627791.

Ridgway, Cathy J., Patrick A. C. Gane, and Joachim Schoelkopf. 2002. 'Effect of Capillary Element Aspect Ratio on the Dynamic Imbibition within Porous Networks'. *Journal of Colloid and Interface Science* 252 (2): 373–82. https://doi.org/10.1006/jcis.2002.8468.

Riepma, K. A., J. Veenstra, A. H. de Boer, G. K. Bolhuis, K. Zuurman, C. F. Lerk, and H. Vromans. 1991. 'Consolidation and Compaction of Powder Mixtures: II. Binary Mixtures of Different Particle Size Fractions of α-Lactose Monohydrate'. *International Journal of Pharmaceutics* 76 (1): 9–15. https://doi.org/10.1016/0378-5173(91)90338-O.

Riepma, K. A., H. Vromans, K. Zuurman, and C. F. Lerk. 1993. 'The Effect of Dry Granulation on the Consolidation and Compaction of Crystalline Lactose'. *International Journal of Pharmaceutics* 97 (1): 29–38. https://doi.org/10.1016/0378-5173(93)90123-W.

Riippi, Merja, Jouko Yliruusi, Tapani Niskanen, and Juha Kiesvaara. 1998. 'Dependence between Dissolution Rate and Porosity of Compressed Erythromycin Acistrate Tablets'. *European Journal of Pharmaceutics and Biopharmaceutics* 46 (2): 169–75. https://doi.org/10.1016/S0939-6411(98)00003-4.

Rioboo, R., M. Marengo, and C. Tropea. 2002. 'Time Evolution of Liquid Drop Impact onto Solid, Dry Surfaces'. *Experiments in Fluids* 33 (1): 112–24. https://doi.org/10.1007/s00348-002-0431-x.

Roberge, Dominique M., Bertin Zimmermann, Fabio Rainone, Michael Gottsponer, Markus Eyholzer, and Norbert Kockmann. 2008. 'Microreactor Technology and Continuous Processes in the Fine Chemical and Pharmaceutical Industry: Is the Revolution Underway?' *Organic Process Research & Development* 12 (5): 905–10. https://doi.org/10.1021/op8001273.

Roberts, A. W. 1999. 'The Influence of Granular Vortex Motion on the Volumetric Performance of Enclosed Screw Conveyors'. *Powder Technology* 104 (1): 56–67. https://doi.org/10.1016/S0032-5910(99)00039-X.

Roberts, A. W., and A. H. Willis. 1962. 'Performance of Grain Augers'. *Proceedings of the Institution of Mechanical Engineers* 176 (1): 165–94. https://doi.org/10.1243/PIME_PROC_1962_176_021_02.

Rojas, John, Santiago Guisao, and Vanesa Ruge. 2012. 'Functional Assessment of Four Types of Disintegrants and Their Effect on the Spironolactone Release Properties'. *AAPS PharmSciTech* 13 (4): 1054–62. https://doi.org/10.1208/s12249-012-9835-y.

Ruban, Olena, Yurii Pidpruzhnykov, and Tetiana Kolisnyk. 2018. 'Excipient Risk Assessment: Possible Approaches to Assessing the Risk Associated with Excipient Function'. *Journal of Pharmaceutical Investigation* 48 (4): 421–29. https://doi.org/10.1007/s40005-017-0354-4.

Rudd, David R. 2004. 'The Use of Acoustic Monitoring for the Control and Scale-Up of a Tablet Granulation Process'. *Journal of Process Analytical Technology* 1 (1–2): 8–11.

Sakr, Walid F., Mohamed A. Ibrahim, Fars K. Alanazi, and Adel A. Sakr. 2012. 'Upgrading Wet Granulation Monitoring from Hand Squeeze Test to Mixing Torque Rheometry'. *Saudi Pharmaceutical Journal : SPJ* 20 (1): 9–19. https://doi.org/10.1016/j.jsps.2011.04.007.

Saleh, Mohammed, Ranjit Dhenge, James Cartwright, Michael Hounslow, and Agba Salman. 2015. 'Twin Screw Wet Granulation: Effect of Process and Formulation Variables on

Powder Caking during Production'. *International Journal of Pharmaceutics* 496 (November). https://doi.org/10.1016/j.ijpharm.2015.10.069.
Salman, Agba D., Gavin K. Reynolds, Hong Sing Tan, Ian Gabbott, and Michael J. Hounslow. 2007. 'Chapter 21 Breakage in Granulation'. In *Handbook of Powder Technology*, 11:979–1040. Elsevier. https://doi.org/10.1016/S0167-3785(07)80056-X.
Santiso, Erik, and Erich A. Müller. 2002. 'Dense Packing of Binary and Polydisperse Hard Spheres'. *Molecular Physics* 100 (15): 2461–69. https://doi.org/10.1080/00268970210125313.
Šantl, Maja, Ilija Ilić, Franc Vrecer, and Saša Baumgartner. 2012. 'A Compressibility and Compactibility Study of Real Tableting Mixtures: The Effect of Granule Particle Size'. *Acta Pharmaceutica (Zagreb, Croatia)* 62 (September): 325–40. https://doi.org/10.2478/v10007-012-0028-8.
Sayin, Ridade, Laura Martinez-Marcos, Juan G. Osorio, Paul Cruise, Ian Jones, Gavin W. Halbert, Dimitrios A. Lamprou, and James D. Litster. 2015. 'Investigation of an 11mm Diameter Twin Screw Granulator: Screw Element Performance and in-Line Monitoring via Image Analysis'. *International Journal of Pharmaceutics*, Special Issue on "Continuous Manufacturing and Process Analytical Tools", 496 (1): 24–32. https://doi.org/10.1016/j.ijpharm.2015.09.024.
Scannell, Jack W., Alex Blanckley, Helen Boldon, and Brian Warrington. 2012. 'Diagnosing the Decline in Pharmaceutical R&D Efficiency'. *Nature Reviews Drug Discovery* 11 (3): 191–200. https://doi.org/10.1038/nrd3681.
Schaafsma, Stefan, Pieter Vonk, and N.W.F Kossen. 2000. 'Fluid Bed Agglomeration with a Narrow Droplet Size Distribution'. *International Journal of Pharmaceutics* 193 (2): 175–87. https://doi.org/10.1016/S0378-5173(99)00329-4.
Schaefer, T., P. Holm, and H.G. Kristensen. 1992. 'Melt Pelletization in a High Shear Mixer III. Effects of Lactose Quality'. *Acta Pharm. Nord.* 4: 245–52.
Schæfer, Torben. 1996. 'Melt Pelletization in a High Shear Mixer VI. Agglomeration of a Cohesive Powder'. *International Journal of Pharmaceutics* 132 (1): 221–30. https://doi.org/10.1016/0378-5173(95)04374-8.
Schæfer, Torben, and Christina Mathiesen. 1996. 'Melt Pelletization in a High Shear Mixer. IX. Effects of Binder Particle Size'. *International Journal of Pharmaceutics* 139 (1): 139–48. https://doi.org/10.1016/0378-5173(96)04548-6.
Schæfer, Torben, and O. Worts. 1978. 'Control of Fluidized Bed Granulation, V: Factors Affecting Granule Growth'. *Archiv Der Pharmazie - Chemistry in Life Sciences* 311 (5): 69–82.
Schoelkopf, Joachim, Patrick A. C Gane, Cathy J Ridgway, and G. Peter Matthews. 2002. 'Practical Observation of Deviation from Lucas–Washburn Scaling in Porous Media'. *Colloids and Surfaces A: Physicochemical and Engineering Aspects* 206 (1): 445–54. https://doi.org/10.1016/S0927-7757(02)00066-3.
Schoneker, Dave. 2008. 'The Impact of Excipient Variability on QbD'. Powerpoint presented at the APEC LSIF JCCT Training Workshop, Beijing, China, December. https://admin.ich.org/sites/default/files/inline-files/Impact_of_Excipient.pdf.
Seem, Tim Chan, Neil A. Rowson, Andy Ingram, Zhenyu Huang, Shen Yu, Marcel de Matas, Ian Gabbott, and Gavin K. Reynolds. 2015. 'Twin Screw Granulation — A Literature Review'. *Powder Technology* 276 (May): 89–102. https://doi.org/10.1016/j.powtec.2015.01.075.
Shah, U. 2005. 'Use of a Modified Twin-Screw Extruder to Develop a High-Strength Tablet Dosage Form'. *Pharmaceutical Technology* 29 (June): 52–66.

Shibuichi, S., T. Yamamoto, T. Onda, and K. Tsujii. 1998. 'Super Water- and Oil-Repellent Surfaces Resulting from Fractal Structure'. *Journal of Colloid and Interface Science* 208 (1): 287–94. https://doi.org/10.1006/jcis.1998.5813.

Shirazian, Saeed, Jacek Zeglinski, Shaza Darwish, Manuel Kuhs, Ahmad B. Albadarin, Denise M. Croker, and Gavin M. Walker. 2018. 'Continuous Twin Screw Wet Granulation: The Combined Effect of Process Parameters on Residence Time, Particle Size, and Granule Morphology'. *Journal of Drug Delivery Science and Technology* 48 (December): 319–27. https://doi.org/10.1016/j.jddst.2018.09.016.

Sikalo, Sefko, Marco Marengo, Cameron Tropea, and E.N Ganić. 2002. 'Analysis of Impact of Droplets on Horizontal Surfaces'. *Experimental Thermal and Fluid Science* 25 (January): 503–10. https://doi.org/10.1016/S0894-1777(01)00109-1.

Sikalo, Sefko, Marco Marengo, Cameron Tropea, and E N. Ganic. 2002. 'ANALYSIS OF IMPACT OF DROPLETS ON HORIZONTAL SURFACES'. In , 347–52. https://doi.org/10.1615/ICHMT.2000.TherSieProcVol2TherSieProcVol1.460.

Silva, Sérgio M. C., Fátima V. Pinto, Filipe E. Antunes, Maria G. Miguel, João J. S. Sousa, and Alberto A. C. C. Pais. 2008. 'Aggregation and Gelation in Hydroxypropylmethyl Cellulose Aqueous Solutions'. *Journal of Colloid and Interface Science* 327 (2): 333–40. https://doi.org/10.1016/j.jcis.2008.08.056.

Singh, Sanchit K., Sameer Khandekar, Dheeraj Pratap, and S. Anantha Ramakrishna. 2013. 'Wetting Dynamics and Evaporation of Sessile Droplets on Nano-Porous Alumina Surfaces'. *Colloids and Surfaces A: Physicochemical and Engineering Aspects*, WETTING AND EVAPORATION: DROPLETS OF PURE AND COMPLEX FLUIDS, 432 (September): 71–81. https://doi.org/10.1016/j.colsurfa.2013.04.070.

Siramshetty, Vishal B., Janette Nickel, Christian Omieczynski, Bjoern-Oliver Gohlke, Malgorzata N. Drwal, and Robert Preissner. 2016. 'WITHDRAWN—a Resource for Withdrawn and Discontinued Drugs'. *Nucleic Acids Research* 44 (Database issue): D1080–86. https://doi.org/10.1093/nar/gkv1192.

Soh, Josephine L. P., Lei Yang, Celine V. Liew, Fu D. Cui, and Paul W. S. Heng. 2008. 'Importance of Small Pores in Microcrystalline Cellulose for Controlling Water Distribution during Extrusion–Spheronization'. *AAPS PharmSciTech* 9 (3): 972–81. https://doi.org/10.1208/s12249-008-9134-9.

Somani, Amit A., Kirstin Thelen, Songmao Zheng, Mirjam N. Trame, Katrin Coboeken, Michaela Meyer, Katrin Schnizler, Ibrahim Ince, Stefan Willmann, and Stephan Schmidt. 2016. 'Evaluation of Changes in Oral Drug Absorption in Preterm and Term Neonates for Biopharmaceutics Classification System (BCS) Class I and II Compounds'. *British Journal of Clinical Pharmacology* 81 (1): 137–47. https://doi.org/10.1111/bcp.12752.

Soppela, Ira, Sari Airaksinen, Matti Murtomaa, Mikko Tenho, Juha Hatara, Heikki Räikkönen, Jouko Yliruusi, and Niklas Sandler. 2010. 'Investigation of the Powder Flow Behaviour of Binary Mixtures of Microcrystalline Celluloses and Paracetamol'. *Journal of Excipients and Food Chemicals* 1 (1): 55–67.

Sorbie, K. S., Y. Z. Wu, and S. R. McDougall. 1995. 'The Extended Washburn Equation and Its Application to the Oil/Water Pore Doublet Problem'. *Journal of Colloid and Interface Science* 174 (2): 289–301. https://doi.org/10.1006/jcis.1995.1394.

Spence, Julie K., Shobha N. Bhattachar, James A. Wesley, Peter J. Martin, and Suresh R. Babu. 2005. 'Increased Dissolution Rate and Bioavailability Through Comicronization with Microcrystalline Cellulose'. *Pharmaceutical Development and Technology* 10 (4): 451–60. https://doi.org/10.1080/10837450500299636.

Srai, Jagjit Singh, Clive Badman, Markus Krumme, Mauricio Futran, and Craig Johnston. 2015. 'Future Supply Chains Enabled by Continuous Processing—Opportunities and Challenges. May 20–21, 2014 Continuous Manufacturing Symposium'. *Journal of Pharmaceutical Sciences* 104 (3): 840–49. https://doi.org/10.1002/jps.24343.

Srai, Jagjit Singh, Mukesh Kumar, Gary Graham, Wendy Phillips, James Tooze, Simon Ford, Paul Beecher, et al. 2016. 'Distributed Manufacturing: Scope, Challenges and Opportunities'. *International Journal of Production Research* 54 (23): 6917–35. https://doi.org/10.1080/00207543.2016.1192302.

Srivastava, Ajit K., Carroll E. Goering, Roger P. Rohrbach, and Dennis R. Buckmaster. 2006. 'Chapter 14 - Conveying of Agricultural Materials'. In *Engineering Principles of Agricultural Machines, Second Edition*, by Ajit K. Srivastava, Carroll E. Goering, Roger P. Rohrbach, and Dennis R. Buckmaster, 2nd ed., 491–524. St. Joseph, MI: American Society of Agricultural and Biological Engineers. https://doi.org/10.13031/2013.41476.

Staniforth, John N., Anand R. Baichwal, Jo P. Hart, and Paul W.S. Heng. 1988. 'Effect of Addition of Water on the Rheological and Mechanical Properties of Microcrystalline Celluloses'. *International Journal of Pharmaceutics* 41 (3): 231–36. https://doi.org/10.1016/0378-5173(88)90198-6.

Stapelbroek, B. B. J., H. P. Jansen, E. S. Kooij, J. H. Snoeijer, and A. Eddi. 2014. 'Universal Spreading of Water Drops on Complex Surfaces'. *Soft Matter* 10 (15): 2641–48. https://doi.org/10.1039/C3SM52464G.

Starov, V. M., S. R. Kosvintsev, V. D. Sobolev, M. G. Velarde, and S. A. Zhdanov. 2002. 'Spreading of Liquid Drops over Saturated Porous Layers'. *Journal of Colloid and Interface Science* 246 (2): 372–79. https://doi.org/10.1006/jcis.2001.8077.

Stevens, Ruth E., Vivian Gray, Angelica Dorantes, Lynn Gold, and Loan Pham. 2015. 'Scientific and Regulatory Standards for Assessing Product Performance Using the Similarity Factor, F2'. *The AAPS Journal* 17 (2): 301–6. https://doi.org/10.1208/s12248-015-9723-y.

Sturtevant, Heather. 2013. 'The IPEC-Americas Significant Change Guideline'. Powerpoint presented at the ExcipientFest Workshop, Baltimore, Maryland, U.S., April 29. https://ipecamericas.org/sites/default/files/EF_RegulatoryWorkshopPresentation_SigChangeGuide_HeatherSturtevant.pdf.

Su, Qinglin, Sudarshan Ganesh, Mariana Moreno, Yasasvi Bommireddy, Marcial Gonzalez, Gintaras Reklaitis, and Zoltan Nagy. 2019. 'A Perspective on Quality-by-Control (QbC) in Pharmaceutical Continuous Manufacturing'. *Computers & Chemical Engineering* 125 (March). https://doi.org/10.1016/j.compchemeng.2019.03.001.

Subrahmanyam, T.V., M.B.M. Monte, A. Middea, E. Valdiviezo, and F.F. Lins. 1999. 'Contact Angles of Quartz by Capillary Penetration of Liquids and Captive Bubble Techniques'. *Minerals Engineering* 12 (11): 1347–57. https://doi.org/10.1016/S0892-6875(99)00122-3.

Subrahmanyam, T.V., C.A. Prestidge, and J. Ralston. 1996. 'Contact Angle and Surface Analysis Studies of Sphalerite Particles'. *Minerals Engineering* 9 (7): 727–41. https://doi.org/10.1016/0892-6875(96)00064-7.

Sun, Changquan Calvin. 2008. 'Mechanism of Moisture Induced Variations in True Density and Compaction Properties of Microcrystalline Cellulose'. *International Journal of Pharmaceutics* 346 (1–2): 93–101. https://doi.org/10.1016/j.ijpharm.2007.06.017.

Supakar, T., M. Moradiafrapoli, G. F. Christopher, and J. O. Marston. 2016. 'Spreading, Encapsulation and Transition to Arrested Shapes during Drop Impact onto

Hydrophobic Powders'. *Journal of Colloid and Interface Science* 468 (April): 10–20. https://doi.org/10.1016/j.jcis.2016.01.028.
Suresh, Pradeep, and Prabir Basu. 2008. 'Improving Pharmaceutical Product Development and Manufacturing: Impact on Cost of Drug Development and Cost of Goods Sold of Pharmaceuticals'. *J. Pharm. Innov* 3 (September): 175–87. https://doi.org/10.1007/s12247-008-9043-1.
Susana, Laura, Filippo Campaci, and Andrea C. Santomaso. 2012. 'Wettability of Mineral and Metallic Powders: Applicability and Limitations of Sessile Drop Method and Washburn's Technique'. *Powder Technology* 226 (August): 68–77. https://doi.org/10.1016/j.powtec.2012.04.016.
Sweeney, Sean M., and Merrilea J. Mayo. 1999. 'Relation of Pore Size to Green Density: The Kozeny Equation'. *Journal of the American Ceramic Society* 82 (7): 1931–33. https://doi.org/10.1111/j.1151-2916.1999.tb02020.x.
T Lee, Kai, A Ingram, and N Rowson. 2012. 'Twin Screw Wet Granulation: The Study of a Continuous Twin Screw Granulator Using Positron Emission Particle Tracking (PEPT) Technique'. *European Journal of Pharmaceutics and Biopharmaceutics : Official Journal of Arbeitsgemeinschaft Für Pharmazeutische Verfahrenstechnik e.V* 81 (April): 666–73. https://doi.org/10.1016/j.ejpb.2012.04.011.
Tang, Chenglong, Mengxiao Qin, Xinyan Weng, Xuhui Zhang, Peng Zhang, Jianling Li, and Zuohua Huang. 2017. 'Dynamics of Droplet Impact on Solid Surface with Different Roughness'. *International Journal of Multiphase Flow* 96 (July). https://doi.org/10.1016/j.ijmultiphaseflow.2017.07.002.
Tanner, L. H. 1979. 'The Spreading of Silicone Oil Drops on Horizontal Surfaces'. *Journal of Physics D: Applied Physics* 12 (9): 1473–84. https://doi.org/10.1088/0022-3727/12/9/009.
Thalberg, Kyrre, David Lindholm, and Anders Axelsson. 2004. 'Comparison of Different Flowability Tests for Powders for Inhalation'. *Powder Technology* 146 (3): 206–13. https://doi.org/doi:10.1016/j.powtec.2004.08.003.
Thapa, Prakash, Du Hyung Choi, Min Soo Kim, and Seong Hoon Jeong. 2019. 'Effects of Granulation Process Variables on the Physical Properties of Dosage Forms by Combination of Experimental Design and Principal Component Analysis'. *Asian Journal of Pharmaceutical Sciences* 14 (3): 287–304. https://doi.org/10.1016/j.ajps.2018.08.006.
The British Pharmacopoeia Commission. 2017. *The British Pharmacopoeia 2017*. Vol. 1. Six vols. Medicines and Healthcare Products Regulatory Agency (MHRA). https://www.pharmacopoeia.com/BP2019.
The United States Pharmacopeial Convention. 2011a. '<1217> Tablet Breaking Force'. In *The United States Pharmacopeia*, 6th ed., 31:1695. Pharmacopeial Forum.
———. 2011b. '<905> Uniformity of Dosage Units'. In *The United States Pharmacopeia*.
Thiel, W. J., and L. T. Nguyen. 1982. 'Fluidized Bed Granulation of an Ordered Powder Mixture'. *The Journal of Pharmacy and Pharmacology* 34 (11): 692–99. https://doi.org/10.1111/j.2042-7158.1982.tb06202.x.
Thompson, M. R. 2015. 'Twin Screw Granulation – Review of Current Progress'. *Drug Development and Industrial Pharmacy* 41 (8): 1223–31. https://doi.org/10.3109/03639045.2014.983931.
Thompson, M. R., and J. Sun. 2010. 'Wet Granulation in a Twin-Screw Extruder: Implications of Screw Design'. *Journal of Pharmaceutical Sciences* 99 (4): 2090–2103. https://doi.org/10.1002/jps.21973.

Thompson, M. R., S. Weatherley, R. N. Pukadyil, and P. J. Sheskey. 2012. 'Foam Granulation: New Developments in Pharmaceutical Solid Oral Dosage Forms Using Twin Screw Extrusion Machinery'. *Drug Development and Industrial Pharmacy* 38 (7): 771–84. https://doi.org/10.3109/03639045.2011.633265.

Thompson, M.R., and J Sun. 2009. 'Wet Granulation in a Twin-Screw Extruder: Implications of Screw Design'. *Journal of Pharmaceutical Sciences* 99 (January): 2090–2103. https://doi.org/10.1002/jps.21973.

Ticehurst, M. D., P. York, R. C. Rowe, and S. K. Dwivedi. 1996. 'Characterisation of the Surface Properties of α-Lactose Monohydrate with Inverse Gas Chromatography, Used to Detect Batch Variation'. *International Journal of Pharmaceutics* 141 (1): 93–99. https://doi.org/10.1016/0378-5173(96)04619-4.

Tomas, J., and S. Kleinschmidt. 2009. 'Improvement of Flowability of Fine Cohesive Powders by Flow Additives'. *Chemical Engineering & Technology* 32 (10): 1470–83. https://doi.org/10.1002/ceat.200900173.

Tomer, G., H. Patel, F. Podczeck, and J. M. Newton. 2001. 'Measuring the Water Retention Capacities (MRC) of Different Microcrystalline Cellulose Grades'. *European Journal of Pharmaceutical Sciences: Official Journal of the European Federation for Pharmaceutical Sciences* 12 (3): 321–25. https://doi.org/10.1016/s0928-0987(00)00188-3.

Tu, Wei-Da, A Ingram, and J.P.K. Seville. 2013. 'Regime Map Development for Continuous Twin Screw Granulation'. *Chemical Engineering Science* 87 (January): 315–26. https://doi.org/10.1016/j.ces.2012.08.015.

Turner, Thomas D., Lauren E. Hatcher, Chick C. Wilson, and Kevin J. Roberts. 2019. 'Habit Modification of the Active Pharmaceutical Ingredient Lovastatin Through a Predictive Solvent Selection Approach'. *Journal of Pharmaceutical Sciences* 108 (5): 1779–87. https://doi.org/10.1016/j.xphs.2018.12.012.

Tyson, Tim. 2019. 'Solving the Industry's Capacity Utilization Problem'. *Pharma's Almanac* (blog). 2019. https://www.pharmasalmanac.com/articles/solving-the-industrys-capacity-utilization-problem.

Uddin, Md Sahab, Abdullah Al Mamun, Tanjuma Tasnu, and Md Asaduzzaman. 2015. 'In-Process and Finished Products Quality Control Tests for Pharmaceutical Tablets According to Pharmacopoeias'. *Journal of Chemical and Pharmaceutical Research* 7 (9). http://www.jocpr.com/abstract/inprocess-and-finished-products-quality-control-tests-for-pharmaceutical-tablets-according-to-pharmacopoeias-6069.html.

Ukiwe, Chijioke, Ali Mansouri, and Daniel Y. Kwok. 2005. 'The Dynamics of Impacting Water Droplets on Alkanethiol Self-Assembled Monolayers with Co-Adsorbed CH3 and CO2H Terminal Groups'. *Journal of Colloid and Interface Science* 285 (2): 760–68. https://doi.org/10.1016/j.jcis.2004.12.027.

United Nations, Department of Economic and Social Affairs, and Population Division. 2015. 'World Population Ageing'. UN. https://www.un.org/en/development/desa/population/publications/ageing/WPA2015_Infochart.asp.

United States Pharmacopeial Convention. 2015. '<616> Bulk Density and Tapped Density of Powders'. In *United States Pharmacopeia*, 3rd ed., 31:909–9011. North Bethesda, Maryland.

———. 2016. '<711> Dissolution'. In *United States Pharmacopeia*, 4th ed., 33:540–55. North Bethesda, Maryland.

V. Lute, Sushma, Ranjit Dhenge, and Michael J. Hounslow & Agba D. Salman. 2016. 'TWIN SCREW GRANULATION: Understanding the Mechanism of Granule Formation along the Barrel Length'. *Chemical Engineering Research and Design*, March. https://doi.org/10.1016/j.cherd.2016.03.008.

Vaikuntanathan, V., and D. Sivakumar. 2014. 'Transition from Cassie to Impaled State during Drop Impact on Groove-Textured Solid Surfaces'. *Soft Matter* 10 (17): 2991–3002. https://doi.org/10.1039/C4SM00050A.

Vaikuntanathan, Visakh, and D. Sivakumar. 2016. 'Maximum Spreading of Liquid Drops Impacting on Groove-Textured Surfaces: Effect of Surface Texture'. *Langmuir* 32 (10): 2399–2409. https://doi.org/10.1021/acs.langmuir.5b04639.

Van Arnum, Patricia. 2013. 'Advancing Flow Chemistry in API Manufacturing'. *Pharmaceutical Technology* 37 (4): 78–82.

Van Melkebeke, B., C. Vervaet, and J. P. Remon. 2008. 'Validation of a Continuous Granulation Process Using a Twin-Screw Extruder'. *International Journal of Pharmaceutics* 356 (1): 224–30. https://doi.org/10.1016/j.ijpharm.2008.01.012.

Vanhoorne, V., L. Janssens, J. Vercruysse, T. De Beer, J. P. Remon, and C. Vervaet. 2016. 'Continuous Twin Screw Granulation of Controlled Release Formulations with Various HPMC Grades'. *International Journal of Pharmaceutics* 511 (2): 1048–57. https://doi.org/10.1016/j.ijpharm.2016.08.020.

Vargas, Jenny M., Sarah Nielsen, Vanessa Cárdenas, Anthony Gonzalez, Efrain Y. Aymat, Elvin Almodovar, Gustavo Classe, Yleana Colón, Eric Sanchez, and Rodolfo J. Romañach. 2018. 'Process Analytical Technology in Continuous Manufacturing of a Commercial Pharmaceutical Product'. *International Journal of Pharmaceutics* 538 (1–2): 167–78. https://doi.org/10.1016/j.ijpharm.2018.01.003.

Vemavarapu, Chandra, Madhu Surapaneni, Munir Hussain, and Sherif Badawy. 2009. 'Role of Drug Substance Material Properties in the Processibility and Performance of a Wet Granulated Product'. *International Journal of Pharmaceutics* 374 (1–2): 96–105. https://doi.org/10.1016/j.ijpharm.2009.03.014.

Vercruysse, J., U. Delaet, I. Van Assche, P. Cappuyns, F. Arata, G. Caporicci, T. De Beer, J. P. Remon, and C. Vervaet. 2013. 'Stability and Repeatability of a Continuous Twin Screw Granulation and Drying System'. *European Journal of Pharmaceutics and Biopharmaceutics: Official Journal of Arbeitsgemeinschaft Fur Pharmazeutische Verfahrenstechnik e.V* 85 (3 Pt B): 1031–38. https://doi.org/10.1016/j.ejpb.2013.05.002.

Vercruysse, Jurgen, Anneleen Burggraeve, Margot Fonteyne, Philippe Cappuyns, U Delaet, Ivo Van Assche, Thomas De Beer, jp Remon, and Chris Vervaet. 2015. 'Impact of Screw Configuration on the Particle Size Distribution of Granules Produced by Twin Screw Granulation'. *International Journal of Pharmaceutics* 479 (January): 171–80. https://doi.org/10.1016/j.ijpharm.2014.12.071.

Vercruysse, Jurgen, Damian Cordoba-Diaz, Elisabeth Peeters, Margot Fonteyne, U Delaet, Ivo Van Assche, Thomas De Beer, jp Remon, and Chris Vervaet. 2012. 'Continuous Twin Screw Granulation: Influence of Process Variables on Granule and Tablet Quality'. *European Journal of Pharmaceutics and Biopharmaceutics : Official Journal of Arbeitsgemeinschaft Für Pharmazeutische Verfahrenstechnik e.V* 82 (June): 205–11. https://doi.org/10.1016/j.ejpb.2012.05.010.

Vercruysse, Jurgen, Maunu Toiviainen, Margot Fonteyne, Niko Helkimo, Jarkko Ketolainen, Mikko Juuti, Urbain Delaet, et al. 2014. 'Visualization and Understanding of the Granulation Liquid Mixing and Distribution during Continuous Twin Screw

Granulation Using NIR Chemical Imaging'. *European Journal of Pharmaceutics and Biopharmaceutics: Official Journal of Arbeitsgemeinschaft Fur Pharmazeutische Verfahrenstechnik e.V* 86 (3): 383–92. https://doi.org/10.1016/j.ejpb.2013.10.012.

Verstraeten, Maxim, Daan Van Hauwermeiren, Kai Lee, Neil Turnbull, David Wilsdon, Mary Am Ende, Pankaj Doshi, et al. 2017. 'In-Depth Experimental Analysis of Pharmaceutical Twin-Screw Wet Granulation in View of Detailed Process Understanding'. *International Journal of Pharmaceutics* 529 (1–2): 678–93. https://doi.org/10.1016/j.ijpharm.2017.07.045.

Visser, J. 1989. 'Van Der Waals and Other Cohesive Forces Affecting Powder Fluidization'. *Powder Technology* 58 (1): 1–10. https://doi.org/10.1016/0032-5910(89)80001-4.

Vonk, P, C. P. F Guillaume, J. S Ramaker, H Vromans, and N. W. F Kossen. 1997. 'Growth Mechanisms of High-Shear Pelletisation'. *International Journal of Pharmaceutics* 157 (1): 93–102. https://doi.org/10.1016/S0378-5173(97)00232-9.

Vromans, H., G.K. Bolhuis, C.F. Lerk, and K.D. Kussendrager. 1987. 'Studies on Tableting Properties of Lactose. VIII. The Effect of Variations in Primary Particle Size, Percentage of Amorphous Lactose and Addition of a Disintegrant on the Disintegration of Spray-Dried Lactose Tablets'. *International Journal of Pharmaceutics* 39 (3): 201–6. https://doi.org/10.1016/0378-5173(87)90217-1.

Vu, Henry, Darren Banks, and Guillermo Aguilar. 2011. 'Examining Viscosity and Surface Wettability on Lamella Lift Dynamics and Droplet Splashing'. *Atomization and Sprays* 21 (4). https://doi.org/10.1615/AtomizSpr.2011002818.

Wade, J. B., G. P. Martin, and D. F. Long. 2015. 'The Evolution of Granule Fracture Strength as a Function of Impeller Tip Speed and Granule Size for a Novel Reverse-Phase Wet Granulation Process'. *International Journal of Pharmaceutics* 488 (1–2): 95–101. https://doi.org/10.1016/j.ijpharm.2015.04.033.

Wade, Jonathan B., Gary P. Martin, and David F. Long. 2015. 'An Assessment of Powder Pycnometry as a Means of Determining Granule Porosity'. *Pharmaceutical Development and Technology* 20 (3): 257–65. https://doi.org/10.3109/10837450.2013.860550.

Wang, Jennifer, Hong Wen, and Divyakant Desai. 2010. 'Lubrication in Tablet Formulations'. *European Journal of Pharmaceutics and Biopharmaceutics* 75 (1): 1–15. https://doi.org/10.1016/j.ejpb.2010.01.007.

Wang, Jiayu, Minh Do-Quang, James J. Cannon, Feng Yue, Yuji Suzuki, Gustav Amberg, and Junichiro Shiomi. 2015. 'Surface Structure Determines Dynamic Wetting'. *Scientific Reports* 5 (1): 1–7. https://doi.org/10.1038/srep08474.

Wang, Meng-Jiy, Fang-Hsing Lin, Yi-Lin Hung, and Shi-Yow Lin. 2009a. 'Dynamic Behaviors of Droplet Impact and Spreading: Water on Five Different Substrates'. *Langmuir* 25 (12): 6772–80. https://doi.org/10.1021/la9002862.

———. 2009b. 'Dynamic Behaviors of Droplet Impact and Spreading: Water on Five Different Substrates'. *Langmuir* 25 (12): 6772–80. https://doi.org/10.1021/la9002862.

Wang, Yifan, Zhanjie Liu, Fernando Muzzio, German Drazer, and Gerardo Callegari. 2018. 'A Drop Penetration Method to Measure Powder Blend Wettability'. *International Journal of Pharmaceutics* 538 (1–2): 112–18. https://doi.org/10.1016/j.ijpharm.2017.12.034.

Washburn, Edward W. 1921. 'The Dynamics of Capillary Flow'. *Physical Review* 17 (3): 273–83. https://doi.org/10.1103/PhysRev.17.273.

Watson, N. J., M. J. W. Povey, G. K. Reynolds, B. H. Xu, and Y. Ding. 2014. 'Acoustic Emission Monitoring from a Lab Scale High Shear Granulator--a Novel Approach'. *International Journal of Pharmaceutics* 465 (1–2): 262–74. https://doi.org/10.1016/j.ijpharm.2014.01.032.

Weatherley, S, M.R. Thompson, and P.J. Sheskey. 2013. 'A Study of Foam Granulation and Wet Granulation in a Twin Screw Extruder'. *The Canadian Journal of Chemical Engineering* 91 (April). https://doi.org/10.1002/cjce.21748.

Wenzel, Robert N. 1936. 'Resistance of Solid Surfaces to Wetting by Water'. *Industrial & Engineering Chemistry* 28 (8): 988–94. https://doi.org/10.1021/ie50320a024.

Werner, Stephen R. L., Jim R. Jones, Anthony H. J. Paterson, Richard H. Archer, and David L. Pearce. 2007. 'Droplet Impact and Spreading: Droplet Formulation Effects'. *Chemical Engineering Science* 62 (9): 2336–45. https://doi.org/10.1016/j.ces.2006.12.024.

Westermarck, S., A. M. Juppo, L. Kervinen, and J. Yliruusi. 1999. 'Microcrystalline Cellulose and Its Microstructure in Pharmaceutical Processing'. *European Journal of Pharmaceutics and Biopharmaceutics: Official Journal of Arbeitsgemeinschaft Fur Pharmazeutische Verfahrenstechnik e.V* 48 (3): 199–206. https://doi.org/10.1016/s0939-6411(99)00051-x.

Westman, A. E. R., and H. R. Hugill. 1930. 'The Packing of Particles'. *Journal of the American Ceramic Society* 13 (10): 767–79. https://doi.org/10.1111/j.1151-2916.1930.tb16222.x.

Whitaker, Mark, Guy R Baker, Julian Westrup, Paul A Goulding, David R Rudd, Ron M Belchamber, and Michael P Collins. 2000. 'Application of Acoustic Emission to the Monitoring and End Point Determination of a High Shear Granulation Process'. *International Journal of Pharmaceutics* 205 (1): 79–91. https://doi.org/10.1016/S0378-5173(00)00479-8.

Wikberg, Martin, and Göran Alderborn. 1990a. 'Compression Characteristics of Granulated Materials II. Evaluation of Granule Fragmentation during Compression by Tablet Permeability and Porosity Measurements'. *International Journal of Pharmaceutics* 62 (2): 229–41. https://doi.org/10.1016/0378-5173(90)90236-W.

———. 1990b. 'Compression Characteristics of Granulated Materials II. Evaluation of Granule Fragmentation during Compression by Tablet Permeability and Porosity Measurements'. *International Journal of Pharmaceutics* 62 (2): 229–41. https://doi.org/10.1016/0378-5173(90)90236-W.

———. 1991. 'Compression Characteristics of Granulated Materials. IV. The Effect of Granule Porosity on the Fragmentation Propensity and the Compatibility of Some Granulations'. *International Journal of Pharmaceutics* 69 (3): 239–53. https://doi.org/10.1016/0378-5173(91)90366-V.

Winkels, Koen G., Joost Weijs, Antonin Eddi, and Jacco H. Snoeijer. 2012. 'Initial Spreading of Low-Viscosity Drops on Partially Wetting Surfaces'. *Physical Review E* 85 (January). https://doi.org/10.1103/PhysRevE.85.055301.

Wouters, Ilse M. F., and Derek Geldart. 1996. 'Characterising Semi-Cohesive Powders Using Angle of Repose'. *Particle & Particle Systems Characterization* 13 (4): 254–59. https://doi.org/10.1002/ppsc.19960130408.

Wu, Mingming, Thomas Cubaud, and Chih-Ming Ho. 2004. 'Scaling Law in Liquid Drop Coalescence Driven by Surface Tension'. *Physics of Fluids* 16 (7): L51–54. https://doi.org/10.1063/1.1756928.

Xiao, Junfeng, Howard A. Stone, and Daniel Attinger. 2012. 'Source-like Solution for Radial Imbibition into a Homogeneous Semi-Infinite Porous Medium'. *Langmuir* 28 (9): 4208–12. https://doi.org/10.1021/la204474f.

Yajima, Toshio, Shigeru Itai, Hidefumi Hayashi, Kozo Takayama, and Tsuneji Nagai. 1996. 'Optimization of Size Distribution of Granules for Tablet Compression.' *CHEMICAL & PHARMACEUTICAL BULLETIN* 44 (5): 1056–60. https://doi.org/10.1248/cpb.44.1056.

Yang, Bingqiao, Shaoxian Song, and Alejandro Lopez-Valdivieso. 2014. 'Effect of Particle Size on the Contact Angle of Molybdenite Powders'. *Mineral Processing and Extractive Metallurgy Review* 35 (3): 208–15. https://doi.org/10.1080/08827508.2013.763802.

Yang, Jing-Tang, Zong-Han Yang, Chien-Yang Chen, and Da-Jeng Yao. 2008. 'Conversion of Surface Energy and Manipulation of a Single Droplet across Micropatterned Surfaces'. *Langmuir* 24 (17): 9889–97. https://doi.org/10.1021/la8004695.

Yang, Jun, Ales Sliva, Amit Banerjee, Rajesh N. Dave, and Robert Pfeffer. 2005. 'Dry Particle Coating for Improving the Flowability of Cohesive Powders'. *Powder Technology* 158 (1–3): 21–33. https://doi.org/10.1016/j.powtec.2005.04.032.

Yang, Wolong, and Jinliang Xu. 2017. 'Drop Spreading and Penetrating on Micro/Nano Particle Sintering Porous with Multiscale Structure'. *Colloids and Surfaces A: Physicochemical and Engineering Aspects* 516 (March): 9–22. https://doi.org/10.1016/j.colsurfa.2016.12.005.

Yang, Yanjie, Xiaoqian Chen, and Yiyong Huang. 2019. 'Spreading Dynamics of Droplet Impact on a Wedge-Patterned Biphilic Surface'. *Applied Sciences* 9 (11): 2214. https://doi.org/10.3390/app9112214.

Yang, Ya-Wun, George Zografi, and Edward E Miller. 1988. 'Capillary Flow Phenomena and Wettability in Porous Media: I. Static Characteristics'. *Journal of Colloid and Interface Science* 122 (1): 24–34. https://doi.org/10.1016/0021-9797(88)90284-6.

Ye, Xianjue, Yunping Li, Yanling Ai, and Yan Nie. 2018. 'Novel Powder Packing Theory with Bimodal Particle Size Distribution-Application in Superalloy'. *Advanced Powder Technology* 29 (9): 2280–87. https://doi.org/10.1016/j.apt.2018.06.012.

Yerazunis, S., S. W. Cornell, and B. Wintner. 1965. 'Dense Random Packing of Binary Mixtures of Spheres'. *Nature* 207 (4999): 835–37. https://doi.org/10.1038/207835a0.

York, Peter. 1992. 'Crystal Engineering and Particle Design for the Powder Compaction Process'. *Drug Development and Industrial Pharmacy* 18 (6–7): 677–721. https://doi.org/10.3109/03639049209058558.

Young, Thomas. 1805. 'An Essay on the Cohesion of Fluids'. *Philosophical Transactions of the Royal Society of London* 95 (65–87). https://doi.org/10.1098/rstl.1805.0005.

Yu, A. B., J. Bridgwater, and A. Burbidge. 1997. 'On the Modelling of the Packing of Fine Particles'. *Powder Technology* 92 (3): 185–94. https://doi.org/10.1016/S0032-5910(97)03219-1.

Yu, A. B., R. P. Zou, and N. Standish. 1996. 'Modifying the Linear Packing Model for Predicting the Porosity of Nonspherical Particle Mixtures'. *Industrial & Engineering Chemistry Research* 35 (10): 3730–41. https://doi.org/10.1021/ie950616a.

Yu, A.B., and N. Standish. 1993. 'A Study of the Packing of Particles with a Mixture Size Distribution'. *Powder Technology* 76 (2): 113–24. https://doi.org/10.1016/S0032-5910(05)80018-X.

Yu, Lawrence X., Gregory Amidon, Mansoor A. Khan, Stephen W. Hoag, James Polli, G. K. Raju, and Janet Woodcock. 2014. 'Understanding Pharmaceutical Quality by Design'. *The AAPS Journal* 16 (4): 771–83. https://doi.org/10.1208/s12248-014-9598-3.

Yu, Shen, Gavin K. Reynolds, Zhenyu Huang, Marcel de Matas, and Agba D. Salman. 2014. 'Granulation of Increasingly Hydrophobic Formulations Using a Twin Screw Granulator'. *International Journal of Pharmaceutics* 475 (1–2): 82–96. https://doi.org/10.1016/j.ijpharm.2014.08.015.

Yu, Weili, Koji Muteki, Lin Zhang, and Gloria Kim. 2011. 'Prediction of Bulk Powder Flow Performance Using Comprehensive Particle Size and Particle Shape Distributions'. *Journal of Pharmaceutical Sciences* 100 (1): 284–93. https://doi.org/10.1002/jps.22254.

Yuan, Quanzi, and Ya-Pu Zhao. 2013. 'Multiscale Dynamic Wetting of a Droplet on a Lyophilic Pillar-Arrayed Surface'. *Journal of Fluid Mechanics* 716 (February): 171–88. https://doi.org/10.1017/jfm.2012.539.

Yuan, Yuehua, and T. Randall Lee. 2013. 'Contact Angle and Wetting Properties'. In *SurfaceScience Techniques*, 51:3–34. Surface Sciences. Berlin and Heidelberg, Germany: Springer.

Zakhvatayeva, A., W. Zhong, H.A. Makroo, C. Hare, and C.Y. Wu. 2018. 'An Experimental Study of Die Filling of Pharmaceutical Powders Using a Rotary Die Filling System'. *International Journal of Pharmaceutics* 553 (1–2): 84–96. https://doi.org/10.1016/j.ijpharm.2018.09.067.

Zarmpi, P., T. Flanagan, E. Meehan, J. Mann, and N. Fotaki. 2017. 'Biopharmaceutical Aspects and Implications of Excipient Variability in Drug Product Performance'. *European Journal of Pharmaceutics and Biopharmaceutics: Official Journal of Arbeitsgemeinschaft Fur Pharmazeutische Verfahrenstechnik e.V* 111 (February): 1–15. https://doi.org/10.1016/j.ejpb.2016.11.004.

Zhao, Na, and Larry L. Augsburger. 2006. 'The Influence of Granulation on Super Disintegrant Performance'. *Pharmaceutical Development and Technology* 11 (1): 47–53. https://doi.org/10.1080/10837450500463828.

Zheng, Jingmin, William B. Carlson, and James S. Reed. 1995. 'The Packing Density of Binary Powder Mixtures'. *Journal of the European Ceramic Society* 15 (5): 479–83. https://doi.org/10.1016/0955-2219(95)00001-B.

Zou, R. P., M. L. Gan, and A. B. Yu. 2011. 'Prediction of the Porosity of Multi-Component Mixtures of Cohesive and Non-Cohesive Particles'. *Chemical Engineering Science* 66 (20): 4711–21. https://doi.org/10.1016/j.ces.2011.06.037.

Zuurman, K., K. A. Riepma, G. K. Bolhuis, H. Vromans, and C. F. Lerk. 1994. 'The Relationship between Bulk Density and Compactibility of Lactose Granulations'. *International Journal of Pharmaceutics* 102 (1): 1–9. https://doi.org/10.1016/0378-5173(94)90033-7.

Zuurman, K., K. Van der Voort Maarschalk, and G. K. Bolhuis. 1999. 'Effect of Magnesium Stearate on Bonding and Porosity Expansion of Tablets Produced from Materials with Different Consolidation Properties'. *International Journal of Pharmaceutics* 179 (1): 107–15. https://doi.org/10.1016/s0378-5173(98)00389-5.